Dissertation
submitted to the
Combined Faculties of the Natural Sciences and Mathematics
of the
Ruperto-Carola-University of Heidelberg, Germany
for the degree of
Doctor of Natural Sciences

Put forward by

Isara Chantesana
born in Bangkok, Thailand

Oral examination: 18.01.2018

Strong Wave Turbulence and Non-Thermal Fixed Points in a Kinetic Theory

Referees: Prof. Dr. Thomas Gasenzer
Priv.-Doz. Dr. Michael Scherer

Isara Chantesana

Institut für Theoretische Physik
Philosophenweg 16
D-69120 Heidelberg
Germany

Supervisor

Prof. Dr. Thomas Gasenzer

Kirchhoff-Institut für Physik
Im Neuenheimer Feld 227
D-69120 Heidelberg
Germany

Abstract

Universal dynamics of a dilute Bose gas is studied within the kinetic regime where the time evolution of the mode occupation number is governed by a wave-Boltzmann equation. The universality manifests itself in the form of the dynamical evolution which can be a cascade in the context of Kolmogorov-Zakharov wave turbulence or a self-similar shift in time and space. Which is the case depends on the relevant global conservation laws and on the particular range of scales in which the respective dynamics takes place. A nonperturbative kinetic equation is derived by applying the Schwinger-Keldysh closed-time functional integral and the 2-particle-irreducible formalism to an action of complex scalar Bose fields with quartic interaction. The resulting dynamic equation for two-point correlations are reduced to a wave-Boltzmann-type kinetic equation with an effective T-matrix which depends explicitly on the mode occupation numbers. This nonperturbative dependence on the solution occurs in the infrared regime where wave numbers are large and collective scattering of many particles prevails. Thus, the scaling analysis of wave turbulence theory can be applied. We explicitly calculate the effective T-matrix analytically taking into account an infrared cutoff for dealing with the infrared divergences. Our results show that the scaling behaviour of the T-matrix departs from the one predicted by naive dimensional counting due to the presence of the infrared cutoff. The Kolmogorov-Zakharov and the self-similar exponents are evaluated by power counting using our T-matrix and the results are confirmed by numerical integration of the wave-Boltzmann scattering integral. The scaling exponents governing the time evolution are determined by means of the global conservation laws and the kinetic equation. Depending on the scaling properties of the quasiparticle spectrum, the momentum cutoff scale in the infrared evolves critically slowed in time. The respective scaling exponent is universal in the nonperturbative regime regardless of whether the process is an inverse cascade or a self-similar shift towards the infrared. Thus, our results provide a general framework for classifying nonthermal fixed points in dilute ultracold Bose gases. They pave the way to a straightforward generalisation and application to trapped systems in different dimensionalities and to systems with more than one internal degree of freedom. Our results furthermore provide a possible interpretation of recent experimental results on wave turbulence in an ultracold Bose gas.

Kurzzusammenfassung

Wir studieren die universelle Dynamik eines verdünnten Bose-Gases im kinetischen Regime, in dem die Zeitentwicklung der Besetzungszahlen durch eine Boltzmann-Gleichung gegeben ist. Die Universalität zeigt sich in der dynamischen Entwicklung der Besetzungszahlen, die entweder die Form einer Kolmogorov-Zakharov wellenturbulenten Kaskade oder einer selbstähnlichen Verschiebung in Zeit und Raum annehmen kann. Welcher Fall eintritt, hängt von den relevanten globalen Erhaltungssätzen und dem entsprechenden Skalenbereich ab, in dem die Dynamik stattfindet. Eine nicht-perturbative dynamische Gleichung für die Zweipunkt-Korrelatoren wird durch Anwendung des Schwinger-Keldysh closed-time Funktionalintegrals und der 2-Teilchen-irreduziblen Formulierung der effektiven Wirkung für ein komplexes skalares Bosefeld mit quartischer Wechselwirkung hergeleitet. Aus dieser Gleichung erhält man eine der Wellen-Boltzmann-Gleichung ähnliche kinetische Gleichung mit einer effektiven T-Matrix, welche explizit von den Moden-Besetzungszahlen abhängt. Diese nicht-perturbative Abhängigkeit von der Lösung tritt im Infrarotbereich auf, in dem die Wellenzahlen groß sind und kollektive Streuung von vielen Teilchen überwiegt. Daher kann die Skalenanalyse der Wellenturbulenz-Theorie angewendet werden. Wir regularisieren die Divergenz im Infraroten mit Hilfe eines physikalischen Cutoffs und berechnen damit analytisch die effektive T-Matrix. Unsere Ergebnisse zeigen, dass das Skalierungsverhalten der T-Matrix aufgrund des infraroten Cutoffs von dem mittels einfachen Abzählens der Impuls-Dimensionen erhaltenen Wert abweicht. Der Kolmogorov-Zakharov Exponent sowie die Exponenten der selbstähnlichen Verschiebung werden mit Hilfe der T-Matrix ausgewertet und durch numerische Integration des Boltzmann-Streuintegrals bestätigt. Die Exponenten, welche die Zeitentwicklung beschreiben, werden durch globale Erhaltungssätze und die kinetische Gleichung bestimmt. Abhängig von den Skalierungseigenschaften des Spektrums der Quasiteilchen entwickelt sich die Impuls-Cutoff Skala kritisch verlangsamt in der Zeit. Der entsprechende Skalierungsexponent ist universell innerhalb des nicht-perturbativen Regimes, unabhängig davon, ob der Prozess eine inverse Kaskade oder eine selbstähnlichen Verschiebung darstellt. Unsere Resultate liefern daher einen allgemeinen Rahmen für die Klassifizierung von nichtthermischen Fixpunkten in verdünnten ultrakalten Bose-Gasen. Außerdem schaffen sie die Grundlage für weitere Anwendungen von (in Fallen eingeschlossenen) Systemen in unterschiedlichen Dimensionen und von Systemen mit mehr als einem internen Freiheitsgrad. Zudem geben unsere Resultate eine mögliche Interpretation der Ergebnisse aktueller Experimente zur Wellenturbulenz in einem ultrakalten Bose-Gas.

Declaration by Author

This thesis is composed of my original work, and contains no material previously published or written by another person except where due reference has been made in the text. I have clearly stated the contribution by other authors to jointly-authored works that I have included in my thesis. The content of my thesis is the result of work I have carried out since the commencement of my graduate studies at the Heidelberg Graduate School of Fundamental Physics, Institut für Theoretische Physik, Universität Heidelberg and does not include material that has been submitted by myself to qualify for the award of any other degree or diploma in any university or other tertiary institution.

Contents

Abstract/Kurzzusammenfassung v

Declaration by Author vii

1 Introduction 1

2 Universal dynamics and nonthermal fixed points 11
- 2.1 Model and observables . . . 12
- 2.2 Momentum scaling and universal scaling functions . . . 14
  - 2.2.1 Momentum scaling in number distributions . . . 14
  - 2.2.2 Bulk integrals . . . 15
  - 2.2.3 Scaling function . . . 16
- 2.3 Universal dynamics . . . 18
  - 2.3.1 Global conservation laws . . . 19
  - 2.3.2 Nonthermal fixed points . . . 20
  - 2.3.3 Wave-turbulent transport . . . 23
  - 2.3.4 Summary of scaling relations . . . 27
- 2.4 Summary . . . 27

3 Kinetic theory of weak and strong wave turbulence 29
- 3.1 Quantum and wave-Boltzmann equations . . . 32
- 3.2 Wave turbulent scaling exponents . . . 33
  - 3.2.1 Weak-wave turbulence scaling exponents . . . 35
  - 3.2.2 Strong wave turbulence scaling exponents . . . 37
  - 3.2.3 Self-similar scaling exponent . . . 38
- 3.3 Universal dynamics (revisited) . . . 39
  - 3.3.1 Time scaling behaviour . . . 39
  - 3.3.2 General scaling of T-matrix . . . 40
  - 3.3.3 Scaling evolution . . . 41
- 3.4 Summary . . . 45

4 Kinetic equation from nonequilibrium quantum field theory 49
- 4.1 Nonequilibrium description of a Bose field with quartic interaction . . . 50
  - 4.1.1 Dynamical equations of a Bose field with quartic interaction . . . 50
  - 4.1.2 Dynamical equations of statistical and spectral function . . . 56
  - 4.1.3 Stationarity condition . . . 59

4.2 The s-channel resummation of the self-energy and Boltzmann's scattering integral . . . 63
4.3 Kinetic equation of quasi-particle occupation number . . . 68
4.3.1 Particle and quasi-particle correlation functions . . . 69
4.3.2 Nonperturbative kinetic equation . . . 71
4.4 Effective many-body coupling function . . . 75
4.4.1 Effective many-body coupling function for free particles . . . 77
4.4.2 Effective many-body coupling function for Bogoliubov quasiparticles . . . 82
4.5 Summary . . . 86

5 Numerical evaluation of scattering integral **89**
5.1 Analytical simplification of the scattering integral . . . 90
5.1.1 Free particles . . . 90
5.1.2 Bogoliubov quasiparticles . . . 92
5.2 The scaling solutions of integrals . . . 95
5.2.1 Weak-wave turbulence solutions . . . 95
5.2.2 Strong-wave turbulence solutions . . . 99
5.2.3 Self-similar solutions . . . 104
5.3 Dynamical exponents . . . 105
5.4 Time evolution of Bose gas in the kinetic regime . . . 109
5.5 Summary . . . 110

6 Conclusion **113**

A Convention and useful symmetries **115**

B Nonequilibrium quantum field theory **119**
B.1 Closed-time-path integral . . . 119
B.1.1 Single-time-contour formalism . . . 119
B.1.2 Closed-time-path formalism . . . 121
B.1.3 Path integral representation of CTP formalism and its effective action . . . 123
B.2 2-particle irreducible effective action . . . 128
B.2.1 The generating of n-particle irreducible (nPI) formalism . . . 128
B.2.2 2-particle-irreducible (2PI) effective action . . . 130
B.3 Nonequilibrium Quantum Field Theory . . . 134

C Spectral function of free and Bogoliubov particles **137**

D Evaluation of integrals **141**
D.1 Integrals involving the many-body coupling . . . 141
D.2 Evaluation of the scattering integral . . . 143
D.2.1 Evaluation of $I_1^{\rm free}$ and $I_2^{\rm free}$ . . . 143
D.2.2 Evaluation of $I_1^{\rm bog}$, $I_2^{\rm bog}$, $I_3^{\rm bog}$ and $I_4^{\rm bog}$ . . . 145

E Expansion of the hypergeometric functions **149**

F Evaluation of the scaling form of T-matrix elements **153**

Bibliography **157**

Chapter 1

Introduction

Bose-Einstein condensation (BEC) was predicted by S.N. Bose and A. Einstein [1–3] as a condensed state of matter in the ground state. In 1995, BEC in a dilute gas was first observed in several experiments, using different types of atomic vapor [4–6]. Since then, the range of isotopes that are successfully condensed into BEC has been rapidly expanded including some lanthanide elements such as Yb, Dy and Er. In many-body physics, the BEC is described as a phase of spontaneously broken global $U(1)$ symmetry of the underlying field theoretical model. The Bogoliubov mean-field theory treats the ground state of the BEC differently from the excited states. In the condensate phase, the field operator which creates the ground state is replaced by a complex-number-valued *macroscopic field*, such that the ground state field expectation value is non-zero while the excited states still have zero field expectation values due to the nature of creation/annihilation operators. The transition from noncondensed to condensed phase can be viewed as a phase transition that occurs below a critical temperature (on the order of nano Kelvins) and the expectation value of the ground state field serves as an order parameter distinguishing the noncondensed state (being zero) from the condensed state (being nonzero). The transition from the noncondensate phase to the condensate phase (which can be viewed as thermal equilibrium states of the ultracold Bose gas) implies that a large amount of particles, comparable to the total number of particles in the system, is shifted into the ground state. In most physical realisations, the formation of a condensate is, however, a highly nonequilibrium process and is not captured by a model that only accounts for slight deviations from thermal equilibrium [7].

In the following, we would like to emphasize how the formation of a Bose-Einstein condensate, wave turbulence and nonthermal fixed points are related to each other and what role each of them plays in the context of nonequilibrium universal physics.

The process of condensation requires cooling of the Bose gas such the temperature drops below the critical temperature. There is a series of techniques to achieve BEC where typically, the evaporate cooling is used in the last step [8, 9]. By allowing high-energy particles to leave the system, the energy of the system is being lowered. This process is equivalent to removing particles from the high-energy tail of the number distribution and then letting the Bose gas to re-equilibrate. This is also termed a "cooling quench". Once the temperature drops down below the critical temperature, the wave functions of the particles start to overlap and a BEC starts to form. During

this procedure, the gas is kept isolated from its surrondings to prevent it from heating up. Hence, the process shifting the particles into the ground state originates from the interparticle collisions alone. As such, the condensation process is expected to be captured by a kinetic-theory description. As we will see, this allows us to identify wave turbulence as a generic feature of this process [10–12].

E. Levich and V. Yakhot investigated the time scale that is needed for condensation to occur. In [13], the Bose gas was coupled with a heat bath and it was shown that the time scale for condensate formation is infinite if there is no condensate in the first place. However, when treating the Bose gas within a kinetic-theory framework, the time scale of condensation is found to be finite [14]. This result suggests that kinetic equations can serve to describe the process of forming a BEC. The process of condensation can then be analysed within the theory of weak wave turbulence.

This analysis of wave turbulence in weakly interacting Bose gases is done in [15], and it is emphasized that an inverse particle cascade is a very convenient means to transport particles into the zero-mode. Numerical calculations supported this claim [16, 17], though the results are slightly different in the values of scaling exponents. It needs to be stressed, however, that weak-wave turbulence can not describe the whole process since it is subject to the weak-wave approximation. This means it is only valid at sufficiently low wave amplitude and in the random phase approximation [10] This approximation breaks down when phase coherence starts to appear and, typically, vortices are formed and begin to reconnect.

In a series of papers, Stoof [18–21] analyzed the Bose gas by applying the Schwinger-Keldysh time integral contour in a 1-particle-irreducible (1PI) formulation of the Gross-Pitaevskii action. Instead of using the process of truncation that is normally done in the 1PI approach, the effective action of the Gross-Pitaevskii model (GPE) was considered as a classical action and a generating functional was derived in the classical limit ($\hbar \to 0$) to avoid over counting of loop-diagrams that are now in the (effective) classical action. Although the author chose the truncation in way that it preserves the symmetry of the original action, he still had to go through several steps of approximations in order to build up a self-consisted correction term for the effective action. The major conclusion was that the instability creates a small amount of condensate in the ground state nucleating the further condensation process. Furthermore, the time scale of nucleation was found to be very short, likely to be observed in laboratory experiments.

In stark contrast, Svistunov, Kagan and Shlyapnikov [7, 22, 23] suggested that the particles in the coherent regime already behave much like a condensate in the ground state. A precondensate peak would form at $k > 0$ due to the suppression of quantum fluctuations. Such a state is called *quasicondensate* and numerical calculations done later [24] show that this quasicondensate induces superfluid turbulence with a very long life-time, indicating that the time scale of condensate formation might be much longer than the one derived by Stoof.

Such an intermediate state apparently fits with the idea of a *nonthermal fixed point* [25, 26], stating that there exists a nonequilibrium fixed point characterized by universal scaling exponents. While there is no mentioning of scaling behaviour

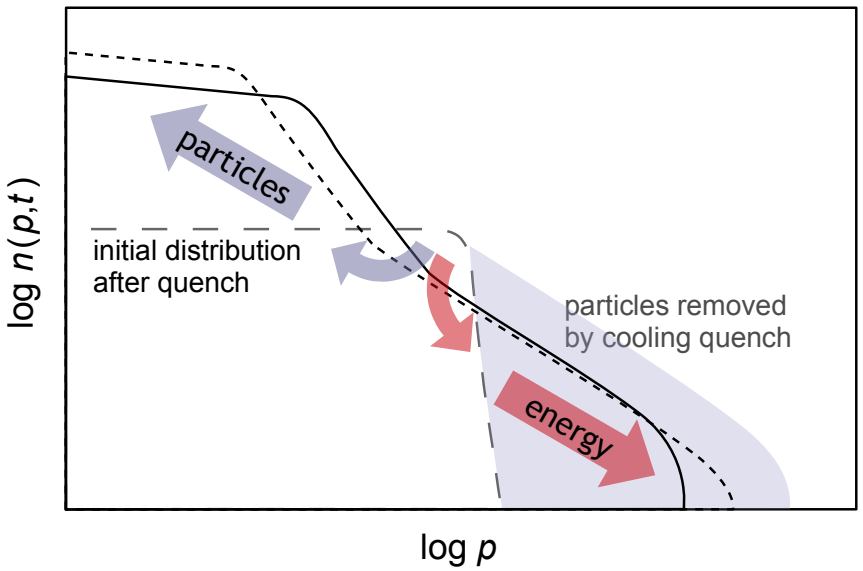

Figure 1.1: Universal dynamics of a dilute Bose gas in the vicinity of a non-thermal fixed point, as induced by a strong cooling quench. The sketch indicates the single-particle radial number distribution $n(p,t)$ as function of momentum p for two different times t (solid and short-dashed lines). Starting from the extreme initial distribution $n(p,t_0)$ (long-dashed line) resulting, e.g., from a strong cooling quench which removes a previous thermal tail (grey shaded area), a bidirectional redistribution of particles in momentum space (arrows) occurs. This eventually builds up a quasicondensate in the infrared while refilling the thermal tail at large momenta. The particle transports towards zero as well as large momenta is characterized by self-similar scaling evolution in space and time, $n(p,t) = t^{\alpha} f(t^{\beta} p)$, with characteristic scaling exponents α, β, in general different for the two directions. The infrared transport moves particles to low-p modes (blue arrow) while their energy is deposited by the scattering of much fewer particles to higher momenta (red arrow), conserving total energy and particle number. Note the double-logarithmic scale.

in [24], the universal scaling of superfluid turbulence in a Bose gas described by the Gross-Pitaevskii model has been observed in numerical simulations [27–29]. See the recent review of condensate formation [30] for a discussion of other, related theories of condensation [31–36]. There, the kinetic equations are derived by different methods and they all seem to agree to a certain extent. However, there are limitations due to the approximations done in the derivations and, thus might not provide sufficient means to treat the nonequilibrium problem of BEC.

The number of particles needs to be sufficiently large in the coherent regime for a quasicondensate to be formed. This is achieved by an inverse particle flux as a result of wave turbulence in the kinetic regime. Before the condensate is formed, the kinetic transport is dominated by the 4-wave interaction process [37, 38] and there are two types of transport here: inverse particle flux and direct energy flux. This two-way transport or dual cascade is an efficient mechanism to achieve a condens-

ate. The inverse particle flux shuffles the particles into the coherent regime while a direct energy flux moves high-energy particles into the ultraviolet tail where they can be removed via evaporation, leading to a further cooling down of the system. In comparison to Richardson's cascade in hydrodynamic turbulence where the energy is passed down in the high-momentum regime by breaking down large eddies into the smaller ones [39], wave turbulence transports particles and energy through the interaction between wave modes at nearby wave numbers.

Like in hydrodynamic turbulence, wave turbulence also involves driving forces and dissipation and assumes that the driving and dissipation scales are set apart by the *inertial range*, a window where there is no effect of driving or dissipation. Therefore, the transport of particles/energy in this inertial range happens in a conserved manner. The steady state of turbulent fluxes in the inertial window enforces a constraint on the particle and energy spectra such that they show unique scaling behaviour. In hydrodynamic turbulence, the exponent of the energy spectrum is the Kolmogorov 5/3 exponent [40], The corresponding power-law particle or energy cascades in wave turbulence are set by the Kolmogorov-Zakharov exponents [10, 37]. Also these Kolmogorov-Zakharov exponents are universal, independent from the microscopic details of the underlying theory.

In [15] wave turbulence in a weakly interacting Bose gas was studied to understand the time evolution of a Bose gas in the kinetic regime. Although 4-wave resonant interactions were considered, the phenomenon of a dual cascade was ruled out due to a single power law assumed to describe the number distribution and the presumption that driving forces and dissipation occur in the deep infrared and the high ultraviolet, respectively.

As will be shown in detail in this thesis, there are, in fact, three situations that could happen in the kinetic regime: a direct energy cascade, an inverse particle cascade or self-similar evolution. In the case of a weakly interacting Bose gas and in the perturbative regime, the inverse cascade is expected to occur. Weak-wave turbulence theory predicts the power-law of the number distribution to be $n(\varepsilon) \sim \varepsilon^{-7/6}$ where $n(\varepsilon)$ is the number distribution as a function of energy ε [15]. The time evolution of the particle flux is encoded in the time-dependent energy scale $\varepsilon_0(t)$ which is the energy scale determining the position of the wave front of particles flux[1]. A scaling analysis shows that time dependence of the wave front as follows $\varepsilon_0(t) \sim (t_c - t)^3$. A later numerical calculation by D. Semikoz and I. Tkachev showed the build up of particles in the infrared through an inverse particle cascade [16, 17]. The power law that has been observed there was slightly different from the prediction: $n(\varepsilon) \sim \varepsilon^{-1.24}$ was found together with the wave front evolution $\varepsilon_0(t) \sim (t_c - t)^{2.6}$.

Recently, an experiment by Navon et al. in Cambridge performed on a quantum gas [41] within a flat-bottom cylindrical trap, has provided a first test of the theoretical predictions made for a homogeneous system. A direct cascade has been observed,

[1]This means flux of particles is established within energy scale $\varepsilon > \varepsilon_0$ and power-law $n(\varepsilon) \sim \varepsilon^{-7/6}$ can be observed here. There is no such power law in the windows $\varepsilon < \varepsilon_0$ since flux of particles has not yet reached.

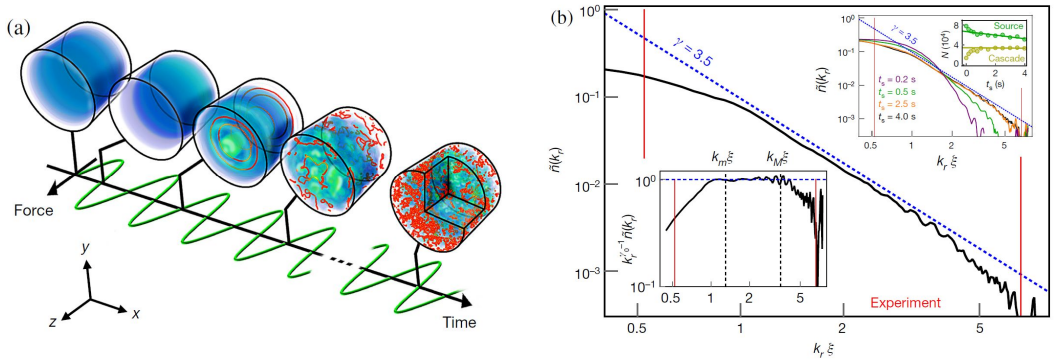

Figure 1.2: The experimental setup in Ref. [41] is illustrated in (a). Bose gases in the cylindrical optical box is driven out-of-equilibrium by a spatially uniform, oscillating force. The blue shading represents the gas density while the red lines indicate the lines of vortices. The momentum distribution during turbulent cascade is presented in (b). The power-law scaling 3.5 is observed within the momentum window bounded by k_m and k_M. The upper inset shows the time evolution of the number distribution which is interpreted as a direct transport toward the ultraviolet regime. Both of figures are taken from Ref. [41].

with number distribution $n(k) \sim k^{-3.5}$ where k is the modulus of momentum. Assuming that in this regime $\varepsilon \sim k^2$, the number distribution was measured to depend on the energy as $n(\varepsilon) \sim \varepsilon^{-1.75}$ which is slightly different from that in a direct energy cascade with Komogorov-Zakharov exponent, $n(\varepsilon) \sim \varepsilon^{-1.5}$. It is not clear yet whether the difference is due to the finite size of the experimental set up or if there are other fundamental concepts that lie outside the kinetic description. The experiment might not yet give a full answer to the questions related to condensate formation but nevertheless, seems to support the validity of kinetic theory in an ultracold Bose gas.

We remark that all discussions about Kolmogorov-Zakharov exponents so far have been based on the context of weak-wave turbulence where wave amplitudes are assumed to be small such that all higher-order correlation functions can be broken down into occupation numbers (and thus to second-order correlation functions). This is an advantage of wave turbulence that is absent in its hydrodynamic counter part, the closed equation describing fluid turbulence. The kinetic equation of weak-wave turbulence takes the form of a wave-Boltzmann equation [10, 11]. The interaction between wave modes is described by a scattering integral over product of occupation numbers and T-matrix elements. The resulting Kolmogorov-Zakharov exponents are universal in the sense that they are fully determined by dimension, energy spectrum and scaling behaviour of the T-matrix elements.

Field-theory approach to universal dynamics is used to avoid the perturbative limitation. In the present work, we demonstrate that this is conveniently achieved with an effective action in a nonequilibrium quantum field theory approach. Here, the Schwinger-Keldysh contour is used but instead of applying the 1PI approach as Stoof has done, we choose the 2-particle-irreducible (2PI) effective-action formalism

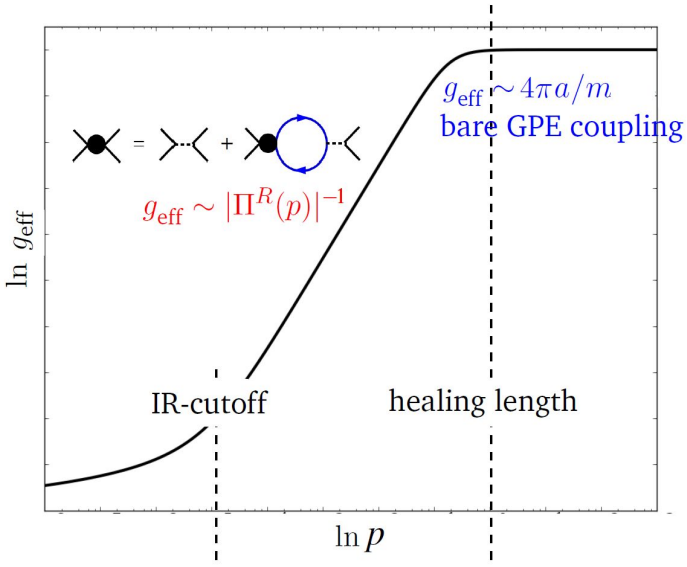

Figure 1.3: A sketch of an effective coupling which is equivalent to an effective T-matrix shows the value of the effective coupling varying on the momentum scales. In the UV regime, the coupling is a bare GPE coupling which is an approximation of many-body coupling in the perturbative calculation. In the IR regime, the effective coupling becomes a momentum-dependent function due to the collective scatterings in the nonperterbative regime. The effect of the collective scatterings is encoded in the self-energy function Π^R.

[42–44]. The advantage of 2PI is having a closed, self consistent dynamical equation for the mean field and propagators. The opportunity to evaluate propagators nonperturbatively opens a path-way to go beyond a mean-field calculation. The $\mathcal{N}$-component scalar field theory with ϕ^4-interaction and orthogonal symmetry, $\mathcal{O}(\mathcal{N})$, has been studied in this nonperturbative approach in Refs. [45–47]. In the language of the large-$\mathcal{N}$ expansion, the leading order (LO) terms lead us back to the mean-field calculation, while the next-to-leading order (NLO) describes the scattering physics which is required to describe the interaction between wave modes [48]. Assuming homogeneity and choosing the classical approximation, the integro-differential dynamical equation for the propagator [25] yields a kinetic equation resembling Bolzmann's equation but involving a many-body momentum dependent T-matrix. The analysis done in wave-turbulence can be applied here in an analogous way. The T-matrix is crucially modified due its the nonperturbative calculation and this effects the values of the scaling exponents in a nontrivial way.

The effective T-matrix has two limits: in the ultraviolet regime where mode occupations are sufficiently low, it turns back to the T-matrix evaluated within the weak-wave turbulence context. Thus, we call this the *perturbative regime*, and all evaluations reproduce the weak-wave turbulence results. In the infrared limit where the population is high, the effective T-matrix exhibits a different, universal scaling behaviour. Within this *nonperturbative regime* the weak-wave turbulence is modi-

fied to so-called *strong-wave turbulence* [11]. Note that strong-wave turbulence here still occurs within the kinetic regime (not yet the coherent regime). The notable feature is that even though strong-wave turbulence is the result of a nonperturbative calculation, the kinetic equation is similar to the one in weak-wave turbulence, apart from the momentum-frequency dependent effective T-matrix. Thus, the scaling of weak-wave turbulence equally applies here, only giving different values for the Kolmogorov-Zakharov exponents. Within scalar Bose field models, the exponents of weak- and strong-wave turbulence have been derived in [25, 26] and [49], calculated in the relativistic and nonrelativistic cases respectively. The exponents in both cases fully agree with each other both in the in perturbative or nonperturbative regimes. This again emphasizes the universality since whether the theory describes relativistic or nonrelativistic particles does not affect the scaling derived from the kinetic equations.

Strong-wave turbulence gives us a supportive argument for the existence of a nonthermal fixed point. The universal character of the fixed point (turbulent steady state) occurs in the regime where the perturbative calculation fails. However, the steady state of transport demands a driving force and dissipation which, in turn, should be absent in an isolated system. As mentioned in the beginning, the process of condensation in an ultracold Bose gas is taking place in a closed and isolated way if no high-energy particles are evaporated out. In such a case, if there exists a nonthermal fixed point, it can not be a steady state of wave turbulence but nevertheless, it shows two characteristic features, long life time and universal scaling. In [50], the numerical calculation for an isolated Bose gas shows scaling behaviour in the occupation number but instead of being stationary, the number distribution evolves *self-similarly* in time conserving particles and energy, at the infrared and the ultraviolet ends of the momentum range, respectively. We note that the self-similar evolution was discussed already in [15] and in there, the scaling exponents are completely fixed by the kinetic equation and somehow differ from the exponents observed in [50]. A plausible explanation is that superfluid turbulence may play some role here. A nonrelativistic calculation shows that the scaling exponents in the occupation number are apparently identical to other classical statistical calculations of Gross-Pitaevskii model [27, 28] where vortices are clearly seen. Although the full picture is not yet available, it is enough to say that nonthermal fixed points in isolated system are possible and in such case, the universal scalings manifest in both space and time.

The scenario of the Bose gas after the cooling quench in the vicinity of a nonthermal fixed point is illustrated in Fig. 1.1. The bimodal transport is necessary for a typical situation where the energy spectrum scales as $\varepsilon(p) \sim p^z$ with $z > 0$ since This implies that the energy content $\varepsilon(p)\, n(p)$ is concentrated on large momentum scales. A particle needs to take energy from several particles to move forward into the UV-direction, and thus, those particles which loose energy need to scatter backward into the IR-direction. The concept here is similar to the one describing the dynamics in the language of the turbulence dual-cascade scheme [37], however, there is no steady state of turbulence flux here due to lack of driving and dissipation forces

in an isolated system.

In this thesis, we study the universal dynamics of a homogeneous Bose gas after a strong cooling quench. We consider the general situation of universal dynamics where the observable, the occupation number, takes the form of a power-law with or without time-dependent cut-off scales regularizing the divergences of the particle and energy integrals. The dynamics is categorized into three cases, particle cascade, energy cascade and self-similar evolution, distinguished by the power-law scaling of occupation number and constraints from global conservation laws. Similar arguments have been introduced in [15] showing that the dynamics can be categorized by the scaling exponent of the T-matrix. We show in Table 2.1 that even without the knowledge of kinetic equation, some of the dynamical exponents are already fixed by the global conservation laws alone.

Later, we analyse the kinetic equation and evaluate scaling exponents, both of the Kolmogorov-Zakharov type and dynamical scalings exponents. In the perturbative regime, the exponents we find fully agree with the ones obtained in [15] in the weak-wave turbulence analysis. In the nonperturbative regime, the main task is to evaluate the scaling behaviour of the effective T-matrix which we achieve here by evaluating the integral giving the self-energy in loop-resummation. We find that the T-matrix in the perturbative regime is evaluated with the bare coupling $g = 4\pi a/m$ independent of the momentum scale where in the nonperturbative regime the T-matrix is calculated with momentum dependent effective coupling, $g_{\text{eff}}(p) \sim p^2$. Using this, we determine the scaling of the effective T-matrix, and with this the Kolmogorov-Zakharov exponents. Our results are different from the ones obtained in [26] and [49] in the strong-wave turbulence regime. This is because the scaling arguments used there gave $g(p) \sim p^4$ assuming that the integral converges without the need of having cut-off scales. In our calculation, we now take into account the necessary infrared cutoff. Related differences appear in the dynamical scalings when we compare with the results of [50].

Apart from Kolmogorov-Zakharov exponents for the turbulence cascades, we evaluate also the self-similar scaling exponents, a universal scaling in isolated systems as depicted in Fig. 1.1. The exponent in the perturbative regime is again identical to the one predicted in [15]. Our prediction in the nonperturbative regime is that the exponent $\kappa = d + (3z - 4 - \eta)/2$ determines the momentum power law of the occupation number, $n(p) \sim p^{-\kappa}$, in d dimensions, with energy spectrum $\varepsilon(p) \sim p^z$ and anomalous scaling η. The exponent we obtain is apparently different from the scaling of the occupation number presented in [50]. We attribute this discrepancy to the fact that there are influences from superfluid turbulence there which is beyond the scope of the kinetic equation.

Our analysis yields a picture of the universal dynamics of Bose gas as follows. In the perturbative regime, an inverse particle cascade occurs however, not with critically slowing of the wave front with $t^{-\beta}$ but with an accelerating wave front, $(t_* - t)^{-\beta}$ due to the negative β. Note that this confirms the earlier predictions of Refs. [15–17]. In the nonperturbative regime where the single-particle spectrum is considered free i.e. $\varepsilon(p) \sim p^2$, the self-similar dynamics manifests itself with a

momentum scaling exponent of the occupation number $\kappa = d + 1 - \eta/2$. Below the healing length scale where the spectrum is linear $\omega(p) \sim p$, an inverse cascade takes place with an exponent $\kappa = d - 1/3 - \eta/6$. In either case, the time evolution of the infrared wave front is critically slowed down with the cutoff evolving proportional to $t^{-\beta}$, with the same exponent $\beta = 1/(z - \eta)$. Our results suggest that the exponent β in the nonperturbative regime is a universal feature of the nonthermal fixed point.

The scenario we predict has not yet been observed in numerical calculations and as before, we suspect that superfluid turbulence plays a role there. The momentum scaling exponent κ deriving from the vortex-statistics is higher than the scaling exponent within kinetic theory/ Thus, the kinetic exponent appears to be subdominant. This is corroborated by the numerical calculation done in [28]. There the exponent of the incompressible part shows the sound-wave excitation spectrum to scale with the exponent $\zeta = 3.6$ in the moment shortly after vortex decay. This corresponds to $\kappa = 2.6$ in our notation which closely resembles $\kappa = 8/3$ of our prediction in $d = 3$ dimensions (neglecting η). The same number has also been found in the scaling analysis of the Kardar-Parisi-Zhang equation [51] using functional renormalization group methods.

The thesis is organized as follows. In Ch.2, we discuss the general form of the universal scaling function and analyse the dynamical exponents using the global conservation laws. In Ch.3, we introduce the kinetic equation without derivation and evaluate the exponents in both the turbulence cascade and the self-similar evolution in an isolated system. The dynamical exponents are finally determined with the constraint arising from kinetic equation. In Ch.4, we derive the closed equation of motion of mean-field and propagators using the nonperturbative approach of nonequilibrium quantum field theory. We recover the kinetic equation and calculate the many-body coupling for the effective T-matrix which we have in Ch.3. Using an ansatz, we explicitly evaluate analytically the many-body T-matrix. In Ch.5, we use this to calculate numerically Kolmogorov-Zakharov exponents, the self-similar exponent and the dynamical scaling of Boltzmann's scattering integral. The technical calculation and supplement materials are in the appendices.

After completion of this thesis I became aware of the recent work [52] discussing questions related to the ones studied in this thesis.

Chapter 2

Universal dynamics and nonthermal fixed points

Universality is a phenomenon where the relevant observables become insensitive to the underlying microscopic theory [53, 54]. Near a second-order phase transition universal behaviour of system is usually signalled by the divergence of the correlation length because fluctuations spread across all length scales, enforcing the whole system to be in a unique state, exhibiting self-similar character. As a consequence, the observables show scaling behaviour with specific *critical exponents*. Systems which might have totally different microscopic properties show the very same set of critical exponents, thus, are classified to be in the same universality class.

Universal physics is not limited to equilibrium physics. Rather, the question whether there is an equivalent nonequilibrium version of universal phenomena has become one the most relevant topics in (quantum) many-body studies. The theory of dynamical critical pheonomena based on stochastic field theory and the renormalisation group has been summarised in [55, 56] where the universality of several physical models has been examined. The universal behaviour during the relaxation after a quench has also been found in purely dissipative cases [57, 58]. In ageing phenomena [59–61], the system persists in the nonequilibrium state for a long time after the relaxation and the fluctuation dissipation relation is violated. However, the fluctuation dissipation ratio has been observed to have universal properties in ferromagnet models [62, 63]. Turbulence (especially wave turbulence) [10, 11, 39] and superfluid or quantum turbulence [64, 65] are also closely related to dynamical critical phenomena even though turbulence involves driving and dissipation forces. The conserved fluxes that go through different scales can be viewed as analogue to the fluctuation that spreads out in critical phenomena, leading to the self-similar character in both cases.

A cooling quench is one of many techniques that have been used to study dynamical critical scaling. By quenching across a critical point, the effects of the universal character of the critical point are expected to influence the dynamics towards the new equilibrium. This means universal scaling should also be observed during the time evolution which is clearly a nonequilibrium process. Universal scaling would emerge if the system was drawn towards a nonthermal fixed point during the time evolution [25, 48]. Classical statistical simulations reveal the scaling character dur-

ing the dynamics towards equilibrium after a cooling quench in a single-component [27–29] and in two-component Bose gases [66, 67]. Thereby, universality showing up in the scaling time evolution implies critical slow down in the evolution towards equilibrium.

In this chapter, we do not yet discuss how precisely universal dynamics is manifested in Bose gases but will presume that the occupation number $n(\boldsymbol{p}, t)$ which is a general observable in the numerical calculations, takes the scaling form in both momentum and time. Then, we analyze the possible time-evolution of the system and the dynamical exponents in each case. In contrast to the analysis in [15], instead of combing global conservations and kinetic equations in the first place, we for the first only consider the constraints from the global conservation laws. It will be seen by the end of this chapter that the constraints set by the global conservation laws alone are already sufficient to give us a general idea of the time evolution assuming a universal character of the occupation number distribution.

2.1 Model and observables

We study the Gross-Pitaevskii model for bosons of mass m with a quartic self-interaction

$$H = \int \mathrm{d}^d x \left[-\Phi^\dagger(x) \frac{\nabla^2}{2m} \Phi(x) + \frac{g}{2} \Phi^\dagger(x) \Phi^\dagger(x) \Phi(x) \Phi(x) \right] . \tag{2.1}$$

where g is a coupling parameter[1]. The Hamiltonian in Eq. (2.1) represents a system of a dilute Bose gas without trapping potential such that it is enough to keep only the 2-body collision term in the interaction $\int \mathrm{d}^d x \mathrm{d}^d x' \Phi^\dagger(x') \Phi^\dagger(x) V(x, x') \Phi(x) \Phi(x')$, while the contact interaction, $V(x, x') \sim \delta(x - x')$, reduces the term further down to a simple quartic interaction with a single parameter a, the s-wave scattering length[2]. In units of $\hbar = k_B = 1$, the coupling g relates to a via $g = 4\pi a/m$. The field variables $\Phi \equiv \Phi(\mathbf{x}, t)$ satisfy Bose equal-time commutation relations,

$$[\Phi(\boldsymbol{x}, t), \Phi^\dagger(\boldsymbol{x}', t)] = \delta^d(\boldsymbol{x} - \boldsymbol{x}') , \tag{2.2}$$

$$[\Phi(\boldsymbol{x}, t), \Phi(\boldsymbol{x}', t)] = [\Phi^\dagger(\boldsymbol{x}, t), \Phi^\dagger(\boldsymbol{x}', t)] = 0 . \tag{2.3}$$

The single-particle momentum distribution

$$n(\mathbf{p}, t) = \langle \Phi^\dagger(\mathbf{p}, t) \Phi(\mathbf{p}, t) \rangle \tag{2.4}$$

counts the directly measurable number of particles with momentum $\mathbf{p}$. In free-particle limit (no condensate and sufficiently weak interactions and occupation numbers), the eigenmodes of the Hamiltonian are approximately determined by only the Laplacian term which gives the free particle energy spectrum

$$\varepsilon_{\mathbf{p}} = \mathbf{p}^2/(2m) . \tag{2.5}$$

[1] The coordinate variable x stands for the $d+1$ dimensional space-time variable $(x_0, \boldsymbol{x})$.

[2] Note that this notion of the scattering length a is only valid in three-dimensions. In terms of the scattering length, the term *dilute* means $na^3 \ll 1$ where n is the total number of particles [68].

In the case of a dilute Bose gas with a condensate fraction, the field operator $\Phi(x)$ becomes a macroscopic field and has a nonzero expectation value, $\langle\Phi(x)\rangle \equiv \phi_0$, assuming that the condensate is homogeneous. Then, the condensate density ρ_0 is determined by $\rho_0 = |\phi_0|^2$. The field $\Phi(x)$ can be expanded around its expectation value $\Phi(x) = \phi_0 + \tilde{\Phi}(x)$ where $\tilde{\Phi}(x)$ represents the fluctuation around the condensate (implies $\langle\tilde{\Phi}(x)\rangle = 0$). In this case, the Hamiltonian can be expanded to second order in the fluctuation fields $\tilde{\Phi}(x)$ around the condensate, $\Phi(x) = \phi_0 + \tilde{\Phi}(x)$, where, by definition, $\langle\tilde{\Phi}(x)\rangle \equiv 0$. A Bogoliubov canonical transformation to bosonic quasiparticle operators Φ_Q, defined in momentum space by $\tilde{\Phi}(\boldsymbol{p}, t) = u_{\boldsymbol{p}}\Phi_Q(\boldsymbol{p}, t) - v_{\boldsymbol{p}}\Phi_Q^\dagger(-\boldsymbol{p}, t)$, with $u_{\boldsymbol{p}}^2 - v_{\boldsymbol{p}}^2 = 1$, diagonalises the resulting quadratic Hamiltonian,

$$H = \sum_{\boldsymbol{p}} \omega_{\boldsymbol{p}} \left(\Phi_Q^\dagger(\boldsymbol{p}, t)\Phi_Q(\boldsymbol{p}, t) + 1/2\right) . \tag{2.6}$$

The Bogoliubov dispersion and mode functions read

$$\omega_{\boldsymbol{p}} = \left[\varepsilon_{\boldsymbol{p}}\Big(\varepsilon_{\boldsymbol{p}} + 2g\rho_0\Big)\right]^{1/2}, \tag{2.7}$$

$$u_{\boldsymbol{p}} = \left(\frac{\varepsilon_{\boldsymbol{p}} + g\rho_0 + \omega_{\boldsymbol{p}}}{2\omega_{\boldsymbol{p}}}\right)^{1/2}, \quad v_{\boldsymbol{p}} = \left(\frac{\varepsilon_{\boldsymbol{p}} + g\rho_0 - \omega_{\boldsymbol{p}}}{2\omega_{\boldsymbol{p}}}\right)^{1/2} . \tag{2.8}$$

For momenta much larger than the healing-length momentum scale, $|\mathbf{p}| \gg p_\xi = \sqrt{2mg\rho_0} = \sqrt{8\pi a\rho_0}$, the Bogoliubov dispersion resembles that of the free fundamental bosons, $\omega_{\boldsymbol{p}} \simeq g\rho_0 + \varepsilon_{\boldsymbol{p}}$, and $u_{\boldsymbol{p}} \simeq 1$, $v_{\boldsymbol{p}} \simeq 0$. In the opposite limit, $|\mathbf{p}| \ll p_\xi = [2mg\rho_0]^{1/2}$, the quasiparticles are sound waves, i.e.

$$\omega_{\boldsymbol{p}} \simeq c_{\rm s}|\boldsymbol{p}| , \tag{2.9}$$

$$u_{\boldsymbol{p}}^2 \simeq v_{\boldsymbol{p}}^2 \simeq g\rho_0/(2\omega_{\boldsymbol{p}}) \simeq mc_{\rm s}/(2|\boldsymbol{p}|) , \tag{2.10}$$

with speed of sound $c_{\rm s} = \sqrt{g\rho_0/m} = p_\xi/(\sqrt{2}m)$. The occupation number of sound-wave field modes with wave-number $\mathbf{p}$ is measured by

$$n_Q(\mathbf{p}, t) = \langle\Phi_Q^\dagger(\mathbf{p}, t)\Phi_Q(\mathbf{p}, t)\rangle . \tag{2.11}$$

According to the Bogoliubov transformation, particle and quasiparticle mode occupation numbers are related by

$$n(\boldsymbol{p}, t) = (u_p^2 + v_p^2)\, n_Q(\boldsymbol{p}, t) + v_p^2 . \tag{2.12}$$

For momenta much larger than the healing-length momentum scale, $|\mathbf{p}| \gg p_\xi = \sqrt{2mg\rho_0} = \sqrt{8\pi a\rho_0}$, the Bogoliubov dispersion $\omega_{\boldsymbol{p}}$ resembles that of the free fundamental bosons, $\omega_{\boldsymbol{p}} \simeq g\rho_0 + \varepsilon_{\boldsymbol{p}}$, and $u_{\boldsymbol{p}} \simeq 1$, $v_{\boldsymbol{p}} \simeq 0$. In the opposite limit, $|\mathbf{p}| \ll p_\xi = [2mg\rho_0]^{1/2}$, the quasiparticles are sound waves, i.e.

$$\omega_{\boldsymbol{p}} \simeq c_{\rm s}|\boldsymbol{p}| , \tag{2.13}$$

$$u_{\boldsymbol{p}}^2 \simeq v_{\boldsymbol{p}}^2 \simeq g\rho_0/(2\omega_{\boldsymbol{p}}) \simeq mc_{\rm s}/(2|\boldsymbol{p}|) , \tag{2.14}$$

with speed of sound $c_{\rm s} = \sqrt{g\rho_0/m} = p_\xi/(\sqrt{2}m)$. In thermal equilibrium, the particle and quasiparticle distributions are given by grand-canonical and canonical Bose-Einstein distributions, respectively. In general, $n_{\rm BE}(\mathbf{p}) = \{\exp[(\omega(\mathbf{p}) - \mu)/T] - 1\}^{-1}$ for excitations with dispersion $\omega_{\mathbf{p}}$ is set by the temperature T and the chemical potential μ. We point out that, in the sound-wave limit, $0 < |\mathbf{p}| \ll p_\xi$, and for large quasiparticle occupations, $n_Q(\boldsymbol{p}, t) \gg 1$, relation (2.12) together with Eq. (2.14) means that

$$n(\boldsymbol{p}, t) \simeq n_Q(\boldsymbol{p}, t)\, g\rho_0/\omega_{\boldsymbol{p}}\,. \tag{2.15}$$

Hence, in the Rayleigh-Jeans regime of the equilibrium Bose-Einstein distribution, $-\mu \ll \omega(\boldsymbol{p}) \ll T$, where the occupancies are $n(\boldsymbol{p}, t) \simeq T/\varepsilon_{\boldsymbol{p}} \sim T/p^2$ and $n_Q(\boldsymbol{p}, t) \simeq T/\omega_{\boldsymbol{p}} \sim T/p$, the extra factor $1/p$ from the mode functions, $u_p^2 + v_p^2 \sim 1/p$, ensures the same power-law dependence on p on both sides of Eq. (2.12) and thus adjusts the quasiparticle number distribution to the modified density of states in the sound-wave limit.

2.2 Momentum scaling and universal scaling functions

In equilibrium, universality is widely studied in the context of phase transition and critical phenomena due to the manifestation of scale invariance around critical point. The indicator of universality, power-law exponents in various observables that are insensitive to microscopic details but depend solely on the particular universality class the system belong to [54]. Analogously, in nonequilibrium, systems are expected to show universal scaling behaviour near so-called nonthermal fixed points. These fixed points can manifest themselves in the form of wave turbulence corresponding to a steady turbulent flux in scale (i.e. momentum) space, or as a self-similar evolution. Here, we are interested in the universal dynamics of the number distribution in nonequilibrium for the Hamiltonian in Eq. (2.1) which means the number distributions (2.4) and (2.11) are expected to take, at a particular moment in time, the form of scaling functions different from a thermal Rayleigh–Jeans law, i.e. $n(\boldsymbol{p}) \sim T/\omega(\boldsymbol{p})$ where $\omega(\boldsymbol{p})$ is a quasiparticle energy.

2.2.1 Momentum scaling in number distributions

We presuppose a scaling behaviour of the number distribution according to,

$$n(s\mathbf{p}) = s^{-\zeta} n(\mathbf{p})\,, \tag{2.16}$$

where s is a positive, real number and ζ is a universal scaling exponent which we assume to be a real number. Notice that Eq. (2.16) is able to generate the whole function in momentum space given its value only on an arbitrarily surface enclosing the origin. This should not be possible if there is no correlation between very different momentum scale in the first place. In physical situations, however, such

correlations stretch over a finite interval in momenta only. So far, we have neglected time dependence. We also consider the situation that the dispersion relation, at least in a region where Eq. (2.16) fulfilled, satisfies scaling according to

$$\omega(s\boldsymbol{p}) = s^z \omega(\boldsymbol{p})\,. \tag{2.17}$$

This is, e.g., everywhere the case for the free dispersion (2.5) and, in the free-particle and sound-wave limits, for the Bogoliubov quasiparticle dispersion (2.7).

In the following we will account for the scaling of $\omega(\boldsymbol{p})$, as far as possible, by means of an arbitrary dynamical exponent z. We anticipate in this way that self-energy corrections can lead to a modified scaling of the quasiparticle dispersion and that, in a treatment beyond kinetic scattering of free modes, a more general scaling between frequency and momentum is expected.

2.2.2 Bulk integrals

The momentum integral over the single-particle distribution $n(\boldsymbol{p})$ yields the density of non-condensed atoms ρ_{nc} and thus the observable total particle density

$$\rho_{\mathrm{tot}} = \rho_0 + \rho_{\mathrm{nc}} = \rho_0 + \int \frac{\mathrm{d}^d p}{(2\pi)^d}\, n(\boldsymbol{p}) \tag{2.18}$$

and therefore must be finite. Hence, if $n(\boldsymbol{p})$ shows power-law scaling (2.16) in a certain range of momenta $p = |\boldsymbol{p}|$, this range can not extend over all possible p from 0 to ∞. This is because the radial, i.e., p-integral over $p^{d-1-\zeta}$, which includes the volume factor, has a power-law divergence either in the ultraviolet (UV), or in the infrared (IR), or is logarithmically divergent in both limits.

This means that in any physically meaningful situation, in the continuum and thermodynamic limits, the distribution $n(\boldsymbol{p})$ must take the form of a more general scaling function which ensures convergence of the integral (2.18). Alternatively, the finite size of a generic physical system and its definition on a discrete grid would provide IR and UV cutoffs, respectively. We are, however, interested in universal dynamics which, within first approximation, is not affected by such boundary conditions. To this end, we demand the scaling region to be sufficiently far away from the boundaries of the system and will study the intrinsic conditions under which scaling dynamics can occur.

The integral over the occupancies of the quasiparticle eigenmodes of the Hamiltonian defines the density

$$\rho_Q = \int \frac{\mathrm{d}^d p}{(2\pi)^d}\, n_Q(\boldsymbol{p}) \tag{2.19}$$

which is in general different from the particle density (2.18). In situations where the interactions between quasiparticles are dominated by elastic 2-to-2 scattering, their total number and thus the density ρ_Q are conserved in time. From Eq. (2.12), we can deduce that, in the momentum regime where both dispersion relations and

occupation numbers show the power-law behavior, the particle and the quasiparticle distributions are related by [3]

$$n(\boldsymbol{p}) = \left(\frac{|\boldsymbol{p}|}{\tilde{p}}\right)^{z-2} n_Q(\boldsymbol{p})\,, \tag{2.20}$$

where $\tilde{p}$ is a momentum scale that encoded in the Bogoliubov transformation i.e. in the case of sound-wave dispersion ($z = 1$) satisfying Eqs. (2.13) and (2.14), $\tilde{p} = p_\xi/\sqrt{2}$. Given a scaling (2.16) of $n(\boldsymbol{p})$, the quasiparticle distribution, in the scaling region, would satisfy

$$n_Q(s\mathbf{p}) = s^{-\kappa} n_Q(\mathbf{p})\,, \tag{2.21}$$

with

$$\kappa = \zeta + \sigma = \zeta + z - 2\,. \tag{2.22}$$

Here, the exponent $\sigma = z - 2$ governing the relative scaling of the two distributions accounts for the z-dependent density of states. It is *not* equal to $-z$ as one may naively infer from Eq. (2.15), cf. the discussion concerning Eq. (4.104) in Sect. 4.3.1.

Assuming contributions from outside the scaling region with a fixed z to be negligible, the relation between particle density and quasiparticle spectrum is

$$\rho_{\mathrm{nc}} = \int \frac{\mathrm{d}^d p}{(2\pi)^d} \left(\frac{p}{\tilde{p}}\right)^{\sigma} n_Q(\boldsymbol{p}, t)\,, \tag{2.23}$$

with $\tilde{p} = g\rho_0/c_s = p_\xi/\sqrt{2}$ for $z = 1$ while for $z = 2$, $\sigma = 0$ and there is no $\tilde{p}$ scale because the Bogoliubov transformation for the free theory is trivial, $u_{\boldsymbol{p}} = 1$ and $v_{\boldsymbol{p}} = 0$. In this $z = 2$ case, quasiparticles and particles are identical. Besides the density of (quasi)particles, also the energy density,

$$\varepsilon = \int \frac{\mathrm{d}^d p}{(2\pi)^d}\, \omega(\boldsymbol{p}) n_Q(\boldsymbol{p})\,, \tag{2.24}$$

is a physical observable and therefore must be finite.

2.2.3 Scaling function

Where not otherwise stated, we assume the momentum distributions to be isotropic in the following, $n_Q(\boldsymbol{p}) \equiv n_Q(p)$. Assume, for the first, that $n_Q(p) \sim p^{-\kappa}$ is a pure power law in the radial momentum direction, satisfying Eq. (2.21) for all momenta.

[3] In the scaling regime $\omega_{\boldsymbol{p}} \sim p^z$ implies $\omega_{\boldsymbol{p}} = \tilde{p}^{2-z} p^z/m$ since $\omega_{\boldsymbol{p}}$ itself is an energy (neglecting some other dimensionless constants). Although we are interested in an interacting theory, we can use the energy expectation value of the free theory, $\langle H\rangle = \Sigma\varepsilon_{\boldsymbol{p}}[n(\boldsymbol{p}) + 1/2]$ to derive scaling relations. Comparing the energy of the free theory with the expectation value of Hamiltonian in Eq. (C.18), we obtain the relation $\tilde{p}^{2-z} p^z n_Q(\boldsymbol{p}) \sim p^2 n(\boldsymbol{p})$ which leads us to Eq. (2.20) (also neglecting the ground state energy $\varepsilon_{\boldsymbol{p}}/2$). This can be verified explicitly in case of $z = 1$. Note that we used an equality in Eq. (2.20) because both $n(\boldsymbol{p})$ and $n_Q(\boldsymbol{p})$ have the same dimension. The dimensionless constants that might appear can be absorbed in $\tilde{p}$ nevertheless.

Furthermore, presume a power-law form for $\omega(p)$, Eq. (2.17), with $z \neq 0$, such that the integrand in Eq. (2.24) is a pure power law.

The exponent κ then determines whether the IR or the UV regime dominates quasiparticle and energy densities. If $\kappa > d$, the integral (2.19) is dominated by quasiparticles with IR momenta, while for $\kappa < d$ UV momenta dominate. Similarly, $\kappa > d + z$ leads to an IR dominance of the integral (2.24) for the energy density whereas, for $\kappa < d + z$, energy is concentrated in the high-momentum modes. In summary, the exponent κ determines where quasiparticle and energy densities are concentrated,

$$\kappa > d + z\,, \qquad \text{quasiparticles and energy: IR;} \tag{2.25}$$

$$d \leq \kappa \leq d + z\,, \qquad \text{quasiparticles: IR; energy: UV;} \tag{2.26}$$

$$\kappa < d\,, \qquad \text{quasiparticles and energy: UV.} \tag{2.27}$$

According to the above, the minimum regularization a power-law momentum distribution requires is provided by a modified power law in the IR or the UV limit. This is the case when both, quasiparticles and energy are concentrated at the same end of the spectrum, i.e. for κ satisfying (2.25) or (2.27). As a consequence, the quasiparticle distribution can be parametrized as

$$n_Q(p) = f(p/p_\Lambda; f_1) \tag{2.28}$$

in terms of a scaling function $f(x)$ of the form

$$f(x; f_1) = 2f_1 \left[x^{\bar{\kappa}} + x^{\kappa}\right]^{-1} . \tag{2.29}$$

$f(x)$ interpolates between two different power laws, with universal exponents $\bar{\kappa} \neq \kappa$. It exhibits a non-universal point at $x = 1$ where the scaling crosses over from one power law to the other. In the distribution function n_Q, this crossover thus occurs at the non-universal momentum scale $p = p_\Lambda$. The amplitude $f_1 = f(1; f_1)$ is a further non-universal quantity the scaling function depends on. Note that different functional forms are possible for describing the crossover, and that determining the precise form of the universal scaling function requires solving the dynamic equations. Note also that a sharp IR (UV) cutoff, i.e., $f(x) \sim \Theta(x-1)\, x^{-\kappa}$ ($f(x) \sim \Theta(1-x)\, x^{-\kappa}$), can be realized by choosing $\bar{\kappa} \to -\infty$ ($\to \infty$). The simultaneous IR and UV convergence of both integrals, Eqs. (2.19) and (2.24), requires $\bar{\kappa} < d$ and $\kappa > d + z$, or vice versa.

Within the interval (2.26) either the quasiparticle or the energy density diverges, such that an extended scaling function, with an additional regulator, is required. A straightforward extension of the scaling function (2.29) involves two crossover scales, $p_\lambda > p_\Lambda$. To make the expression more transparent, we introduce a third scale p_0. Hence, we write

$$n_Q(p) = f(p/p_0; p_\Lambda/p_0, p_\lambda/p_0, f_0)\,, \tag{2.30}$$

with the scaling function

$$f(x; y, z, f_1) = f_1 \left[y^{\kappa}(x/y)^{\kappa_\Lambda} + x^{\kappa} + z^{\kappa}(x/z)^{\kappa_\lambda}\right]^{-1} , \tag{2.31}$$

such that, for $\kappa_\Lambda < \kappa < \kappa_\lambda$, the amplitude f_1 fixes f at $x = 1$ if the crossover scales are taken to the IR and UV limits, $f_1 = f(1; y \to 0, z \to \infty, f_1)$, see the sketch in Fig. 2.1. $\kappa_\Lambda < d$ ensures convergence of the integral for the quasiparticle density in the IR, while $\kappa_\lambda > d + z$ renders the energy integral finite in the UV.

As p_0 above only sets the unit, we can simplify the parametrization such that the scaling function has only two arguments,

$$n_Q(p) = f_\Lambda(p/p_\Lambda; p_\lambda/p_\Lambda, f_0[p_0/p_\Lambda]^\kappa)\,, \tag{2.32}$$

$$f_\Lambda(x; y, f_1) = f_1 \left[x^{\kappa_\Lambda} + x^\kappa + x^{\kappa_\lambda} y^{\kappa-\kappa_\lambda}\right]^{-1}\,, \tag{2.33}$$

or, equivalently,

$$n_Q(p) = f_\lambda(p/p_\lambda; p_\Lambda/p_\lambda, f_0[p_0/p_\lambda]^\kappa)\,, \tag{2.34}$$

$$f_\lambda(x; y, f_1) = f_1 \left[x^{\kappa_\Lambda} y^{\kappa-\kappa_\Lambda} + x^\kappa + x^{\kappa_\lambda}\right]^{-1}\,. \tag{2.35}$$

In the parametrizations (2.32) and (2.34), all momenta are expressed in units of the IR scale p_Λ and the UV scale p_λ, respectively. Note that this leads to individual redefinitions of the amplitude f_0. In the special cases that $\kappa_\lambda = \kappa$ or that the UV scale is sent to $p_\lambda \to \infty$, the scaling function (2.33), up to constant factors, reduces to the function (2.29). The same applies to the function (2.35) if $\kappa_\Lambda = \kappa$ or $p_\Lambda \to 0$.

In general, the precise form of the scaling function requires solving the dynamic equations. As a result, it can, e.g., exhibit regions with different momentum power laws as sketched in Fig. 1.1 which can relax the condition (2.26) for self-similar evolution, allowing $\kappa > d+z$ in the IR and $\kappa < d$ in the UV. Corresponding dynamics has been discussed in Refs. [28, 29, 50, 69, 70] in the context of non-thermal fixed points and the formation of topological defects. In the following we will focus on the case that a single momentum power law prevails between the cutoffs, discussing possible extensions where applicable.

2.3 Universal dynamics

Our aim is to describe possible forms of universal dynamics realized in the model (2.1). We demand that, at a given instant in time, the quasiparticle number distribution $n_Q(p, t)$ is parametrized by a scaling function of the type (2.31) which disposes of the essential properties discussed in the previous subsection, i.e., power-law behavior (2.21) within a region of momenta, $p_\Lambda \ll p \ll p_\lambda$, and convergence of the integrals (2.18) and (2.24) for quasiparticle and energy density, respectively. The question then is, how such a distribution can evolve in time in a universal manner, i.e., in a way that it keeps its parametrization in terms of the initial scaling function, varying only the non-universal scales p_Λ and p_λ, and the amplitude f_0. The considerations of the previous subsection already provide an intuition of what types of dynamics are possible, depending on the scaling exponent κ.

2.3.1 Global conservation laws

In most cases, one or more global conservation law constrain the dynamics, which plays an important role for the dynamical scaling phenomena possible in the system. For a closed system and if quasiparticle number changing processes are absent, the total quasiparticle density is conserved in time,

$$\rho_Q = \int \frac{\mathrm{d}^d p}{(2\pi)^d}\, n_Q(\boldsymbol{p}, t) \equiv \text{const.} \tag{2.36}$$

If, furthermore, neither internal excitations nor interactions with an energy reservoir are possible, also the energy density is a constant of motion,

$$\varepsilon = \int \frac{\mathrm{d}^d p}{(2\pi)^d}\, \omega(\boldsymbol{p}) n_Q(\boldsymbol{p}, t) \equiv \text{const.} \tag{2.37}$$

In addition to the above also real particle number ρ_{nc}, Eq. (2.18) is a viable conserved quantity. In the present work we will eventually only consider quasiparticle number conserving processes due to the discussions in subsequent chapters will be based on Boltzmann's scattering integral which determines the time evolution of the quasiparticle distribution. A generalization to dynamics which, for $z \neq 2$, explicitly accounts also for particle number conservation requires an extend discussion which we consider beyond the scope of this thesis. In the following, we will use the terms "quasiparticles" for the respective quasiparticle eigenmodes of the Hamiltonian, and "particles" to refer to the distribution $\zeta_{\mathrm{nc}}(p) \sim p^{z-2} n_Q(p)$, where both are identical for $z = 2$.

The above conservation laws strongly constrain the dynamics the system can undergo. As was pointed out in Ref. [15] and we will discuss in detail, they limit the possibilities of how the cutoff scales p_Λ and p_λ, and the amplitude f_0 can vary in time. For example, if $\kappa > d$, quasiparticles are concentrated in the IR. In this case, shifting the infrared cutoff p_Λ implies a violation of the conservation law (2.36) unless the amplitude f_0 is adjusted appropriately. Similarly, for $\kappa < d + z$, the bulk of energy sits in the UV, and p_λ can in general only be varied together with f_0. If these conditions are simultaneously fulfilled, $d \leq \kappa \leq d + z$, both, IR and UV cutoffs are needed, cf. Eqs. (2.26) and (2.31), such that a change of f_0 requires also a shift of both of these cutoff scales. On the contrary, if $\kappa > d + z$, both, quasiparticles and energy are concentrated at the IR cutoff scale. In this case, an additional UV cutoff $p_\lambda \gg p_\Lambda$, which is expected to limit a realistic physical distribution, can be shifted without significantly 'renormalizing' the entire function since neither conservation law is strongly affected by the shift. The same applies to shifting the IR cutoff p_Λ if $\kappa < d$.

We remark again that for bimodal distributions such as the one sketched in Fig. 1.1, also for $\kappa > d + z$ energy can be concentrated in the UV, requiring a UV cutoff and allowing for the dynamics anticipated in the case of $d \leq \kappa \leq d + z$. This will in general be the case for superfluid turbulence [27–29, 70, 71].

In the next two subsections we discuss in more detail how these constraints distinguish the kinds of universal dynamics possible in the system.

2.3.2 Nonthermal fixed points

Nonthermal fixed points refer to nonequilibrium attractor solutions that show universal scalings [48]. The phrase *nonequilibrium attraactor* implies that the fixed points are not fully attractors since the system has to be thermalized after some time scale. At the early state of studies, nonthermal fixed points was understood as a turbulence state due to the similarity of dynamic equation compare to the kinetic equation and the focus was the exponents of stationary state [25, 49, 72] or the Kolmogorov-Zakharov exponets. Later, the concept of nonthermal fixed points has been extended to the nonstationary situation [50] which is more typical for an isolated system where there are constraints from the global conservation laws. Though, the dynamics still evolves self-similarly and number distributions show universal scalings.

Dynamical scaling hypothesis

Scaling hypotheses are at the basis of critical phenomena such as continuous, symmetry breaking phase transitions in equilibrium systems. They are, in general, mathematically justified by fixed points appearing in the renormalisation-group (RG) flows of the effective Hamiltonian or action functional describing phenomena within a particular range of scales. These flows describe, e.g., the change of the effective Hamiltonian under a variation of the scale limiting that range in the infrared. Choosing the initial, microscopic Hamiltonian such that the flow reaches, on macroscopic scales, an RG fixed point is equivalent to tuning the system to a phase transition. Close to the fixed point, correlations become universal, meaning that they show scaling and no longer depend on the microscopic details of the system, except for a few symmetry properties of the underlying Hamiltonian.

Isolated systems by definition do not allow for the driving and dissipation which are required to keep a universal non-equilibrium state stationary. Nevertheless, when a closed system quenched out of equilibrium re-equilibrates, universal time evolution can occur. This is equivalent to extending the scaling hypothesis to time evolution, saying that time evolution can have the form of an RG flow. When the RG flow approaches a fixed point, critical slowing down occurs, and the time evolution is well approximated by a rescaling. This evolution is captured, in the simplest case, by a scaling hypothesis for the time-dependent, angle-averaged quasiparticle number distribution,

$$n_Q(p,t) = (t/t_0)^\alpha f([t/t_0]^\beta p)\,. \tag{2.38}$$

Here, f is a universal scaling function in momentum space, and t_0 is an arbitrary reference time within the temporal scaling regime, where $n_Q(p,t_0) = f(p)$. The universal exponents α and β determine the self-similar rescaling of the distribution during the evolution. These exponents are to be associated with the particular RG fixed point which the system approaches in time. In contrast to the attractive thermal fixed point of the evolution where both, α and β are by definition zero, non-vanishing exponents indicate the existence of a non-thermal fixed point [25, 26, 49, 50].

Determining the universal scaling function $f(p)$ requires solving the dynamic equations. Instead of this, we will work with a minimal ansatz for f as the one given in Eq. (2.29), which interpolates between two momentum power laws. If the parameters have the power-law time dependence $f_\Lambda(t) = n_Q(p_\Lambda(t), t) \sim t^\alpha$, $p_\Lambda(t) \sim t^{-\beta}$ this implies a scaling evolution $n_Q(p,t) = f(p/p_\Lambda(t), f_\Lambda(t))$ satisfying Eq. (2.38). Choosing, e.g., both exponents to be positive real numbers, time evolution shifts the distribution $n_Q(p,t)$ self-similarly to smaller momenta and larger values of $n_Q(p_\Lambda(t),t) = f_1(t)$.

Constraints from conservation laws

As discussed in the previous section, global conservation laws in general constrain the dynamics and thus play an important role for the scaling phenomena possible in the system. With regard to the scaling hypothesis (2.38), they imply scaling relations between the exponents α and β. For example, if the dynamics conserves the total quasiparticle density, Eq. (2.36),

$$\begin{aligned}\rho_Q &= \int \frac{\mathrm{d}^d p}{(2\pi)^d}\,(t/t_0)^\alpha f([t/t_0]^\beta p) \\ &= (t/t_0)^{\alpha-\beta d}\int \frac{\mathrm{d}^d p'}{(2\pi)^d}\, f(p') \sim (t/t_0)^0\,, \end{aligned} \tag{2.39}$$

where $p'(t) = (t/t_0)^\beta p$, the relation

$$\alpha = \beta d \tag{2.40}$$

must be fulfilled. Analogously, the conservation of the energy density, Eq. (2.37), requires

$$\alpha = \beta(d+z)\,. \tag{2.41}$$

Here we always presuppose, that the respective integrals converge without the cut-off scales that might be time-dependent. Given one of the above relations, determining the remaining exponent can be determined by a scaling analysis of the dynamic equations as we will discuss in more detail in Ch. 3.

Scaling evolution of the closed system

In the closed system, quasiparticle number and energy are simultaneously conserved in time. For non-zero exponents α and β, however, the scaling relations (2.40) and (2.41) can not both be satisfied for $z \neq 0$. This means that either $\alpha = \beta = 0$ or that the scaling hypothesis (2.38) has to be extended.

Suppose that the scaling function has the form given in Eq. (2.29). As discussed in Sect. 2.2.3, quasiparticles and energy are concentrated at the same end of the momentum scaling region, within which $n_Q(p,t) \sim p^{-\kappa}$, if κ is outside the interval (2.26). In this case, $\alpha = \beta = 0$ is required, and a scaling evolution is only possible

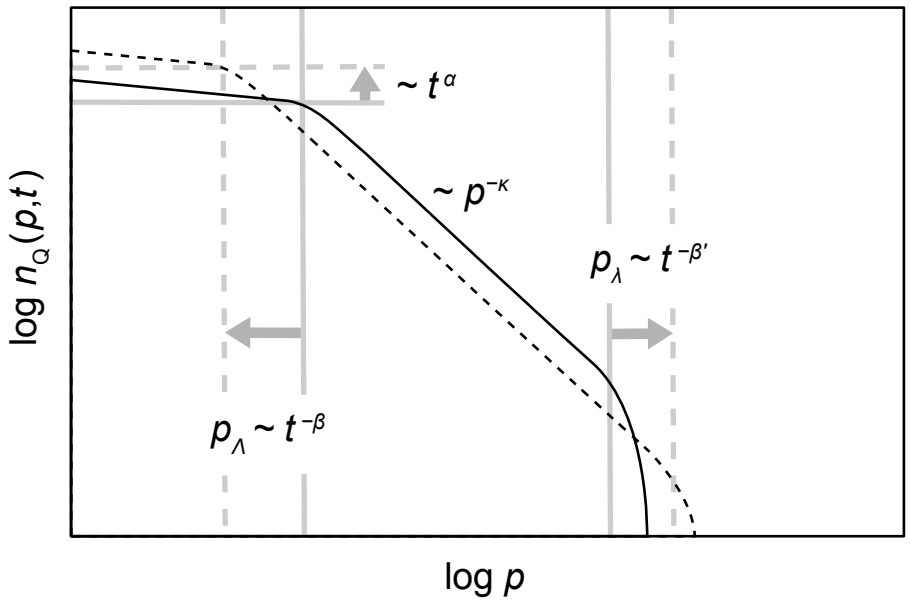

Figure 2.1: Sketch of the self-similar evolution of the scaling form (2.43) for $n_Q(p,t)$ according to Eq. (2.42). Note the double-logarithmic scale. The IR cutoff scale p_Λ and the UV scale p_λ, as well as the amplitude f_0 rescale with time t such that the area under the curve remains invariant. The sketch shows the case of an inverse particle transport following a strong cooling quench. See Table 5.1 for our predictions for the scaling exponents (first row, NTFP).

at the opposite end of the scaling region. This evolution leads to a wave-turbulent cascade which we discuss in Sect. 2.3.3 below.

On the contrary, if κ is within the interval (2.26), particles and energy are concentrated at opposite ends of the scaling region. In this case, a more general scaling hypothesis is needed which allows for different rescalings of the IR and the UV parts of the scaling function. We choose the ansatz (2.30) in terms of the scaling function (2.31), and suppose that the non-universal parameters follow the scaling evolution

$$f_0(t) \sim t^{\alpha_0}\,, \quad p_\Lambda(t) \sim t^{-\beta}\,, \quad p_\lambda(t) \sim t^{-\beta'}\,. \tag{2.42}$$

This ansatz satisfies the extended scaling hypothesis

$$n_Q(p,t) = \tau^{\,\alpha_0+(\beta+\beta')\kappa} f\Big[\tau^{\,\beta+\beta'} p; \tau^{\,\beta'} p_\Lambda(t_0), \tau^{\,\beta} p_\lambda(t_0)\Big]\,, \tag{2.43}$$

where

$$\tau = t/t_0\,, \tag{2.44}$$

see the sketch in Fig. 2.1. It is useful to express the momenta p and p_λ in Eq. (2.43) alternatively in terms of the IR scale p_Λ and to rewrite the scaling hypothesis in terms of a scaling function of the type (2.33),

$$n_Q(p,t) = \tau^{\,\alpha} f_\Lambda\Big[\tau^{\,\beta}\frac{p}{p_\Lambda(t_0)}; \tau^{\,\beta-\beta'}\frac{p_\lambda(t_0)}{p_\Lambda(t_0)}\Big]\,. \tag{2.45}$$

Here we introduced the exponent α, defined as

$$\alpha = \alpha_0 + \beta\kappa\,, \tag{2.46}$$

such that the scaling hypothesis (2.45) is equivalent to Eq. (2.38) in the regime $p \ll p_\lambda$, i.e., in the limit $p_\lambda \to \infty$. Alternatively, we can rewrite Eq. (2.43), by expressing p and p_Λ in terms of p_λ, as

$$n_Q(p,t) = \tau^{\,\alpha'} f_\lambda\Big[\tau^{\,\beta'}\frac{p}{p_\lambda(t_0)}; \tau^{\,\beta'-\beta}\frac{p_\Lambda(t_0)}{p_\lambda(t_0)}\Big]\,, \tag{2.47}$$

with

$$\alpha' = \alpha_0 + \beta'\kappa\,. \tag{2.48}$$

Also Eq. (2.47) is equivalent to the simpler scaling hypothesis (2.38), with the replacements $\alpha \leftrightarrow \alpha'$, $\beta \leftrightarrow \beta'$, $p_\Lambda \leftrightarrow p_\lambda$, in the limit $p \gg p_\Lambda$ or $p_\Lambda \to 0$.

The scaling hypotheses (2.45), in the limit $p_\lambda \to \infty$, and (2.47), in the limit $p_\Lambda \to 0$, can now be used, in the same way as before, to obtain the scaling relations (2.40) between α and β and (2.41) between α' and β', respectively,

$$\alpha = \alpha_0 + \beta\kappa = \beta d\,, \tag{2.49}$$
$$\alpha' = \alpha_0 + \beta'\kappa = \beta'(d+z)\,. \tag{2.50}$$

Eliminating α' by means of Eqs (2.46) and (2.48), i.e., $\alpha' = \alpha + (\beta' - \beta)\kappa$, energy and (quasi)particle densities are time independent if

$$\alpha = \beta d\,, \tag{2.51}$$
$$\beta'(d + z - \kappa) = \beta(d - \kappa)\,. \tag{2.52}$$

Note that, in the self-similar window (2.26), this implies $\beta\,\beta' \leq 0$, i.e., the IR and UV scales p_Λ, p_λ rescale in opposite directions. These relations hold in the limit of a large scaling region, i.e., for $p_\lambda \gg p_\Lambda$. Thereby, particle conservation only affects the infrared shift with β, Eq. (2.51), while energy conservation gives the condition (2.52) for β' in the UV. The scalings (2.42) represent the leading power-law behavior in t while further non-leading terms account for the exact conservation of the energy and particle densities.

2.3.3 Wave-turbulent transport

Stationary turbulent flows

According to Boltzmann, stationarity of the maximum-entropy state is related to detailed balance between the collision processes [73]. In contrast, out-of-equilibrium stationary states generally do not require detailed balance. In particular when considering driven open systems, stationary states can exist on the basis of a balanced but directed flow through the momentum shells or energy levels. This is possible

when, e.g., kinetic energy is inserted into the system predominantly at one length scale while being ejected or dissipated at a different length scale.

A well-known example is turbulence in a three-dimensional incompressible fluid driven continuously at a particular length scale, e.g., by a stirrer [39]. Fully developed turbulence is characterized by a stationary energy distribution within an extended 'inertial range' of wave numbers. The limiting scales of the inertial range are typically set, on the low-energy side, by the size of eddies stirred into the fluid, and, at the opposite end, by viscosity which causes kinetic energy to dissipate into heat.

Within the inertial range, on average and per unit of time, the same amount of energy is transported unidirectionally through each momentum shell, from large to small characteristic length scales, or vice versa, as is the case in Kraichnan turbulence in two dimensions [74]. This implies that the turbulent transport is quasi local in momentum space.

The dilute Bose gas, Eq. (2.1), is compressible such that also quantities other than the energy can be locally conserved in their transport through momentum space. As the interactions are spatially isotropic, these local conservation laws can be expressed in the form of one-dimensional transport equations for either the radial quasiparticle number,

$$N_Q(p) = (2p)^{d-1}\pi n_Q(p)\,, \tag{2.53}$$

or the energy distribution,

$$E_Q(p) = (2p)^{d-1}\pi \varepsilon_Q(p)\,. \tag{2.54}$$

Here $\varepsilon_Q(p) = \omega(p) n_Q(p)$, and as quasiparticles we again consider free particles or Bogoliubov sound waves using the same notation. The respective transport equations are written as

$$\partial_t N_Q(p,t) = -\partial_p Q(p,t)\,, \tag{2.55}$$
$$\partial_t E_Q(p,t) = -\partial_p P(p,t)\,, \tag{2.56}$$

with radial quasiparticle current Q and energy current P. Non-thermal, scaling, stationary solutions of these equations are studied in wave-turbulence theory, usually within a Boltzmann kinetic approach [10, 11]. We discuss such solutions in further detail in Sect. 3.2. Beforehand, we extend, as for the self-similar case above, our discussion to the dynamics of the closed system and study the constraints set by global conservation laws.

Build-up of wave-turbulence in the closed system

Let us consider the build-up of wave turbulence in a closed system from an initially non-equilibrated quasiparticle distribution. Suppose that this distribution has the form (2.31), with a power law $n_Q(p) \sim p^{-\kappa}$ in the region $p_\Lambda \ll p \ll p_\lambda$ between the IR and UV cutoff scales. Again, taking into account the integrals for particle and

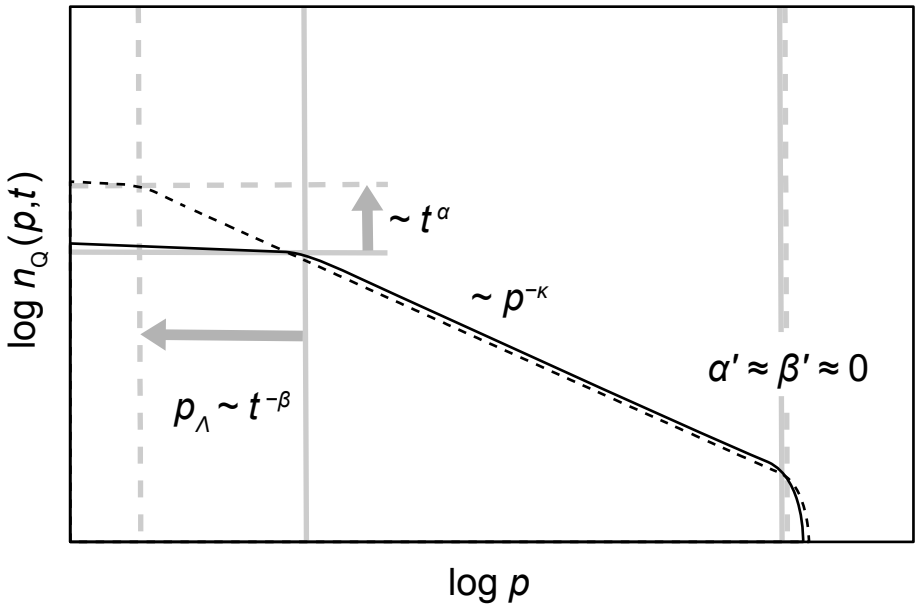

Figure 2.2: Sketch of the build-up of the inverse quasiparticle cascade, self-similar evolution of the scaling form (2.57) for $n_Q(p,t)$ according to Eq. (2.59), with $\alpha = \beta\kappa$ and, to leading order, $\alpha' = \beta' = 0$. Note the double-logarithmic scale. The IR cutoff scale p_Λ shifts without significantly changing the area under the curve, i.e., the total quasiparticle number. Only a small non-leading-order rescaling of the UV scale p_λ is required to satisfy number conservation.. The sketch shows the case of an inverse particle transport following a cooling quench. See Table 5.1 for our predictions for the scaling exponents (row 3, NTFP). In the case of a weak-wave-turbulence quasiparticle cascade, p_Λ shifts in an accelerated way, with t replaced by τ_1, see Eq. (2.60).

energy densities, Eqs. (2.18), (2.24), the value of the exponent κ tells us at which end of this region energy and particle number are concentrated.

If the power law is sufficiently steep, $\kappa > d + z$, both, particles and energy are in the IR, and both, Eqs. (2.40) and (2.41) need to be fulfilled, presupposing that the UV cutoff is sufficiently large, $p_\lambda \gg p_\Lambda$. This is only possible for $\alpha = \beta = 0$. As a consequence, the amplitude f_0 and the infrared scale p_Λ are, to a first approximation, constant in time.

Nonetheless, a wave-turbulent, quasilocal flux can build up and thereby satisfy also the global conservations laws while the UV scale p_λ grows in time. As before, global conservation laws demand that this process in leading order confirms the scaling hypothesis (2.45),

$$n_Q(p,t) = \tau^{\alpha} f_\Lambda\Big[\tau^{\beta}\frac{p}{p_\Lambda(t_0)}; \tau^{\beta-\beta'}\frac{p_\lambda(t_0)}{p_\Lambda(t_0}\Big]\,. \tag{2.57}$$

Here, $\alpha = \beta = 0$, and thus $\alpha_0 = 0$, cf. Eq. (2.46). In turn, Eq. (2.48) implies that

$\alpha' = \beta'\kappa$ in an equivalent scaling hypothesis of the form (2.47),

$$n_Q(p,t) = \tau^{\alpha'} f_\lambda\Big[\tau^{\beta'}\frac{p}{p_\lambda(t_0)}; \tau^{\beta'-\beta}\frac{p_\Lambda(t_0)}{p_\lambda(t_0)}\Big]\,. \tag{2.58}$$

To determine β' requires the analysing the kinetic equation and the scaling properties the interactions. We will do this in Ch. 3. Depending on these scaling properties, β' can be positive or negative. If $\beta' < 0$, the wave-turbulent flux builds up similarly as the self-similar scaling evolution. The non-universal scales evolve according to

$$f_\Lambda(t) \sim \tau^{\alpha}\,, \quad p_\Lambda(t) \sim \tau^{-\beta}\,, \quad p_\lambda(t) \sim \tau^{-\beta'} \tag{2.59}$$

with $\alpha = \beta = 0$ and $\tau = t/t_0$.

On the contrary, if $\beta' > 0$, building up a wave-turbulent cascade towards the UV is possibly only through a wave front [15], in which $\tau = \tau_1$,

$$\tau_1 = \frac{t_1 - t}{t_1 - t_0}\,, \tag{2.60}$$

see the sketch in Fig. 2.2. At time t_1, the wave front reaches infinity, before which the solution, however, will become invalid as arbitrarily high momenta are usually not captured by a given model. The value of t_1 is determined by the given initial distribution at time t_0. The scaling evolution (2.59) is valid for $\tau_1 < 1$, and $t_1 - t_0$ much smaller than the overall evolution time. Only in this limit, the physics behind the wave front becomes nearly stationary when taking into account the global conservation of particle and energy density. Note that, as a result of these conservation laws, the scaling (2.59) represent the leading behaviour, while subleading terms form corrections which are the more important the further away t is from t_1.

For $\kappa < d$, both, quasiparticles and energy are concentrated in the UV, and an inverse cascade can build up according to the scaling form (2.57), with $\alpha = \beta\kappa$, $\alpha' = \beta' = 0$. If $\beta < 0$ the evolution takes the form of a wave front while for $\beta > 0$ a self-similar evolution is possible. At $t = t_1$, the wave front reaches zero momentum, before which the solution, however, is expected to break down as no information can be spread over infinite distances in a finite time.

We will show in Ch. 3 that, for the cases of free particles and Bogoliubov sound in the perturbative wave-Boltzmann regime of weakly occupied modes, following a cooling quench, an inverse cascade builds up behind a wave front described by the scaling evolution (2.59), with scaling parameter $\tau = \tau_1$, Eq. (2.60), see also Refs. [15–17]. One may say that this wave-front scaling evolution is critically accelerating.

We emphasize that, in physically realistic situations, this scaling evolution breaks down at a finite length scale, $1/p_\lambda < \infty$, i.e., before $t = t_1$ is reached, when the processes underlying the kinetics of the system change in a fundamental way. We will show that this change can be caused by collective many-body scattering becoming relevant at momenta below the chemical potential. This makes the further time evolution to become self-similar and critically slowed.

Table 2.1: Scaling relations. The table summarizes the relations between the scaling exponents as obtained, in Sect. 2.3, from the constraints set by global conservation laws. Depending on the relative size of the momentum-scaling exponent κ, the dimension d, and the dynamical exponent z, one expects either an inverse cascade, a self-similar evolution, or a direct cascade of quasiparticles.

	α	β	α'	β'	τ
inverse cascade $\kappa < d$	$\beta\kappa$	< 0	0	0	τ_1
		> 0			t/t_0
self-similar evol. $d < \kappa < d + z$	βd		$\beta'(d+z)$	$\dfrac{\beta(d-\kappa)}{d+z-\kappa}$	
direct cascade $d + z < \kappa$	0	0	$\beta'\kappa$	< 0	t/t_0
				> 0	τ_1

2.3.4 Summary of scaling relations

In summary, a wave-turbulent, quasilocal transport of either quasiparticles or energy, which does not renormalize n_Q in time, is possible only if both these quantities are concentrated at the same end of the inertial range, i.e., if κ is outside the interval (2.26). Depending on the relative size of κ one expects either an inverse cascade, a self-similar evolution, or a direct cascade, with scaling relations between the exponents as summarized in Table 2.1. Note that at the boundaries, $\kappa = d$ and $\kappa = d+z$, a more careful analysis would be in order.

2.4 Summary

The Gross-Pitaevskii model Eq. (2.1) gives us two types of observables, particle and quasiparticle occupations related to the cases of whether a condensate is prevails or not, respectively. As a result we consider two types of quasiparticles: free particles with quadratic dispersion, $\varepsilon(p) \sim p^2$, and Bogoliubov quasiparticles with linear dispersion $\omega(p) \sim p$. This will provide us with the possibility to compare the respective results obtained later on. We furthermore considered universal scaling functions characterising the occupation-number distribution, including physical cutoffs at the infrared and ultraviolet ends of the momentum spectrum. The universal dynamics of the occupation number under the constraints of global conservation laws follows three possible scenarios depending on the exponent κ of the occupation number: an inverse particle cascade, a direct energy cascade or a self-similar evolution where the local occupation number evolves in time, also within the regime where it shows a power law in momentum. For each case, we evaluated the dynamical scaling exponents of the cutoff scales and presented them in Table 2.1. In the forthcoming

chapters we will include the constraints by the kinetic equations.

Chapter 3

Kinetic theory of weak and strong wave turbulence

Turbulence is well-known in the context of hydrodynamics as an irregular motion of the fluid in the form of *eddies* of different sizes. The turbulence emerges when the life-time of large eddies is significantly shorter than their decay rate due to the fluid viscosity [75]. Thus, instead of dissipating, the large eddies break down into smaller-size eddies which, in turn, also break down into the even smaller-size eddies if the viscosity is not yet strong enough to cause their energy being dissipated into heat. The generation of smaller-scale motions is a unique characteristic of turbulence and is understood to be a reason why turbulence enhances diffusion dramatically [76].

In more general terms, turbulence can be viewed as a transport phenomenon where the driving force and the dissipation act at different scales. The window in between these scales is called *inertial range* where conserved transport of energy or some other quantity occurs. The breaking down of eddies in turbulent transport forms the so-called Richardson cascade in which the energy is transported in a conserved manner from large to smaller-scale eddies [77]. This process continues until the eddies are small enough for viscosity to take over and dissipate the eddies motional energy into heat. The transport is called a *cascade* because the energy is transported to continuously smaller eddies.

While in Richardson's cascade the energy moves forward, towards smaller eddies, the cascade can also be directed into the opposite direction, as is the case, e.g., for Kraichnan turbulence in two-dimensional fluids. A transport from small to large momentum scales (i.e. the Richardson's cascade) is called *direct cascade* while the transport in the opposite direction is called *inverse cascade* [78].

There are many faces of turbulence but what we are interested in is its self-similar and universal features. In the steady state, the rate of transport is fixed to a particular value at every momentum scale within the inertial range. Such a condition constrains the amount of the energy that can exist in each momentum shell and gives a specific relation between energy and momentum. A well-known relation is the Kolmogorov 5/3-law in hydrodynamic turbulence predicted in the 1941 seminal paper [40]. Later, many experimental observations confirmed Komogorov's prediction [79–81]. The 5/3-law is universal, completely independent from the microscopic details and how the driving force generates turbulence. Towards the ultraviolet end of the

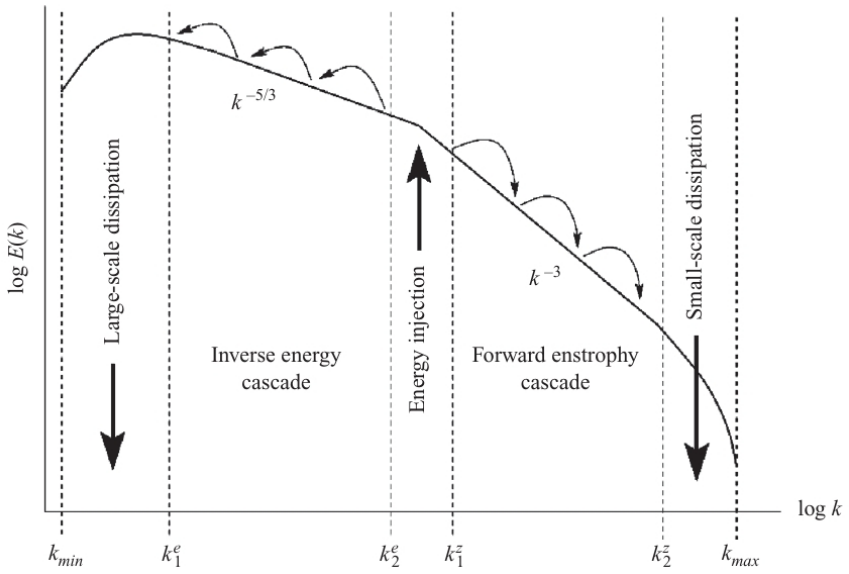

Figure 3.1: The schematic represents the dual cascade in two dimensional turbulence (the Kraichnan-Leith-Batchelor theory). In contrast to three dimensional turbulence, the energy flux is an inverse cascade while the entropy flux is a direct cascade. The figure is taken from Ref. [83].

inertial region self-similarity and also the 5/3-law break down due to intermittency. A detailed discussion of intermittency can be found in [39].

Wave turbulence is a form of turbulence where the transport affects propagating waves instead of eddies [11]. The major advantage of wave turbulence is the existence of a closed equation though this is the case only for *weak-wave* turbulence where the wave amplitudes are small. In such a case, the higher-order correlation functions can be expressed in the terms of lower ones, terminating the hierarchy [10, 11, 82]. The statistical quantities can eventually be derived from a number distribution $n(\boldsymbol{p})$ and which satisfies a kinetic equation of the form of a wave-Boltzmann equation describing the interaction of waves in resonances. In the most simple cases, the leading contributions are the resonant interactions between three or four waves depending on the particular physical situation. As in fluid turbulence, the wave-Boltzmann equation has stationary solutions of the power-law form, $n(\boldsymbol{p}) \sim |\boldsymbol{p}|^{-\zeta}$. The exponent ζ is a Kolmogorov-Zakharov exponent defining the particular steady state of wave-turbulence transport and it is a direct analogue to Kolmogorov 5/3 exponent in hydrodynamic turbulence [10]. The ζ exponent is universal and independent of the detials of the underlying microscopic theory. The exponent depends only on basic properties of the kinetic equation, including dimensionality, scaling properties of the interaction, and the number of modes interacting.

The number of stationary solutions is different for the 3- and 4-wave resonant interactions. In 3-wave resonances, only energy can be transported in a conserved manner, and thus, there is only one stationary solution corresponding to an energy

cascade. In contrast, in 4-wave resonances, both energy and particle numbers can be transported in a conserved manner which gives rise to two possible stationary solutions representing the steady fluxes of particles and energy. As mentioned above, these cascades are directed in opposite ways, namely, a direct cascade for energy and an inverse cascade for particles [37]. So, it is possible to observe two different exponents in 4-wave resonances. Typically, the exponent of particle transport is smaller than that of energy transport so the occupation number will show, at low momententa, a weaker power-law fall off due to an inverse cascade followed by a steeper law at large momenta within the direct cascade [84], see Fig. 3.1.

The physical phenomena that can be explained by wave turbulence are vast and cover the large range of scales [12]. Famous examples are turbulence of capillary waves [85–90] and surface gravity waves [91–93]. In ultracold Bose gases which we are interested in here, wave turbuelence is believed to drive the formation of a condensate when cooling down the system non-adiabatically [15, 37, 38, 94, 95].

To go beyond weak-wave turbulence, one needs to derive kinetic equations beyond the perturbative order corresponding to the wave-kinetic equations. This can be done, e.g. in the context of nonequilibrium quantum field theory within the s-channel resummation in the language of a large-$\mathcal{N}$ expansion [45]. The major differences are, first, that the nonperturbative kinetic equation is not limited to low occupation numbers (which can be translated to low wave amplitudes since number occupation is a second-order correlation function of the wave amplitude) and second, T-matrix elements in the kinetic equation becomes an effective many-body coupling function depending on the occupation numbers themselves. This many-body coupling recovers the perturbative bare one beyond a certain momentum scale where the approximation entering weak-wave-turbulence theory are valid. To distinguish the two limits, in the infrared non-perturbative region, one refers to *strong-wave* turbulence. We will see that the kinetic equation takes the same structure as in the weak-wave case but with the effective coupling replacing the bare one. Then, the idea of transport and stationary solutions in weak-wave turbulence can still be applied including the dual cascade in 4-wave resonant interactions.

In this chapter, we analyse the integral of 4-wave resonant interactions and evaluate the stationary solutions for determining the Kolmogorov-Zakharov exponents using the scaling arguments in both weak- and strong-wave turbulence. We furthermore analyse the non-stationary evolution and determine the corresponding exponents of self-similar shifts of the occupation numbers in space and time [15]. We will work out the differences between wave-turbuelent cascades and self-similar shifts. By the end, we return again to the arguments of dynamical exponents as we have done by the end of Ch. 2. The constraints set by the kinetic equation will help us determine the value of the exponent β which can not be determined from global conservation laws alone. We emphasize that the results of the weak-wave turbulence analysis for free particles agree with the previous studies in [15]. The resulting exponents for strong-wave turbulence are different from the prediction in [49] due to the scaling behaviour of the many-body coupling being different. The dynamical exponents in the strong-wave regime are also different from the ones evaluated in [50] for similar

reasons and, furthermore, different constraints.

3.1 Quantum and wave-Boltzmann equations

The time evolution of the momentum distribution $n_{\mathbf{p}} \equiv n_Q(\mathbf{p}, t)$ of Bose-field (quasiparticle) excitations is described by [10]

$$\partial_t n_Q(\boldsymbol{p}, t) = I[n_Q](\boldsymbol{p}, t) + \Gamma(\boldsymbol{p}) n_Q(\boldsymbol{p}, t)\,, \tag{3.1}$$

where $I[n_Q](\boldsymbol{p}, t)$ is a scattering integral, representing the interaction between wave-modes. $\Gamma(\boldsymbol{p})$ represents the influences of external forces whether they are driving forces ($\Gamma(\boldsymbol{k}) > 0$) or give rise to dissipation ($\Gamma(\boldsymbol{k}) < 0$). In the context of wave turbulence, $\Gamma(\boldsymbol{k})$ does not act at every momentum scale. Typically, there will be scales k_+ where $\Gamma(\boldsymbol{k})$ is positive, meaning that energy (and/or particles) are entering the system in this region. Analogously, within a range of scales k_-, $\Gamma(\boldsymbol{k})$ is negative implying a loss of energy (and/or particles). The scales k_+ and k_- are assumed to be well separated, with the inertial range in between where $\Gamma(\boldsymbol{k})$ vanishes. Within the inertial range, the kinetic wave- or Quantum-Boltzman equation (QBE),

$$\partial_t n_Q(\boldsymbol{p}, t) = I[n_Q](\boldsymbol{p}, t)\,, \tag{3.2}$$

governs the transport between the different scales. The scattering integral $I[n_Q]$ is specified by

$$\begin{aligned} I[n_Q](\boldsymbol{p}, t) = \int_{\boldsymbol{kqr}} |T_{\boldsymbol{pkqr}}|^2 \delta(\boldsymbol{p} + \boldsymbol{k} - \boldsymbol{q} - \boldsymbol{r}) \\ \times\ \delta(\omega_{\boldsymbol{p}} + \omega_{\boldsymbol{k}} - \omega_{\boldsymbol{q}} - \omega_{\boldsymbol{r}}) \\ \times\ [(n_{\boldsymbol{p}} + 1)(n_{\boldsymbol{k}} + 1) n_{\boldsymbol{q}} n_{\boldsymbol{r}} \\ -\ n_{\boldsymbol{p}} n_{\boldsymbol{k}} (n_{\boldsymbol{q}} + 1)(n_{\boldsymbol{r}} + 1)], \end{aligned} \tag{3.3}$$

where we use the short-hand notation $\int_{\boldsymbol{k}} \equiv \int \mathrm{d}^d k\, (2\pi)^{-d}$. The scattering integral $I[n_Q](\mathbf{p}, t)$ describes the redistribution of the occupations $n_{\boldsymbol{p}}$ of momentum modes $\boldsymbol{p}$ with eigenfrequency $\omega_{\boldsymbol{p}}$ due to elastic $2 \to 2$ collisions. These $2 \to 2$ collisions can be inferred from the delta distribution $\delta(\boldsymbol{p} + \boldsymbol{k} - \boldsymbol{q} - \boldsymbol{r})$ which is interpreted as two momenta $\boldsymbol{q}$ and $\boldsymbol{r}$ coming in and $\boldsymbol{p}$ and $\boldsymbol{k}$ going out. The delta function $\delta(\omega_{\boldsymbol{p}} + \omega_{\boldsymbol{k}} - \omega_{\boldsymbol{q}} - \omega_{\boldsymbol{r}})$ ensures that the scattering process conserves the total energy. Moreover, the $2 \to 2$ collisions also conserve the number of quasiparticles [1] since the numbers that are going in and out are unchanged. Both conserved quantities, the total energy and the number of quasiparticles, play a critical role for the studies of the scattering integral in Eq. (3.3).

Note that the QBE does not take into account coherences between the modes. It is because the random phase approximation was used in the derivation of the kinetic

[1] The wave-Boltzmann equation is the kinetic equation for quasiparticle occupations. Thus, the time evolution of particle occupations has to be inferred from the that of quasiparticles. In the case of a quadratic dispersion, $\varepsilon(\boldsymbol{p}) \sim |\boldsymbol{p}|^2$, quasiparticle and particle numbers are identical.

equation so the higher-order correlation functions can be reduced into products of a number distribution. The scattering integral then becomes a functional of $n_Q(\boldsymbol{p},t)$ (as in Eq. (3.3) if the interaction is dominated by 4-wave resonances), see Ch. 2 in [10] for a derivation.

The QBE scattering integral (3.3) has two classical limits: If $n_{\boldsymbol{p}} \ll 1$, the scattering integral reduces to the usual Boltzmann integral with its integrand proportional to $n_{\boldsymbol{q}}n_{\boldsymbol{r}} - n_{\boldsymbol{p}}n_{\boldsymbol{k}}$. In the opposite, classical-wave limit of large bosonic mode occupations, $n_{\boldsymbol{p}} \gg 1$, the wave-Boltzmann scattering integral applies,

$$\begin{aligned} I[n_Q](\boldsymbol{p},t) = \int_{\boldsymbol{kqr}} |T_{\boldsymbol{pkqr}}|^2 \delta(\boldsymbol{p}+\boldsymbol{k}-\boldsymbol{q}-\boldsymbol{r}) \\ \times\ \delta(\omega_{\boldsymbol{p}}+\omega_{\boldsymbol{k}}-\omega_{\boldsymbol{q}}-\omega_{\boldsymbol{r}}) \\ \times\ \left[(n_{\boldsymbol{p}}+n_{\boldsymbol{k}})n_{\boldsymbol{q}}n_{\boldsymbol{r}} - n_{\boldsymbol{p}}n_{\boldsymbol{k}}(n_{\boldsymbol{q}}+n_{\boldsymbol{r}})\right], \end{aligned} \tag{3.4}$$

as the terms of third order in the distribution function $n_{\mathbf{p}}$ dominate over the classical-particle, second-order Boltzmann terms. As we are interested, in this work, in wave-turbulent dynamics of the near-degenerate Bose gas we will restrict our discussion to the integral (3.4) of the wave-Boltzmann equation (WBE).

As we are, for now, assuming isotropic distributions $n_Q(\boldsymbol{p},t) = n_Q(p,t) \equiv n_p$, it is convenient to write the WBE in the form

$$\partial_t n_Q(p,t) = I[n_Q](p,t) = \int \mathrm{d}\Omega_{\mathbf{p}}\, I[n_Q](\boldsymbol{p},t)\,, \tag{3.5}$$

$$I[n_Q](p,t) = \int_{kqr} W_{pkqr}\delta(\omega_p+\omega_k-\omega_q-\omega_r)[(n_p+n_k)n_qn_r - n_pn_k(n_q+n_r)], \tag{3.6}$$

with the angle-averaged transition matrix squared ($d = 2, 3$)

$$W_{pkqr} = 2^{1-d}\pi^{-1}\int \mathrm{d}\Omega_{\mathbf{p}}\,\mathrm{d}\Omega_{\mathbf{k}}\,\mathrm{d}\Omega_{\mathbf{q}}\,\mathrm{d}\Omega_{\mathbf{r}}\, k^{d-1}q^{d-1}r^{d-1}|T_{\boldsymbol{pkqr}}|^2\delta(\boldsymbol{p}+\boldsymbol{k}-\boldsymbol{q}-\boldsymbol{r})\,. \tag{3.7}$$

3.2 Wave turbulent scaling exponents

The well-known solutions of the WBE are stationary solutions where $n_Q(\boldsymbol{p},t)$ satisfies $\partial_t n_Q(p,t) = 0$ or, in other words, nulltifies the scattering integral, $I[n_Q](p,t) = 0$. Interestingly, this depends solely on the functional form of $n_Q(p,t)$ as a function of momentum because it is the only thing that has an effect on the momentum integration. There are two trivial solutions, a constant solution, $n_Q(p,t) \sim$ const. and the Rayleigh-Jeans distribution, $n_Q(p,t) \sim p^{-z}$. Both solutions can be verified by inspecting Boltzmann's factor,

$$[(n_p+n_k)n_qn_r - n_pn_k(n_q+n_r)] = n_pn_kn_qn_r\Big[\frac{1}{n_k}+\frac{1}{n_p}-\frac{1}{n_r}-\frac{1}{n_q}\Big]. \tag{3.8}$$

The constant solution is inferred directly while, for a Rayleigh-Jeans solution, we substitute n_p by p^{-z},

$$[(n_p+n_k)n_qn_r - n_pn_k(n_q+n_r)] \sim (pkqr)^{-z}[k^z+p^z-r^z-q^z]\,. \tag{3.9}$$

The bracket is zero due to the energy conservation, $\delta(\omega_p + \omega_k - \omega_q - \omega_r)$. Both cases are called *detailed-balance* since they make the integrand vanish which implies a symmetry between in and out scattering process. As for non-trivial solutions or the Kolmogorov-Zakharov exponents, the case of $n_Q(p,t)$ having power-law behavior is considered,

$$n_Q(sp) = s^{-\kappa} n_Q(p)\,. \tag{3.10}$$

The trivial solutions correspond to $\kappa = 0$ and $\kappa = z$ but there are other κ's that also nulltify the scattering integral without making a zero integrand. The exponents κ of non-trivial solutions are analytically derived within wave-turbulence theory by means of an integral transformation (Zahkarov transformation [10]). The procedure is to transform and reshape the integral such that a set of exponent κ's that nulltifies the scattering integral can be read off directly. The full demonstration of this technique can be found in [10, 26, 37, 49] as well as many other references on wave-turbulence studies. All possible solutions, including trivial ones, can be found in this way. However, in the following we are going to evaluate the scaling exponents in a simplified manner, by assuming steady fluxes and analysing the scaling behaviour of the scattering integral.

The transport equations (2.55) and (2.56) are related to the scattering integral Eqs. (3.2) and (3.3) by

$$\partial_p Q(p,t) = -(2p)^{d-1}\pi\, I[n_Q](p,t)\,, \tag{3.11}$$

$$\partial_p P(p,t) = -(2p)^{d-1}\omega(p)\pi\, I[n_Q](p,t)\,. \tag{3.12}$$

The turbulence or stationary state of transport equations therefore correspond to gradientless fluxes, i.e. $\partial_p Q(p,t) = 0$ and $\partial_p P(p,t) = 0$. Assuming that the number distribution is a single power-law function as in Eq. (3.10) and $n_Q(p,t) \gg 1$ such that the scattering integral is well approximated by Eq. (3.4), the non-trivial exponents κ that satisfy $I[n_Q](p,t) = 0$ can be obtained by power counting of the momentum scale. If the scattering T-matrix, $T(\boldsymbol{p},\boldsymbol{k},\boldsymbol{q},\boldsymbol{r}) \equiv T_{\boldsymbol{pkqr}}$, has the following scaling behaviour,

$$T(s\boldsymbol{p}, s\boldsymbol{k}, s\boldsymbol{q}, s\boldsymbol{r}) = s^{m_\kappa} T(\boldsymbol{p},\boldsymbol{k},\boldsymbol{q},\boldsymbol{r})\,, \tag{3.13}$$

the scaling of the W_{pkqr} function in Eq. (3.7) becomes

$$W(sp, sk, sq, sr) = s^{2(d+m_\kappa)-3} W(p,k,q,r)\,. \tag{3.14}$$

and it implies

$$I[n_Q](sp,t) = s^{2(d+m_\kappa)-z-3\kappa} I[n_Q](p,t)\,. \tag{3.15}$$

Eq. (3.11) requires $p^d I(p) \sim p^0$ to coincide with $\partial_p Q = 0$, therefore the exponent $\kappa = \kappa_Q$ must obey a following constraint,

$$\begin{aligned} 0 &= d + 2(d + m_\kappa) - z - 3\kappa_Q\,, \\ \Rightarrow \kappa_Q &= \frac{3d + 2m_\kappa - z}{3}\,. \end{aligned} \tag{3.16}$$

The same argument applies to Eq. (3.12) giving the condition $p^{d+z}I(p) \sim p^0$ and thus,

$$\begin{aligned} 0 &= d + z + 2(d + m_\kappa) - z - 3\kappa_P \,, \\ \Rightarrow \kappa_P &= \frac{3d + 2m_\kappa - z}{3} + \frac{z}{3} = \kappa_Q + \frac{z}{3} \,. \end{aligned} \tag{3.17}$$

The exponents κ_Q and κ_P are the exponents governing the power-law dependence of the occupancies in the quasiparticle and energy cascade respectively. It should be noted that whether by means of power-counting or the scaling transformatiion, the exponent κ_Q and κ_P are subject to the condition that the scattering integral is finite without requiring any cutoff scales. This is crucial because both scaling transformation and power-counting fail in the presence of cutoff scales. Recall that, in the 4-wave resonance, the quasiparticle cascade is an inverse cascade while the energy cascade is a direct cascade. This can be verified by the sign of the fluxes $Q(p,t)$ and $P(p,t)$, requiring a negative sign for an inverse and a positive one for a direct cascade which is impossible to check analytically solely within the power-counting scheme. The direction of transport is most easily determined by evaluating derivative $\partial I[n_Q](p,t)/\partial\kappa$ with a power-law ansatz for $n_Q(p)$ inserted. For example, the sign of $Q(p,t)$ is proportional to $\partial I[n_Q](p,t)/\partial\kappa\big|_{\kappa=\kappa_Q}$. See [10, 37] for a detailed discussions of the direction of wave-turbulence cascade.

3.2.1 Weak-wave turbulence scaling exponents

In our context, weak wave turbulence refers to a case where the many-body coupling is well approximated by a bare coupling g in the Hamiltonian (2.1). The situation is realized in the perturbative regime where the coupling is weak and the occupation number is sufficiently low, however, the occupation shold be large enough for the classical Boltzmann equation (3.4) being applicable. The scaling behaviour of the coupling has a strong effect on the scaling of the T-matrix and, as a consequence, determines the Kolmogorov-Zakharov exponents κ_Q and κ_P. In realistic physical situation, the T-matrix usaully does not show a single momentum exponent as assumed in Eq. (3.13) but within the scaling analysis, we will always assume that we are within a regime characterized by a single exponent and that effectively, the scaling there is independent of the precise scaling behaviour outside the respective limiting scales. This assumption is justified if the scattering accounted for in the kinetic equation is sufficiently local such that the major contribution to the integral, $I[n_Q](p)$, comes from the scattering of waves in the momentum modes around p.

Free particles

If the single-particle dispersion is quadratic, $\varepsilon_{\boldsymbol{p}} = p^2/2m$, and thus, $z = 2$, quasiparticles are identical to the fundamental fields themselves, $n_Q \equiv n$. The scattering

T-matrix is approximated by

$$|T_{\boldsymbol{pkqr}}|^2 = (2\pi)^4 g^2 \,, \tag{3.18}$$

where, in $d = 3$ dimensions, g is given by the GPE coupling $g = 4\pi a/m$. Eq. (3.18) applies up to an ultraviolet cutoff scale p_λ and $|T_{\boldsymbol{pkqr}}|$ falls off to zero beyond this scale, which ensures the unitarity of the scattering amplitude. $p_\lambda \sim 1/a$ scales with the inverse of the scattering length a and is typically much larger than the highest significantly occupied momentum mode. The T-matrix in this case is momentum independent and the scaling exponent defined in Eq. (3.13) corresponds to

$$m_\kappa = 0 \,. \tag{3.19}$$

Inserting this into Eqs. (3.16) and (3.17), one obtains the respective weak-wave-turbulence exponents [10, 49]

$$\kappa_Q^{\mathrm{WWT}} = d - 2/3, \qquad \kappa_P^{\mathrm{WWT}} = d. \tag{3.20}$$

Bogoliubov quasiparticles

For comparison, we consider the case when a condensate with density $\rho_0 \leq \rho$ is present, such that the quasiparticle excitations below the healing-length scale $p_\xi = \sqrt{2g\rho_0 m}$ take the form of sound waves on the background of the bulk condensate, cf. Sect. 2.1. We assume that in the regime where weak-wave turbulence applies, the dispersion is also that of sound waves, $\omega(\boldsymbol{p}) = c_s p$, such that in this case $z = 1$. Far below p_ξ, the T-matrix takes the approximate form

$$|T_{\boldsymbol{pkqr}}|^2 = \ (2\pi)^4 \frac{(mc_s)^4}{pkqr} \frac{3g^2}{2} \,, \tag{3.21}$$

where the speed of sound c_s is defined in terms of the healing-length momentum scale $mc_s = p_\xi/\sqrt{2} = \sqrt{g\rho_0 m}$. See Sect. 4.3.2 for a derivation of the corresponding wave-Boltzmann scattering integral. According to Eq. (3.21), the scaling exponent defined in Eq. (3.13) is

$$m_\kappa = -2 \,. \tag{3.22}$$

Inserting this into Eqs. (3.16) and (3.17), one obtains the respective weak-wave-turbulence exponents [49]

$$\kappa_Q^{\mathrm{WsWT}} = d - 5/3 \,, \qquad \kappa_P^{\mathrm{WsWT}} = d - 4/3 \,. \tag{3.23}$$

We remark that perturbative expressions for the T-matrix in Eqs. (3.18) and (3.21) as well as the scaling exponents in Eqs. (3.20) and (3.23), in general, are of limited applicability for solutions showing scaling in the far infrared due to the over occupation in the infrared scale.

3.2.2 Strong wave turbulence scaling exponents

The scaling solution of $n_Q(\boldsymbol{p}, t)$ implies that in the deep infrared, the occupation will eventually become large to the point that a perturbative calculation is no longer valid. Typically, this happens where $g^2 n_Q^2 \gg 1$ because there, terms that are of higher order than $g^2 n_Q^3$ become important. Note that the over occupation is even able to break the perturbative approximation in the weak-coupling limit $g \ll 1$. To include those terms, the non-perturbative calculation is needed.

In our work, we use the resummation of the class of s-channel loop-chain diagrams contributing to the two-particle irreducible effective action (2PI) to find a non-perturbative expression of the many-body coupling. The details of derivation within the 2PI scheme are given in the App. B and the derivation of the resulting of many-body coupling $g_{\text{eff}}(p)$ will be discussed in the Ch. 4. To keep the discussion of its application concise, we here only quote the results. The many-body coupling $g_{\text{eff}}(p)$ turns out to be a momentum dependent function scaling according to,

$$g_{\text{eff}}(s^z p_0, s\boldsymbol{p}) = s^2 g_{\text{eff}}(p_0, \boldsymbol{p})\,, \tag{3.24}$$

which, to our knowledge, does not depend on the choice of systems as long as the (quasi)particle has a well-defined spectral function. Since $g_{\text{eff}} \neq g$, the scaling exponents m_κ of the T-matrix are different, in the perturbative and the nonperturbative cases. We, again, compare the scaling for free and Bogoliubov quasiparticles. Note that the result in Eq. (3.24) was checked explicitly in one [96] and three (cf. Ch. 4) spatial dimensions.

Free particles

In the term of the effective many-body coupling, the T-matrix reads

$$|T_{\boldsymbol{pkqr}}|^2 = (2\pi)^4 g_{\text{eff}}^2(\varepsilon_{\mathbf{p}} - \varepsilon_{\mathbf{r}}, \boldsymbol{p} - \boldsymbol{r})\,. \tag{3.25}$$

Here, $\boldsymbol{p}-\boldsymbol{r}$ and $\varepsilon_{\mathbf{p}}-\varepsilon_{\mathbf{r}}$ are the momentum and energy transfer in a scattering process, respectively. See Fig. 4.1 for a diagrammatic representation. Hence, the T-matrix scaling exponent becomes

$$m_\kappa = 2\,. \tag{3.26}$$

Inserting the result back into Eqs. (3.16) and (3.17), the strong-wave-turbulence exponents read

$$\kappa_Q^{\text{SWT}} = d + 2/3, \quad \kappa_P^{\text{SWT}} = d + 4/3. \tag{3.27}$$

Bogoliubov quasiparticles

For sound waves, there are two types of momentum and energy transfer collisional processes, distinguished by the many-body coupling in the T-matrix element,

$$|T_{\boldsymbol{pkqr}}|^2 = (2\pi)^4 \frac{(g\rho_0)^4}{\omega_p \omega_k \omega_q \omega_r} \Big[g_{\text{eff}}^2(\omega_p - \omega_r, \boldsymbol{p} - \boldsymbol{r}) + \frac{1}{2} g_{\text{eff}}^2(\omega_p - \omega_k, \boldsymbol{p} + \boldsymbol{k}) \Big]\,, \tag{3.28}$$

Therefore, the exponent m_κ of the T-matrix vanished,

$$m_\kappa = 0\,, \tag{3.29}$$

and the strong-sound-wave turbulence exponents read :

$$\kappa_Q^{\mathrm{SsWT}} = d - 1/3\,, \qquad \kappa_P^{\mathrm{SsWT}} = d\,. \tag{3.30}$$

These exponents apply only in the regime $p \ll p_\xi$ where the Bogoliubov sound dispersion applies.

3.2.3 Self-similar scaling exponent

The self-similar exponents are not related to particles or energy fluxes, unlike the wave turbulence exponents. They are governing solutions of the kinetic equation evolving via a space-time rescaling which become important when taking into account global conservation laws. The simplest form of the self-similar solution reads

$$n_Q(p,t) \sim p^{-\kappa} t^{\nu}\,. \tag{3.31}$$

which is now explicitly time-dependent. At $\nu = 0$, $n_Q(p,t)$ collapses to the stationary solutions. In the similar manner as in the turbulence cascade, there is a constraint that fixes the exponent κ to a specific value κ_S if such an evolution occurs. All we need here is Eq. (3.4) because the nonstationary solution implies that both sides of the equation are nonzero and, thus, the dimension of momentum and time on both sides must be equal. On the LHS, $\partial_t n_Q(p,t) \sim p^{-\kappa}$ and on the RHS, $I[n_Q](p,t) \sim p^{2(d+m_\kappa)-z-3\kappa}$. By comparing the exponents from both sides, we obtain

$$\begin{aligned} -\kappa &= 2(d+m_\kappa) - z - 3\kappa\,, \\ \Rightarrow \kappa_S &= d + m_\kappa - \frac{z}{2}\,. \end{aligned} \tag{3.32}$$

Observe that the scattering integral $I[n_Q](p,t) \sim p^{-\kappa_S}$ for the self-similar exponent κ_S. This property is very useful for clarifying whether an exponent corresponds to a self-similar exponent.

In principle, the time exponent ν can be deduced from the condition that both sides of Eq. (3.4) rescale equally with time. The difficulty here lies in extracting the time dependence scales from all parameters in the scattering integral which is not always straightforward. However, if the time dependence arises from the number distribution $n_Q(\boldsymbol{p},t)$ alone, we have

$$\begin{aligned} \nu - 1 &= 3\nu\,, \\ \Rightarrow \nu &= -\frac{1}{2}\,. \end{aligned} \tag{3.33}$$

Eqs. (3.32) and (3.33) imply that the self-similar form of the number distribution is $n_Q(p,t) \sim p^{-\kappa_S} t^{-1/2}$ [15]. Under the assumption we made, the temporal exponent

is totally independent of the details of the system (dimension, dipersion relation, etc.) and we also note that the results in Eqs. (3.32) and (3.33) are independent of the global conservation laws. It is sensible to look back to Eqs. (2.49) and (2.50). The exponents α and β are fixed by quasiparticle conservation alone without the constraint from energy conservation. The same is true for α' and β' with respect to energy conservation. To ensure that particles and energy are simultaneously conserved, a constraint is needed which is the self-similar form, (3.31), governed by the kinetic equation.

3.3 Universal dynamics (revisited)

In Sect. 2.3, we have evaluated the scaling exponents corresponding to the universal dynamics based on the global conservation laws alone. However, the values of the exponents have not been determined. In this section, we will evaluate the values of all exponents in Table 2.1 using the information from the kinetic equation. Recall that in physical situations, cutoff scales whether in IR, UV or both are inevitable to ensure convergence of the integrals. Therefore, care has to be taken in power counting when determining the scaling behaviour of an integral. Here, we will clarify the power-law behaviour of the cutoff scales before counting. The results we are going to present crucially depend on the presence of a cutoff regularishing the IR divergences of the loop-integral, Π^R, that is evaluated in Ch. 4.

3.3.1 Time scaling behaviour

If observables are time-dependent, the scaling hypotheses is not limited to the momentum dependence but can be extended to the time argument as well. For example, the general scaling of the quasiparticle distribution reads

$$n_Q(p,t) = s^{\alpha/\beta} n_Q(sp, s^{-1/\beta}t)\,, \tag{3.34}$$

where the scaling in time is inspired by the time-dependent of the cutoff scale i.e. $p_\Lambda(t) \sim t^{-\beta}$ and, hence, $p_\Lambda(s^{-1/\beta}t) \sim (s^{-1/\beta}t)^{-\beta} \sim s\, p_\Lambda(t)$, cf. Sect. 2.3.2. Similar scaling occurs for $p_\lambda(t) \sim t^{-\beta'}$ with α' and β' exponents. s is an arbitrary positive parameter and if it is chosen to be $s = (t/t_0)^\beta$, Eq. (3.34) gives Eq. (2.38). The exponents extracted from the scaling hypotheses in Eq. (3.10) and Eq. (3.34) are not necessary to coincide. To see this explicitly, we assume the most simplest form that satisfies both conditions simultaneously,

$$n_Q(p,t) \sim p^{-\kappa}[p_\Lambda(t)]^{\kappa-\alpha/\beta}\,. \tag{3.35}$$

Whenever only momentum scaling is considered, only $p^{-\kappa}$ contributes to the exponent but, with scaling hypotheses in Eq. (3.34), both p and $p_\Lambda(t)$ give the contributions. This kind of differences appears in every time-dependent observable. Note that the exponent solutions in Sect. 3.2, except ν in Eq. (3.33), remain the same because they are evaluated from the scalings in momentum alone.

3.3.2 General scaling of T-matrix

The general scaling of the T-matrix elements can not be identified straightforwardly since, at least, a scaling in momentum and of the time-dependent scales must be known. To proceed in this direction, we need to recall the many-body coupling g_{eff} obtained from the 2PI resummation for making an estimation of the general scaling. Therefore, the following arguments are inevitably subject to the 2PI calculation. Again, we skip the detailed derivation within dynamic field theory which is given in the subsequent chapters and provide further details of the evaluation in App. F. We note that in the following, we also take into account the dependence on an anomalous dimension η which governs the spectral function of (quasi)particles.

Due to a lot of information from the subsequent chapters are needed, we skip the discussion how one obtain the general scaling and give the details in App. F. We only need to mention that there is an anomalous dimension η that excluded from the calculation in Ch.4 thus, there is no appearance of η there. However, we would like to recover the η-dependence in the following expressions so the pure momentum exponents will be given again. The general scaling of the T-matrix elements obeys

$$|T(s\boldsymbol{p}, s\boldsymbol{k}, s\boldsymbol{q}, s\boldsymbol{r}; s^{-1/\beta}t)| = s^{m}|T(\boldsymbol{p}, \boldsymbol{k}, \boldsymbol{q}, \boldsymbol{r}; t)|\,, \tag{3.36}$$

$$|T(s\boldsymbol{p}, s\boldsymbol{k}, s\boldsymbol{q}, s\boldsymbol{r}; t)| = s^{m_\kappa}|T(\boldsymbol{p}, \boldsymbol{k}, \boldsymbol{q}, \boldsymbol{r}; t)|\,, \tag{3.37}$$

where

$$m = \gamma + 2(z-2) + \frac{\eta}{2}\,, \tag{3.38}$$

$$m_\kappa = \gamma_\kappa + 2(z-2) + \frac{\eta}{2}\,, \tag{3.39}$$

cf. Eqs. (F.12) and (F.28). In the Bogoliubov quasiparticle case, the inverse healing length $p_\xi = [2mg\rho_0]^{1/2}$ is assumed to be time-independent, implies no condesation and depletion in the zero mode. The exponents γ and γ_κ are the scaling exponents of the many-body coupling,

$$g_{\text{eff}}(s^z p_0, s\boldsymbol{p}; s^{-1/\beta}t) = s^{\gamma} g_{\text{eff}}(p_0, \boldsymbol{p}; t)\,, \tag{3.40}$$

$$g_{\text{eff}}(s^z p_0, s\boldsymbol{p}; t) = s^{\gamma_\kappa} g_{\text{eff}}(p_0, \boldsymbol{p}; t)\,. \tag{3.41}$$

The subscript κ is used to distinguish the pure momentum scaling from the scaling hypotheses in Eq. (3.34). Assuming that the scattering integral $I[n_Q]$ converges which should be the case if there exists stationary solutions, the scaling exponents of the scattering integral can be directly counted from Eq. (3.4),

$$I[n_Q](s\boldsymbol{p}, s^{-1/\beta}t) = s^{\mu} I[n_Q](\boldsymbol{p}, t)\,, \tag{3.42}$$

$$I[n_Q](s\boldsymbol{p}, t) = s^{\mu_\kappa} I[n_Q](\boldsymbol{p}, t)\,, \tag{3.43}$$

where

$$\mu = 2(d+m) - z - \frac{3\alpha}{\beta}\,, \tag{3.44}$$

$$\mu_\kappa = 2(d+m_\kappa) - z - 3\kappa\,. \tag{3.45}$$

3.3.3 Scaling evolution

The scaling hypotheses Eq. (3.34) give a further constraints for the time-related exponents i.e. α, β, μ etc. if the kinetic equation is taken into account. To see this, we apply Eq. (3.34) with the choice $s = (t/t_0)^\beta$ into Eq. (3.2) [50],

$$(t/t_0)^{\alpha-1}(\alpha + \beta\, q\, \partial_q) f(q)\Big|_{q=(t/t_0)^\beta p} = \; t_0 (t/t_0)^{-\beta\mu} I[f](q)\,. \tag{3.46}$$

The function $f(p) = n_Q(p, t_0)$ is now time-independent, then, for Eq. (3.46) being valid at any time t, including t_0, the time-independent fixed point equation

$$(\alpha + \beta\, q\, \partial_q) f(q) = \; t_0 I[f](q)\,. \tag{3.47}$$

must hold. At the same time, the exponents of the factor t/t_0 on both sides of Eq. (3.46) need to be equal. This means

$$\alpha = 1 - \beta\,\mu\,. \tag{3.48}$$

The condition (3.48) allows us to evaluate the exponent β using μ which governs the scaling of the scattering integral in the kinetic equation. Inserting μ from Eq. (3.44) and rearranging the terms, we obtain

$$\beta = \frac{1}{2(d+m) - z - 2\alpha/\beta}\,. \tag{3.49}$$

The further discussion will be separated between the turbulent transport and self-similar evolution due to the different constraints on the ratio α/β.

Time evolution in turbulent transport

If we substitute $f(q)$ on the LHS of Eq. (3.47) with a simple power-law function $f(q) \sim q^{-\kappa}$, we get

$$(\alpha - \beta\,\kappa) f(q) = \; t_0 I[f](q)\,. \tag{3.50}$$

The condition $I[f](q) = 0$ on the RHS demands $\alpha = \beta\,\kappa$ on the LHS, otherwise Eq. (3.50) does not hold. Note that this is true only in the power-law regime where there are turbulent fluxes with the Kolmogorov-Zakharov exponents κ_Q or κ_P. In the momentum regime that fluxes have not reached, the scattering integral does not vanish and we do not expect κ to describe a stationary solution. The constraint of turbulent transport is $\alpha/\beta = \kappa$ as presented in Table 2.1. Substituting this into Eq. (3.49) yeilds

$$\beta = \frac{1}{2(d+m) - z - 2\kappa_Q}\,. \tag{3.51}$$

β' is subject to the same relation except that κ_Q is replaced with κ_P. Note that in the case of turbulence, Eq. (3.48) does not apply for the momentum scale that have no

dynamics. For example, Eq. (3.48) can not be used to constrain the exponents α' and β' in the regime of $\kappa < d$ where both particle number and energy are concentrated in the UV, p_λ because in that case $\alpha' = \beta' = 0$ in the first approximation to ensure global particle and energy conservation. Although Eq. (3.48) is not fulfilled, Eq. (3.46) and $\alpha' = \beta' = 0$ imply the vanishing of the of scattering integral. We insert Eqs. (3.16) and (3.17) into Eq. (3.51) to evaluate $\beta = \beta_Q$ for an inverse cascade and $\beta' = \beta_P$ for a direct cascade, respectively,

$$\beta_Q = \frac{1}{2(m - 2m_\kappa/3) - z/3}\,, \tag{3.52}$$

$$\beta_P = \frac{1}{2(m - 2m_\kappa/3) - z}\,. \tag{3.53}$$

The further analysis will be separately discussed for weak- and strong-wave turbulence due to the different values of m and m_κ.

Weak-wave turbulence.— In the perturbative limit, the many-body coupling is the bare coupling constant, see Eqs. (3.18) and (3.21), therefore,

$$\gamma = \gamma_\kappa = 0\,. \tag{3.54}$$

Substituting Eq. (3.54) into Eqs. (3.38) and (3.39) simply gives

$$m = m_\kappa = 2(z-2) + \frac{\eta}{2}\,, \tag{3.55}$$

and we can now determine β_Q and β_P from Eqs. (3.52) and (3.53),

$$\beta_Q = \frac{3}{3z - 8 + \eta}\,, \tag{3.56}$$

$$\beta_P = \frac{3}{z - 8 + \eta}\,. \tag{3.57}$$

In the free particle case where $z = 2$, we get $\beta_Q = -3/2$ (neglecting the anomalous exponent η) which gives $p_\Lambda(t) \sim (t_1 - t)^{3/2}$ where p_Λ is an IR cutoff. We thus recover the temporal rescaling of the IR energy scale, $\varepsilon_\Lambda(t) \sim (t_1 - t)^3$ due to $\varepsilon(p) \sim p^2$ which agrees with the energy rescaling obtained in [15].

Strong-wave turbulence.— In the strong-wave regime, an infinite number of diagrams in s-channel resummation is taken into account to calculate the effective coupling. The resummation modifies the functional form of the many-body coupling and its scaling behaviour, Eqs. (3.25), (3.28), (F.11) and (F.27) implying that

$$\gamma = 2 - \eta - \frac{2\delta}{\beta}\,, \tag{3.58}$$

$$\gamma_\kappa = 2 - \eta\,. \tag{3.59}$$

Here, we assumed that the noncondensed particle density $\rho_{\rm nc}$ in general changes in time with the exponent δ, $\rho_{\rm nc}(t) \sim t^{-2\delta}$. This is the generally the case whenever

particles and quasiparticle degrees of freedom do not coincide such tht quasiparticle conservation violates that of particle number and vice versa, see Eqs. (2.18) and (2.19). Inserting Eqs. (3.58) and (3.59) into (3.38) and (3.39) repectively, yields

$$m = 2(z-1) - \frac{\eta}{2} - \frac{2\delta}{\beta}\,, \tag{3.60}$$

$$m_\kappa = 2(z-1) - \frac{\eta}{2}\,. \tag{3.61}$$

Substituting Eqs. (3.60) and (3.61) into Eqs. (3.52) and (3.53) give

$$\beta_Q = \frac{3}{3z-4-\eta-12\delta/\beta}\,, \tag{3.62}$$

$$\beta_P = \frac{3}{z-4-\eta-12\delta/\beta}\,. \tag{3.63}$$

In the limit $\delta = 0$, one gets $\beta_Q = 3/(3z-4-\eta)$ and $\beta_P = 3/(z-4-\eta)$ which bear a similar form as in Eqs. (3.56) and (3.57) in the perturbative case. However, the results imply the violation of quasiparticle conservation. Demanding quasiparticle conservation as ensured by the 2-to-2 resonant interaction in the kinetic equation, delta does no longer vanish and can be inferred from Eq. (2.23),

$$2\delta/\beta = d + z - 2 - \alpha/\beta\,. \tag{3.64}$$

The further step are not straightforward because it depends on the divergence of $\rho_{\rm nc}$. Here, we assume that $\rho_{\rm nc}$ diverges in the infrared, therefore, α and β are governing the rescaling at the IR end. For an inverse particle cascade, α/β is constrained by $\alpha/\beta = \kappa_Q$ and we can replace the ratio α/β in Eq. (3.64) by κ_Q from Eq. (3.16) to obtain

$$\begin{aligned}\beta_Q &= \frac{3}{3z-4-\eta-6(d+z-2-\kappa_Q)} \\ &= \frac{3}{3z-4-\eta-6(-2+4/3+\eta/3)} \\ &= \frac{1}{z-\eta}\,.\end{aligned} \tag{3.65}$$

For a direct energy cascade, the infrared cutoff p_Λ has no dynamics in a first order approximation. Thus, we simply take $2\delta/\beta = 0$ in this case because we assumed $\rho_{\rm nc}$ depends on the infrared scale p_Λ. As a result, β_P becomes

$$\beta_P = \frac{3}{z-4-\eta}\,. \tag{3.66}$$

Time evolution in the self-similar dynamics

In the self-similar time evolution, the constraints come from the global conservation laws, $\alpha/\beta = d$ and $\alpha'/\beta' = d + z$, see Eqs. (2.40) and (2.41). Inserting these two

constraints into Eq. (3.49) gives

$$\beta_Q = \frac{1}{2m - z}\,, \tag{3.67}$$

$$\beta_P = \frac{1}{2m - 3z}\,. \tag{3.68}$$

The further discussions are again separately discussed into the perturbative and the nonperturbative regimes.

Perturbative regime.—

In the perturbative regime, the T-matrix scalings is the one in Eq. (3.55). We insert Eq. (3.55) into Eqs. (3.67) and (3.68) to obtain

$$\beta = \frac{1}{3z - 8 + \eta}\,, \tag{3.69}$$

$$\beta' = \frac{1}{z - 8 + \eta}\,. \tag{3.70}$$

From Eqs. (3.32) and (3.55), we evaluate the self-similar momentum scaling exponent,

$$\kappa_S = d + 3z/2 - 4 + \eta/2\,, \tag{3.71}$$

and verify the relation (2.52),

$$\begin{aligned}\beta' &= \frac{d - \kappa_S}{d + z - \kappa_S}\,\beta \\ &= \Big(\frac{-3z/2 + 4 - \eta/2}{-z/2 + 4 - \eta/2}\Big)\Big(\frac{1}{3z - 8 + \eta}\Big) \\ &= \Big(\frac{3z - 8 + \eta}{z - 8\eta}\Big)\Big(\frac{1}{3z - 8 + \eta}\Big) = \frac{1}{z - 8 + \eta}\,.\end{aligned} \tag{3.72}$$

The result is identical to Eq. (3.70) which means the scenario describing in Sect. 2.3.2 is well defined.

In the free particle case where $z = 2$, we then have $\beta = -1/2$ and $\beta' = -1/6$. This means the time evolution of the momentum scales in the infrared p_Λ and the ultraviolet p_λ are $p_\Lambda(t) \sim t^{1/2}$ and $p_\lambda(t) \sim t^{1/6}$ respectively, which translate to the time evolution of the energy scales as $\varepsilon_\Lambda(t) \sim t$ and $\varepsilon_\lambda(t) \sim t^{1/3}$. The results are agree with [15]. Notice that $\beta < 0$ despite the expectation $\beta > 0$ in Sect. 2.3.2. The requirements $\beta > 0$ and $\beta' < 0$ imply $8/3 < z < 8$ in the perturbative regime. This is an indicator that the self-similar time evolution can not occur in the perturbative regime where $z \in \{1, 2\}$.

Nonperturbative regime.—

In the nonperturbative regime, the scalings of T-matrix are those in Eqs. (3.60) and (3.61). Inserting Eq. (3.60) into Eqs. (3.67) and (3.68) gives

$$\beta = \frac{1}{3z - 4 - \eta - 4\delta/\beta}\,, \tag{3.73}$$

$$\beta' = \frac{1}{z - 4 - \eta - 4\delta/\beta}\,. \tag{3.74}$$

This brings us back to the problem of determining the exponent δ as before. We again assume that the divergence of $\rho_{\rm nc}$ is in the infrared such that the ratio α/β in the relation (3.64) is replaced by the quasiparticle constraint, $\alpha/\beta = d$. Thus, Eq. (3.64) becomes

$$2\delta/\beta = z - 2\,. \tag{3.75}$$

We insert this relation into Eqs. (3.73) and (3.74) to evaluate β and β' respectively,

$$\beta = \frac{1}{z-\eta}\,, \tag{3.76}$$

$$\beta' = \frac{1}{-z-\eta}\,. \tag{3.77}$$

However, in this $\delta \neq 0$ limit, further constraints are needed to satisfy the relation (2.52). This can be seen from

$$\begin{aligned} \beta' &= \frac{d-\kappa_S}{d+z-\kappa_S}\ \beta \\ \frac{1}{-z-\eta} &= \Big(\frac{3z-4-\eta}{z-4-\eta}\Big)\Big(\frac{1}{z-\eta}\Big)\,, \end{aligned} \tag{3.78}$$

where $\kappa_S = d + 3z/2 - 2 - \eta/2$, evaluated from Eqs. (3.32) and (3.61). In the limit $\delta = 0$, the relation (2.52) is fully satisfied, cf. Eqs. (3.73) and (3.74). The problem is more transparent if we insert the general expressions in terms of m and m_κ into relation (2.52), see Eqs. (3.32), (3.67), and (3.68),

$$\frac{1}{2m-3z} = \Big(\frac{2m_\kappa - z}{2m_\kappa - 3z}\Big)\frac{1}{2m-z}\,. \tag{3.79}$$

The relation (2.52) will be satisfied as in the perturbative case or the nonperturbative case where $\delta = 0$ if $m = m_\kappa$. It is an open question whether the case of $m \neq m_\kappa$ means the failure of the scenario in Sect. 2.3.2, for example, the single power-law function may not be a proper way to describe the universal dynamics in this case, or this means a way to determine the value of the anomalous scaling η which, so far, is completely undetermined in the kinetic theory.

3.4 Summary

We have analysed the kinetic equation of 4-wave resonances in the classical limit where the occupation number is sufficiently large and dominates the quantum ground state. The stationary solutions of the kinetic equation andin particular the Kolmogorov-Zakharov exponents are evaluated by means of dimensional counting. The alternative approach involving integral transforms witnin the scattering integral after which exponents can be read off directly [10, 26, 37, 49]. Our analysis is more straightforward

Table 3.1: Scaling relations in the purturbative regime. The table summarizes the relations between the scaling exponents as obtained in Sect. 2.3 and further constrained by the kinetic equation in Sect. 3.3. η was set to be zero and the value of τ is determined with the values of $z \in \{1, 2\}$.

	α	β	α'	β'	τ
inverse cascade $\kappa_Q = d + z - 8/3$	$\beta\kappa_Q$	$\frac{3}{3z-8}$	0	0	τ_1
self-similar evol. $\kappa_S = d + 3z/2 - 4$	βd	$\frac{1}{3z-8}$	$\beta'(d+z)$	$\frac{1}{z-8}$	
direct cascade $\kappa_P = d + 4(z-2)/3$	0	0	$\beta'\kappa_P$	$\frac{3}{z-8}$	t/t_0

Table 3.2: Scaling relations in the nonpurturbative regime. The table summarizes the relations between the scaling exponents as obtained in Sect. 2.3 and further constrained by the kinetic equation in Sect. 3.3. η was set to be zero and the value of τ is determined with the value of $z \in \{1, 2\}$. We present the results of the cases where there is time-evolution in the contents of noncondensed particle ρ_{nc}, except in a direct cascade case.

	α	β	α'	β'	τ
inverse cascade $\kappa_Q = d + z - 4/3$	$\beta\kappa_Q$	$\frac{1}{z}$	0	0	t/t_0
self-similar evol. $\kappa_S = d + 3z/2 - 2$	βd	$\frac{1}{z}$	$\beta'(d+z)$	$-\frac{1}{z}$	
direct cascade $\kappa_P = d + 4(z-1)/3$	0	0	$\beta'\kappa_P$	$\frac{3}{z-4}$	τ_1

and yields the same set of exponents while it has to be taken with more care concerning the role of divergence. Our approach is motivated by the way the scaling analysis was done in Ref. [15]. We eventually have evaluated exponents governing the dynamical evolution of the momentum distribution using Eq. (3.48) obtained from Eq. (3.46) to determine β before the other dynamical exponents can be evaluated by relations given in Table 2.1. Our results are summarized in Tables 3.1 and 3.2. One thereby has to keep in mind that Eq. (3.46) is subject to the condition of self-similar time evolution (turbulence cascade included). So Eq. (3.48) is valid only for the case of self-similar dynamics.

The exponents of the time evolution in the perturbative regime are well agreed with the scenarios describing in Sect. 2.3. However, this is not completely the case in the nonperturbative regime. We have seen that when m does not coincide with m_κ, some discrepancies may occur. This means the scenarios of the universal dynamics needs to be modified, or a new constraint for determining the value of the anomalous exponent η. In any case, it is not conclusive.

In the case that we neglect the inconsistencies, we have a universal value of β

in the nonperturbative regime regardless of whether the type of dynamics represents an inverse cascade or a self-similar shift in time. This is a nontrivial result in the kinetic theory and may signal the particular character of the nonthermal fixed point in the nonperturbative regime. We anticipate that, in order to obtain a full picture of the universal properties of the fixed point, the question of what possible values the anomalous dimension η can take and in which way this is related to the condition giving in the dynamical exponent z.

Chapter 4

Kinetic equation from nonequilibrium quantum field theory

Nonequilibrium quantum field theory is an attempt to construct a nonperturbative approach for evaluating the n-point functions in a way that all quantities respect causality given their values at an initial time. We review the formalism in App. B but would like to summarize the main points here. The conventional quantum field theory is constructed to be a boundary value problem in the sense that the observables are defined through the S-matrix which is generally a transition between in and out states [97]. This feature contrasts with the nature of nonequilibrium problems that observables are calculated from the time-evolution of their initial conditions. Two ingredients are needed to modify conventional quantum field theory: the Schwinger-Keldysh closed-time-path (CTP) integral [98, 99] and the 2-particle-irreducible (2PI) effective action [43]. The CTP formalism is necessary to make all observables being expectation values with respect to the initial states instead of the matrix elements between in and out states (hence the name in-in formalism used sometimes in the literature). Moreover, the observables in the CTP formalism respect causality in the sense that the observables at time t are evaluated only from information at time $t' < t$. The 2PI formalism gives a nonpertubative way to evaluate the 1- and 2-point functions through a set of dynamic equations.[1] Unfortunately, this set of equations is usually a set of integro-differential coupled equations which is not practically solvable.

Despite such difficulties, some information is still available through other means. For a theory with ϕ^4 interaction, the dynamic equation for the 2-point functions can be transformed into the kinetic equation of wave turbulence [25, 45, 49]. Therefore, the arguments that have been discussed in Ch. 3 are applied. The main advantage is that the kinetic equation derived within this approach is free from the perturbative constraint that occupation numbers are low. This allows us to go beyond the weak-wave turbulence limit which is called strong-wave turbulence. Some aspects of nonequilibrium dynamics of Bose fields can now be studied using the concepts of wave turbulence and universal dynamics. Our interest is still in the momentum scaling of occupation numbers which include the Kolmogorov-Zakharov, κ_Q and κ_P, and the self-similar, κ_S, exponents.

The Kolmogorov-Zakharov exponents or the stationary solutions of the kinetic

[1] In principle, it can be extended to the n-point functions if one uses nPI formalism instead [44, 45].

equation deriving from nonequilibrium quantum field theory have been discussed previously in [49] using the scaling arguments and the technique of re-mapping the integral, similarly to the analysis in [10, 26, 37]. We have shown in Ch. 3 that the exponents we obtained are different from the result in [49]. This is because the scaling behaviour of the effective coupling $g_{\rm eff}(p)$ does not agree with the prediction from dimensional counting. This can be verified by replacing the scaling exponent of the effective coupling by ours, recovering then also our scaling exponents of the solutions. The evaluation of $g_{\rm eff}(p)$ to determine its scaling behaviour is the one of the central result in this thesis.

This chapter is organized as follows. We start by applying the nonequilibrium quantum field theory to the Gross-Pitaevskii action and evaluate a set of dynamic equations of 1- and 2-point functions. Then, we concentrate on turning the dynamic equation of 2-point functions into the kinetic equation similarly to Eq. (3.2) under the homogeneous assumption. The procedure is analogous to the one presented in [45] but here, we apply it to a complex scalar field so symmetries and expressions will be slightly different. We finally explicitly evaluate the effective coupling $g_{\rm eff}(p)$ using an ansatz to determine its scaling behaviour which we used throughout the analysis in Ch. 3. We remark that the kinetic equation we derive in this chapter can be used to analyse both, the momentum or and the temporal scaling exponents. The respective results obtained from scaling arguments are presented in Ch. 3. Our scaling ansatz leads to an explicit form of the kinetic equation. To confirm the validity of this ansatz we perform a numeric integration of the T-matrix and the scattering integrals which we will discuss in Ch. 5.

4.1 Nonequilibrium description of a Bose field with quartic interaction

The quartic interaction is the simplest, non-trivial self-interaction that appears in many theoretical models, including the Gross-Pitaevskii Hamiltonian (2.1). Here, we will study nonequilibrium quantum field theory of a Bose field with quartic interaction. The aim is deriving the dynamic equations of mean-fields an propagators so we can study the time evolution of Bose gases.

4.1.1 Dynamical equations of a Bose field with quartic interaction

The classical action of a complex Bose field with ϕ^4 interaction reads

$$S[\phi,\phi^*] = \frac{1}{2}\int_{xy} \phi_a^*(x)(iD_{ab}^{-1}(x,y))\phi_b(y) - \frac{g}{8}\int_x \phi_a^*(x)\phi_a(x)\phi_b^*(x)\phi_b(x), \qquad (4.1)$$

where the variable x refers to $d+1$ space-time coordinate in d spatial dimensions. The notation $\int_x$ stands for $\int_{-\infty}^{\infty} d^4x$ and $\int_{xy}$ for $\int_{-\infty}^{\infty} d^4x \int_{-\infty}^{\infty} d^4y$. The field components

are labelled by an index $a \in \{1, 2\}$ where $\phi_1(x) = \phi(x)$ and $\phi_2(x) = \phi^*(x)$ and the operator $iD^{-1}_{ab}(x, y)$ is defined by

$$iD^{-1}_{ab}(x, y) = \delta^{d+1}(x - y)\Big(i\sigma^3_{ab}\partial_{x_0} - \delta_{ab}H_{1B}(x)\Big). \tag{4.2}$$

The σ^3 is the third Pauli matrix and H_{1B} is the one-body Hamiltonian,

$$H_{1B} = -\hbar^2\Sigma^d_{i=1}\partial^2_i/2m + V(x)\,, \tag{4.3}$$

where $V(x)$ is an external potential i.e. a trap potential which we neglect from now on. Note that the action in Eq. (4.1) gives back the Gross-Pitaevskii Hamiltonian in Eq. (2.1). However, the action (4.1) has second class constraints, therefore, its Hamiltonian has to be formulated properly if one wishes to recover the dynamic equations of the field variables from the Hamilton equations. This can be seen from an absence of the conjugate-momentum from (2.1). The scheme for treating a constrained system can be found in [100, 101]. The quantum field description is done by promoting the field variables into operators. In the case of Bose fields, operators must satisfy the Bose version of equal-time commutation relations

$$[\Phi(t, \boldsymbol{x}), \Phi^\dagger(t, \boldsymbol{y})] = \delta^d(\boldsymbol{x} - \boldsymbol{y}), \tag{4.4}$$

$$[\Phi(t, \boldsymbol{x}), \Phi(t, \boldsymbol{y})] = [\Phi^\dagger(t, \boldsymbol{x}), \Phi^\dagger(t, \boldsymbol{y})] = 0. \tag{4.5}$$

It will be seen later that the commutation relations do not play any role in the derivation of dynamic equations. Therefore, the Fermion fields will give the same set of the dynamic equations as long as the form of the interaction and the procedure of truncation remain the same. However, the commutation relations is used to determine the properties of the propagators at equal times.

We recall the 2PI effective action from App. B

$$\begin{aligned}\Gamma[\phi, \phi^*, G] =& S[\phi, \phi^*] + \frac{i\hbar}{2}\mathrm{Tr}_{\mathcal{C}} \ln G^{-1} \\ &+ \frac{\hbar}{2}\int^{\mathcal{C}}_{xy} \frac{\delta^2 S[\phi, \phi^*]}{\delta\phi^*_b(y)\delta\phi_a(x)} G_{ab}(x, y) + \Gamma_2[\phi, \phi^*, G],\end{aligned} \tag{4.6}$$

where the symbol $\mathcal{C}$ indicates that the time contour is the Schwinger-Keldysh closed-time loop. We need to calculate the functional derivative of each term in (4.6) with respect to $\phi(x)$ to derive the dynamic equation of the field variable which it can be done explicitly for the first three terms. We start with the first derivative of the

classical action with respect to a field variable and its complex conjugate[2],

$$\begin{aligned}\frac{\delta S[\phi,\phi^*]}{\delta\phi_a^*(x)} &= \frac{1}{2}\int_{uv}^{\mathcal{C}}\Big(\delta_{\mathcal{C}}^{d+1}(x-u)\delta_{ac}\Big(iD_{cd}^{-1}(u,v)\Big)\phi_d(v)\\ &\qquad+\delta_{\mathcal{C}}^{d+1}(x-v)\sigma^1_{ad}\sigma^1_{dm}\Big(iD_{mn}^{-1}(v,u)\Big)\sigma^1_{nc}\phi_c^*(u)\Big)\\ &\qquad-\frac{g}{8}\int_u^{\mathcal{C}}\delta_{\mathcal{C}}^{d+1}(x-u)\Big[\Big(\delta_{ac}\phi_c(u)+\sigma^1_{ac}\phi_c^*(u)\Big)\phi_d^*(u)\phi_d(u)+(c\leftrightarrow d)\Big]\\ &= \frac{1}{2}\Big[\int_v^{\mathcal{C}}\Big(iD_{ad}^{-1}(x,v)\Big)\phi_d(v)+\int_u^{\mathcal{C}}\Big(iD_{an}^{-1}(x,u)\Big)\phi_n(u)\Big]-\frac{g}{2}\phi_a(x)\phi_d^*(x)\phi_d(x)\\ &= \int_u^{\mathcal{C}}\Big(iD_{ad}^{-1}(x,u)\Big)\phi_d(u)-\frac{g}{2}\phi_a(x)\phi_d^*(x)\phi_d(x)\,, \qquad (4.7)\\ \frac{\delta S[\phi,\phi^*]}{\delta\phi_a(x)} &= \int_u^{\mathcal{C}}\sigma^1_{ac}\Big(iD_{cd}^{-1}(x,u)\Big)\sigma^1_{dn}\phi_n^*(u)-\frac{g}{2}\phi_a^*(x)\phi_d^*(x)\phi_d(x)\,. \qquad (4.8)\end{aligned}$$

Since $\phi_1(x)$ and $\phi_2(x)$ are not completely independent (i.e. $\phi_1^*(x)=\phi_2(x)$), we need to modify the functional variation rules,

$$\frac{\delta\phi_a(x)}{\delta\phi_b(y)} = \delta_{\mathcal{C}}^{d+1}(x-y)\delta_{ab}\,, \qquad (4.9)$$

$$\frac{\delta\phi_a^*(x)}{\delta\phi_b(y)} = \frac{\delta\phi_a(x)}{\delta\phi_b^*(y)} = \delta_{\mathcal{C}}^{d+1}(x-y)\sigma^1_{ab}\,, \qquad (4.10)$$

together with the field transformation $\sigma^1_{ab}\phi_b(x)=\phi_a^*(x)$ where σ^1 is the first Pauli matrix. The second derivative can be done in a similar manner,

$$\begin{aligned}&\frac{\delta^2 S[\phi,\phi^*]}{\delta\phi_b^*(y)\delta\phi_a(x)}\\ &\quad= \int_u^{\mathcal{C}}\delta_{bd}\delta_{\mathcal{C}}^{d+1}(y-u)\sigma^1_{ac}\sigma^1_{cm}\Big(iD_{mp}^{-1}(x,u)\Big)\sigma^1_{pd}\sigma^1_{dn}\delta_{nb}\\ &\qquad-\frac{g}{2}\delta_{\mathcal{C}}^{d+1}(x-y)\Big(\delta_{ab}\phi_d(x)\phi_d^*(x)+\phi_a^*(x)(\delta_{bd}\phi_d(x)+\sigma^1_{bd}\phi_d^*(x)\Big)\\ &\quad= iD_{ba}^{-1}(y,x)-g\Big(\frac{\delta_{ab}}{2}\phi_d^*(x)\phi_d(x)+\phi_a^*(x)\phi_b(x)\Big)\delta_{\mathcal{C}}^{d+1}(x-y)\\ &\quad= \delta_{\mathcal{C}}^{d+1}(x-y)\Big(i\sigma^3_{ab}\partial_{x_0}-\delta_{ab}H_{1B}(x)-g[\frac{\delta_{ab}}{2}\phi_d^*(x)\phi_d(x)+\phi_a^*(x)\phi_b(x)]\Big)\,, \qquad (4.11)\end{aligned}$$

[2]The first term in the action can also be written as $\int_{uv}\phi_d(v)[(iD_{dc}^{-1}(v,u))\phi_c(u)]^*$ where the differential operators have been moved to act on $\phi^*(x)$ instead of $\phi(x)$ and we use this form when we need to perform the derivative with respect to $\phi(x)$. Also, we express the $(iD_{dc}^{-1}(v,u))^*$ term by $\sigma^1_{dm}(iD_{mn}^{-1}(v,u))\sigma^1_{nc}$ since $\sigma^1_{dm}\sigma^3_{mn}\sigma^1_{nc}=-\sigma^3_{dc}$ and $\sigma^1_{dm}\delta_{mn}\sigma^1_{nc}=\delta_{dc}$.

$$
\begin{aligned}
&\frac{\delta^2 S[\phi,\phi^*]}{\delta\phi_b(y)\delta\phi_a^*(x)} \\
&\quad = \sigma^1_{bm}\Big(iD^{-1}_{mn}(y,x)\Big)\sigma^1_{na} - g\Big(\frac{\delta_{ab}}{2}\phi_d^*(x)\phi_d(x) + \phi_a(x)\phi_b^*(x)\Big)\delta_{\mathcal{C}}^{d+1}(x-y) \\
&\quad = \delta_{\mathcal{C}}^{d+1}(x-y)\Big(- i\sigma^3_{ab}\partial_{x_0} - \delta_{ab}H_{1B}(x) - g[\frac{\delta_{ab}}{2}\phi_d^*(x)\phi_d(x) + \phi_a(x)\phi_b^*(x)]\Big)\,.
\end{aligned}
\tag{4.12}
$$

For the $\Gamma_2[\phi,\phi^*,G]$ term, we need to decide which 2PI diagrams are going to be kept in the derivation through the process of truncation. The procedure we use follows the context of a large-$\mathcal{N}$ approximation that is commonly used in the theory of $\mathcal{N}$-component fields with an $\mathcal{O}(\mathcal{N})$ symmetry, although in our case, $\mathcal{N}=2$. We keep the Feynman diagrams up to the next-to-leading order (NLO) terms such that the nonlocal diagrams which capture the scattering processes are taken into account. It is necessary to recall that the interaction in $\Gamma_2[\phi,\phi^*,G]$ is determined by $iS_Q/\hbar$, not only by interaction terms in the classical action (4.1). For quartic interaction, S_Q reads

$$
\begin{aligned}
S_Q[\varphi,\varphi^*] &= \frac{1}{3!}\int_{xyz}^{\mathcal{C}} \frac{\delta^3 S}{\delta\phi_c^*(z)\delta\phi_b(y)\delta\phi_a^*(x)}\varphi_a^*(x)\varphi_b(y)\varphi_c^*(z) \\
&\qquad + \frac{1}{4!}\int_{xyzw}^{\mathcal{C}} \frac{\delta^4 S}{\delta\phi_d(w)\delta\phi_c^*(z)\delta\phi_b(y)\delta\phi_a^*(x)}\varphi_a^*(x)\varphi_b(y)\varphi_c^*(z)\varphi_d(w) \\
&= -\frac{g}{2}\int_x^{\mathcal{C}} \Big(\varphi_a(x)\varphi_a^*(x)\Big)\Big(\phi_c(x)\varphi_c^*(x)\Big) - \frac{g}{8}\int_x^{\mathcal{C}} \Big(\varphi_a(x)\varphi_a^*(x)\Big)\Big(\varphi_c(x)\varphi_c^*(x)\Big) \\
&= -\frac{g}{4}\int_x^{\mathcal{C}} \varphi_a(x)\varphi_a^*(x)\Big(\phi_c(x)\varphi_c^*(x) + \phi_c^*(x)\varphi_c(x)\Big) - \frac{g}{8}\int_x^{\mathcal{C}} \varphi_a(x)\varphi_a^*(x)\varphi_c(x)\varphi_c^*(x).
\end{aligned}
\tag{4.13}
$$

There are two types of vertices in $\Gamma_2[\phi,\phi^*,G]$, a 3-point vertex with a field insertion and a 4-point vertex. In the leading order (LO), there is only one possible 2PI-Feynman diagram,

$$
\begin{aligned}
\Gamma_2^{\mathrm{LO}}[G] &= (-i\hbar)\Big(\frac{i}{\hbar}\Big)\Big(-\frac{g}{8}\Big)\int_x^{\mathcal{C}} (\hbar G_{aa}(x,x))(\hbar G_{bb}(x,x)) \\
&= -\frac{g}{8}\hbar^2\int_x^{\mathcal{C}} G_{aa}(x,x)G_{bb}(x,x)\,.
\end{aligned}
\tag{4.14}
$$

In NLO, there is one local diagram,

$$
\Gamma_2^{\mathrm{NLO-Local}}[G] = -\frac{g}{4}\hbar^2\int_x^{\mathcal{C}} G_{ab}(x,x)G_{ba}(x,x)\,,
\tag{4.15}
$$

where we also included the symmetry factor. For the 4-point vertex, the symmetry factors for each of the Feynman diagrams are given by $4^n/2n$ where n is the number

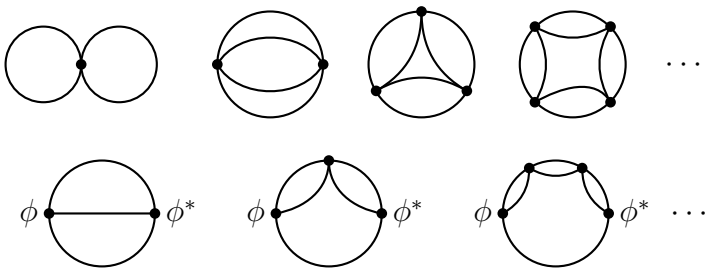

Figure 4.1: 2PI diagrams that contribute to Γ_2 up to NLO. The diagrams in the upper row, except the first double-bubble, are included in $\Gamma_2^{\mathrm{NLO}-4}[G]$. The lower row shows the diagrams contained in $\Gamma_2^{\mathrm{NLO}-3}[\phi,\phi^*,G]$. Note that the number of diagrams in each row is infinite because adding one loop of propagators and one vertex does not change the order in $1/\mathcal{N}$ expansion.

of vertices. The number comes from $(n-1)!$ ways to arrange n vertices into a ring multiplied by 2^{2n-1} possible ways to contract internal indices, and is multiplied by $1/n!$ since n vertices are indistinguishable. As for the nonlocal contributions, there are infinitely many diagrams because the order of the $1/\mathcal{N}$ expansion does not change when adding one loop of propagators and one vertex. However, the diagrams have the systematic structures as shown in Fig. 4.1. We separate the nonlocal contribution into two parts,

$$\Gamma_2^{\mathrm{NLO-Nonlocal}}[\phi,\phi^*,G] = \Gamma_2^{\mathrm{NLO}-4}[G] + \Gamma_2^{\mathrm{NLO}-3}[\phi,\phi^*,G] \tag{4.16}$$

where $\Gamma_2^{\mathrm{NLO}-4}[\phi,\phi^*,G]$ is a series of diagrams that contain only 4-point vertices,

$$\begin{aligned}\Gamma_2^{\mathrm{NLO}-4}[G] = {} & i\frac{\hbar^3}{4}\Big(\frac{g}{2}\Big)^2\int_{xy}^{\mathcal{C}} G_{ab}(x,y)G_{ba}(y,x)G_{cd}(x,y)G_{dc}(y,x) \\ & + \frac{\hbar^4}{6}\Big(\frac{g}{2}\Big)^3\int_{xyz}^{\mathcal{C}} G_{ab}(x,y)G_{ba}(y,x)G_{cd}(y,z)G_{dc}(z,y)G_{ef}(z,x)G_{fe}(x,z) \\ & + \cdots\end{aligned} \tag{4.17}$$

and $\Gamma_2^{\mathrm{NLO}-3}[\phi,\phi^*,G]$, a series of diagrams that have two 3-point vertices with a field insertion,

$$\begin{aligned}\Gamma_2^{\mathrm{NLO}-3}[\phi,\phi^*,G] = {} & i\frac{\hbar^2}{2}\Big(\frac{g}{2}\Big)^2\int_{xy}^{\mathcal{C}} \phi_a(x)\phi_b^*(y)G_{ba}(y,x)G_{cd}(x,y)G_{dc}(y,x) \\ & + \frac{\hbar^3}{2}\Big(\frac{g}{2}\Big)^3\int_{xyz}^{\mathcal{C}} \phi_a(x)\phi_b^*(y)G_{ba}(y,x)G_{cd}(y,z)G_{dc}(z,y)G_{ef}(z,x)G_{fe}(x,z) \\ & + \cdots .\end{aligned} \tag{4.18}$$

The first comes from $\delta\Gamma[\phi,\phi^*,G]/\delta\phi_a^*(x)=0$,

$$\begin{aligned}
0 &= \frac{\delta S[\phi,\phi^*]}{\delta\phi_a^*(x)} + \frac{\hbar}{2}\int_{uv}^{\mathcal{C}} \frac{\delta^3 S[\phi,\phi^*]}{\delta\phi_a^*(x)\delta\phi_d^*(v)\delta\phi_c(u)} G_{cd}(u,v) + \frac{\delta\Gamma_2[\phi,\phi^*,G]}{\delta\phi_a^*(x)} \\
&= \int_u^{\mathcal{C}} \Big(iD_{ad}^{-1}(x,u)\Big)\phi_d(u) - \frac{g}{2}\phi_a(x)\phi_d^*(x)\phi_d(x) \\
&\quad + \frac{\hbar}{2}\int_{uv}^{\mathcal{C}} (-g)\delta_{\mathcal{C}}^{d+1}(u-v)\delta_{\mathcal{C}}^{d+1}(x-u)\Big(\delta_{cd}\phi_a(u) + \sigma_{ac}^1\phi_d^*(u) + \delta_{ad}\phi_c(u)\Big)G_{dc}(v,u) \\
&\quad + \frac{\delta\Gamma_2^{\mathrm{NLO}-3}[\phi,\phi^*,G]}{\delta\phi_a^*(x)} \\
&= \Big(i\sigma_{ad}^3\partial_{x_0} - g\hbar G_{ad}\Big)\phi_d(x) - \Big(H_{1B}(x) + \frac{g}{2}\Big(\phi_c^*(x)\phi_c(x) + \hbar G_{cc}(x,x)\Big)\Big)\phi_a(x) \\
&\quad + \frac{\delta\Gamma_2^{\mathrm{NLO}-3}[\phi,\phi^*,G]}{\delta\phi_a^*(x)}\,,
\end{aligned} \tag{4.19}$$

where the relation $G_{ba}(y,x)=\sigma_{na}^1\sigma_{bm}^1 G_{nm}(x,y)$ is needed.[3] The equations for the propagators can be obtained through the relation $\delta\Gamma[\phi,\phi^*,G]/\delta G_{ab}(x,y)=0$ and the result is identical to Eq. (B.99) (with external non-local currents $K_{ab}=0$),

$$iG_{ba}^{-1}(y,x) = \frac{\delta^2 S[\phi,\phi^*]}{\delta\phi_b^*(y)\delta\phi_a(x)} + \frac{2}{\hbar}\frac{\delta\Gamma_2[\phi,\phi^*,G]}{\delta G_{ab}(x,y)}\,, \tag{4.20}$$

then, multiplying with $G_{ac}(x,z)$ and integrating over the x variable, we get[4]

$$\begin{aligned}
i\int_x^{\mathcal{C}} G_{ba}^{-1}(y,x)G_{ac}(x,z) &= \int_x^{\mathcal{C}} \frac{\delta^2 S[\phi,\phi^*]}{\delta\phi_b^*(y)\delta\phi_a(x)} G_{ac}(x,z) + \frac{2}{\hbar}\int_x^{\mathcal{C}} \frac{\delta\Gamma_2[\phi,\phi^*,G]}{\delta G_{ab}(x,y)} G_{ac}(x,z) \\
i\delta_{bc}\delta_{\mathcal{C}}^{d+1}(y-z) &= \int_y^{\mathcal{C}} iD_{ab}^{-1}(x,y)G_{ac}(x,z) \\
&\quad - g\Big(\frac{\delta_{ab}}{2}\phi_d^*(y)\phi_d(y) + \phi_a^*(y)\phi_b(y)\Big)G_{ac}(y,z) \\
&\quad + \frac{2}{\hbar}\int_x^{\mathcal{C}} \frac{\delta\Gamma_2[\phi,\phi^*,G]}{\delta G_{ab}(x,y)} G_{ac}(x,z)
\end{aligned}$$

[3] Observe that $G_{ba}(y,x) = \langle T_{\mathcal{C}}\Phi_b(y)\Phi_a^\dagger(x)\rangle = \sigma_{bm}^1\langle T_{\mathcal{C}}\Phi_m^\dagger(y)\Phi_n(x)\rangle\sigma_{na}^1 = \sigma_{na}^1\sigma_{bm}^1 G_{nm}(x,y)$, therefore, $\sigma_{ac}^1\phi_d^*(x)G_{dc}(x,x) = \sigma_{ac}^1\phi_d^*(x)\sigma_{nc}^1\sigma_{dm}^1 G_{nm}(x,x) = \phi_m(x)G_{am}(x,x)$ where $\sigma_{ab}^1\sigma_{bc}^1=\delta_{ac}$ has been used.

[4] We chose the definition in Eqs. (4.11) and (4.12) in such a way that the differential operators live at point x. Therefore, it is more straight forward to do the convolution over the point x such that it can be seen that the differential operators always act on different spatio-temporal arguments i.e. $i\partial_{x_0}$ acts on the argument of ϕ and $-i\partial_{x_0}$ acts on the argument ofϕ^*. The convolution over the point y means the differential operators need to operate to the left which can be achieved by moving the operators to the other argument first i.e. $i\partial_{x_0}\to -i\partial_{x_0}$ and then choosing $x=y$ due to $\delta_{\mathcal{C}}^{d+1}(x-y)$.

$$= \Big(i\sigma^3_{ab}\partial_{y_0} - \delta_{ab}[H_{1B}(y) + \frac{g}{2}\phi^*_d(y)\phi_d(y)] - g\phi^*_a(y)\phi_b(y)\Big) G_{ac}(y,z) + \frac{2}{\hbar}\int_x^{\mathcal{C}} \frac{\delta\Gamma_2[\phi,\phi^*,G]}{\delta G_{ab}(x,y)} G_{ac}(x,z)\,, \tag{4.21}$$

where the identity $\int_y^{\mathcal{C}} G^{-1}_{ba}(y,x)G_{ac}(x,z) = \delta_{ac}\delta^{d+1}_{\mathcal{C}}(y-z)$ has been used. It is convenient to separate $\delta\Gamma_2/\delta G_{ba}$ which is proportional to the self-energy into local and non-local contributions,

$$\frac{2i}{\hbar}\frac{\delta\Gamma_2[\phi,\phi^*,G]}{\delta G_{ab}(x,y)} = \Sigma^{\rm local}_{ba}(y,x) + \Sigma_{ba}(y,x)\,. \tag{4.22}$$

The local contribution which contains double-bubble diagrams from both LO and NLO reads

$$\Sigma^{\rm local}_{ba}(y,x) = -i\hbar g\delta^{d+1}_{\mathcal{C}}(y-x)\Big(\frac{\delta_{ba}}{2}G_{cc}(y,y) + G_{ba}(y,y)\Big)\,. \tag{4.23}$$

The effect of the local contribution in self-energy is to shift the mass into an effective mass while the nonlocal contribution represents the scattering processes. The s of propagators then become

$$i\delta_{ac}\delta^{d+1}_{\mathcal{C}}(x-z) = [i\sigma^3_{ab}\partial_{x_0} - M^G_{ab}(x)]G_{bc}(x,z) - i\int_y^{\mathcal{C}} \Sigma_{ab}(x,y)G_{bc}(y,z)\,, \tag{4.24}$$

where the effective mass $M^G_{ab}(x)$ reads

$$M^G_{ab}(x) = \delta_{ab}\Big(H_{1B}(x) + \frac{g}{2}[\phi_d(x)\phi^*_d(x) + \hbar G_{dd}(x,x)]\Big) + g\Big(\phi_a(x)\phi^*_b(x) + \hbar G_{ab}(x,x)\Big)\,. \tag{4.25}$$

In principle, solving the set of coupled integro-differential equations (4.19) and (4.24) gives the field expectation value and propagators as functions of their space-time coordinates in $d+1$ dimensions. However, the task is very formidable in practice due to the complication of integro-differential equations. We are going to show that despite its complexities, we can still extract useful information from these equations by using the knowledge of wave turbulence but we need a further manipulation and approximation in order to write down Boltzmann's integral which is our central equation of the wave turbulence studies.

4.1.2 Dynamical equations of statistical and spectral function

One of the complications in Eqs. (4.19) and (4.24) is the presence of the closed-time contour since it duplicates the number of propagators (the field is identical on the forward and backward branches of the contour but this is not the case for propagators, see Sect. B.1). We are going to decompose propagators which live on the closed-time

contour into two functions where each living on a single time contour. These two functions are the statistical and spectral function defined by

$$F_{ab}(x,y) = \frac{1}{2}\langle\{\Phi_a(x), \Phi_b^\dagger(y)\}\rangle\,, \tag{4.26}$$

$$\rho_{ab}(x,y) = i\langle[\Phi_a(x), \Phi_b^\dagger(y)]\rangle\,, \tag{4.27}$$

where $\{,\}$ and $[,]$ are anti-commutator and commutator respectively. Using the identity $2\Phi_a(x)\Phi_b^\dagger(y) = \{\Phi_a(x), \Phi_b^\dagger(y)\} + [\Phi_a(x), \Phi_b^\dagger(y)]$, one can verify the following relation

$$\begin{aligned} G_{ab}(x,y) &= \theta_{\mathcal{C}}(x^0-y^0)\langle\Phi_a(x)\Phi_b^\dagger(y)\rangle + \theta_{\mathcal{C}}(y^0-x^0)\langle\Phi_b^\dagger(y)\Phi_a(x)\rangle \\ &= \frac{1}{2}\Big(\theta_{\mathcal{C}}(x^0-y^0)\langle\{\Phi_a(x), \Phi_b^\dagger(y)\}\rangle + \theta_{\mathcal{C}}(y^0-x^0)\langle\{\Phi_b^\dagger(y), \Phi_a(x)\}\rangle\Big) \\ &\quad + \frac{1}{2}\Big(\theta_{\mathcal{C}}(x^0-y^0)\langle[\Phi_a(x), \Phi_b^\dagger(y)]\rangle + \theta_{\mathcal{C}}(y^0-x^0)\langle[\Phi_b^\dagger(y), \Phi_a(x)]\rangle\Big) \\ &= F_{ab}(x,y) - \frac{i}{2}\rho_{ab}(x,y)\mathrm{sgn}_{\mathcal{C}}(x^0-y^0)\,, \end{aligned} \tag{4.28}$$

where $\theta_{\mathcal{C}}(x^0)$ is Heaviside function living on the closed-time contour, $\mathrm{sgn}_{\mathcal{C}}(x^0) = \theta_{\mathcal{C}}(x^0) - \theta_{\mathcal{C}}(-x^0)$ and $\theta_{\mathcal{C}}(x^0) + \theta_{\mathcal{C}}(-x^0) = 1$. We also used the symmetry (anti-symmetry) of the anti-commutator (commutator) to combine terms. The self-energy which is a functional of $G_{ab}(x,y)$ is expected to decompose into statistical and spectral components in a similar way

$$\Sigma_{ab}(x,y) = \Sigma^F_{ab}(x,y) - \frac{i}{2}\Sigma^\rho_{ab}(x,y)\mathrm{sgn}_{\mathcal{C}}(x^0-y^0)\,. \tag{4.29}$$

The aim is to replace propagators and self-energy in Eqs. (4.19) and (4.24) into statistical and spectral components. The decomposition allows us to evaluate the term that involves closed-time integration into a single time integration, for example,

$$\begin{aligned} -i\int_y^{\mathcal{C}} &\Sigma_{ab}(x,y)G_{bc}(y,z) \\ &= -i\int_y^{\mathcal{C}}\Big(\Sigma^F_{ab}(x,y)F_{bc}(y,z) - \frac{i}{2}\Sigma^\rho_{ab}(x,y)F_{bc}(y,z)\mathrm{sgn}_{\mathcal{C}}(x^0-y^0) \\ &\quad - \frac{i}{2}\Sigma^F_{ab}(x,y)\rho_{bc}(y,z)\mathrm{sgn}_{\mathcal{C}}(y^0-z^0) \\ &\quad - \frac{1}{4}\Sigma^\rho_{ab}(x,y)\rho_{bc}(y,z)\mathrm{sgn}_{\mathcal{C}}(x^0-y^0)\mathrm{sgn}_{\mathcal{C}}(y^0-z^0)\Big) \\ &= -\int_{t_0}^{x_0} dy\Sigma^\rho_{ab}(x,y)F_{bc}(y,z) + \int_{t_0}^{z_0}\Sigma^F_{ab}(x,y)\rho_{bc}(y,z) \\ &\quad + \frac{i}{2}\int_{z_0}^{x_0} dy\Sigma^\rho_{ab}(x,y)\rho_{bc}(y,z)\mathrm{sgn}_{\mathcal{C}}(x^0-z^0)\,, \end{aligned} \tag{4.30}$$

where the short-hand notation $\int_{t_0}^{z_0} dy$ stands for $\int_{t_0}^{z_0} dy_0 d^d y$. The first term has no signum function and vanishes identically under the closed-time integration. The

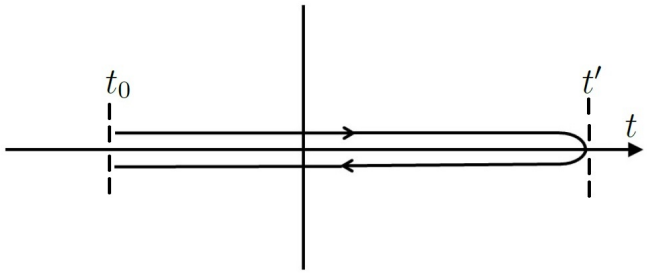

Figure 4.2: Diagram represents the Schwinger-Keldysh closed-time contour. The contour runs from the initial time t_0, to the time t' and goes backward to t_0 again.

other terms have non-zero contribution in a certain window depending on the type of signum function. For example, the second term came from the following evaluation,

$$\begin{aligned}
&\int_y^{\mathcal{C}} \Sigma^{\rho}_{ab}(x,y)F_{bc}(y,z)\mathrm{sgn}_{\mathcal{C}}(x^0-y^0) \\
&\quad = \Big(\int_{t_0}^{x_0} dy + \int_{x_0}^{t'} dy + \int_{t'}^{t_0} dy\Big)\Sigma^{\rho}_{ab}(x,y)F_{bc}(y,z)\mathrm{sgn}_{\mathcal{C}}(x^0-y^0) \\
&\quad = \Big(\int_{t_0}^{x_0} dy(1) + \int_{x_0}^{t'} dy(-1) + \int_{t'}^{x_0} dy(-1) + \int_{x_0}^{t_0} dy(-1)\Big)\Sigma^{\rho}_{ab}(x,y)F_{bc}(y,z) \\
&\quad = \Big(\int_{t_0}^{x_0} dy(1) + \int_{x_0}^{t_0} dy(-1)\Big)\Sigma^{\rho}_{ab}(x,y)F_{bc}(y,z) = 2\int_{t_0}^{x_0} dy\Sigma^{\rho}_{ab}(x,y)F_{bc}(y,z))\,.
\end{aligned} \tag{4.31}$$

Here, the time contour starts at t_0 and the largest time before the closed-time contour turns back is t', see Fig. 4.2. We also assumed that the point x_0 lies in forward time branch, but the result is the same for x_0 living on the backward time branch. Using the same procedure, the last two terms in Eq. (4.30) can be verified

$$\int_y^{\mathcal{C}} \Sigma^{F}_{ab}(x,y)\rho_{bc}(y,z)\mathrm{sgn}_{\mathcal{C}}(y^0-z^0) = -2\int_{t_0}^{z_0} dy\Sigma^{F}_{ab}(x,y)\rho_{bc}(y,z)\,, \tag{4.32}$$

$$\begin{aligned}
&\int_y^{\mathcal{C}} \Sigma^{\rho}_{ab}(x,y)\rho_{bc}(y,z)\mathrm{sgn}_{\mathcal{C}}(x^0-y^0)\mathrm{sgn}_{\mathcal{C}}(y^0-z^0) \\
&\qquad\qquad = 2\int_{z_0}^{x_0} dy\Sigma^{\rho}_{ab}(x,y)\rho_{bc}(y,z)\mathrm{sgn}_{\mathcal{C}}(x^0-z^0)\,.
\end{aligned} \tag{4.33}$$

The decomposition of Eq. (4.24) can be separated into two equations arising from its real and imaginary parts

$$[i\sigma^3_{ab}\partial_{x_0} - M_{ab}(x)]F_{bc}(x,z) = \int_{t_0}^{x_0} dy\Sigma^{\rho}_{ab}(x,y)F_{bc}(y,z) - \int_{t_0}^{z_0} dy\Sigma^{F}_{ab}(x,y)\rho_{bc}(y,z)\,, \tag{4.34}$$

$$[i\sigma^3_{ab}\partial_{x_0} - M_{ab}(x)]\rho_{bc}(x,z) = \int_{z_0}^{x_0} dy\Sigma^{\rho}_{ab}(x,y)\rho_{bc}(y,z)\,, \tag{4.35}$$

where the effective mass now reads

$$M_{ab}(x) = \delta_{ab}\Big(H_{1B}(x) + \frac{g}{2}[\phi_d(x)\phi_d^*(x) + \hbar F_{dd}(x,x)]\Big) + g\Big(\phi_a(x)\phi_b^*(x) + \hbar F_{ab}(x,x)\Big)\,. \tag{4.36}$$

We had neglected all terms that have $\mathrm{sgn}_{\mathcal{C}}(x^0 - x^0)$ since the signum function is an anti-symmetric function and the following result is also needed,

$$\begin{aligned} -i\sigma^3_{ab}\rho_{bc}(x,z)\partial_{x_0}\mathrm{sgn}_{\mathcal{C}}(x^0 - z^0) &= 2\delta_{\mathcal{C}}(x^0 - z^0)\langle[\sigma^3_{ab}\Phi_b(x), \Phi_c^\dagger(z)]\rangle \\ &= 2\delta_{\mathcal{C}}(x^0 - z^0)\langle[\sigma^3_{a1}\Phi_1(x^0,\boldsymbol{x}), \Phi_c^\dagger(x^0,\boldsymbol{z})] + [\sigma^3_{a2}\Phi_2(x^0,\boldsymbol{x}), \Phi_c^\dagger(x^0,\boldsymbol{z})]\rangle \\ &= 2\delta_{\mathcal{C}}(x^0 - z^0)\delta_{ac}\delta^d_{\mathcal{C}}(\boldsymbol{x} - \boldsymbol{z}) = 2\delta_{ac}\delta^{d+1}_{\mathcal{C}}(x - z)\,. \end{aligned} \tag{4.37}$$

This term will cancel out with the LHS of Eq. (4.24). For the further usage, instead of Eq. (4.20), we may start with the relation

$$iG^{-1}_{ab}(x,y) = \frac{\delta^2 S[\phi,\phi^*]}{\delta\phi_b(y)\delta\phi_a^*(x)} + \frac{2}{\hbar}\frac{\delta\Gamma_2[\phi,\phi^*,G]}{\delta G_{ba}(y,x)}\,, \tag{4.38}$$

and its convolution,

$$i\int_x^{\mathcal{C}} G^{-1}_{ab}(x,y)G_{ca}(z,x) = \int_x^{\mathcal{C}}\Big(\frac{\delta^2 S[\phi,\phi^*]}{\delta\phi_b(y)\delta\phi_a^*(x)} + \frac{2}{\hbar}\frac{\delta\Gamma_2[\phi,\phi^*,G]}{\delta G_{ba}(y,x)}\Big)G_{ca}(z,x)\,, \tag{4.39}$$

in order to obtain of $G_{ca}(z,x)$,

$$i\delta_{ac}\delta^{d+1}_{\mathcal{C}}(x - z) = [-i\sigma^3_{ba}\partial_{x_0} - M^G_{ba}(x)]G_{cb}(z,x) - i\int_y^{\mathcal{C}}\Sigma_{ba}(y,x)G_{cb}(z,y)\,. \tag{4.40}$$

It should be noted that the differential operator now acts on the second arguments of the propagator and that equation gives us another set of equations of F and ρ,

$$[-i\sigma^3_{ba}\partial_{x_0} - M_{ba}(x)]F_{cb}(z,x) = -\int_{t_0}^{x_0} dy\Sigma^\rho_{ba}(y,x)F_{cb}(z,y) + \int_{t_0}^{z_0} dy\Sigma^F_{ba}(y,x)\rho_{cb}(z,y)\,, \tag{4.41}$$

$$[-i\sigma^3_{ba}\partial_{x_0} - M_{ba}(x)]\rho_{cb}(z,x) = \int_{x_0}^{z_0} dy\Sigma^\rho_{ba}(y,x)\rho_{cb}(z,y)\,, \tag{4.42}$$

which are the conjugate equations of Eqs. (4.34) and (4.35).

4.1.3 Stationarity condition

From Eqs. (4.34) and (4.35), we next derive the expressions in momentum space for our later derivation of the kinetic equation. We firstly send t_0 into the infinite past, $t_0 \to -\infty$, based on an assumption that we are interested in late-time dynamics of

the system, not the early time where instabilities are dominant processes [48, 102]. Eqs. (4.34) and (4.35) can be rewritten with the help of the Heaviside function

$$\begin{aligned}
&[i\sigma^3_{ac}\partial_{x_0} - M_{ac}(x)]F_{cb}(x,y) \\
&\qquad = \int_z \theta(x_0-z_0)\Sigma^\rho_{ac}(x,z)F_{cb}(z,y) - \int_z \theta(y_0-z_0)\Sigma^F_{ac}(x,z)\rho_{cb}(z,y) \\
&\qquad = \int_z \Sigma^R_{ac}(x,z)F_{cb}(z,y) + \int_z \Sigma^F_{ac}(x,z)G^A_{cb}(z,y)\,, \qquad (4.43) \\
&[i\sigma^3_{ac}\partial_{x_0} - M_{ac}(x)]\rho_{cb}(x,y) \\
&\qquad = \int_z \theta(x_0-z_0)\Sigma^\rho_{ac}(x,z)\rho_{cb}(z,y) - \int_z \theta(y_0-z_0)\Sigma^\rho_{ac}(x,z)\rho_{cb}(z,y) \\
&\qquad = \int_z \Sigma^R_{ac}(x,z)\rho_{cb}(z,y) + \int_z \Sigma^\rho_{ac}(x,z)G^A_{cb}(z,y)\,, \qquad (4.44)
\end{aligned}$$

where we have defined

$$G^R_{ab}(x,y) = \theta(x_0-y_0)\rho_{ab}(x,y)\,, \qquad (4.45)$$
$$G^A_{ab}(x,y) = -\theta(y_0-x_0)\rho_{ab}(x,y)\,, \qquad (4.46)$$

and the same applies for Σ^ρ to obtain Σ^R and Σ^A. Similar results can be retrieved from Eqs. (4.41) and (4.42),

$$[-i\sigma^3_{ca}\partial_{y_0} - M_{ca}(y)]F_{bc}(x,y) = \int_z \Sigma^A_{ca}(z,y)F_{bc}(x,z) + \int_z \Sigma^F_{ca}(z,y)G^R_{bc}(x,z)\,, \qquad (4.47)$$
$$[-i\sigma^3_{ca}\partial_{y_0} - M_{ca}(y)]\rho_{bc}(x,y) = \int_z \Sigma^A_{ca}(z,y)\rho_{bc}(x,z) + \int_z \Sigma^\rho_{ca}(z,y)G^R_{bc}(x,z)\,. \qquad (4.48)$$

In the homogeneous situation, the dynamics of $F_{ab}(x,y)$ and $\rho_{ab}(x,y)$ do not depend directly on local points (x,y) but rather on the distance between x and y, therefore, it is more appropriate to use Wigner coordinates to change the local coordinate into center and relative coordinates u and s where

$$u = \frac{1}{2}(x+y)\,, \qquad s = x-y\,. \qquad (4.49)$$

Using the simple chain-rule, one can verify that $\partial_x = \frac{1}{2}\partial_u + \partial_s\,, \partial_y = \frac{1}{2}\partial_u - \partial_s$. Although we claimed the homogeneous nature of $F_{ab}(x,y)$ and $\rho_{ab}(x,y)$ which means only relative coordinate s are relevant, we still wish to keep the center-time coordinate u_0 and say this is the time variable for the observable dynamics. Therefore, we're looking for the dynamics of $F_{ab}(x,y)$ and $\rho_{ab}(x,y)$ with respect to this center time

u_0. Taking Eqs. (4.43) and (4.47) and rewriting them in Wigner coordinates gives

$$\begin{aligned}
&\Big[i\sigma^3_{ac}(\frac{1}{2}\partial_{u_0}+\partial_{s_0})-M_{ac}(u+\frac{s}{2})\Big]F_{cb}(u,s)\\
&\qquad=\int_{s'}\Sigma^R_{ac}(u+\frac{s'}{2},s-s')F_{cb}(u+\frac{s'-s}{2},s')\\
&\qquad\quad+\int_{s'}\Sigma^F_{ac}(u+\frac{s'}{2},s-s')G^A_{cb}(u+\frac{s'-s}{2},s')\,, \qquad (4.50)\\
&\Big[-i\sigma^3_{ca}(\frac{1}{2}\partial_{u_0}-\partial_{s_0})-M_{ca}(u-\frac{s}{2})\Big]F_{bc}(u,s)\\
&\qquad=\int_{s'}\Sigma^A_{ca}(u+\frac{s'-s}{2},s')F_{bc}(u+\frac{s'}{2},s-s')\\
&\qquad\quad+\int_{s'}\Sigma^F_{ca}(u+\frac{s'-s}{2},s')G^R_{bc}(u+\frac{s'}{2},s-s')\\
&\qquad=\int_{s'}\Sigma^A_{ca}(u-\frac{s'}{2},s-s')F_{bc}(u-\frac{s'-s}{2},s')\\
&\qquad\quad+\int_{s'}\Sigma^F_{ca}(u-\frac{s'}{2},s-s')G^R_{bc}(u-\frac{s'-s}{2},s')\,, \qquad (4.51)
\end{aligned}$$

where we have defined $s'=z-y$ and as a consequence $x-z=s-s'$, $(x+z)/2=u+s'/2$ and $(z+y)/2=u+(s'-s)/2$. The first and second arguments of all functions are now their center and relative coordinates respectively. Subtracting Eq. (4.50) with Eq. (4.51) yields

$$\begin{aligned}
&\frac{i}{2}\partial_{u_0}[\sigma^3_{ac}F_{cb}(u,s)+\sigma^3_{ca}F_{bc}(u,s)]-[M_{ac}(u+\frac{s}{2})F_{cb}(u,s)-M_{ca}(u-\frac{s}{2})F_{bc}(u,s)]\\
&\qquad=\int_{s'}\Big[\Sigma^R_{ac}(u+\frac{s'}{2},s-s')F_{cb}(u+\frac{s'-s}{2},s')\\
&\qquad\qquad-\Sigma^A_{ca}(u-\frac{s'}{2},s-s')F_{bc}(u-\frac{s'-s}{2},s')\Big]\\
&\qquad\quad+\int_{s'}\Big[\Sigma^F_{ac}(u+\frac{s'}{2},s-s')G^A_{cb}(u+\frac{s'-s}{2},s')\\
&\qquad\qquad-\Sigma^F_{ca}(u-\frac{s'}{2},s-s')G^R_{bc}(u-\frac{s'-s}{2},s')\Big]\,. \qquad (4.52)
\end{aligned}$$

We then would like to keep only leading-order terms in a gradient expansion in the center coordinate, for example, we approximate $M_{ab}(u\pm s/2)\approx M_{ab}(u)$. All spatial components of the center coordinate will also be neglected due to the homogeneity assumption. Then, Eq. (4.52) becomes

$$\begin{aligned}
&\frac{i}{2}\partial_{u_0}[\sigma^3_{ac}F_{cb}(u_0,s)+\sigma^3_{ca}F_{bc}(u_0,s)]-[M_{ac}(u_0)F_{cb}(u_0,s)-M_{ca}(u_0)F_{bc}(u,s)]\\
&\qquad=\int_{s'}\Big[\Sigma^R_{ac}(u_0,s-s')F_{cb}(u_0,s')-\Sigma^A_{ca}(u_0,s-s')F_{bc}(u_0,s')\Big]\\
&\qquad\quad+\int_{s'}\Big[\Sigma^F_{ac}(u_0,s-s')G^A_{cb}(u_0,s')-\Sigma^F_{ca}(u_0,s-s')G^R_{bc}(u_0,s')\Big]\,. \qquad (4.53)
\end{aligned}$$

Lastly, we trace over the whole equation and combine the terms in the each square brackets,

$$i\partial_{u_0}\sigma^3_{ac}F_{ca}(u_0,s)=\int_{s'}\Big[\Sigma^\rho_{ac}(u_0,s-s')F_{ca}(u_0,s')-\Sigma^F_{ac}(u_0,s-s')\rho_{ca}(u_0,s')\Big]\,, \tag{4.54}$$

$$i\partial_t\sigma^3_{ac}F_{ca}(t,p_0,\boldsymbol{p})=\Sigma^\rho_{ac}(t,p_0,\boldsymbol{p})F_{ca}(t,p_0,\boldsymbol{p})-\Sigma^F_{ac}(t,p_0,\boldsymbol{p})\rho_{ca}(t,p_0,\boldsymbol{p})\,, \tag{4.55}$$

where we have performed a Fourier transform $(s_0,\boldsymbol{s})\to(p_0,\boldsymbol{p})$ in the last equation and relabelled u_0 with t. Since the statistical function F contains the information of number occupation, the fixed-point of the occupation number is determined by a vanishing the RHS in Eq. (4.55),

$$\Sigma^\rho_{ac}(t,p_0,\boldsymbol{p})F_{ca}(t,p_0,\boldsymbol{p})-\Sigma^F_{ac}(t,p_0,\boldsymbol{p})\rho_{ca}(t,p_0,\boldsymbol{p})=0\,. \tag{4.56}$$

This is the stationarity condition for the number occupation and one of the solutions that satisfies this condition is the thermal solution.

In thermal equilibrium the statistical and spectral functions are related by a fluctuation-dissipation relation

$$F_T(p_0,\boldsymbol{p})=-i\Big(n_{\rm BE}(p_0)+\frac{1}{2}\Big)\rho_T(p_0,\boldsymbol{p})\,, \tag{4.57}$$

where $n_{\rm BE}(p_0)$ is the Bose-Einstein distribution function, $n_{\rm BE}(p_0)=[\exp(\beta p_0)-1]^{-1}$. In this limit, the statisical and spectral components of the self-energy also share the same relation,

$$\Sigma^F_T(p_0,\boldsymbol{p})=-i\Big(n_{\rm BE}(p_0)+\frac{1}{2}\Big)\Sigma^\rho_T(p_0,\boldsymbol{p})\,. \tag{4.58}$$

Thus, in thermal equilibrium, the stationary condition (4.56) is fulfilled [48]. We will show lateron that Eq. (4.55) can be turned into the kinetic equation, such that other solutions satisfying the stationary condition will be power-law functions associated with turbulent cascades.

The same procedure could be applied to the equation for $\rho_{ab}(x,y)$. In Wigner coordinates, Eqs. (4.44) and (4.48) read

$$\begin{aligned}\Big[i\sigma^3_{ac}(\frac{1}{2}\partial_{u_0}+\partial_{s_0})-M_{ac}(u+\frac{s}{2})\Big]\rho_{cb}(u,s)&\\ =\int_{s'}\Sigma^R_{ac}(u+\frac{s'}{2},s-s')\rho_{cb}(u+\frac{s'-s}{2},s')&\\ +\int_{s'}\Sigma^\rho_{ac}(u+\frac{s'}{2},s-s')G^A_{cb}(u+\frac{s'-s}{2},s')\,,&\end{aligned} \tag{4.59}$$

$$\begin{aligned}\Big[-i\sigma^3_{ca}(\frac{1}{2}\partial_{u_0}-\partial_{s_0})-M_{ca}(u-\frac{s}{2})\Big]\rho_{bc}(u,s)&\\ =\int_{s'}\Sigma^A_{ca}(u-\frac{s'}{2},s-s')\rho_{bc}(u-\frac{s'-s}{2},s')&\\ +\int_{s'}\Sigma^\rho_{ca}(u-\frac{s'}{2},s-s')G^R_{bc}(u-\frac{s'-s}{2},s')\,.&\end{aligned} \tag{4.60}$$

Following the same approximations and exactly the same steps as we have done for $F_{ab}(p)$, we obtain the equation of motion of $\rho_{ab}(p)$ in the center time coordinate,

$$i\partial_{u_0}\sigma^3_{ac}\rho_{ca}(u_0,s) = \int_{s'}\Big[\Sigma^\rho_{ac}(u_0,s-s')\rho_{ca}(u_0,s') - \Sigma^\rho_{ac}(u_0,s-s')\rho_{ca}(u_0,s')\Big] = 0\,, \tag{4.61}$$

$$i\partial_t\sigma^3_{ac}\rho_{ca}(t,p_0,\boldsymbol{p}) = 0\,, \tag{4.62}$$

where we again relabelled u_0 by t. Eq. (4.62) reveals that $\rho_{ab}(p)$ is a constant during the time evolution. This is a very essential point for the rest of the discussion because $\rho_{ab}(p)$ can be approximated with some ansatz and will then remain the same for a certain window of time as long as Eqs. (4.55) and (4.62) are valid.

4.2 The s-channel resummation of the self-energy and Boltzmann's scattering integral

So far, $\Sigma_{ab}(x,y)$ was treated as a nonlocal contribution of the self-energy and the derivations were made without explicit functional forms. Therefore, as long as the self-energy contains the nonlocal contribution and if the homogeneity assumption can be made, the stationarity condition (4.56) should be valid. However, to render stationarity condition into Boltzmann's scattering integral, one needs a specific form of the self-energy. In the following, we are going to analytically sum the Feynman diagrams up to NLO and derive an integral equation that closely resembles Boltzmann's integral.

We recall the nonlocal contribution of the self energy,

$$\begin{aligned}\Sigma_{ab}(x,y) &= \frac{2i}{\hbar}\frac{\delta\Gamma^{\mathrm{NLO}-4}}{\delta G_{ba}(y,x)}\\ &= -\hbar g G_{ab}(x,y)I(y,x)\,,\end{aligned} \tag{4.63}$$

where $I(y,x)$ is defined by

$$I(y,x) = \frac{\hbar g}{2}\Big[G_{cd}(x,y)G_{dc}(y,x) - i\int_w^{\mathcal{C}} I(y,w)G_{cd}(w,x)G_{dc}(x,w)\Big]\,. \tag{4.64}$$

We have neglected the contribution from $\Gamma^{\mathrm{NLO}-3}$ by claiming that the integral generated from $\Gamma^{\mathrm{NLO}-4}$ dominates when we compare their scaling behaviour [49]. Each term in $\delta\Gamma^{\mathrm{NLO}-4}/\delta G_{ba}(x,y)$ can be retrieved by iteration of $I(x,y)$. We then decompose $\Sigma_{ab}(x,y)$ to find its $\Sigma^F_{ab}(x,y)$ and $\Sigma^\rho_{ab}(x,y)$ components

$$\Sigma^F_{ab}(x,y) = -\hbar g\Big[F_{ab}(x,y)I^F(y,x) + \frac{1}{4}\rho_{ab}(x,y)I^\rho(y,x)\Big]\,, \tag{4.65}$$

$$\Sigma^\rho_{ab}(x,y) = -\hbar g\Big[\rho_{ab}(x,y)I^F(y,x) - F_{ab}(x,y)I^\rho(x,y)\Big]\,, \tag{4.66}$$

where we have decomposed $I(y,x)$ in the same way,

$$I(y,x) = I^F(y,x) - \frac{i}{2} I^\rho(y,x)\mathrm{sgn}_\mathcal{C}(y^0 - x^0)\,. \tag{4.67}$$

The statistical and spectral components of $I(x,y)$ can be obtained by decomposing both $G_{ab}(x,y)$ and $I(x,y)$ itself in Eq. (4.64),

$$\begin{aligned} I(y,x) = \hbar g\Big\{ &\Pi^F(y,x) + \frac{i}{2}\Pi^\rho(y,x)\mathrm{sgn}_\mathcal{C}(y^0 - x^0) \\ &- i\int_w^\mathcal{C} \Big[\Pi^F(w,x)I^F(y,w) - \frac{1}{4}\Pi^\rho(w,x)I^\rho(y,w)\mathrm{sgn}_\mathcal{C}(w^0 - x^0)\mathrm{sgn}_\mathcal{C}(y^0 - w^0) \\ &\quad - \frac{i}{2}\Pi^F(w,x)I^\rho(y,w)\mathrm{sgn}_\mathcal{C}(y^0 - w^0) \\ &\quad - \frac{i}{2}\Pi^\rho(w,x)I^F(y,w)\mathrm{sgn}_\mathcal{C}(w^0 - x^0)\Big]\Big\}\,, \end{aligned} \tag{4.68}$$

where we have defined

$$\Pi^F(y,x) = \frac{1}{2}\Big[F_{cd}(x,y)F_{dc}(y,x) + \frac{1}{4}\rho_{cd}(x,y)\rho_{dc}(y,x)\Big]\,, \tag{4.69}$$

$$\Pi^\rho(y,x) = \frac{1}{2}\Big[\rho_{cd}(x,y)F_{dc}(y,x) - F_{cd}(x,y)\rho_{dc}(y,x)\Big]\,. \tag{4.70}$$

The closed-time integration is treated in the same way as we have done with Eq. (4.30). Then, we can read off $I^F(y,x)$ and $I^\rho(y,x)$ from its real and imaginary parts,

$$I^F(y,x) = \Pi^F(y,x) - \int_{t_0}^{y_0} dw \Pi^F(w,x)I^\rho(y,w) + \int_{t_0}^{x_0} \Pi^\rho(w,x)I^F(y,w)\,, \tag{4.71}$$

$$I^\rho(y,x) = \Pi^\rho(y,x) + \int_{y_0}^{x_0} dw \Pi^\rho(w,x)I^\rho(y,w)\,. \tag{4.72}$$

These equations are necessary for writing down Σ^F and Σ^ρ as an infinite sum in terms of F and ρ in configuration space. However, we would like to have all expressions in momentum space so they can be substituted into Eq. (4.55). Before doing so, we introduce the multiplication $(\cdot)$ and convolution $(*)$ operators

$$(f\cdot g)(x) = f(x)g(-x)\,, \tag{4.73}$$

$$(f * g)(x) = \int_y f(x-y)g(-y)\,, \tag{4.74}$$

and it can be seen that these two operators are related through a Fourier transform,

$$\begin{aligned} (f\cdot g)(x) &= \int \frac{d^{d+1}p}{(2\pi)^{d+1}} e^{-ipx}\Big[\int \frac{d^{d+1}q}{(2\pi)^{d+1}} f(p-q)g(-q)\Big] \\ &= \int \frac{d^{d+1}p}{(2\pi)^{d+1}} e^{-ipx}(f*g)(p)\,, \end{aligned} \tag{4.75}$$

$$\begin{aligned} (f * g)(x) &= \int \frac{d^{d+1}p}{(2\pi)^{d+1}} e^{-ipx} f(p)g(-p) \\ &= \int \frac{d^{d+1}p}{(2\pi)^{d+1}} e^{-ipx}(f\cdot g)(p)\,, \end{aligned} \tag{4.76}$$

where $\int_q$ needs to include a factor $1/(2\pi)^{d+1}$ if q is a variable in momentum space. The homogeneity is also needed to be taken into account such that we can choose Wigner coordinates and write Eqs. (4.71) and (4.72) in terms of $\cdot$ and $*$ operators. Here, we will drop the center coordinate arguments because the Fourier transform will be done only on relative coordinate variables. The center time variable remains untouched by the calculation we are going to do. We again define $s = x - y$ and $s' = w - y$ which implies $x - w = s - s'$. Eqs. (4.71) and (4.72) become

$$\begin{aligned} I^F(-s) &= \hbar g\Big[\Pi^F(-s) - \int_{s'} \theta(-s'^0) I^\rho(-s')\Pi^F(s'-s) \\ &\qquad + \int_{s'} \theta(s^0 - s'^0) I^F(-s')\Pi^\rho(s'-s)\Big] \\ &= \hbar g\Big\{\Pi^F(-s) - [\Pi^F * (\theta^- \cdot I^\rho)](-s) + [(\theta\cdot\Pi^\rho) * I^F](s)\Big\}, \qquad (4.77) \\ I^\rho(-s) &= \hbar g\Big[\Pi^\rho(-s) - \int_{s'} \theta(-s'^0) I^\rho(-s')\Pi^\rho(s'-s) \\ &\qquad + \int_{s'} \theta(s^0 - s'^0) I^\rho(-s')\Pi^\rho(s'-s)\Big] \\ &= \hbar g\Big\{\Pi^\rho(-s) - [\Pi^\rho * (\theta^- \cdot I^\rho)](-s) + [(\theta\cdot\Pi^\rho) * I^\rho](s)\Big\}, \qquad (4.78) \end{aligned}$$

where the Fourier transform of $\Pi^F(u,s)$ and $\Pi^\rho(u,s)$ in relative coordinates s are derived from Eqs. (4.69) and (4.70) (the center coordinates also drop out),

$$\Pi^F(-p) = \frac{1}{2}\Big[(F_{cd} * F_{dc})(p) + \frac{1}{4}(\rho_{cd} * \rho_{dc})(p)\Big], \qquad (4.79)$$

$$\Pi^\rho(-p) = \frac{1}{2}\Big[(\rho_{cd} * F_{dc})(p) - (F_{cd} * \rho_{dc})(p)\Big]. \qquad (4.80)$$

We can read off the Fourier transform of Eq. (4.78) directly from the relationships between $\cdot$ and $*$ operators,

$$\begin{aligned} I^F(-p) &= \hbar g\Big\{\Pi^F(-p) - [\Pi^F \cdot (\theta^- * I^\rho)](-p) + [(\theta * \Pi^\rho)\cdot I^F](p)\Big\} \\ &= \hbar g\Big\{[1 - (\theta^- * I^\rho)(p)]\Pi^F(-p) + (\theta * \Pi^\rho)(p) I^F(-p)\Big\}, \qquad (4.81) \\ I^\rho(-p) &= \hbar g\Big\{[1 - (\theta^- * I^\rho)(p)]\Pi^\rho(-p) + (\theta * \Pi^\rho)(p) I^\rho(-p)\Big\}, \qquad (4.82) \\ & \qquad (4.83) \end{aligned}$$

where the initial time t_0 is sent to the infinite past, $t_0 \to -\infty$. The terms can be

rearranged to obtain

$$gI^F(-p) = \hbar g^2\Big[\frac{1-(\theta^-*I^\rho)(p)}{1-g\hbar(\theta*\Pi^\rho)(p)}\Big]\Pi^F(-p)$$
$$= \hbar\Pi^F(-p)g^2_{\rm eff}(p) \qquad = \hbar(\Pi^F\cdot g^2_{\rm eff})(-p)\,, \tag{4.84}$$
$$gI^\rho(-p) = \hbar g^2\Big[\frac{1-(\theta^-*I^\rho)(p)}{1-g\hbar(\theta*\Pi^\rho)(p)}\Big]\Pi^\rho(-p)$$
$$= \hbar\Pi^\rho(-p)g^2_{\rm eff}(p) \qquad = \hbar(\Pi^\rho\cdot g^2_{\rm eff})(-p)\,, \tag{4.85}$$

where we have defined the effective coupling $g^2_{\rm eff}(p)$ by

$$g^2_{\rm eff}(p) = g^2\Big[\frac{1-(\theta^-*I^\rho)(p)}{1-g\hbar(\theta*\Pi^\rho)(p)}\Big]. \tag{4.86}$$

To write the effective coupling in a more compact form, one needs to verify the identity

$$\Big[1-g\hbar(\theta*\Pi^\rho)(-p)\Big]\Big[1-(\theta^-*I^\rho)(p)\Big] = 1, \tag{4.87}$$

observing that $(\theta*\Pi^\rho)(-p) = (\theta*\Pi^\rho)^*(p)$. Distributing the terms and then transforming the equation back into the configuration space yields

$$\begin{aligned}0 &= -\hbar g(\theta\cdot\Pi^\rho)(-x) + g\hbar[(\theta\cdot\Pi^\rho)*(\theta^-\cdot I^\rho)](-x) - (\theta^-\cdot I^\rho)(x)\\
&= -\hbar g\theta(-x_0)\Pi^\rho(x) + \hbar g\int_y \theta(-x_0+y_0)\Pi^\rho(-y+x)\theta^-(y_0)I^\rho(-y)\\
&\quad + \hbar g\Big[-\theta^-(x_0)\Pi^\rho(-x) - \int_y \theta(-x_0)I^\rho(-y)\theta(x_0-y_0)\Pi^\rho(y-x)\\
&\quad + \int_y \theta(-x_0)\theta(-y_0)I^\rho(-y)\Pi^\rho(y-x)\Big]\\
&= \hbar g\Big[-\int_{-\infty}^{x_0}dy + \int_{-\infty}^{0}dy - \int_{x_0}^{0}dy\Big]I^\rho(-y)\Pi^\rho(y-x)\theta(-x_0) = 0\,,\end{aligned} \tag{4.88}$$

where Eq. (4.82) is needed to expand the third term in the first equality and the symmetry relation of $\Pi^\rho(x)$ are necessary for changing $x\to -x$. With the identity having been proved, we can claim

$$1-(\theta^-*I^\rho)(p) = \frac{1}{1-g\hbar(\theta*\Pi^\rho)(-p)}\,, \tag{4.89}$$

and redefine $g^2_{\rm eff}(p)$,

$$g^2_{\rm eff}(p) = \frac{g^2}{|1+g\hbar\Pi^R(p)|^2}\,, \tag{4.90}$$

where the retarded self-energy Π^R is $\Pi^R(s) = -\theta(s)\Pi^\rho(-s)$ in configuration space which becomes $\Pi^R(p) = -(\theta*\Pi^\rho)(p)$ in momentum space. By introducing the effective coupling, I^F and I^ρ can be resummed to a single term instead of infinite terms and it becomes much easier to manage despite the fact that evaluation of

the effective coupling itself is still complicated. The last approximation we need is a classical approximation saying that the statistical component of the propagator is much larger than its spectral component. This approximation is expected to be satisfied with sufficiently large occupation numbers and the dynamics are dominated by the Feynman diagrams with classical vertices [103]. Under such a condition, all spectral components can be neglected if there is a statistical component with an equal power. To be precise, we make following approximations

$$\Pi^F(x,y) \approx F_{cd}(x,y)F_{dc}(y,x)\,, \tag{4.91}$$
$$\Sigma^F_{ab}(x,y) \approx -\hbar g F_{ab}(x,y)I^F(y,x)\,. \tag{4.92}$$

Then, Σ^F and Σ^ρ in momentum space now read

$$\Sigma^F_{ab}(p) = -\hbar g(F_{ab} * I^F)(p)\,, \tag{4.93}$$
$$\Sigma^\rho_{ab}(p) = -\hbar g(\rho_{ab} * I^F - F_{ab} * I^\rho)(p)\,. \tag{4.94}$$

Substituting the results from Eqs. (4.84) and (4.85) into Eqs. (4.93) and (4.94), then expanding the $\cdot$ and $*$ operators into the product and convolution will give integrals over momenta. For example, Eq. (4.93) yields

$$\begin{aligned}
\Sigma^F_{ab}(p) &= -\hbar g \int_k F_{ab}(p-k)I^F(-k) \\
&= -\frac{\hbar^2}{2}\int_k F_{ab}(p-k)g^2_{\rm eff}(k)(F_{cd}*F_{dc})(-k) \\
&= -\frac{\hbar^2}{2}\int_k F_{ab}(p-k)g^2_{\rm eff}(k)(F_{cd}*F_{dc})(k) \\
&= -\frac{\hbar^2}{2}\int_k\int_q F_{ab}(p-k)g^2_{\rm eff}(k)F_{cd}(k-r)F_{dc}(-r) \\
&= -\frac{\hbar^2}{2}\int_k\int_q g^2_{\rm eff}(p+k)F_{ab}(-k)F_{cd}(p+k-r)F_{dc}(-r) \\
&= -\frac{(2\pi)^{d+1}\hbar^2}{2}\int_{kqr}\delta^{d+1}(p+k-q-r)g^2_{\rm eff}(p+k)F_{ab}(-k)F_{cd}(q)F_{dc}(-r)\,,
\end{aligned} \tag{4.95}$$

where we have used the symmetry $\Pi^F(-p) = \Pi^F(p)$ in the third equality, changed the variable k to $p+k$ in the fifth equality and introduced an integral over r and a delta function in the last equality. The results can be obtained for $\Sigma^\rho_{ab}(p)$,

$$\begin{aligned}
\Sigma^\rho_{ab}(p) = -\frac{(2\pi)^{d+1}\hbar^2}{2}\int_{kqr}&\delta^{d+1}(p+k-q-r)g^2_{\rm eff}(p+k) \\
&\times\Big[\rho_{ab}(-k)F_{cd}(q)F_{dc}(-r) + F_{ab}(-k)\rho_{cd}(q)F_{dc}(-r) \\
&\qquad - F_{ab}(-k)F_{cd}(q)\rho_{dc}(-r)\Big]\,,
\end{aligned} \tag{4.96}$$

where the symmetry $\Pi^\rho(-p) = \Pi^\rho(p)$ has been used too. Putting Eqs. (4.95) and (4.96) back into the RHS of Eq. (4.55) to obtain the kinetic equation for $F_{ab}(p)$

$$\begin{aligned} i\partial_t \sigma^3_{ac} F_{ca}(t, p_0, \boldsymbol{p}) = -\frac{(2\pi)^{d+1}\hbar^2}{2} \int_{kqr} \delta^{d+1}(p+k-q-r) g^2_{\text{eff}}(p+k) \\ \times \{ F_{ba}(p)\rho_{ab}(-k)F_{cd}(q)F_{dc}(-r) \\ + F_{ba}(p)F_{ab}(-k)\rho_{cd}(q)F_{dc}(-r) \\ - F_{ba}(p)F_{ab}(-k)F_{cd}(q)\rho_{dc}(-r) \\ - \rho_{ba}(p)F_{ab}(-k)F_{cd}(q)F_{dc}(-r) \} \,. \end{aligned} \tag{4.97}$$

The RHS of Eq. (4.97) is a Boltzmann scattering integral which represents the 4-wave resonant interaction with an effective coupling $g^2_{\text{eff}}(p+k)$. Although the structure of the RHS of Eq. (4.97) is very similar to the integral in the kinetic equation Eq. (3.4), we are not yet there. It needs further manipulation which demands a quasi-particle assumption.

4.3 Kinetic equation of quasi-particle occupation number

We have seen that $F_{ab}(p)$ and $\rho_{ab}(p)$ are related by a fluctuation-dissipation relation in thermal equilibrium and that Eq. (4.62) shows that there is no dynamics of $\rho_{ab}(p)$. If we assume that Eqs. (4.55) and (4.62) are valid until the point the system reaches thermal equilibrium, it is not too wild to also assume that the spectral function $\rho_{ab}(p)$ has become thermal at the very beginning where the system is governed by Eqs. (4.55) and (4.62). This has been seen in [104, 105] that $\rho_{ab}(p)$ exhibits a well-defined peak at a single frequency mode and does not change much during the time evolution. In comparison, the occupation number changes much more drastically on the same time scale.

There are two things that are useful to us. First, we can assume $\rho_{ab}(p)$ having equilibrium shape while we analyse Eq. (4.97). Second, since $F_{ab}(p)$ and $\rho_{ab}(p)$ follow the fluctuation-dissipation relation at the end, we might be able to assume further that during the time evolution governed by Eqs. (4.55) and (4.62), the following relation needs to hold,

$$F_{ab}(t, p_0, \boldsymbol{p}) = -if(t, p_0)\rho_{ab}(p_0, \boldsymbol{p}) \,, \tag{4.98}$$

where $f(t, p_0)$ is a quasi-occupation number. The symmetry of $F_{ab}(p)$ requires

$$f(t, -p_0) = -f(t, p_0) \,. \tag{4.99}$$

We do not require $f(t, p_0)$ being a Bose-Einstein distribution unless in thermal equilibrium. Thus, Eq. (4.98) is generally not an equilibrium fluctuation-dissipation relation. The dynamics of $F_{ab}(p)$ is now encoded in $f(p; t)$ which will play the role

of $n_Q(\boldsymbol{p})$ in the kinetic equation. In [106], it has been shown that the quantity $F_{ab}(p)/f(t,p_0)$ approached $\rho_{ab}(p)$ at a much earlier time scale, compared to the time scale where $f(t,p_0)$ reached equilibrium. After this early-time setting of the spectral peak the mode population are clearly seen to further evolve in time.

4.3.1 Particle and quasi-particle correlation functions

The relation (4.98) turns Eq. (4.97) into a functional of $\rho_{ab}(p)$ and $f(t;p_0)$ but we need to reduce it further until we have a kinetic equation which is only a functional of $f(t;p_0)$. The full knowledge of $\rho_{ab}(p)$ is required and the possible choice here is through the commutators of field operators. Note that this is accessible because we are allowed to assume the equilibrium shape of $\rho_{ab}(p)$ which can be generated from equilibrium field operators. Despite all that, there are two cases within our reach, a free theory and a weakly-interacting theory such that there exists a free-theory representation through a Bogoliubov transformation. This sounds a bit extreme but we recall that the well-defined peak of the spectral function has been seen at a very early time-scale, so, the free spectral function with delta-like peak should be, more of less, justified.

The matrix elements of the spectral function in the free-field limit read

$$\begin{aligned}
&\rho_{11}(p_0,\mathbf{p}) = \rho^*_{22}(-p_0,-\mathbf{p}) = -\rho_{22}(-p_0,-\mathbf{p}) = 2\pi i\,\delta(p_0-\varepsilon_{\mathbf{p}})\,,\\
&\rho_{12}(p_0,\mathbf{p}) = \rho^*_{21}(p_0,\mathbf{p}) = 0\,,
\end{aligned} \tag{4.100}$$

with free dispersion $\varepsilon_{\boldsymbol{p}} = p^2/2m$ while the Bogoliubov spectral function is given by

$$\begin{aligned}
\rho_{\mathrm{B},11}(p) &= 2\pi i\left[u^2_{\boldsymbol{p}}\delta(p_0-\omega_{\boldsymbol{p}}) - v^2_{\boldsymbol{p}}\delta(p_0+\omega_{\boldsymbol{p}})\right],\\
\rho_{\mathrm{B},22}(p) &= 2\pi i\left[v^2_{\boldsymbol{p}}\delta(p_0-\omega_{\boldsymbol{p}}) - u^2_{\boldsymbol{p}}\delta(p_0+\omega_{\boldsymbol{p}})\right],\\
\rho_{\mathrm{B},12}(p) &= 2\pi i\,u_{\boldsymbol{p}}v_{\boldsymbol{p}}\Big[\delta(p_0-\omega_{\boldsymbol{p}}) - \delta(p_0+\omega_{\boldsymbol{p}})\Big]\\
&= \rho^*_{\mathrm{B},21}(-p)\,,
\end{aligned} \tag{4.101}$$

with Bogoliubov dispersion (2.7) and mode functions (2.8). For momenta much smaller than the healing-length scale, $|\mathbf{p}| \ll p_\xi = [2mgn_0]^{1/2}$, the quasiparticles are sound waves, i.e., $\omega_{\boldsymbol{p}} \simeq c_{\mathrm{s}}|\boldsymbol{p}|$, see Eqs. (2.13), (2.14), with speed of sound $c_{\mathrm{s}} = \sqrt{gn_0/m} = p_\xi/(\sqrt{2}m)$. In this sound-wave limit, the spectral function simplifies to

$$\rho_{\mathrm{B}}(p) = \frac{i\pi gn_0}{\omega_{\boldsymbol{p}}}(1-\sigma^1)\left[\delta(p_0-\omega_{\boldsymbol{p}}) - \delta(p_0+\omega_{\boldsymbol{p}})\right], \tag{4.102}$$

such that, for $p_0, r_0 \geq 0$,

$$\begin{aligned}
&\rho_{\mathrm{B},ab}(sp_0,\boldsymbol{p})\rho_{\mathrm{B},ba}(s'r_0,\boldsymbol{r})\\
&\qquad = -\frac{(2\pi gn_0)^2}{\omega_{\boldsymbol{p}}\omega_{\boldsymbol{r}}}\,ss'\delta(p_0-\omega_{\boldsymbol{p}})\delta(r_0-\omega_{\boldsymbol{r}})\,.
\end{aligned} \tag{4.103}$$

The details of the evaluation of the matrix elements in Eqs. (4.100) and (4.101) can be found in App. C. We remark that although the form of ρ in Eq. (4.102) leads us to deduce that ρ in general takes the form of $\rho \sim p^{-z}\delta(p_0 - p^z)$, this is not true since it would break the canonical scaling $\rho \sim p^{-2}$ following from the commutation relation in Eq. (4.27). In fact, the general form of ρ should be

$$\rho(p) \sim \frac{iA}{p^{2-z}}(\sigma^3 + C\sigma^1)\left[\delta(p_0 - \omega_{\boldsymbol{p}}) - \delta(p_0 + \omega_{\boldsymbol{p}})\right], \tag{4.104}$$

with some constants A, C, and where we have set $\eta = 0$. This is consistent with both the free ($z = 2$), Eq. (4.100), and the sound-wave dispersion ($z = 1$), Eq. (4.102). Using an explicit form of the spectral function, it is very useful to observe the following two quantities for both types of spectral function,[5]

$$\int_0^\infty \frac{\mathrm{d}p_0}{2\pi}\,\mathrm{Tr}\left[F(t, p_0, \boldsymbol{p})\right], \tag{4.105}$$

$$\int_0^\infty \frac{\mathrm{d}p_0}{2\pi}\,\mathrm{Tr}\left[\sigma^3 F(t, p_0, \boldsymbol{p})\right]. \tag{4.106}$$

Assuming the relation (4.98), free spectral function gives

$$\begin{aligned}\int_0^\infty \frac{\mathrm{d}p_0}{2\pi}\,\mathrm{Tr}\left[F(t, p_0, \boldsymbol{p})\right] &= \int_0^\infty \frac{\mathrm{d}p_0}{2\pi} f(t, p_0)(F_{11} + F_{22}) \\ &= \int_0^\infty \mathrm{d}p_0\, f(t, p_0)\Big(\delta(p_0 - \varepsilon_{\boldsymbol{p}}) - \delta(p_0 + \varepsilon_{\boldsymbol{p}})\Big) \\ &= f(t, \varepsilon_{\boldsymbol{p}}), \end{aligned} \tag{4.107}$$

$$\begin{aligned}\int_0^\infty \frac{\mathrm{d}p_0}{2\pi}\,\mathrm{Tr}\left[\sigma^3 F(t, p_0, \boldsymbol{p})\right] &= \int_0^\infty \frac{\mathrm{d}p_0}{2\pi} f(t, p_0)(F_{11} - F_{22}) \\ &= \int_0^\infty \mathrm{d}p_0\, f(t, p_0)\Big(\delta(p_0 - \varepsilon_{\boldsymbol{p}}) + \delta(p_0 + \varepsilon_{\boldsymbol{p}})\Big) \\ &= f(t, \varepsilon_{\boldsymbol{p}}). \end{aligned} \tag{4.108}$$

The same applies to the Bogoliubov case,

$$\begin{aligned}\int_0^\infty \frac{\mathrm{d}p_0}{2\pi}\,\mathrm{Tr}\left[F_{\mathrm{B}}(t, p_0, \boldsymbol{p})\right] &= \int_0^\infty \frac{\mathrm{d}p_0}{2\pi}(F_{\mathrm{B},11} + F_{\mathrm{B},22}) \\ &= \int_0^\infty \mathrm{d}p_0\, f(t, p_0)\Big((u_{\boldsymbol{p}}^2 + v_{\boldsymbol{p}}^2)\delta(p_0 - \omega_{\boldsymbol{p}}) - (u_p^2 + v_p^2)\delta(p_0 + \omega_{\boldsymbol{p}})\Big) \\ &= f(t, \omega_{\boldsymbol{p}})(u_{\boldsymbol{p}}^2 + v_{\boldsymbol{p}}^2) = f(t, \omega_{\boldsymbol{p}})\frac{mc_s}{|\boldsymbol{p}|}, \end{aligned} \tag{4.109}$$

$$\begin{aligned}\int_0^\infty \frac{\mathrm{d}p_0}{2\pi}\,\mathrm{Tr}\left[\sigma^3 F_{\mathrm{B}}(t, p_0, \boldsymbol{p})\right] &= \int_0^\infty \frac{\mathrm{d}p_0}{2\pi}(F_{\mathrm{B},11} - F_{\mathrm{B},22}) \\ &= \int_0^\infty \mathrm{d}p_0\, f(t, p_0)\Big((u_{\boldsymbol{p}}^2 - v_{\boldsymbol{p}}^2)\delta(p_0 - \omega_{\boldsymbol{p}}) + (u_p^2 - v_p^2)\delta(p_0 + \omega_{\boldsymbol{p}})\Big) \\ &= f(t, \omega_{\boldsymbol{p}})(u_{\boldsymbol{p}}^2 - v_{\boldsymbol{p}}^2) = f(t, \omega_{\boldsymbol{p}}). \end{aligned} \tag{4.110}$$

[5] If the integration is done on both positive and negative frequency, the kinetic equation that we are going to derive will vanish identically.

The results are different depending on the particular spectral function we used. This coincides with the relation between particles and quasiparticles mentioned in Sect. 2.1. This observation discussed that $f(t, p_0)$ is not related to a particle occupation but rather shows a quasiparticle occupation and we can define particle and quasiparticle mode occupation numbers, $n(\boldsymbol{p}, t)$ and $n_Q(\boldsymbol{p}, t)$ respectively, from the statistical correlator $F(t, p_0, \boldsymbol{p})$,

$$n(\boldsymbol{p}, t) = \int_0^\infty \frac{\mathrm{d}p_0}{2\pi} \mathrm{Tr} F(t, p_0, \boldsymbol{p}) - 1/2\,, \tag{4.111}$$

$$n_Q(\boldsymbol{p}, t) = \int_0^\infty \frac{\mathrm{d}p_0}{2\pi} \mathrm{Tr}[\sigma^3 F(t, p_0, \boldsymbol{p})] - 1/2\,, \tag{4.112}$$

where we used $f(t, \boldsymbol{p}) = n_Q(\boldsymbol{p}, t) + 1/2$. Due to $\mathrm{Tr}[\sigma^3 F]$ relates to n_Q, the kinetic equation that is derived from Eq. (4.97) will also describes the dynamics of quasiparticle occupation $n_Q(\boldsymbol{p}, t)$.

4.3.2 Nonperturbative kinetic equation

Our main interest is the scaling solution in the infrared regime where quasiparticles are highly populated i.e. $n_Q(\boldsymbol{p}) \gg 1$. In this regime, the quantum ground state $1/2$ in Eq. (4.112) can be neglected. Therefore, the kinetic equation for the quasiparticle number takes the form

$$\partial_t n_Q(t, \boldsymbol{p}) = \int_0^\infty \frac{\mathrm{d}p_0}{2\pi} \partial_t \sigma^3_{ab} F_{ba}(t, p_0, \boldsymbol{p}) = I(t, \boldsymbol{p})\,, \tag{4.113}$$

with the scattering integral

$$I(t, \mathbf{p}) = -i \int_0^\infty \frac{\mathrm{d}\omega}{2\pi} \mathrm{Tr}\Big[\Sigma^\rho(t, p_0, \boldsymbol{p}) F(t, p_0, \boldsymbol{p}) - \Sigma^F(t, p_0, \boldsymbol{p}) \rho(p_0, \boldsymbol{p})\Big]. \tag{4.114}$$

We have dropped the time argument of spectral function due to the assumption of its time independence but if that is not the case, the time argument can be restored without changing anything else as long as Eq. (4.112) holds. In the context of the s-channel resummation, the scattering integral Eq. (4.97) can be expressed in terms of Boltzmann's integral,

$$\begin{aligned} I(\mathbf{p}) = \frac{(2\pi)^{d+1}\hbar^2}{2} \int_0^\infty \frac{\mathrm{d}p_0}{2\pi} \int_{kqr} \delta^{d+1}(p + k - q - r) g^2_{\mathrm{eff}}(p + k) \\ \times \rho_{ba}(p_0, \boldsymbol{p}) \rho_{ab}(-k_0, -\boldsymbol{k}) \rho_{cd}(q_0, \boldsymbol{q}) \rho_{dc}(-r_0, -\boldsymbol{r}) \\ \times \{-f(p_0) f(q_0) f(-r_0) - f(p_0) f(-k_0) f(-r_0) \\ + f(p_0) f(-k_0) f(q_0) + f(-k_0) f(q_0) f(-r_0)\} \end{aligned} \tag{4.115}$$

$$
\begin{aligned}
&= \frac{(2\pi)^d\hbar^2}{2}\int_0^\infty \mathrm{d}p_0 \int_{kqr} \delta^{d+1}(p-k-q+r) g_{\mathrm{eff}}^2(p-k) \\
&\qquad \times \rho_{ba}(p_0,\boldsymbol{p})\rho_{ab}(k_0,\boldsymbol{k})\rho_{cd}(r_0,\boldsymbol{r})\rho_{dc}(q_0,\boldsymbol{q}) \\
&\qquad \times \{-f(p_0)f(q_0)f(r_0) - f(p_0)f(k_0)f(r_0) \\
&\qquad\qquad + f(p_0)f(k_0)f(q_0) + f(k_0)f(q_0)f(r_0)\} \\
&= \frac{(2\pi)^d\hbar^2}{2}\int_0^\infty \mathrm{d}p_0 \int_{kqr} \delta^{d+1}(p+k-q-r) g_{\mathrm{eff}}^2(p-r) \\
&\qquad \times \rho_{ba}(p_0,\boldsymbol{p})\rho_{ab}(k_0,\boldsymbol{k})\rho_{cd}(r_0,\boldsymbol{r})\rho_{dc}(q_0,\boldsymbol{q}) \\
&\qquad \times \{-f(p_0)f(k_0)f(q_0) - f(p_0)f(k_0)f(r_0) \\
&\qquad\qquad + f(p_0)f(q_0)f(r_0) + f(k_0)f(q_0)f(r_0)\}\,,
\end{aligned}
\tag{4.116}
$$

where we have replaced all F functions by Eq. (4.112) (without the factor 1/2) and made all argument positive using the symmetry of $f(t,p_0)$ and changing integration variables. We also dropped the time argument t in $f(t,p_0)$. The integrations over frequencies are rewritten to range over the positive domain only,

$$
I(\boldsymbol{p}) = \frac{(2\pi)^d\hbar^2}{2}\int_0^\infty \mathrm{d}p_0\,\mathrm{d}k\,\mathrm{d}q\,\mathrm{d}r\,\delta(\boldsymbol{p}+\boldsymbol{k}-\boldsymbol{q}-\boldsymbol{r}) \sum_{s,s'\in\{-1,1\}} \left[\mathcal{I}_{1sss'} + \mathcal{I}_{1s(-s)s'}\right],
\tag{4.117}
$$

where $\int_0^\infty \mathrm{d}k = (2\pi)^{-4}\int_0^\infty \mathrm{d}k_0 \int \mathrm{d}^d k$, and

$$
\begin{aligned}
\mathcal{I}_{s\sigma\sigma's'} = \delta(sp_0+\sigma k_0-\sigma' q_0 - s' r_0)\, g_{\mathrm{eff}}^2(sp_0 - s' r_0, \boldsymbol{p}-\boldsymbol{r}) \\
\times\ \rho_{ab}(sp_0,\boldsymbol{p})\rho_{ba}(s' r_0,\boldsymbol{r})\,\rho_{cd}(\sigma' q_0,\boldsymbol{q})\rho_{dc}(\sigma k_0,\boldsymbol{k}) \\
\times\ \Big\{\sigma' s'\Big[s f(p_0) + \sigma f(k_0)\Big] f(q_0) f(r_0) \\
-\ s\sigma f(p_0) f(k_0)\left[\sigma' f(q_0) + s' f(r_0)\right]\Big\}\,.
\end{aligned}
\tag{4.118}
$$

Eq. (4.117) gives the perturbative kinetic equation if the many-body coupling g_{eff}^2 reduces to the bare coupling g^2. This limit coincides with the case that one keeps only second Feynman diagram presented in the upper row in Fig. 4.1. However, with loop-resummation, the many-body coupling is in general different from the bare one and thus, Eq. (4.117) includes contributions beyond the perturbative calculation. The many-body coupling makes it harder to obtain the time-dependent solution but nevertheless, we can analyse the possible scaling solutions and make an implication about time development in case that a particular scaling solution exists.

Kinetic scattering integral for free particles

The kinetic equation for free particle can be obtained by inserting the free spectral function Eq. (4.100) into Eq. (4.117). It can be seen that only $\mathcal{I}_{1ss1}$ contributes to

the integral,

$$\begin{aligned}\mathcal{I}_{1ss1} = (2\pi)^4\delta(p_0 + sk_0 - sq_0 - r_0)s\, g^2_{\rm eff}(p_0 - r_0, \boldsymbol{p} - \boldsymbol{r}) \\ \times\ \delta(p_0 - \varepsilon_{\boldsymbol{p}})\delta(k_0 - \varepsilon_{\boldsymbol{k}})\delta(q_0 - \varepsilon_{\boldsymbol{q}})\delta(r_0 - \varepsilon_{\boldsymbol{r}}) \\ \times\ \Big\{\Big[f(p_0) + sf(k_0)\Big]\, f(q_0)f(r_0) \\ -\ f(p_0)f(k_0)\Big[sf(q_0) + f(r_0)\Big]\Big\}\,, \end{aligned} \tag{4.119}$$

where $s \in \{-1, 1\}$. Integrating over the frequencies p_0, k_0, q_0 and r_0 we obtain the scattering integral

$$\begin{aligned} I(\boldsymbol{p}) &= \frac{(2\pi)^d\hbar^2}{2}\int_0^\infty {\rm d}p_0\,\frac{{\rm d}k_0}{2\pi}\,\frac{{\rm d}q_0}{2\pi}\,\frac{{\rm d}r_0}{2\pi}\,\int_{\boldsymbol{kqr}}\delta(\boldsymbol{p}+\boldsymbol{k}-\boldsymbol{q}-\boldsymbol{r})\sum_{s,s'\in\{-1,1\}}\mathcal{I}_{1ss1} \\ &= \frac{(2\pi)^{d+1}\hbar^2}{2}\int_{\boldsymbol{kqr}}\delta(\boldsymbol{p}+\boldsymbol{k}-\boldsymbol{q}-\boldsymbol{r}) \\ &\quad\times\sum_{s\in\{-1,1\}} s\, g^2_{\rm eff}(\varepsilon_{\boldsymbol{p}} - \varepsilon_{\boldsymbol{r}}, \boldsymbol{p} - \boldsymbol{r})\,\delta(\varepsilon_{\boldsymbol{p}} + s[\varepsilon_{\boldsymbol{k}} - \varepsilon_{\boldsymbol{q}}] - \varepsilon_{\boldsymbol{r}}) \\ &\quad\times\Big\{\Big[f(\varepsilon_{\boldsymbol{p}}) + sf(\varepsilon_{\boldsymbol{k}})\Big]\, f(\varepsilon_{\boldsymbol{q}})f(\varepsilon_{\boldsymbol{r}}) - \ f(\varepsilon_{\boldsymbol{p}})f(\varepsilon_{\boldsymbol{k}})\Big[sf(\varepsilon_{\boldsymbol{q}}) + f(\varepsilon_{\boldsymbol{r}})\Big]\Big\} \\ &= \frac{(2\pi)^{d+1}\hbar^2}{2}\int_{\boldsymbol{kqr}}\Big(\delta(\boldsymbol{p}+\boldsymbol{k}-\boldsymbol{q}-\boldsymbol{r}) + \delta(\boldsymbol{p}-\boldsymbol{k}+\boldsymbol{q}-\boldsymbol{r})\Big) \\ &\quad\times\ g^2_{\rm eff}(\varepsilon_{\boldsymbol{p}} - \varepsilon_{\boldsymbol{r}}, \boldsymbol{p} - \boldsymbol{r})\,\delta(\varepsilon_{\boldsymbol{p}} + \varepsilon_{\boldsymbol{k}} - \varepsilon_{\boldsymbol{q}} - \varepsilon_{\boldsymbol{r}}) \\ &\quad\times\Big\{\Big[f(\varepsilon_{\boldsymbol{p}}) + f(\varepsilon_{\boldsymbol{k}})\Big]\, f(\varepsilon_{\boldsymbol{q}})f(\varepsilon_{\boldsymbol{r}}) - \ f(\varepsilon_{\boldsymbol{p}})f(\varepsilon_{\boldsymbol{k}})\Big[f(\varepsilon_{\boldsymbol{q}}) + f(\varepsilon_{\boldsymbol{r}})\Big]\Big\} \\ &= (2\pi)^{d+1}\hbar^2\int_{\boldsymbol{kqr}} g^2_{\rm eff}(\varepsilon_{\boldsymbol{p}} - \varepsilon_{\boldsymbol{r}}, \boldsymbol{p} - \boldsymbol{r})\delta(\boldsymbol{p}+\boldsymbol{k}-\boldsymbol{q}-\boldsymbol{r}) \\ &\quad\times\delta(\varepsilon_{\boldsymbol{p}} + \varepsilon_{\boldsymbol{k}} - \varepsilon_{\boldsymbol{q}} - \varepsilon_{\boldsymbol{r}})\Big\{\Big[f(\varepsilon_{\boldsymbol{p}}) + f(\varepsilon_{\boldsymbol{k}})\Big]\, f(\varepsilon_{\boldsymbol{q}})f(\varepsilon_{\boldsymbol{r}}) \\ &\qquad\qquad - \ f(\varepsilon_{\boldsymbol{p}})f(\varepsilon_{\boldsymbol{k}})\Big[f(\varepsilon_{\boldsymbol{q}}) + f(\varepsilon_{\boldsymbol{r}})\Big]\Big\}\,. \end{aligned} \tag{4.120}$$

In the third equality, we simply distributed the terms and exchanged variable $\boldsymbol{k} \leftrightarrow \boldsymbol{q}$ in the integral that is generated from $s = -1$ so it can be combined with the integral generated from $s = 1$, except the delta function of spatial momenta. The dependence of $\boldsymbol{k}$ and $\boldsymbol{q}$ are in terms of the free particle energies $\varepsilon_{\boldsymbol{k}}$ and $\varepsilon_{\boldsymbol{q}}$ so the momenta $\boldsymbol{k}$ and $\boldsymbol{q}$ could be reversed in the fourth equality to combine two delta functions without disturbing the rest of integral. The Boltzmann equation (3.2) for $n(t, \mathbf{p}) = f(t, \varepsilon(\mathbf{p})) \gg 1$, with the scattering integral (3.4) has been recovered in the classical-wave approximation. We emphasize that our 2PI resummation approach provides us with an expression for the T-matrix elements,

$$|T_{\boldsymbol{pkqr}}|^2 = (2\pi)^{d+1}\hbar^2 g^2_{\rm eff}(\varepsilon_{\mathbf{p}} - \varepsilon_{\mathbf{r}}, \boldsymbol{p} - \boldsymbol{r})\,, \tag{4.121}$$

which depend on the quasi-particle distribution $n_Q(\boldsymbol{p}, t)$ themselves. Making a scaling ansatz for $n(\boldsymbol{p}, t)$, we will explicitly calculate, in Sect. 4.4.1, the dependence of these matrix elements on the energy and momentum arguments.

Kinetic scattering integral for Bogoliubov sound waves

For the Bogoliubov spectral function, we limit ourselves to the sound-wave regime where the dispersion is linear, see Eq. (2.13). Inserting the sound-wave approximation of Bogoliubov spectral function Eq. (4.103) into the integrand (4.118) gives

$$\begin{aligned}\mathcal{I}_{s\sigma\sigma's'} = \frac{(2\pi g n_0)^4}{\omega_{\boldsymbol{p}}\omega_{\boldsymbol{k}}\omega_{\boldsymbol{q}}\omega_{\boldsymbol{r}}}\delta(sp_0+\sigma k_0-\sigma' q_0-s' r_0)\, g_{\text{eff}}^2(sp_0-s'r_0, \boldsymbol{p}-\boldsymbol{r}) \\ \times\ \delta(p_0-\omega_{\boldsymbol{p}})\delta(k_0-\omega_{\boldsymbol{k}})\delta(q_0-\omega_{\boldsymbol{q}})\delta(r_0-\omega_{\boldsymbol{r}}) \\ \times\ \Big\{\Big[\sigma f(p_0)+sf(k_0)\Big] f(q_0)f(r_0) \\ -\ f(p_0)f(k_0)\Big[s' f(q_0)+\sigma' f(r_0)\Big]\Big\}. \end{aligned} \tag{4.122}$$

Again, only a subset of integrands contributes to the integral. We can identify the non-vanishing contributions by first integrating over all frequencies as well as the $\boldsymbol{q}$ variable over the delta function of spatial momenta,

$$\begin{aligned} I(\boldsymbol{p}) = \frac{(2\pi)^3\hbar^2}{2}(2\pi)^{-12}\int \mathrm{d}\boldsymbol{r}\int_0^\infty \mathrm{d}|\boldsymbol{k}|\int_{-1}^1 \mathrm{d}\cos(\theta_k)\int_0^{2\pi}\mathrm{d}\phi_k\,|\boldsymbol{k}|^2 \\ \times\sum_{s,s'\in\{-1,1\}}\Big[\mathcal{I}_{1sss'}+\mathcal{I}_{1s(-s)s'}\Big]\Big|_{\boldsymbol{q}=\boldsymbol{p}+\boldsymbol{k}-\boldsymbol{r}}. \end{aligned} \tag{4.123}$$

The integral is written in $d=3$ since it is an only particular case that we are going to work with. Then, we shift $\boldsymbol{r}$ to $\boldsymbol{p}-\boldsymbol{r'}$ and choose an orientation of $\boldsymbol{k}$-space such that θ_k is an angle between $\boldsymbol{k}$ and $\boldsymbol{r'}$. By introducing $q=|\boldsymbol{r'}+\boldsymbol{k}|$, $\mathrm{d}\cos(\theta_k) = (|\boldsymbol{r'}||\boldsymbol{k}|)^{-1}\,q\,\mathrm{d}q$. The azimuthal angle ϕ_k can also be integrated out because of azimuthal symmetry. The integral then becomes

$$I(\boldsymbol{p}) = \frac{(2\pi)^{-8}\,\hbar^2}{2}\int\frac{\mathrm{d}^d r'}{r'}\int_0^\infty k\mathrm{d}k\int_{|r'-k|}^{|r'+k|} q\mathrm{d}q\sum_{s,s'\in\{-1,1\}}\Big[\tilde{\mathcal{I}}_{1sss'}+\tilde{\mathcal{I}}_{1s(-s)s'}\Big], \tag{4.124}$$

where $r'=|\boldsymbol{r'}|$, $k=|\boldsymbol{k}|$ and

$$\begin{aligned}\tilde{\mathcal{I}}_{s\sigma\sigma's'} = \frac{(2\pi g\rho)^4}{\omega_p\omega_k\omega_q\omega_{|\boldsymbol{p}-\boldsymbol{r'}|}}\, g_{\text{eff}}^2(s\omega_p - s'\omega_{|\boldsymbol{p}-\boldsymbol{r'}|}, \boldsymbol{r'}) \\ \times\ \delta(s\omega_p+\sigma\omega_k-\sigma'\omega_q-s'\omega_{|\boldsymbol{p}-\boldsymbol{r'}|}) \\ \times\ \Big\{\Big[\sigma f_p+sf_k\Big] f_q f_{|\boldsymbol{p}-\boldsymbol{r'}|}) \\ -\ f_p f_k\Big[s' f_q+\sigma' f_{|\boldsymbol{p}-\boldsymbol{r'}|})\Big]\Big\}. \end{aligned} \tag{4.125}$$

Here, we defined $f_p \equiv f(\omega_{\boldsymbol{p}})$. In order to reduce the set of integrands, we analyze the energy conservation delta function for the case of the Bogoliubov dispersion (2.7): $\delta(s\omega_p+\sigma\omega_k-\sigma'\omega_q-s'\omega_{|\boldsymbol{p}-\boldsymbol{r'}|}) = \text{const.}\times\delta(|\boldsymbol{p}-\boldsymbol{r'}|-ss'[p+s\sigma(k-\sigma\sigma' q)])$. Since $|k-q|\le r'$ and $k+q\ge r'$ we find that the argument of the delta distribution can

vanish only if $\sigma\sigma' = 1$ and $ss' = 1$ or if $\sigma\sigma' = -1$ and $ss' = -1$ and $s = -\sigma$. This leaves us with the following terms:

$$I(\boldsymbol{p}) = \frac{(2\pi)^{-8}\,\hbar^2}{2}\int\frac{\mathrm{d}^d r'}{r'}\int_0^\infty k\mathrm{d}k\int_{|r'-k|}^{|r'+k|} q\mathrm{d}q \times\left[\tilde{\mathcal{I}}_{1111}+\tilde{\mathcal{I}}_{1(-1)(-1)1}+\tilde{\mathcal{I}}_{1(-1)1(-1)}\right], \tag{4.126}$$

where $\tilde{\mathcal{I}}_{s\sigma\sigma's'} \equiv \tilde{\mathcal{I}}_{s\sigma\sigma's'}(\boldsymbol{p}, k, q, \boldsymbol{r'})$. To identify the T-matrix element, it is more convenient and clearer to go back to Eq. (4.117) and to keep only the non-vanishing contributions according to Eq. (4.126),

$$\begin{aligned}
I(\boldsymbol{p}) &= \frac{(2\pi)^d\hbar^2}{2}\int_0^\infty \mathrm{d}p_0\,\frac{\mathrm{d}k_0}{2\pi}\,\frac{\mathrm{d}q_0}{2\pi}\,\frac{\mathrm{d}r_0}{2\pi}\int_{\boldsymbol{kqr}}\delta(\boldsymbol{p}+\boldsymbol{k}-\boldsymbol{q}-\boldsymbol{r})\\
&\qquad\times\left[\mathcal{I}_{1111}+\mathcal{I}_{1(-1)(-1)1}+\mathcal{I}_{1(-1)1(-1)}\right]\\
&= \frac{(2\pi)^{d+1}\hbar^2}{2}\int_{\boldsymbol{kqr}}\frac{(g\rho)^4}{\omega_{\boldsymbol{p}}\omega_{\boldsymbol{k}}\omega_{\boldsymbol{q}}\omega_{\boldsymbol{r}}}\,\delta(\omega_{\boldsymbol{p}}+\omega_{\boldsymbol{k}}-\omega_{\boldsymbol{q}}-\omega_{\boldsymbol{r}})\\
&\qquad\times\Big[2g_{\mathrm{eff}}^2(\omega_{\boldsymbol{p}}-\omega_{\boldsymbol{r}},\boldsymbol{p}-\boldsymbol{r})\,\delta(\boldsymbol{p}+\boldsymbol{k}-\boldsymbol{q}-\boldsymbol{r})\\
&\qquad\quad+g_{\mathrm{eff}}^2(\omega_{\boldsymbol{p}}-\omega_{\boldsymbol{k}},\boldsymbol{p}-\boldsymbol{k})\,\delta(\boldsymbol{p}-\boldsymbol{k}-\boldsymbol{q}+\boldsymbol{r})\Big]\\
&\qquad\times\Big\{\Big[f(\omega_{\boldsymbol{p}})+f(\omega_{\boldsymbol{k}})\Big]\,f(\omega_{\boldsymbol{q}})f(\omega_{\boldsymbol{r}})-\;f(\omega_{\boldsymbol{p}})f(\omega_{\boldsymbol{k}})\Big[f(\omega_{\boldsymbol{q}})+f(\omega_{\boldsymbol{r}})\Big]\Big\}\\
&= (2\pi)^{d+1}\hbar^2\int_{\boldsymbol{kqr}}\frac{(g\rho)^4}{\omega_{\boldsymbol{p}}\omega_{\boldsymbol{k}}\omega_{\boldsymbol{q}}\omega_{\boldsymbol{r}}}\Big[g_{\mathrm{eff}}^2(\omega_{\boldsymbol{p}}-\omega_{\boldsymbol{r}},\boldsymbol{p}-\boldsymbol{r})+\frac{1}{2}g_{\mathrm{eff}}^2(\omega_{\boldsymbol{p}}-\omega_{\boldsymbol{k}},\boldsymbol{p}+\boldsymbol{k})\Big]\\
&\qquad\times\delta(\boldsymbol{p}+\boldsymbol{k}-\boldsymbol{q}-\boldsymbol{r})\,\delta(\omega_{\boldsymbol{p}}+\omega_{\boldsymbol{k}}-\omega_{\boldsymbol{q}}-\omega_{\boldsymbol{r}})\\
&\qquad\times\Big\{\Big[f(\omega_{\boldsymbol{p}})+f(\omega_{\boldsymbol{k}})\Big]\,f(\omega_{\boldsymbol{q}})f(\omega_{\boldsymbol{r}})-\;f(\omega_{\boldsymbol{p}})f(\omega_{\boldsymbol{k}})\Big[f(\omega_{\boldsymbol{q}})+f(\omega_{\boldsymbol{r}})\Big]\Big\}.
\end{aligned} \tag{4.127}$$

The integrand $\mathcal{I}_{1111}$ and $\mathcal{I}_{1(-1)(-1)1}$ could be combined in the similar way we did in the free-particle case. As for $\mathcal{I}_{1(-1)1(-1)}$, an interchange $\boldsymbol{k}\leftrightarrow\boldsymbol{r}$ is needed to get the result in the second equality and we reversed the sign of $\boldsymbol{k}$ and $\boldsymbol{r}$ to make the delta functions of the spatial momenta identical in the third equality. Eq. (4.127) is again a Boltzmann integral (3.2) for $n_Q(t,\mathbf{p}) = f(t,\omega(\mathbf{p})) \gg 1$ with T-matrix elements

$$|T_{\boldsymbol{pkqr}}|^2 = (2\pi)^{d+1}\hbar^2\frac{(g\rho)^4}{\omega_{\boldsymbol{p}}\omega_{\boldsymbol{k}}\omega_{\boldsymbol{q}}\omega_{\boldsymbol{r}}}\Big[g_{\mathrm{eff}}^2(\omega_{\boldsymbol{p}}-\omega_{\boldsymbol{r}},\boldsymbol{p}-\boldsymbol{r})+\frac{1}{2}g_{\mathrm{eff}}^2(\omega_{\boldsymbol{p}}-\omega_{\boldsymbol{k}},\boldsymbol{p}+\boldsymbol{k})\Big]. \tag{4.128}$$

4.4 Effective many-body coupling function

The kinetic equation defined by Eqs. (4.120) and (4.127) can be analyzed in the same way we have done in Eq. (3.6). All we need to know is the scaling behaviour of their T-matrix elements. In this section, we are going to evaluate the effective many-body coupling determining these T-matrix elements. Regardless we consider

whether of the free or the Bogoliubov case, the effective many-body coupling reads (cf. Eq. (4.90))

$$g^2_{\text{eff}}(p) = \frac{g^2}{|1 + g\hbar\Pi^R(p)|^2} = \frac{g^2}{|1 - g\hbar(\theta * \Pi^\rho)(p)|^2}\,. \tag{4.129}$$

Recalling Eq. (4.70) and using relations (4.75) and (4.76), we are able to write down Π^ρ as a function in momentum space,

$$\Pi^\rho(y,x) \to \Pi^\rho(-p) = \frac{1}{2}\Big(\rho_{ab} * F_{ba} - F_{ab} * \rho_{ba}\Big)(p)\,, \tag{4.130}$$

and Π^R in momentum space reads

$$\Pi^R(p) = -\int_{-\infty}^{\infty} \frac{\mathrm{d}q_0}{2\pi}\,\theta(q_0)\Pi^\rho(q_0 - p_0, -\boldsymbol{p})\,. \tag{4.131}$$

Within the quasiparticle approximation introduced above, $\Pi^\rho(p)$ can be written in terms of the quasi-particle frequency spectrum $f(t,p_0)$ and the spectral function $\rho(p)$, cf. Eqs. (4.80) and (4.98), as

$$\begin{aligned}\Pi^\rho(-p) &= \frac{1}{2}(\rho_{ab} * F_{ba} - F_{ab} * \rho_{ba})(p) \\ &= \frac{1}{2}\int_k \Big[\rho_{ab}(p-k)F_{ba}(-k) - F_{ab}(p-k)\rho_{ba}(-k)\Big] \\ &= -\frac{i}{2}\int_k \Big[f(-k_0) - f(p_0 - k_0)\Big]\rho_{ab}(-k)\rho_{ba}(p-k)\,,\end{aligned} \tag{4.132}$$

where $\int_k = (2\pi)^{-d-1}\int d^{d+1}k$ and, here and in the following, we suppress the time argument t of $f(t,p_0)$. In order to go further, we need an explicit form of the quasi-particle distribution $f(t,p_0)$ for which we make an ansatz in term of a power-law in momentum with an infrared cut-off. The calculations are separately discussed for the free and the Bogoliubov cases due to the different form of the spectral function and the quasiparticle distribution. It also has to be noted that the following calculation will be carried out in $d = 3$ dimensions.

4.4.1 Effective many-body coupling function for free particles

We first discuss the case of free particles. Inserting the spectral function (4.100) into Eq. (4.132), one obtains

$$\begin{aligned}\Pi^\rho(-p^0,-\boldsymbol{p}) &= -\frac{i}{2}\int_k \Big[f(-k_0)-f(p_0-k_0)\Big]\Big[-(2\pi)^2\delta(-k_0-\varepsilon_{\boldsymbol{k}})\delta(p_0-k_0-\varepsilon_{\boldsymbol{p}-\boldsymbol{k}}) \\ &\qquad -(2\pi)^2\delta(-k_0+\varepsilon_{\boldsymbol{k}})\delta(p_0-k_0+\varepsilon_{\boldsymbol{p}-\boldsymbol{k}})\Big] \\ &= i\pi\int\frac{d^dk}{(2\pi)^d}\Big\{\Big[f(-\varepsilon_{\boldsymbol{k}})-f(-\varepsilon_{\boldsymbol{p}-\boldsymbol{k}})\Big]\delta(p_0-\varepsilon_{\boldsymbol{k}}+\varepsilon_{\boldsymbol{p}-\boldsymbol{k}}) \\ &\qquad +\Big[f(\varepsilon_{\boldsymbol{k}})-f(\varepsilon_{\boldsymbol{p}-\boldsymbol{k}})\Big]\delta(p_0+\varepsilon_{\boldsymbol{k}}-\varepsilon_{\boldsymbol{p}-\boldsymbol{k}})\Big\} \\ &= -i\pi\int\frac{d^dk}{(2\pi)^d}\Big\{f(\varepsilon_{\boldsymbol{k}})\Big[\delta(p_0-\varepsilon_{\boldsymbol{k}}+\varepsilon_{\boldsymbol{p}-\boldsymbol{k}})-\delta(p_0+\varepsilon_{\boldsymbol{k}}-\varepsilon_{\boldsymbol{p}-\boldsymbol{k}})\Big] \\ &\qquad +f(\varepsilon_{\boldsymbol{p}-\boldsymbol{k}})\Big[\delta(p_0+\varepsilon_{\boldsymbol{k}}-\varepsilon_{\boldsymbol{p}-\boldsymbol{k}})-\delta(p_0-\varepsilon_{\boldsymbol{k}}+\varepsilon_{\boldsymbol{p}-\boldsymbol{k}})\Big]\Big\} \\ &= -2\pi i\int\frac{d^dk}{(2\pi)^d}f(\varepsilon_{\boldsymbol{k}})\Big[\delta(p_0-\varepsilon_{\boldsymbol{k}}+\varepsilon_{\boldsymbol{p}-\boldsymbol{k}})-\delta(p_0+\varepsilon_{\boldsymbol{k}}-\varepsilon_{\boldsymbol{p}-\boldsymbol{k}})\Big]. \quad (4.133)\end{aligned}$$

Inserting this into Π^R, Eq. (4.131), we obtain, in $d=2,3$ dimensions,

$$\begin{aligned}\Pi^R(E,p) &= -\int_{-\infty}^{\infty}\frac{dq_0}{2\pi}\frac{i}{q_0+i\epsilon}\Pi^\rho(q_0-p_0,-\boldsymbol{p}) = -\int_{-\infty}^{\infty}\frac{dq_0}{2\pi}\frac{i}{q_0+i\epsilon}\Pi^\rho(-(p_0-q_0),-\boldsymbol{p}) \\ &= -\int\frac{d^dk}{(2\pi)^d}f(\varepsilon_{\boldsymbol{k}})\left[\frac{1}{p_0-\varepsilon_{\boldsymbol{k}}+\varepsilon_{\boldsymbol{p}-\boldsymbol{k}}+i\epsilon}-\frac{1}{p_0+\varepsilon_{\boldsymbol{k}}-\varepsilon_{\boldsymbol{p}-\boldsymbol{k}}+i\epsilon}\right] \\ &= -\frac{2mS_{d-2}}{(2\pi)^d}\int_0^\infty dk\,k^{d-1}\int_{-1}^1\frac{d\cos\theta}{\sin^{3-d}\theta}f(\varepsilon_{\boldsymbol{k}}) \\ &\qquad\times\left[\frac{1}{E-k^2+|\boldsymbol{p}-\boldsymbol{k}|^2+i\epsilon}-\frac{1}{E+k^2-|\boldsymbol{p}-\boldsymbol{k}|^2+i\epsilon}\right], \quad (4.134)\end{aligned}$$

where θ is the angle between $\boldsymbol{p}$ and $\boldsymbol{k}$. We proceed by considering explicitly the case $d=3$,

$$\begin{aligned}\Pi^R(E,p) &= -\frac{1}{(2\pi)^2}\frac{m}{p}\int_0^\infty dk\,k^2\int_{-1}^1 dz\,f(\varepsilon_{\boldsymbol{k}}) \\ &\qquad\times\left[\left(\frac{E+p^2}{2p}-kz+i\epsilon\right)^{-1}-\left(\frac{E-p^2}{2p}+kz+i\epsilon\right)^{-1}\right] \\ &= -\frac{1}{(2\pi)^2}\frac{m}{p}\int_0^\infty dk\,k\,f(\varepsilon_{\boldsymbol{k}})\left[\ln\left(\frac{\frac{E+p^2}{2p}+k+i\epsilon}{\frac{E+p^2}{2p}-k+i\epsilon}\right)-\ln\left(\frac{\frac{E-p^2}{2p}+k+i\epsilon}{\frac{E-p^2}{2p}-k+i\epsilon}\right)\right] \\ &= -\frac{p_\Lambda^2}{(2\pi)^2}\frac{m}{p}\left[\widetilde{\Pi}_f\left(\tfrac{E+p^2}{2pp_\Lambda}\right)-\widetilde{\Pi}_f\left(\tfrac{E-p^2}{2pp_\Lambda}\right)\right], \quad (4.135)\end{aligned}$$

where we defined $E = 2mp^0$ and introduced a characteristic scale p_Λ to be able to write the integral as

$$\widetilde{\Pi}_f(x) = \int_0^\infty dy\, y\, f(\varepsilon_{yp_\Lambda}) \ln\left(\frac{x+y+i\epsilon}{x-y+i\epsilon}\right) . \tag{4.136}$$

In order to proceed, we need to know the quasiparticle distribution $f(\varepsilon_{\boldsymbol{k}})$. As we want to study wave-turbulent transport, this spectrum is anticipated to assume a scaling form. Taking into account that f needs to be regularized in the infrared in order to ensure the convergence of integrals we make the following ansatz for the scaling form,

$$f(p_0) = \mathrm{sgn}(p_0) \left(\frac{\varepsilon_\Lambda}{p_0 + \varepsilon_{p_\Lambda}}\right)^{\kappa/2} , \tag{4.137}$$

with an infrared cut-off p_Λ. This ansatz interpolates in a smooth way between a constant in the infrared limit and a power-law fall-off $f(\varepsilon_p) \sim p^{-\kappa}$, with cross-over scale p_Λ. Note that, while the precise form at and below the cross-over scale can be different we are, here, primarily interested in determining the power-law exponent κ. The signum function is introduced to account for the anti-symmetry of f in p_0, cf. Eq. (4.99). Inserting Eq. (4.137) into Eq. (4.136), we find

$$\widetilde{\Pi}_f(x) = \left(\frac{\Lambda}{p_\Lambda}\right)^\kappa \int_0^\infty \frac{dy\, y}{(1+y^2)^{\kappa/2}} \ln\left(\frac{x+y+i\epsilon}{x-y+i\epsilon}\right) . \tag{4.138}$$

The overall amplitude $2m\varepsilon_\Lambda^{\kappa/2} = \Lambda^\kappa$ is fixed by the normalization of the distribution to the non-condensed particle ρ_{nc},

$$\begin{aligned}
\rho_{\mathrm{nc}} &= \int \frac{\mathrm{d}^d k}{(2\pi)^d} \left(\frac{\Lambda^2}{k^2 + p_\Lambda^2}\right)^{\kappa/2} \\
&= \frac{S_{d-1}\Lambda^\kappa p_\Lambda^{d-\kappa}}{(2\pi)^d} \int_0^\infty dk\, k^{d-1} (1+k^2)^{-\kappa/2} \\
&= \frac{S_{d-1}\Lambda^\kappa p_\Lambda^{d-\kappa}}{2(2\pi)^d} \int_0^\infty du\, u^{(d-2)/2} (1+u)^{-\kappa/2} \\
&= \frac{\Lambda^\kappa p_\Lambda^{d-\kappa}}{2^d \pi^{d/2}} \frac{\Gamma([\kappa-d]/2)}{\Gamma(\kappa/2)} {}_2F_1(\kappa/2, d/2; \kappa/2; 0)
\end{aligned} \tag{4.139}$$

where

$$S_{d-1} = \frac{2\pi^{d/2}}{\Gamma(d/2)} \tag{4.140}$$

is the surface area of the unit sphere in d dimensions. Since ${}_2F_1(a, b; c; 0) = 1$, the infrared cutoff scale is related to the density via (in $d = 3$)

$$\left(\frac{\Lambda}{p_\Lambda}\right)^\kappa = 2^3 \pi^{3/2} \frac{\Gamma(\kappa/2)}{\Gamma([\kappa-3]/2)} \frac{\rho_{\mathrm{nc}}}{p_\Lambda^3} . \tag{4.141}$$

The above expression applies in the case that $\kappa > d = 3$, where the UV cutoff can be neglected and we assume this is the case. With all these, the integral in (4.138) can be evaluated,

$$\Pi^R(E,p) = -\frac{p_\mu^2}{2gpp_\Lambda}\left[\tilde{\pi}_\kappa\Big(\tfrac{E+p^2}{2pp_\Lambda}\Big) - \tilde{\pi}_\kappa\Big(\tfrac{E-p^2}{2pp_\Lambda}\Big)\right], \tag{4.142}$$

where $p_\mu = \sqrt{8\pi a \rho_{\rm nc}}$ is the 'healing'-length wave number set by the noncondensed particle density $\rho_{\rm nc}$. $\tilde{\pi}_\kappa$ contains the integral over y which can be expressed in terms of a Gaussian hypergeometric function,

$$\begin{aligned}\tilde{\pi}_\kappa(x) &= \frac{2}{\sqrt{\pi}}\frac{\Gamma(\frac{\kappa}{2})}{\Gamma(\frac{\kappa-3}{2})}\int_0^\infty dy\,\frac{y}{(1+y^2)^{\kappa/2}}\ln\left(\frac{x+y+i\epsilon}{x-y+i\epsilon}\right)\\ &= \frac{1}{x}\frac{\kappa-3}{\kappa-2}{}_2F_1\left(1,\frac{1}{2};\frac{\kappa}{2};1+[(1\pm i\epsilon)x]^{-2}\right).\end{aligned} \tag{4.143}$$

Here the $+(-)$ sign of the infinitesimal imaginary shift applies in the case $x > 0$ ($x < 0$). The details of evaluation of the integral are in App. D. If $x \gg 1$, i.e., sufficiently far above the infrared cutoff, and assuming that κ is not an integer,[6] the hypergeometric function in $\tilde{\pi}_\kappa(x)$ can be simplified, see App. E for details,

$$\tilde{\pi}_\kappa(x) \simeq \frac{1}{x} - i\sqrt{\pi}\,\frac{\Gamma([\kappa-2]/2)}{\Gamma([\kappa-3]/2)}|x|^{2-\kappa}. \tag{4.144}$$

If $x \ll 1$, i.e., far below the IR cutoff, one finds

$$\tilde{\pi}_\kappa(x) \simeq -i\sqrt{\pi}\,\frac{\Gamma\left(\frac{\kappa-2}{2}\right)}{\Gamma\left(\frac{\kappa-3}{2}\right)}\left(1-\frac{\kappa-2}{2}x^2\right) + (\kappa-3)x + \mathcal{O}(x^3). \tag{4.145}$$

From Eq. (4.144) one finds that, for $\kappa > 3$ as assumed above, the real part dominates above the infrared cutoff such that

$$g\Pi^R(E,p) \simeq -\frac{2p_\mu^2 p^2}{p^4-E^2} + i\sqrt{\pi}\,\frac{p_\mu^2 p_\Lambda^{\kappa-3}}{2p}\frac{\Gamma\left(\frac{\kappa-2}{2}\right)}{\Gamma\left(\frac{\kappa-3}{2}\right)}\left(\left|\frac{E+p^2}{2p\,p_\Lambda}\right|^{2-\kappa} - \left|\frac{E-p^2}{2p\,p_\Lambda}\right|^{2-\kappa}\right), \tag{4.146}$$

while, below the cutoff, the loop function approaches

$$g\Pi^R(E,p) \simeq -\frac{p_\mu^2}{2p_\Lambda^2}\left(\kappa - 3 + i\sqrt{\pi}\,\frac{\Gamma\left(\frac{\kappa}{2}\right)}{\Gamma\left(\frac{\kappa-3}{2}\right)}\frac{E}{pp_\Lambda}\right). \tag{4.147}$$

[6] The case of an integer κ could be discussed and allowed for, too, but in a more complicated way due to the non-simple pole structure of the integral represent of the hypergeometric function (in the form of Mellin-Barnes integral). Since it can be seen from the numerical results in the next chapter that there is no discontinuity in the transition from non-integer to integer values of κ, it should be sufficient to use the expressions for non-integer κ and take the limit to an integer value.

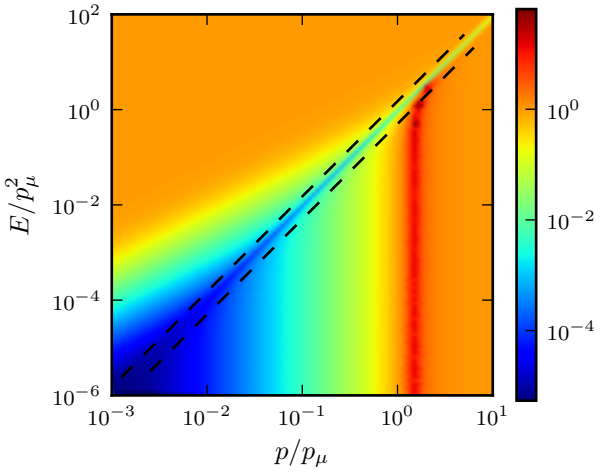

Figure 4.3: Contour plot of $g_{\text{eff}}^2(E,p)/g^2$ defined in Eq. (4.129), with $\Pi^R(E,p)$ given in Eq. (4.142), for $\kappa = 3.5$ and $p_\Lambda = 10^{-3}$.

As a result, for $|E \pm p^2| \gg 2p_\Lambda p$, the loop integral scales as $\Pi^R(s^2E, sp) = s^{-2}\Pi^R(E,p)$. Inserting this into Eq. (4.129), we find that, in the momentum region $p_\Lambda \ll |E \pm p^2|/p \ll p_\xi$ the effective coupling assumes the universal scaling form

$$g_{\text{eff}}(p_0,p) \simeq \frac{\left|\varepsilon_p^2 - p_0^2\right|}{2\rho_{\text{nc}}\,\varepsilon_p}\,, \tag{4.148}$$

independent of both, the microscopic interaction constant g, and the scaling exponent κ of f, and scaling as

$$g_{\text{eff}}(s^2p_0, sp) = s^2 g_{\text{eff}}(p_0,p). \tag{4.149}$$

Together with Eqs. (3.25) and (3.13), this gives the scaling exponents $\gamma_\kappa = m_\kappa = 2$ of the many-body T-matrix reported in Eqs. (3.24) and (3.26). In the IR limit, for $|E \pm p^2|/p \ll p_\Lambda \ll p_\mu$, the effective coupling saturates at the constant value

$$g_{\text{eff}}(p_0,p) \simeq \frac{2\varepsilon_{p_\Lambda}}{\rho_{\text{nc}}}\,. \tag{4.150}$$

At larger energy and momentum scales, above the healing-length scale, $|E \pm p^2|/p \gg p_\mu$, the effective coupling saturates at the microscopic interaction constant, $g_{\text{eff}} \simeq g$, recovering $\gamma_\kappa = 0$ and the perturbative Boltzmann T-matrix Eq. (3.25) with scaling exponent $m_\kappa = 0$. We emphasize that, while the transition scale from the microscopic coupling g to the universal scaling form (4.148) is set by p_μ and thus by the microscopic coupling g, the particular value of the *universal* coupling g_{eff} is independent of g.

Fig. 4.3 shows the effective coupling constant in the E–p plane, on a double-logarithmic scale. Cuts through this graph, for $E = 0.5p^2$ and $E = 1.5p^2$, are shown in Fig. 4.4, for three different values of the infrared cutoff p_Λ. These figures

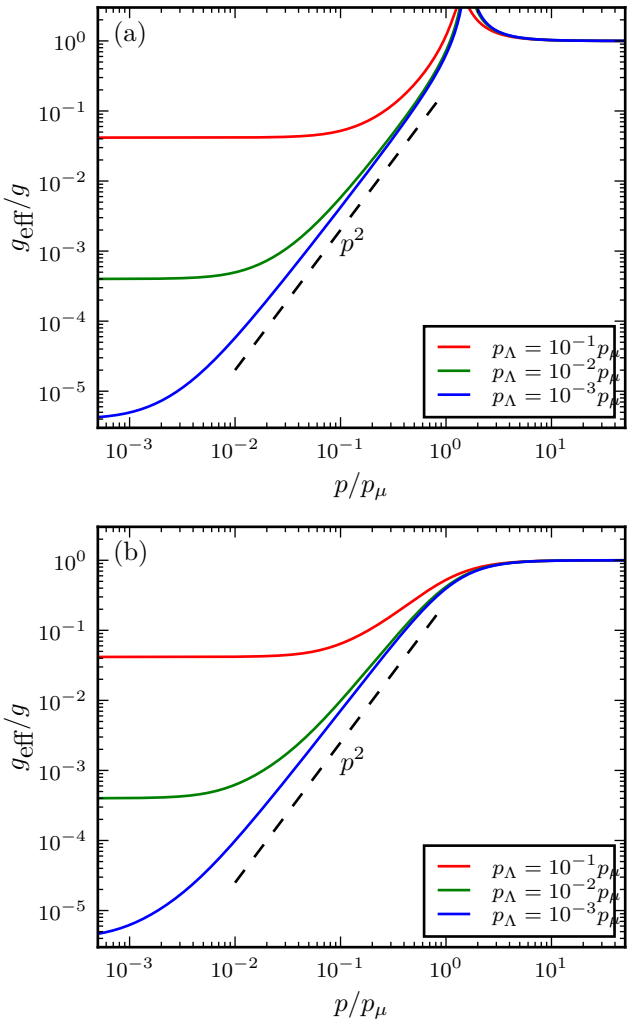

Figure 4.4: Effective coupling $g^2_{\rm eff}(E,p)$ as a function of momentum p. Shown are different cuts in the p–E-plane, with (a) $E = 0.5p^2$ and (b) $E = 1.5p^2$. Different colors refer to different infrared cutoff scales k_Λ as listed in the legends.

demonstrate the scaling of $g_{\rm eff}(E,p) \sim p^2$ within the regime $p_\Lambda \ll p \ll p_\mu$ and the saturation to $g_{\rm eff}(E,p) = g$ for $p \gg p_\mu$.

Depending on the choice of E, a maximum appears in between these scaling regimes, see also Fig. 4.3, at momenta

$$p^4 - E_0(p)^2 = 2p_\mu^2 p^2 \,. \tag{4.151}$$

On this line, the real part of $1 + g\Pi^R$ vanishes, and the denominator of the effective coupling is dominated by the imaginary part,

$$g_{\rm eff}(E_0(p),p) = 1/|{\rm Im}\Pi^R(E_0(p),p)| \,. \tag{4.152}$$

Since ${\rm Im}\Pi^R(s^2E, sp) = s^{1-\kappa}{\rm Im}\Pi^R(E,p)$, see Eq. (4.146), $g_{\rm eff}(s^2E, sp) = s^{\kappa-1} g_{\rm eff}(E,p)$ along the curve of Eq. (4.151). Note that the scaling of the imaginary part of Π^R

alone matches with the dimensional counting of the integral on the RHS of Eq. (4.131) which should be the overall scaling of Π^R if there is no divergence in the integral.

We emphasize that, according to these non-perturbative results, the breakdown of the wave-Boltzmann scattering integral which was argued to appear due to the divergence of occupation numbers in the IR, is counteracted by a strong power-law fall-off of the scattering T-matrix. At very low scales, below the IR cutoff, the effective coupling saturates again to a much smaller constant, reinstating effectively the perturbative approximation in the lowest-p regime where the growth of occupation numbers is regulated to ensure convergence of physical quantities such as particle number and energy.

4.4.2 Effective many-body coupling function for Bogoliubov quasiparticles

For Bogoliubov quasi-particles in the linear, sound-wave regime, Eq. (2.13), the spectral function, in the basis of the fundamental fields Φ_a, is given in Eq. (4.101). Inserting this into Eq. (4.132) we obtain, in $d = 3$ dimensions,

$$\begin{aligned}
\Pi^\rho(-p_0,-\boldsymbol{p}) &= -\frac{i}{2}\int_k \frac{(2\pi g\rho_0)^2}{\omega_{\boldsymbol{k}}\omega_{\boldsymbol{p}-\boldsymbol{k}}}\Big[f(-k_0)-f(p_0-k_0)\Big] \\
&\quad\times\Big[\delta(k_0+\omega_{\boldsymbol{k}})\delta(p_0-k_0+\omega_{\boldsymbol{p}-\boldsymbol{k}})-\delta(k_0-\omega_{\boldsymbol{k}})\delta(p_0-k_0+\omega_{\boldsymbol{p}-\boldsymbol{k}}) \\
&\qquad+\delta(k_0-\omega_{\boldsymbol{k}})\delta(p_0-k_0-\omega_{\boldsymbol{p}-\boldsymbol{k}})-\delta(k_0+\omega_{\boldsymbol{k}})\delta(p_0-k_0-\omega_{\boldsymbol{p}-\boldsymbol{k}})\Big] \\
&= -i\pi\int\frac{d^dk}{(2\pi)^d}\frac{(g\rho_0)^2}{\omega_{\boldsymbol{k}}\omega_{\boldsymbol{p}-\boldsymbol{k}}}\Big\{\Big[f(\omega_{\boldsymbol{k}})-f(-\omega_{\boldsymbol{p}-\boldsymbol{k}})\Big]\delta(p_0+\omega_{\boldsymbol{k}}+\omega_{\boldsymbol{p}-\boldsymbol{k}}) \\
&\qquad-\Big[f(-\omega_{\boldsymbol{k}})-f(-\omega_{\boldsymbol{p}-\boldsymbol{k}})\Big]\delta(p_0-\omega_{\boldsymbol{k}}+\omega_{\boldsymbol{p}-\boldsymbol{k}}) \\
&\qquad+\Big[f(-\omega_{\boldsymbol{k}})-f(\omega_{\boldsymbol{p}-\boldsymbol{k}})\Big]\delta(p_0-\omega_{\boldsymbol{k}}-\omega_{\boldsymbol{p}-\boldsymbol{k}}) \\
&\qquad-\Big[f(\omega_{\boldsymbol{k}})-f(\omega_{\boldsymbol{p}-\boldsymbol{k}})\Big]\delta(p_0+\omega_{\boldsymbol{k}}-\omega_{\boldsymbol{p}-\boldsymbol{k}})\Big\} \\
&= -i\Big(\frac{g\rho_0}{2\pi}\Big)^2\int \mathrm{d}^3k\frac{1}{\omega_k\omega_{|\boldsymbol{p}-\boldsymbol{k}|}}f(\omega_k)\Big[\delta(p_0+\omega_k+\omega_{|\boldsymbol{p}-\boldsymbol{k}|})-\delta(p_0+\omega_k-\omega_{|\boldsymbol{p}-\boldsymbol{k}|}) \\
&\qquad-\delta(p_0-\omega_k-\omega_{|\boldsymbol{p}-\boldsymbol{k}|})+\delta(p_0-\omega_k+\omega_{|\boldsymbol{p}-\boldsymbol{k}|})\Big] \\
&= -\frac{i}{2\pi\omega_p}\Big(\frac{g\rho_0}{c_s}\Big)^2\int_0^\infty \mathrm{d}k\int_{|p-k|}^{p+k}\mathrm{d}r f(\omega_k)\Big[\delta(E+k+r)-\delta(E+k-r) \\
&\qquad-\delta(E-k-r)+\delta(E-k+r)\Big], \qquad (4.153)
\end{aligned}$$

where we have replaced the integral over the angle $\measuredangle(\boldsymbol{p},\boldsymbol{k})$ by an integral over $r = |\boldsymbol{p}-\boldsymbol{k}|$, and defined $p_0 = c_s E$. Inserting this into Π^R, Eq. (4.131), gives

$$\begin{aligned}\Pi^R(p_0,p) &= -\int_{-\infty}^{\infty}\frac{dq_0}{2\pi}\frac{i}{q_0+i\epsilon}\Pi^\rho(-(p_0-q_0),-\boldsymbol{p})\\ &= -\frac{1}{(2\pi)^2\omega_p}\left(\frac{g\rho_0}{c_s}\right)^2\int_0^\infty \mathrm{d}k\int_{|p-k|}^{p+k}\mathrm{d}r f(\omega_k)\Big[\frac{1}{E+k+r+i\epsilon}-\frac{1}{E+k-r+i\epsilon}\\ &\qquad -\frac{1}{E-k-r+i\epsilon}+\frac{1}{E-k+r+i\epsilon}\Big]\\ &= -\frac{p_\Lambda p_\xi}{(2\pi)^2\sqrt{2}}\frac{m}{p}\left[\widetilde{\Pi}'_f\left(\tfrac{E+p}{2p_\Lambda}\right)-\widetilde{\Pi}'_f\left(\tfrac{E-p}{2p_\Lambda}\right)\right], \end{aligned}\tag{4.154}$$

where $\widetilde{\Pi}'_f$ is defined as

$$\widetilde{\Pi}'_f(x) = \int_0^\infty dy\, f(\omega_{yp_\Lambda})\ln\left(\frac{x+y+i\epsilon}{x-y+i\epsilon}\right).\tag{4.155}$$

To proceed, we need to specify the quasi-particle distribution $f(\omega_{\boldsymbol{k}})$. Choosing again the infrared cutoff to be p_Λ, and in view of wave-turbulent solutions, we assume f to have the scaling form

$$f(p_0) = \mathrm{sgn}(p_0)\left(\frac{\omega_\Lambda}{|p_0|+\omega_{p_\Lambda}}\right)^\kappa.\tag{4.156}$$

where the signum function accounts for the symmetry stated in Eq. (4.99), and the scale Λ is fixed by the normalization of $n(p,t)$ to the total density n, see Eq. (4.158). Inserting Eq. (4.156) into Eq. (4.155) and assuming $\kappa > 2$, to ensure that there is no UV-divergence, gives

$$\begin{aligned}\widetilde{\Pi}'_f(x) &= \left(\frac{\Lambda}{p_\Lambda}\right)^\kappa\int_0^\infty dy\,(1+y)^{-\kappa}\ln\left(\frac{x+y+i\epsilon}{x-y+i\epsilon}\right)\\ &= \left(\frac{\Lambda}{p_\Lambda}\right)^\kappa\frac{1}{(\kappa-1)^2 x}\Big[{}_2F_1\left(1,1;\kappa;1-[(1\pm i\epsilon)x]^{-1}\right)\\ &\qquad +{}_2F_1\left(1,1;\kappa;1+[(1\pm i\epsilon)x]^{-1}\right)\Big], \end{aligned}\tag{4.157}$$

where the $+(-)$ sign of the infinitesimal imaginary shift applies for $x > 0\,(x < 0)$, see App. D for details. The factor Λ^κ, resulting from the overall magnitude of f, cf. Eq. (4.156), is fixed by the normalization of the single-particle distribution to the non-condensed density ρ_{nc},

$$\begin{aligned}\rho_{\mathrm{nc}} &= \int\frac{\mathrm{d}^d k}{(2\pi)^d}\frac{p_\xi}{\sqrt{2}k}\left(\frac{\Lambda}{k+p_\Lambda}\right)^\kappa\\ &= \frac{S_{d-1}\Lambda^\kappa p_\Lambda^{d-\kappa-1}p_\xi}{\sqrt{2}(2\pi)^d}\int_0^\infty du\,u^{d-2}(1+u)^{-\kappa}\\ &= \left(\frac{\Lambda}{p_\Lambda}\right)^\kappa\frac{p_\Lambda^{d-1}p_\xi}{2^{d-1/2}\pi^{d/2}}\frac{\Gamma(\kappa-d+1)\Gamma(d-1)}{\Gamma(d/2)\Gamma(\kappa)}. \end{aligned}\tag{4.158}$$

With this, the retarded loop integral (4.154) can be written as

$$\Pi^R(E,p) = -\frac{p_\mu^2}{2gpp_\Lambda}\left[\tilde{\pi}'_\kappa\left(\tfrac{E+p}{2p_\Lambda}\right) - \tilde{\pi}'_\kappa\left(\tfrac{E-p}{2p_\Lambda}\right)\right], \tag{4.159}$$

with

$$\begin{aligned}\tilde{\pi}'_\kappa(x) = \frac{1}{2x}\frac{\kappa-2}{\kappa-1}\Big[&{}_2F_1\left(1,1;\kappa;1-[(1\pm i\epsilon)x]^{-1}\right)\\ &+{}_2F_1\left(1,1;\kappa;1+[(1\pm i\epsilon)x]^{-1}\right)\Big].\end{aligned} \tag{4.160}$$

If $|x| \gg 1$, i.e., sufficiently far above the infrared cutoff, and assuming that κ is not an integer, the hypergeometric functions are approximated, in leading order, by

$$\begin{aligned}&\frac{\kappa-2}{\kappa-1}\,{}_2F_1(1,1;\kappa;1+[(1\pm i\epsilon)|x|]^{-1}) \approx 1 \mp \frac{i\pi(\kappa-2)}{|x|^{\kappa-2}},\\ &\frac{\kappa-2}{\kappa-1}\,{}_2F_1(1,1;\kappa;1-[(1\pm i\epsilon)|x|]^{-1}) \approx 1,\end{aligned} \tag{4.161}$$

see App. E for details. Then, the $\tilde{\pi}$ in this limit becomes

$$\tilde{\pi}'_\kappa(x) \approx \frac{1}{x} - \frac{i\pi}{2|x|^{\kappa-1}}(\kappa-2), \tag{4.162}$$

while below the cutoff, one gets

$$\tilde{\pi}'_\kappa(x) \approx -\frac{i\pi}{2}(\kappa-2) - [C(\kappa) + (\kappa-2)(\kappa-1)\ln x]\,x + \mathcal{O}(x^2), \tag{4.163}$$

with a κ-dependent constant $C(\kappa)$.

The resulting form of Π^R depends on the relative size of E and p. Here we only quote the form applying in the regions where $E > p$ and $E < |p|$ as the scattering integral will receive its dominating contributions there. Inserting Eq. (4.161) into Eq. (4.160) one finds that, for $\kappa > 2$ as assumed above, the real part dominates above the infrared cutoff such that,

$$g\Pi^R(E,p) \simeq -\frac{2p_\mu^2}{p^2-E^2} + i\pi(\kappa-2)\frac{p_\mu^2 p_\Lambda^{\kappa-2}}{4p}\left(\left|\frac{E+p}{2}\right|^{1-\kappa} - \left|\frac{E-p}{2}\right|^{1-\kappa}\right). \tag{4.164}$$

Below the cutoff, the retarded loop approaches

$$g\Pi^R(E,p) \simeq \frac{p_\mu^2}{2p_\Lambda^2}C(\kappa) + \text{log. corrections}. \tag{4.165}$$

As a result, for $p, |E \pm p| \gg p_\Lambda$ and $\kappa > 2$, the loop integral scales as $\Pi^R(s^2E, sp) = s^{-2}\Pi^R(E,p)$. Inserting this into Eq. (4.129), we find that, in the momentum region $p_\Lambda \ll |E \pm p^2|/p \ll p_\mu$ the effective coupling assumes the universal scaling form

$$g_{\text{eff}}(p_0,p) \simeq \frac{|\omega_p^2 - p_0^2|}{4mc_s^2\rho_{\text{nc}}}, \tag{4.166}$$

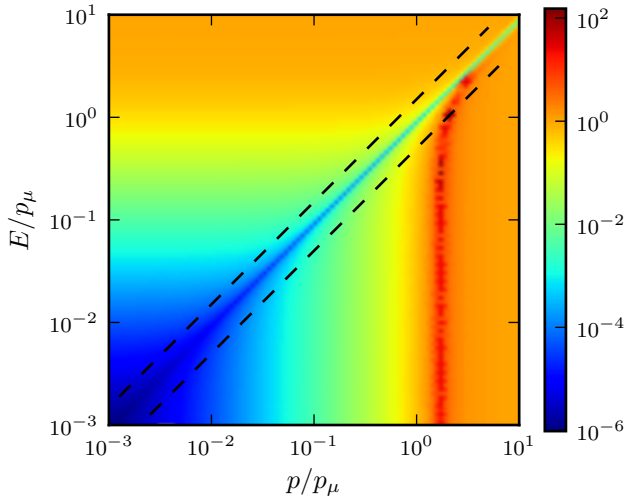

Figure 4.5: Contour plot of $g^2_{\text{eff}}(E,p)$ defined in Eq. (4.129), with $\Pi^R(E,p)$ given in Eq. (4.159), for $\kappa = 3.5$ and $p_\Lambda = 10^{-3}$.

which is, again, effectively independent of the microscopic interaction constant g and scales as

$$g_{\text{eff}}(sp_0, sp) = s^2 g_{\text{eff}}(p_0, p). \tag{4.167}$$

Together with Eqs. (3.28) and (3.13) this gives the scaling exponents $\gamma_\kappa = 2$, $m_\kappa = 0$, of the many-body T-matrix reported in Eqs. (3.24) and (3.29). In the IR limit, the coupling saturates to the same constant (4.150) as for the free case, but, due to the logarithmic terms in a much slower manner.

At larger energy and momentum scales, above the healing-length scale, $|E \pm p^2|/p \gg p_\mu$, the effective coupling saturates at the microscopic interaction constant, $g_{\text{eff}} \simeq g$, recovering the perturbative Boltzmann T-matrix Eq. (3.28) with scaling exponent $m_\kappa = m = -2$. We again emphasize that, while the transition scale from the microscopic coupling g to the universal scaling form (4.166) is set by p_μ and thus by the microscopic coupling g, the particular value of the *universal* coupling g_{eff} is independent of g.

Fig. 4.5 shows the effective coupling constant in the (p,E) plane, on a double-logarithmic scale. While the coupling is constant at large momenta and energies, it falls off as power laws in the infrared. Cuts through Fig. 4.5, for $E = 0.5\,p$ and $E = 1.5\,p$, are shown in Fig. 4.6, for three different values of the infrared cutoff p_Λ. The curves again show the saturation to g at momenta above the healing-length scale, the power-law scaling below, and a weaker scaling below the infrared cutoff scale p_Λ.

The real part of Π^R now vanishes along the curve designated by

$$p^2 - E_0(p)^2 = 2p_\mu^2\,, \tag{4.168}$$

and on this curve, effective coupling is again dominated by imaginary part of Π^R with a scaling $g_{\text{eff}}(sE, sp) = s^\kappa g_{\text{eff}}(E,p)$, see Eq. (4.164). Also in the quasiparticle

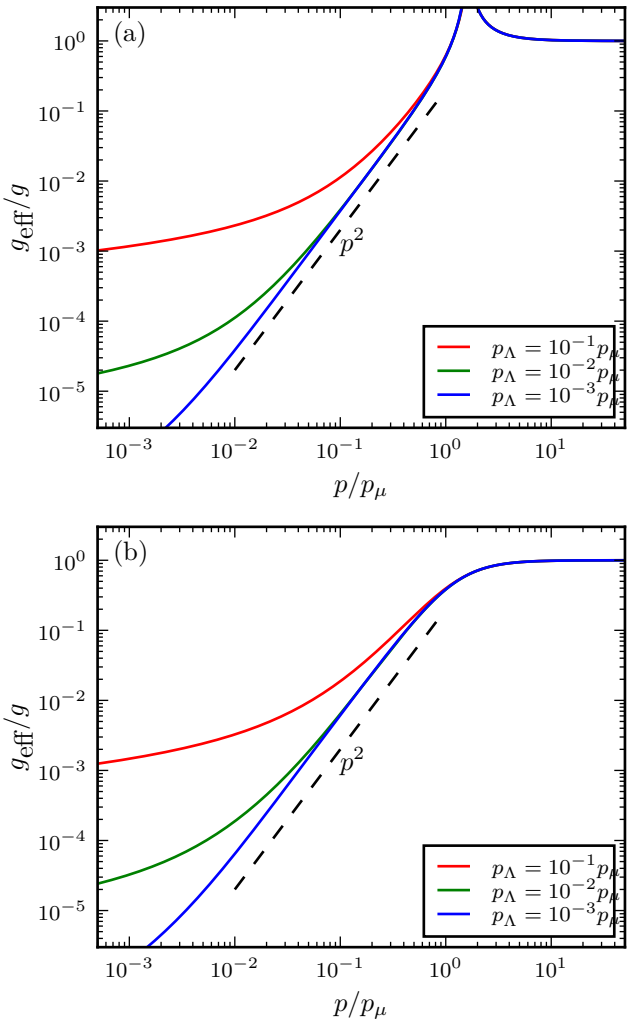

Figure 4.6: Effective coupling $g^2_{\mathrm{eff}}(E,p)$ as a function of momentum p. Shown are different cuts in the p–E-plane, with (a) $E = 0.5p$ and (b) $E = 1.5p$. Different colors refer to different infrared cutoff scales k_Λ as listed in the legends.

case, the imaginary part of Π^R preserves the scaling from dimensional counting. This can be seen from Eq. (4.131) as counting the scaling directly from the dimensions of the factors in the integrand gives

$$\Pi^R(s^z p_0, s\boldsymbol{p}) = s^{d+z-4-\kappa}\Pi^R(p_0, \boldsymbol{p})\,, \tag{4.169}$$

and this result can only be obtained in the absence of a real part.

4.5 Summary

We have derived the closed equations of mean field and propagators of the complex Bose field using nonequilibrium quantum field theory in an expansion of the effective

action in terms of 2PI diagrams. The propagators, self-energies and other composite two-point functions are decomposed into statistical parts F and spectral parts ρ. We have shown how to turn the equations for F and ρ into a kinetic equation by means of Wigner coordinates. In the center coordinate, only F undergoes dynamical evolution while ρ remains static. The kinetic-like equation emerges from the equation for F in center time where we expand the self-energy to next-to-leading order in an expansion in the inverse of the number of field components $\mathcal{N}$. This corresponds to the effective T-matrix being a result of the s-channel resummation and we have used this to explicitly calculate the loop function Π^R which enters the self energy such that we can determine the scaling behaviour of the effective T-matrix which represents the main input for analysing kinetic equation in the nonperturbative infrared regime.

The central result in this chapter and of this thesis is an apparently universal scaling of the effective coupling g_{eff}, see Eqs. (4.149) and (4.167). We can not prove yet its universal nature but we are convinced of it from the calculations presented in this chapter, the analysis in App. F and similar calculations for the one-demensional case [96]. The scaling of g_{eff} is the crucial ingredient allowing for the analysis of the kinetic equation presented in Ch. 3. The deviation of scaling behaviour of g_{eff} in our calculation from the one determined by naive power-counting arguments is due to the presence of the infrared cutoff.Taking this into account our results provide a substantial improvement compared to the results presented in [26, 49]. For the scaling $g_{\text{eff}} \sim p^4$ estimated there, we would, in fact, obtain the very same exponents.

We emphasize that the exponents predicted in [26, 49] rather happen to capture the phenomenon of superfluid turbulence since they fit very well with the numerical calculations [27–29] where vortices are present at the time when the exponents predicted there occur.

Chapter 5

Numerical evaluation of scattering integral

In the previous chapter, we have derived a non-perturbative kinetic equation within a nonequilibrium quantum field theory as well as explicit expressions for effective many-body coupling g_{eff}. Using these, we have performed a scaling analysis to extract the Kolmogorov-Zakharov and the temporal exponents from the nonperturbative kinetic equation as described in detail in Ch. 3. Provided the scaling ansatz for the resulting occupation number distributions we could derive an explicit expression of the scattering integral with which one can evaluate all scaling exponents by means of numerical integration. In the following we will derive the analytical form of this scattering integral and present the results of its numerical evaluation.

First, we evaluate the Kolmogorov-Zakharov exponents κ_Q and κ_P. This can be done by seeking the κ exponents that nullify the scattering integral. We compute the scattering integral as a function of κ while all other parameters fixed, in the same way it was done in Ref. [86]. The values of κ which characterise the stationary solutions are inferred from the position of the zeroes of the scattering integral. At the same time, the sign of the slope of the scattering integral at these zeroes determines the direction of the cascade. In this way we can identify the respective cascade to be a direct or an inverse one. Moreover, we evaluate the scattering integral for a particular exponent κ, as function of the external momentum and calculate the particle and the energy fluxes to see whether there is a window where fluxes are momentum-independent which is a signature of a cascade behaviour.

The self-similar exponent κ_S can not be obtained in the same way since it is a non-stationary solution. However, as we saw in Sect. 3.2.3 the respective scattering integral falls off with the same power law as the quasiparticle occupation number. We thus evaluate the scattering integral as a function of the external momentum to observe its power law behaviour. Note that the existence of a self-similar exponent has been pointed out in Ref. [15] but was neglected because a self-similar time evolution was not found to be possible, for the dilute Bose gas model studied, in the perturbative regime. In Ref. [50], the self-similar time evolution was found to occur in the nonperturbative regime, derived by means of nonequilibrium quantum field theory within the s-channel resummation in the language of a large-$\mathcal{N}$ expansion, as discussed in detail in Ch. 4. However, the momentum exponents found there, as well

as in Refs. [27, 28] are different from the exponents we predict in Eq. (3.32). One possibility is that the exponents observed in Refs. [27, 28, 50] which were obtained numerically may not be described by the kinetic equation.

The temporal exponent μ of the scattering integral can be recovered assumption $\rho_{\mathrm{nc}} = \text{const.}$, or $\delta = 0$, since this leaves only the infrared cutoff scale being a time-independent scale in our calculation. The exponent μ is critical to determine the value of β and β' as we have shown in Sect. 3.3. We have to point out that the recovering of μ in this chapter does not allow to prove the relation (3.48). Here, we can only show that there exists an exponent μ according to the scaling transformation (3.42) and that the value found confirms Eq. (3.44). The LHS of Eq. (3.48) needs the presumption of a self-similar time evolution or turbulent cascade in the first place.

In the following, we present the integrals that are evaluated from Eqs. (4.120) and (4.127) to make them more suitable for the numerical integration. We then present the numerical results for each case. In general, the momentum exponents agree well with the results from power counting in Ch. 3. The exponent μ under the assumption $\rho_{\mathrm{nc}} = \text{const.}$ is universal, $\mu = -1$. Finally, we discuss the scenarios of the universal dynamics of a dilute Bose gas in the kinetic regime based on our results.

5.1 Analytical simplification of the scattering integral

In this section, we perform part of the integrations in the scattering integral that can be done analytically in Eqs. (4.120) and (4.127) to get rid of the delta functions and reduce the numbers of integrals that have to be done numerically. The discussion will be separately presented for the free particles and Bogoliubov quasiparticles in the linear-dispersion regime.

5.1.1 Free particles

We first recall Eq. (4.120) and rearrange the Boltzmann factor terms,

$$\begin{aligned} I(\boldsymbol{p}) = (2\pi)^4 \int_{\boldsymbol{kqr}} g_{\mathrm{eff}}^2(\varepsilon_{\boldsymbol{p}} - \varepsilon_{\boldsymbol{r}}, \boldsymbol{p} - \boldsymbol{r}) \delta(\boldsymbol{p} + \boldsymbol{k} - \boldsymbol{q} - \boldsymbol{r}) \\ \times \delta(\varepsilon_{\boldsymbol{p}} + \varepsilon_{\boldsymbol{k}} - \varepsilon_{\boldsymbol{q}} - \varepsilon_{\boldsymbol{r}}) \Big\{ f(\varepsilon_{\boldsymbol{p}}) f(\varepsilon_{\boldsymbol{r}}) \Big[f(\varepsilon_{\boldsymbol{q}}) - f(\varepsilon_{\boldsymbol{k}}) \Big] \\ + \Big[f(\varepsilon_{\boldsymbol{r}}) - f(\varepsilon_{\boldsymbol{p}}) \Big] f(\varepsilon_{\boldsymbol{q}}) f(\varepsilon_{\boldsymbol{k}}) \Big\}, \end{aligned} \tag{5.1}$$

where the dimension is chosen to be $d = 3$. The terms are such that the integration over $\mathrm{d}\boldsymbol{k}$ and $\mathrm{d}\boldsymbol{q}$ can be done. We leave the $\mathrm{d}\boldsymbol{r}$ integration for the numerical evaluation because $\boldsymbol{r}$ also appears in the arguments of the many-body coupling function g_{eff}. We start by eliminating the delta distribution of the spatial momenta and substitute variables such that there is no term that involves the addition or the subtraction of

more than two vectors,

$$
\begin{aligned}
I(\boldsymbol{p}) &= (2\pi)\int_{\boldsymbol{kr}} g_{\text{eff}}^2(\varepsilon_{\boldsymbol{p}}-\varepsilon_{\boldsymbol{r}},\boldsymbol{p}-\boldsymbol{r})\,\delta(\varepsilon_{\boldsymbol{p}}+\varepsilon_{\boldsymbol{k}}-\varepsilon_{\boldsymbol{p}+\boldsymbol{k}-\boldsymbol{r}}-\varepsilon_{\boldsymbol{r}}) \\
&\quad\times\Big\{f(\varepsilon_{\boldsymbol{p}})f(\varepsilon_{\boldsymbol{r}})\Big[f(\varepsilon_{\boldsymbol{p}+\boldsymbol{k}-\boldsymbol{r}})-f(\varepsilon_{\boldsymbol{k}})\Big]+\Big[f(\varepsilon_{\boldsymbol{r}})-f(\varepsilon_{\boldsymbol{p}})\Big]f(\varepsilon_{\boldsymbol{p}+\boldsymbol{k}-\boldsymbol{r}})f(\varepsilon_{\boldsymbol{k}})\Big\} \\
&= (2\pi)\int_{\boldsymbol{kr}'} g_{\text{eff}}^2(\varepsilon_{\boldsymbol{p}}-\varepsilon_{\boldsymbol{p}-\boldsymbol{r}'},\boldsymbol{r}')\,\delta(\varepsilon_{\boldsymbol{p}}+\varepsilon_{\boldsymbol{k}}-\varepsilon_{\boldsymbol{k}+\boldsymbol{r}'}-\varepsilon_{\boldsymbol{p}-\boldsymbol{r}'}) \\
&\quad\times\Big\{f(\varepsilon_{\boldsymbol{p}})f(\varepsilon_{\boldsymbol{p}-\boldsymbol{r}'})\Big[f(\varepsilon_{\boldsymbol{k}+\boldsymbol{r}'})-f(\varepsilon_{\boldsymbol{k}})\Big]+\Big[f(\varepsilon_{\boldsymbol{p}-\boldsymbol{r}'})-f(\varepsilon_{\boldsymbol{p}})\Big]f(\varepsilon_{\boldsymbol{k}+\boldsymbol{r}'})f(\varepsilon_{\boldsymbol{k}})\Big\} \\
&= (2\pi)^{-2}\int_{\boldsymbol{r}'} g_{\text{eff}}^2(\varepsilon_{\boldsymbol{p}}-\varepsilon_{\boldsymbol{p}-\boldsymbol{r}'},\boldsymbol{r}')\int_0^\infty \mathrm{d}k\,k^2\int_{-1}^{1}\mathrm{d}\cos\theta_{\boldsymbol{k}}\int_0^{2\pi}\mathrm{d}\phi_{\boldsymbol{k}} \\
&\quad\times\delta(\varepsilon_{\boldsymbol{p}}+\varepsilon_{\boldsymbol{k}}-\varepsilon_{\boldsymbol{k}+\boldsymbol{r}'}-\varepsilon_{\boldsymbol{p}-\boldsymbol{r}'}) \\
&\quad\times\Big\{f(\varepsilon_{\boldsymbol{p}})f(\varepsilon_{\boldsymbol{p}-\boldsymbol{r}'})\Big[f(\varepsilon_{\boldsymbol{k}+\boldsymbol{r}'})-f(\varepsilon_{\boldsymbol{k}})\Big]+\Big[f(\varepsilon_{\boldsymbol{p}-\boldsymbol{r}'})-f(\varepsilon_{\boldsymbol{p}})\Big]f(\varepsilon_{\boldsymbol{k}+\boldsymbol{r}'})f(\varepsilon_{\boldsymbol{k}})\Big\} \\
&= (2\pi)^{-1}\int_{\boldsymbol{r}'}\frac{1}{r'}g_{\text{eff}}^2(\varepsilon_{\boldsymbol{p}}-\varepsilon_{\boldsymbol{p}-\boldsymbol{r}'},\boldsymbol{r}')\int_0^\infty \mathrm{d}k\,k\int_{|k-r'|}^{|k+r'|}\mathrm{d}q\,q\,\delta(\varepsilon_{\boldsymbol{p}}+\varepsilon_{\boldsymbol{k}}-\varepsilon_{\boldsymbol{q}}-\varepsilon_{\boldsymbol{p}-\boldsymbol{r}'}) \\
&\quad\times\Big\{f(\varepsilon_{\boldsymbol{p}})f(\varepsilon_{\boldsymbol{p}-\boldsymbol{r}'})\Big[f(\varepsilon_{\boldsymbol{q}})-f(\varepsilon_{\boldsymbol{k}})\Big]+\Big[f(\varepsilon_{\boldsymbol{p}-\boldsymbol{r}'})-f(\varepsilon_{\boldsymbol{p}})\Big]f(\varepsilon_{\boldsymbol{q}})f(\varepsilon_{\boldsymbol{k}})\Big\}. \qquad (5.2)
\end{aligned}
$$

Here, we have changed variables by setting $\boldsymbol{r}=\boldsymbol{p}-\boldsymbol{r}'$ in the second equality and defined $\boldsymbol{q}=\boldsymbol{k}+\boldsymbol{r}'$ in the last equality. The norm of $\boldsymbol{k}$ is now written as k. We set the $\boldsymbol{k}$-coordinate such that the vector $\boldsymbol{r}'$ is parallel to the z-component of $\boldsymbol{k}$ so the polar angle $\theta_{\boldsymbol{k}}$ is also the angle between $\boldsymbol{r}'$ and $\boldsymbol{k}$. This allows us to replace the integral over $\mathrm{d}\cos\theta_{\boldsymbol{k}}$ by the integral over $\mathrm{d}q$. To proceed further, we insert $f(p_0)$ from Eq. (4.137) and the free energy dispersion, $\varepsilon(\boldsymbol{p})=p^2/2m$,

$$
\begin{aligned}
I(\boldsymbol{p}) &= \frac{2m}{2\pi}\int_{\boldsymbol{r}'}\frac{1}{r'}g_{\text{eff}}^2(\varepsilon_{\boldsymbol{p}}-\varepsilon_{\boldsymbol{p}-\boldsymbol{r}'},\boldsymbol{r}')\int_0^\infty \mathrm{d}k\,k\int_{|k-r'|}^{|k+r'|}\mathrm{d}q\,q\,\delta(p^2+k^2-q^2-|\boldsymbol{p}-\boldsymbol{r}'|^2) \\
&\quad\times\Big\{\frac{\Lambda^{2\kappa}}{(p^2+p_\Lambda^2)^{\kappa/2}(|\boldsymbol{p}-\boldsymbol{r}'|^2+p_\Lambda^2)^{\kappa/2}}\Big[\frac{\Lambda^\kappa}{(q^2+p_\Lambda^2)^{\kappa/2}}-\frac{\Lambda^\kappa}{(k^2+p_\Lambda^2)^{\kappa/2}}\Big] \\
&\qquad+\Big[\frac{\Lambda^\kappa}{(|\boldsymbol{p}-\boldsymbol{r}'|^2+p_\Lambda^2)^{\kappa/2}}-\frac{\Lambda^\kappa}{(p^2+p_\Lambda^2)^{\kappa/2}}\Big]\frac{\Lambda^{2\kappa}}{(q^2+p_\Lambda^2)^{\kappa/2}(k^2+p_\Lambda^2)^{\kappa/2}}\Big\} \\
&= \frac{2m\,\Lambda^{3\kappa}}{2\pi}\int_{\boldsymbol{r}'}\frac{1}{r'}g_{\text{eff}}^2(\varepsilon_{\boldsymbol{p}}-\varepsilon_{\boldsymbol{p}-\boldsymbol{r}'},\boldsymbol{r}')\Big\{\frac{I_1^{\text{free}}(\boldsymbol{p},\boldsymbol{r}')}{(p^2+p_\Lambda^2)^{\kappa/2}(|\boldsymbol{p}-\boldsymbol{r}'|^2+p_\Lambda^2)^{\kappa/2}} \\
&\qquad+\Big[\frac{1}{(|\boldsymbol{p}-\boldsymbol{r}'|^2+p_\Lambda^2)^{\kappa/2}}-\frac{1}{(p^2+p_\Lambda^2)^{\kappa/2}}\Big]I_2^{\text{free}}(\boldsymbol{p},\boldsymbol{r}')\Big\}, \qquad (5.3)
\end{aligned}
$$

where we define

$$
\begin{aligned}
I_1^{\text{free}}(\boldsymbol{p},\boldsymbol{r}') &= \int_0^\infty \mathrm{d}k\,k\int_{|k-r'|}^{|k+r'|}\mathrm{d}q\,q\,\delta(p^2+k^2-q^2-|\boldsymbol{p}-\boldsymbol{r}'|^2) \\
&\quad\times\Big[\frac{1}{(q^2+p_\Lambda^2)^{\kappa/2}}-\frac{1}{(k^2+p_\Lambda^2)^{\kappa/2}}\Big], \qquad (5.4) \\
I_2^{\text{free}}(\boldsymbol{p},\boldsymbol{r}') &= \int_0^\infty \mathrm{d}k\,k\int_{|k-r'|}^{|k+r'|}\mathrm{d}q\,q\,\delta(p^2+k^2-q^2-|\boldsymbol{p}-\boldsymbol{r}'|^2) \\
&\quad\times\frac{1}{(q^2+p_\Lambda^2)^{\kappa/2}(k^2+p_\Lambda^2)^{\kappa/2}}. \qquad (5.5)
\end{aligned}
$$

We give the details how to evaluate these two integrals in the App. D. Inserting the results from Eqs. (D.15) and (D.20) into Eq. (5.3) yields

$$
\begin{aligned}
I(\boldsymbol{p}) = \frac{2m}{(2\pi)^3}\frac{\Lambda^{3\kappa}}{p}\int_0^\infty \mathrm{d}r\, r \int_{|p-r|}^{p+r} \mathrm{d}q\, g_{\mathrm{eff}}^2(\varepsilon_{\boldsymbol{p}} - \varepsilon_{\boldsymbol{r}}, \boldsymbol{q}) \\
\times \Big\{ \frac{2^{\kappa/2}}{4(\kappa-2)} \frac{1}{(p^2+p_\Lambda^2)^{\kappa/2}(r^2+p_\Lambda^2)^{\kappa/2}} \\
\times \Big[\Big(\frac{(p^2-r^2+q^2)^2}{2q^2} + 2p_\Lambda^2\Big)^{1-\kappa/2} - \Big(\frac{(p^2-r^2-q^2)^2}{2q^2} + 2p_\Lambda^2\Big)^{1-\kappa/2}\Big] \\
+ \frac{2^{\kappa-1}}{4(\kappa-1)}\Big[\frac{1}{(r^2+p_\Lambda^2)^{\kappa/2}} - \frac{1}{(p^2+p_\Lambda^2)^{\kappa/2}}\Big]\Big(\frac{(p^2-r^2)^2+q^4}{2q^2} + 2p_\Lambda^2\Big)^{1-\kappa} \\
\times {}_2F_1\Big(\frac{\kappa}{2}, \frac{\kappa-1}{2}; \frac{\kappa+1}{2}; \Big(\frac{2q^2(p^2-r^2)}{(p^2-r^2)^2+q^4+4p_\Lambda^2 q^2}\Big)^2\Big)\Big\} \\
= \frac{2m}{(2\pi)^3}\left(\frac{\Lambda}{p_\mu}\right)^{3\kappa} p_\mu^4\, g^2\, \tilde{I}[n_Q](x_p)\,, \qquad (5.6)
\end{aligned}
$$

where we have changed $\boldsymbol{r}'$ back to $\boldsymbol{r} = \boldsymbol{p} - \boldsymbol{r}'$ and define $\boldsymbol{q} = \boldsymbol{p} - \boldsymbol{r}$ so the integration over the polar angle $\mathrm{d}\theta_{\boldsymbol{r}}$ can be replaced by the integral over $\mathrm{d}q$. The dimensionless integral $\tilde{I}(x_p)$ which all momenta are in the unit of p_μ reads

$$
\begin{aligned}
\tilde{I}[n_Q](x_p) = \frac{1}{g^2\, x_p}\int_0^\infty \mathrm{d}x_r\, x_r \int_{|x_p-x_r|}^{x_p+x_r} \mathrm{d}x_q\, g_{\mathrm{eff}}^2(\varepsilon_{\boldsymbol{x}_p} - \varepsilon_{\boldsymbol{x}_r}, \boldsymbol{x}_q) \\
\times \Big\{ \frac{2^{\kappa/2}}{4(\kappa-2)} \frac{1}{(x_p^2+x_{p_\Lambda}^2)^{\kappa/2}(x_r^2+x_{p_\Lambda}^2)^{\kappa/2}} \\
\times \Big[\Big(\frac{(x_p^2-x_r^2+x_q^2)^2}{2x_q^2} + 2x_{p_\Lambda}^2\Big)^{1-\kappa/2} - \Big(\frac{(x_p^2-x_r^2-x_q^2)^2}{2x_q^2} + 2x_{p_\Lambda}^2\Big)^{1-\kappa/2}\Big] \\
+ \frac{2^{\kappa-1}}{4(\kappa-1)}\Big[\frac{1}{(x_r^2+x_{p_\Lambda}^2)^{\kappa/2}} - \frac{1}{(x_p^2+x_{p_\Lambda}^2)^{\kappa/2}}\Big]\Big(\frac{(x_p^2-x_r^2)^2+x_q^4}{2x_q^2} + 2x_{p_\Lambda}^2\Big)^{1-\kappa} \\
\times {}_2F_1\Big(\frac{\kappa}{2}, \frac{\kappa-1}{2}; \frac{\kappa+1}{2}; \Big(\frac{2x_q^2(x_p^2-x_r^2)}{(x_p^2-x_r^2)^2+x_q^4+4x_{p_\Lambda}^2 x_q^2}\Big)^2\Big)\Big\}\,, \qquad (5.7)
\end{aligned}
$$

where $\boldsymbol{x}_p = \boldsymbol{p}/|p_\mu|$. We will evaluate the integral $\tilde{I}[n_Q](x_p)$ numerically.

5.1.2 Bogoliubov quasiparticles

The same procedure applies in the quasiparticle case, starting with Eq. (4.127). However, there is a difference because Eq. (4.127) has two distinct many-body coupling functions which need to be treated differently. We separate the right-hand side of Eq. (4.127) into two integrals, each for one such coupling,

$$
I(\boldsymbol{p}) = I_1(\boldsymbol{p}) + \frac{1}{2} I_2(\boldsymbol{p})\,, \qquad (5.8)
$$

where

$$
\begin{aligned}
I_1(\boldsymbol{p}) = (2\pi)^4 \int_{\boldsymbol{kqr}} \frac{(g\rho)^4}{\omega_{\boldsymbol{p}}\omega_{\boldsymbol{k}}\omega_{\boldsymbol{q}}\omega_{\boldsymbol{r}}}\, g^2_{\text{eff}}(\omega_{\boldsymbol{p}} - \omega_{\boldsymbol{r}}, \boldsymbol{p} - \boldsymbol{r}) \\
\times \delta(\boldsymbol{p} + \boldsymbol{k} - \boldsymbol{q} - \boldsymbol{r})\, \delta(\omega_{\boldsymbol{p}} + \omega_{\boldsymbol{k}} - \omega_{\boldsymbol{q}} - \omega_{\boldsymbol{r}}) \\
\times \Big\{ f(\omega_{\boldsymbol{p}}) f(\omega_{\boldsymbol{r}}) \Big[f(\omega_{\boldsymbol{q}}) - f(\omega_{\boldsymbol{k}}) \Big] + \Big[f(\omega_{\boldsymbol{r}}) - f(\omega_{\boldsymbol{p}}) \Big] f(\omega_{\boldsymbol{k}}) f(\omega_{\boldsymbol{q}}) \Big\}, \qquad (5.9) \\
I_2(\boldsymbol{p}) = (2\pi)^4 \int_{\boldsymbol{kqr}} \frac{(g\rho)^4}{\omega_{\boldsymbol{p}}\omega_{\boldsymbol{k}}\omega_{\boldsymbol{q}}\omega_{\boldsymbol{r}}}\, g^2_{\text{eff}}(\omega_{\boldsymbol{p}} - \omega_{\boldsymbol{k}}, \boldsymbol{p} + \boldsymbol{k}) \\
\times \delta(\boldsymbol{p} + \boldsymbol{k} - \boldsymbol{q} - \boldsymbol{r})\, \delta(\omega_{\boldsymbol{p}} + \omega_{\boldsymbol{k}} - \omega_{\boldsymbol{q}} - \omega_{\boldsymbol{r}}) \\
\times \Big\{ \Big[f(\omega_{\boldsymbol{p}}) + f(\omega_{\boldsymbol{k}}) \Big] f(\omega_{\boldsymbol{q}}) f(\omega_{\boldsymbol{r}}) - f(\omega_{\boldsymbol{p}}) f(\omega_{\boldsymbol{k}}) \Big[f(\omega_{\boldsymbol{q}}) + f(\omega_{\boldsymbol{r}}) \Big] \Big\}. \qquad (5.10)
\end{aligned}
$$

Then, we follow the same steps we did in the free case. The result of $I_1(\boldsymbol{p})$ is almost identical to the free case due to the similarity in the arguments of many-body coupling,

$$
\begin{aligned}
I_1(\boldsymbol{p}) &= \frac{(g\rho)^4}{(2\pi)c_s^5} \int_{r'} \frac{1}{p|\boldsymbol{p} - \boldsymbol{r}'|r'} g^2_{\text{eff}}(\omega_{\boldsymbol{p}} - \omega_{\boldsymbol{p}-\boldsymbol{r}'}, \boldsymbol{r}') \int_0^\infty \mathrm{d}k \int_{|k-r'|}^{k+r'} \mathrm{d}q\, \delta(p - |\boldsymbol{p} - \boldsymbol{r}'| + k - q) \\
&\quad \times \Big\{ f(\omega_{\boldsymbol{p}}) f(\omega_{|\boldsymbol{p}-\boldsymbol{r}'|}) \Big[f(\omega_{\boldsymbol{q}}) - f(\omega_{\boldsymbol{k}}) \Big] + \Big[f(\omega_{|\boldsymbol{p}-\boldsymbol{r}'|}) - f(\omega_{\boldsymbol{p}}) \Big] f(\omega_{\boldsymbol{k}}) f(\omega_{\boldsymbol{q}}) \Big\} \\
&= \frac{(g\rho)^4}{(2\pi)c_s^5} \frac{\Lambda^{3\kappa}}{p} \int_{r'} \frac{1}{|\boldsymbol{p} - \boldsymbol{r}'|r'} g^2_{\text{eff}}(\omega_{\boldsymbol{p}} - \omega_{\boldsymbol{p}-\boldsymbol{r}'}, \boldsymbol{r}') \Big\{ \frac{I_1^{\text{bog}}(\boldsymbol{p}, \boldsymbol{r}')}{(p + p_\Lambda)^\kappa (|\boldsymbol{p} - \boldsymbol{r}'| + p_\Lambda)^\kappa} \\
&\qquad + \Big[\frac{1}{(|\boldsymbol{p} - \boldsymbol{r}'| + p_\Lambda)^\kappa} - \frac{1}{(p + p_\Lambda)^\kappa} \Big] I_2^{\text{bog}}(\boldsymbol{p}, \boldsymbol{r}') \Big\}, \qquad (5.11)
\end{aligned}
$$

where $\boldsymbol{r}' = \boldsymbol{p} - \boldsymbol{r}$, $\boldsymbol{q} = \boldsymbol{k} + \boldsymbol{r}'$ and

$$
I_1^{\text{bog}}(\boldsymbol{p}, \boldsymbol{r}') = \int_0^\infty \mathrm{d}k \int_{|k-r'|}^{k+r'} \mathrm{d}q\, \delta(p - |\boldsymbol{p} - \boldsymbol{r}'| + k - q) \Big[\frac{1}{(q + p_\Lambda)^\kappa} - \frac{1}{(k + p_\Lambda)^\kappa} \Big], \qquad (5.12)
$$

$$
I_2^{\text{bog}}(\boldsymbol{p}, \boldsymbol{r}') = \int_0^\infty \mathrm{d}k \int_{|k-r'|}^{k+r'} \mathrm{d}q\, \delta(p - |\boldsymbol{p} - \boldsymbol{r}'| + k - q) \frac{1}{(q + p_\Lambda)^\kappa (k + p_\Lambda)^\kappa}. \qquad (5.13)
$$

As for $I_2(\boldsymbol{p}, \boldsymbol{k})$, instead of changing $\boldsymbol{r}$ to $\boldsymbol{r}' = \boldsymbol{p} - \boldsymbol{r}$, we change $\boldsymbol{k}$ to $\boldsymbol{k}' = \boldsymbol{k} + \boldsymbol{p}$ and define $\boldsymbol{q} = \boldsymbol{k}' - \boldsymbol{r}$ to take care the integration over the polar angle of $\boldsymbol{r}$,

$$
\begin{aligned}
I_2(\boldsymbol{p}) &= \frac{(g\rho)^4}{(2\pi)c_s^5} \int_{k'} \frac{1}{p|\boldsymbol{k}' - \boldsymbol{p}|k'} g^2_{\text{eff}}(\omega_{\boldsymbol{p}} - \omega_{\boldsymbol{k}'-\boldsymbol{p}}, \boldsymbol{k}') \int_0^\infty \mathrm{d}r \int_{|k-r'|}^{k+r'} \mathrm{d}q\, \delta(p + |\boldsymbol{k}' - \boldsymbol{p}| - q - r) \\
&\quad \times \Big\{ \Big[f(\omega_{\boldsymbol{p}}) + f(\omega_{|\boldsymbol{k}'-\boldsymbol{p}|}) \Big] f(\omega_{\boldsymbol{q}}) f(\omega_{\boldsymbol{r}}) - f(\omega_{\boldsymbol{p}}) f(\omega_{|\boldsymbol{k}'-\boldsymbol{p}|}) \Big[f(\omega_{\boldsymbol{q}}) + f(\omega_{\boldsymbol{r}}) \Big] \Big\} \\
&= \frac{(g\rho)^4}{(2\pi)c_s^5} \frac{\Lambda^{3\kappa}}{p} \int_{k'} \frac{1}{|\boldsymbol{k}' - \boldsymbol{p}|k'} g^2_{\text{eff}}(\omega_{\boldsymbol{p}} - \omega_{\boldsymbol{k}'-\boldsymbol{p}}, \boldsymbol{k}') \Big\{ - \frac{I_3^{\text{bog}}(\boldsymbol{p}, \boldsymbol{k}')}{(p + p_\Lambda)^\kappa (|\boldsymbol{k}' - \boldsymbol{p}| + p_\Lambda)^\kappa} \\
&\qquad + \Big[\frac{1}{(\boldsymbol{p} + p_\Lambda)^\kappa} + \frac{1}{(|\boldsymbol{k}' - \boldsymbol{p}| + p_\Lambda)^\kappa} \Big] I_4^{\text{bog}}(\boldsymbol{p}, \boldsymbol{k}') \Big\}, \qquad (5.14)
\end{aligned}
$$

where

$$I_3^{\rm bog}(\boldsymbol{p},\boldsymbol{k}') = \int_0^\infty \mathrm{d}r \int_{|k'-r|}^{k'+r} \mathrm{d}q\, \delta(p+|\boldsymbol{k}'-\boldsymbol{p}|-q-r)\Big[\frac{1}{(q+p_\Lambda)^\kappa}+\frac{1}{(r+p_\Lambda)^\kappa}\Big]\,, \tag{5.15}$$

$$I_4^{\rm bog}(\boldsymbol{p},\boldsymbol{k}') = \int_0^\infty \mathrm{d}r \int_{|k'-r|}^{k'+r} \mathrm{d}q\, \delta(p+|\boldsymbol{k}'-\boldsymbol{p}|-q-r)\frac{1}{(q+p_\Lambda)^\kappa(r+p_\Lambda)^\kappa}\,. \tag{5.16}$$

The integrals $I_1^{\rm bog}, I_2^{\rm bog}, I_3^{\rm bog}$ and $I_4^{\rm bog}$ are evaluated in App. D. Substituting the results from Eqs. (D.23), (D.25), (D.28) and (D.30) into Eqs. (5.11) and (5.14), we obtain

$$\begin{aligned} I_1(\boldsymbol{p}) &= \frac{(g\rho)^4}{(2\pi)^3 c_s^5}\frac{\Lambda^{3\kappa}}{p^2}\int_0^\infty \mathrm{d}r \int_{|p-r|}^{p+r} \mathrm{d}q\, g_{\rm eff}^2(\omega_{\boldsymbol{p}}-\omega_{\boldsymbol{r}},\boldsymbol{q}) \\ &\quad\times\Bigg\{\frac{2^{\kappa-1}}{\kappa-1}\frac{1}{(p+p_\Lambda)^\kappa(r+p_\Lambda)^\kappa} \\ &\qquad\times\Big[(q+p-r+2p_\Lambda)^{1-\kappa}-(q-p+r+2p_\Lambda)^{1-\kappa}\Big] \\ &\quad+\frac{2^{2\kappa-1}}{2\kappa-1}\Big[\frac{1}{(r+p_\Lambda)^\kappa}-\frac{1}{(p+p_\Lambda)^\kappa}\Big](q+2p_\Lambda)^{1-2\kappa} \\ &\qquad\times {}_2F_1\Big(\kappa,\kappa-\frac{1}{2};\kappa+\frac{1}{2};\Big(\frac{p-r}{q+2p_\Lambda}\Big)^2\Big)\Bigg\} \\ &= \frac{(g\rho_0)^4}{(2\pi)^3 c_s^5}\Big(\frac{\Lambda}{p_\mu}\Big)^{3\kappa} p_\mu\, g^2\, \tilde{I}_1[n_Q](x_p)\,, \end{aligned} \tag{5.17}$$

and

$$\begin{aligned} I_2(\boldsymbol{p}) &= 2\frac{(g\rho)^4}{(2\pi)^3 c_s^5}\frac{\Lambda^{3\kappa}}{p^2}\int_0^\infty \mathrm{d}k \int_{|p-k|}^{p+k} \mathrm{d}q\, g_{\rm eff}^2(\omega_{\boldsymbol{p}}-\omega_{\boldsymbol{k}},\boldsymbol{q}) \\ &\quad\times\Bigg\{\frac{2^{\kappa-1}}{\kappa-1}\frac{1}{(p+p_\Lambda)^\kappa(k+p_\Lambda)^\kappa} \\ &\qquad\times\Big[(p+k+q+2p_\Lambda)^{1-\kappa}-(p+k-q+2p_\Lambda)^{1-\kappa}\Big] \\ &\quad+2^{2\kappa-1}\Big[\frac{1}{(\boldsymbol{p}+p_\Lambda)^\kappa}+\frac{1}{(k+p_\Lambda)^\kappa}\Big]\frac{q}{(p+k+2p_\Lambda)^{2\kappa}} \\ &\qquad\times {}_2F_1\Big(\kappa,\frac{1}{2};\frac{3}{2};\Big(\frac{q}{p+k+2p_\Lambda}\Big)^2\Big)\Bigg\} \\ &= 2\frac{(g\rho_0)^4}{(2\pi)^3 c_s^5}\Big(\frac{\Lambda}{p_\mu}\Big)^{3\kappa} p_\mu\, g^2\, \tilde{I}_2[n_Q](x_p)\,. \end{aligned} \tag{5.18}$$

Here, $\boldsymbol{r}'$ and $\boldsymbol{k}'$ were replaced by the original $\boldsymbol{r}$ and $\boldsymbol{k}$, respectively. We further define $\boldsymbol{q}=\boldsymbol{p}-\boldsymbol{r}$ in $I_1(\boldsymbol{p})$ and $\boldsymbol{q}=\boldsymbol{p}+\boldsymbol{k}$ in $I_2(\boldsymbol{p})$. The integral $I(\boldsymbol{p})$ in Eq. (5.8) can now be expressed in a term of the dimensionless integral, $\tilde{I}[n_Q](x_p)=\tilde{I}_1[n_Q](x_p)+\tilde{I}_2[n_Q](x_p)$,

$$I(\boldsymbol{p}) = \frac{(g\rho_0)^4}{(2\pi)^3 c_s^5}\Big(\frac{\Lambda}{p_\mu}\Big)^{3\kappa} p_\mu\, g^2\, \tilde{I}[n_Q](x_p)\,, \tag{5.19}$$

where $\tilde{I}_1[n_Q](x_p)$ and $\tilde{I}_2[n_Q](x_p)$ are the dimensionless integrals of $I_1(\boldsymbol{p})$ and $I_2(\boldsymbol{p})$ respectively, defined in the very same way we have done in free particle case. The integral $\tilde{I}[n_Q](x_p)$ will also be evaluated numerically in the following sections.

5.2 The scaling solutions of integrals

In this section, we present the results from numerical integration of dimensionless integral $\tilde{I}[n_Q](x_p)$. Of main interest here are the scaling solutions of the integrals which include both the stationary turbulence solutions (the Kolmogorov-Zakharov exponents) and a nonstationary self-similar solution. The turbulence solutions will be determined by seeking the zeroes of the integral $\tilde{I}[n_Q](x_p)$ when the exponents κ are varied. For a self-similar solution, we make use of the observation that the integral $I(\boldsymbol{p})$ must have the same momentum scaling as $n_Q(\boldsymbol{p})$ if $n_Q(\boldsymbol{p})$ evolves self-similarly, see Sect. 3.2.3. Therefore, we check whether a particular exponent κ_S is a self-similar exponent by observing the power-law behaviour of $I(p)$. The expectation is that $I(p) \sim p^{-\kappa_S}$ if $n_Q(p) \sim p^{-\kappa_S}$. This translates directly to $\tilde{I}[n_Q](x_p) \sim x_p^{\kappa_S}$.

5.2.1 Weak-wave turbulence solutions

In the weak-wave turbulence limit, we evaluated the integral with the condition $g_{\text{eff}} = g$. Note that in principle, the weak-wave scaling exponents can be obtained by using the nonperturbative expressions of g_{eff} but $\tilde{I}[n_Q](x_p)$ needs to be evaluated at a large value of x_p, $x_p \gg 1$. This makes the integral being evaluated in the area where $g_{\text{eff}} = g$. However, the numerical evaluation becomes unstable when the separation between the infrared cutoff p_Λ and p is large. Thus, we simply used the perturbative value $g_{\text{eff}} = g$ to evaluate the scaling solution in the perturbative limit. The results will be presented separately for the free particles and the Bogoliubov quasiparticles.

Free particles

The rescaled integral $\tilde{I}[n_Q](x_p)$ in Eq. (5.6) has been evaluated at $x_p = 1.5$ ($p = 1.5p_\mu$) with exponents κ varied and the results are presented in Fig. 5.1. The scattering integral as a function of κ is shown by a curve for each value of the infrared cutoff p_Λ. The stationary solutions can be identified from the zeroes of $\tilde{I}[n_Q](x_p)$ of which there are three in general. The first stationary solution is $\kappa = 2$ where the number distribution exhibits Rayleigh-Jeans scaling $n(p) = T/\varepsilon_p \sim p^{-2}$. We note that the $\kappa = 2$ solution is slightly dependent on the infrared cutoff which we believe it is due to the numerical accuracies. We expect that $\kappa = 2$ is a cutoff-independent solution because it corresponds to a detail-balance case where the integrand vanishes at each point in the integration domain.

The other two stationary solutions vary and their dependences on the infrared scale are shown in Fig. 5.2. As a separation between the infrared cutoff p_Λ and the external momentum p grows, the solutions approach the predicted values $\kappa_Q = 7/3$

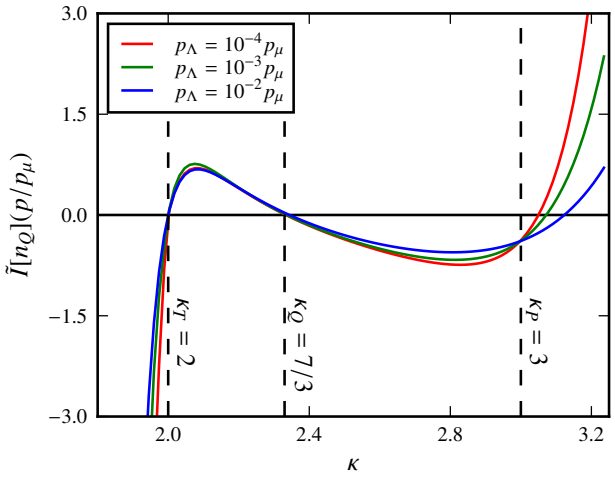

Figure 5.1: Dependence of the weak-wave-Boltzmann scattering integral $I[n_Q](p)$ for free particles ($n = n_Q$) in $d = 3$ spatial dimensions, at the momentum $p = 1.5p_\mu$, on the momentum scaling exponent κ characterizing the occupation number distribution $n(p) \sim p^{-\kappa}$. The vertical dashed lines mark, from the left, the thermal zero at $\kappa_T = 2$, the particle-cascade exponent $\kappa_Q = 7/3$, and the energy-cascade exponent $\kappa_P = 3$. In the figure, the rescaled integral $\tilde{I}[n_Q](p)$ is shown, see Eq. (5.6). The different colors correspond to different values of the IR cutoff p_Λ, as indicated in the legend. As the cutoff is lowered, the zeroes approach the predicted values. The sign of the slope $\partial\tilde{I}[n_Q]/\partial\kappa$ at the zeroes determines the direction of the cascade.

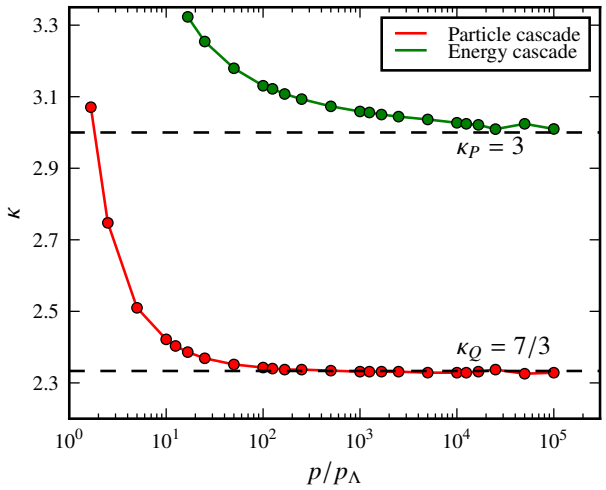

Figure 5.2: Scaling exponents κ of occupation number distribution $n(p) \sim p^{-\kappa}$ for which the weak-wave-Boltzmann scattering integral $I[n](p)$ for free particles in $d = 3$ spatial dimensions has a zero, for different momenta p in units of the IR cutoff scale p_Λ. Red dots correspond to the particle cascade for which κ approaches $\kappa_Q = 7/3$. Green dots mark the zeroes of the energy cascade, approaching $\kappa_P = 3$.

and $\kappa_P = 3$, see Eq. (3.20). Note that the absolute values of p_Λ and p have no meaning here, only the ratio p/p_Λ determines the value of the stationary solutions. The sign of the slope $\partial\tilde{I}[n_Q]/\partial\kappa$ agrees with the direction of the cascades in context of 4-wave resonances, an inverse cascade for particle flux and a direct cascade for energy flux [10].

We emphasize that the deviation of the momentum scaling exponent $\zeta = 3.5$ from the predicted value $\zeta = 3$, observed in the experiment by Navon et al. [41], may be an effect from the finite size of the experimental apparatus. Fig. 5.2 shows that a direct cascade exponent manifests at $\zeta = \kappa = 3.5$ if the observed momentum and the infrared cutoff scales are approximately in the order, $p \simeq p_\Lambda$. Considering Fig. 1.2(b), one estimates $p_\Lambda \xi \simeq 0.5$ and observes the scaling with $\kappa = 3.5$ (γ in their notation) in a momentum regime $p_\xi \lesssim 5$, consistent with our finite-size estimation.

We evaluate the radial fluxes of particle and energy, however, with the rescaled $\tilde{I}[n_Q](x_p)$. The rescaled particle flux $Q[\tilde{I}](x_p)$ and energy flux $P[\tilde{I}](x_p)$ are derived directly from Eqs. (3.11) and (3.12),

$$Q[\tilde{I}](x_p) = -4\pi \int_0^{x_p} \mathrm{d}s\, s^2 \tilde{I}[n_Q](s)\,, \tag{5.20}$$

$$P[\tilde{I}](x_p) = -4\pi \int_0^{x_p} \mathrm{d}s\, s^2 \varepsilon(s) \tilde{I}[n_Q](s)\,. \tag{5.21}$$

where $\varepsilon(s) = s^2$. The evaluation of $Q[\tilde{I}](x_p)$ at $\kappa = 7/3$ and of $P[\tilde{I}](x_p)$ at $\kappa = 3$ is presented in Fig. 5.3. The particle flux $Q[\tilde{I}](x_p)$ shows a flat plateau which indicates a p-independent particle flux and thus a turbulence cascade. In contrast, energy flux $P[\tilde{I}](x_p)$ has no signature of a flat plateau in the momentum window we calculated. This can be understood since, in this window, the energy solution has not yet reached the predicted value $\kappa = 3$, see Fig. 5.2.

Bogoliubov quasiparticles

The rescaled integral $\tilde{I}[n_Q](x_p)$ in Eq. (5.19) is evaluated at $x_p = 0.1$ ($p = 0.1 p_\mu$) with the exponents κ varied. The results are presented in Fig. 5.4 and the structures closely resemble to the free particle results. There is a thermal solution $\kappa = 1$ corresponding to the Rayleigh-Jeans scaling $n(p) = T/\omega_p \sim p^{-1}$ and two solutions with a negative and a positive slope of $\partial\tilde{I}[n_Q]/\partial\kappa$ which can be related to an inverse particle cascade and a direct energy cascade respectively. As the separation between the external momentum p and the infrared cutoff increases, the solutions approach the predicted values, $\kappa = 4/3$ for an inverse particle cascade and $\kappa = 5/3$ for a direct energy cascade, see Eq. (3.23). The solutions also depend solely on the ratio of p/p_Λ as shown in Fig. 5.5.

The quasiparticle and the energy fluxes are calculated from the rescaled integral $\tilde{I}(x_p)$ and presented in Fig. 5.6. The quasiparticle flux $Q[\tilde{I}](x_p)$ is given by a similar integral as the one appearing in Eq. (5.20) but the energy flux needs to be modified because the energy spectrum is now linear in momentum,

$$P[\tilde{I}](x_p) = -4\pi \int_0^{x_p} \mathrm{d}s\, s^2 \omega(s) \tilde{I}(s)\,, \tag{5.22}$$

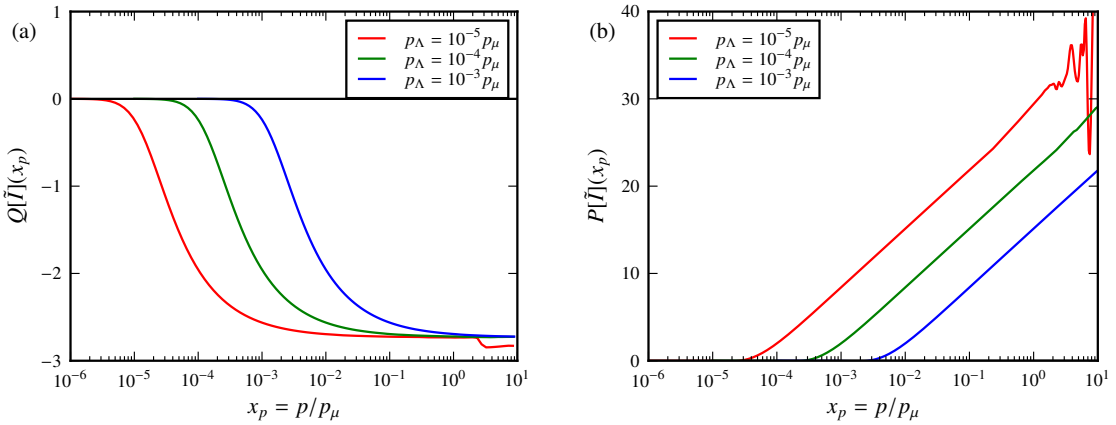

Figure 5.3: The particle flux $Q[\tilde{I}](x_p)$ and the energy flux $P[\tilde{I}](x_p)$ calculated from the rescaled scattering integral $\tilde{I}(x_p)$ are shown as functions of the rescaled momentum x_p in panel (a) and (b) respectively. The evaluation has been done at the analytically predicted scaling exponents, i.e. at $\kappa = 7/3$ for $Q[\tilde{I}](x_p)$ and $\kappa = 3$ for $P[\tilde{I}](x_p)$.

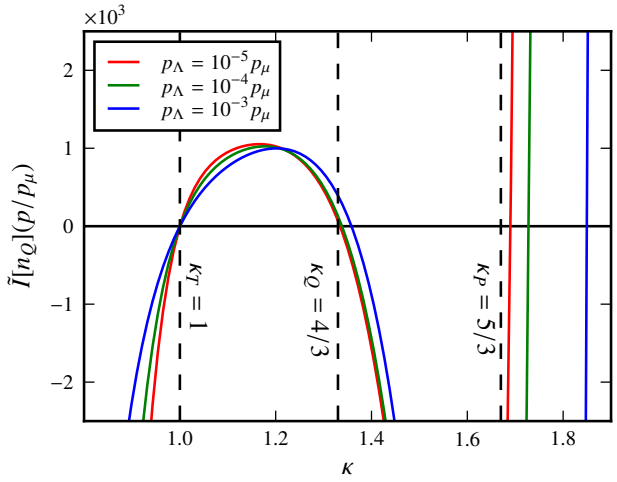

Figure 5.4: Dependence of the weak-wave-Boltzmann scattering integral $I[n_Q](p)$ for Bogoliubov sound in $d = 3$ spatial dimensions, at the momentum $p = 0.1 p_\mu$, on the momentum scaling exponent κ characterizing the occupation number distribution $n_Q(p) \sim p^{-\kappa}$. The vertical dashed lines mark, from the left, the thermal zero at $\kappa_T = 1$, the quasiparticle-cascade exponent $\kappa_Q = 4/3$, and the energy-cascade exponent $\kappa_P = 5/3$. In the figure, the rescaled integral $\tilde{I}[n_Q](p)$ is shown, see Eq. (5.19). The different colors correspond to different values of the IR cutoff p_Λ, as indicated in the legend. As the cutoff is lowered, the zeroes approach the predicted values. The sign of the slope $\partial \tilde{I}[n_Q]/\partial \kappa$ at the zeroes determines the direction of the cascade.

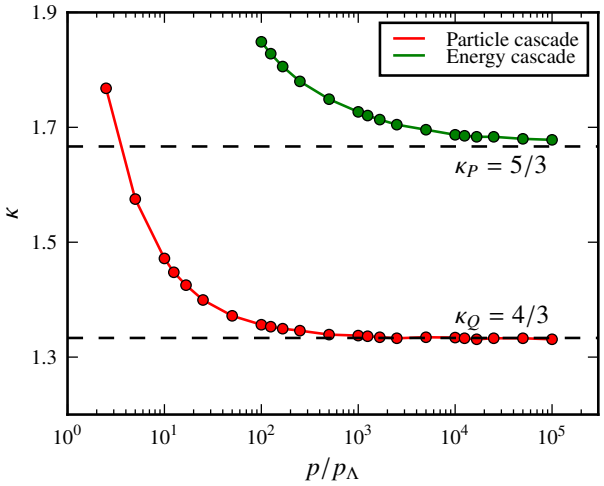

Figure 5.5: Scaling exponents κ of the quasiparticle distribution $n_Q(p) \sim p^{-\kappa}$ for which the weak-wave-Boltzmann scattering integral $I[n_Q](p)$ in $d = 3$ spatial dimensions has a zero, for different momenta p in units of the IR cutoff scale p_Λ. As in Fig. 5.2, red dots correspond to the particle cascade, with the zeroes approaching $\kappa_Q = 4/3$, green dots to the energy cascade, approaching $\kappa_P = 5/3$.

where $\omega(s) = s$. The quasiparticle flux shows again the plateau and this is a signature for a turbulence cascade. The energy flux seems to closely reach the plateau and if we look back to the curve giving the energy solution in Fig. 5.6 (the green line), the plateau is expected to exist since the trend shows a saturation at $\kappa = 5/3$ beyond the momentum window we calculated. However, we conclude that there is no direct energy cascade in the momentum window we considered.

5.2.2 Strong-wave turbulence solutions

The strong-wave calculation is done by using the full expressions for the many-body coupling g_{eff}. However, the strong-wave results are only available for a sufficiently small values of an external momentum p compared to p_μ. This is because the major contributions to the integrals come from the regime where the nonperturbative effects dominate. Since $\tilde{I}[n_Q](x_p)$ falls off as a power-law, the major contributions generally come from the area below the scale x_p. This means the further p away from p_μ, the better chance we have to see the results of strong-wave turbulence.

Free particles

The many-body coupling g_{eff} is now evaluated with the self-energy Π^R in Eq. (4.142) and substituting the Λ scale by the relation (4.141). Then, we numerically calculate $\tilde{I}[n_Q](x_p)$ with κ varied, at $x_p = 0.001$. The results are presented in Fig. 5.7. There are two zeroes which represent the stationary solutions of strong-wave turbulence which vary with the infrared cutoff scale p_Λ. Fig. 5.8 shows that as $p_\Lambda \to 0$, the solu-

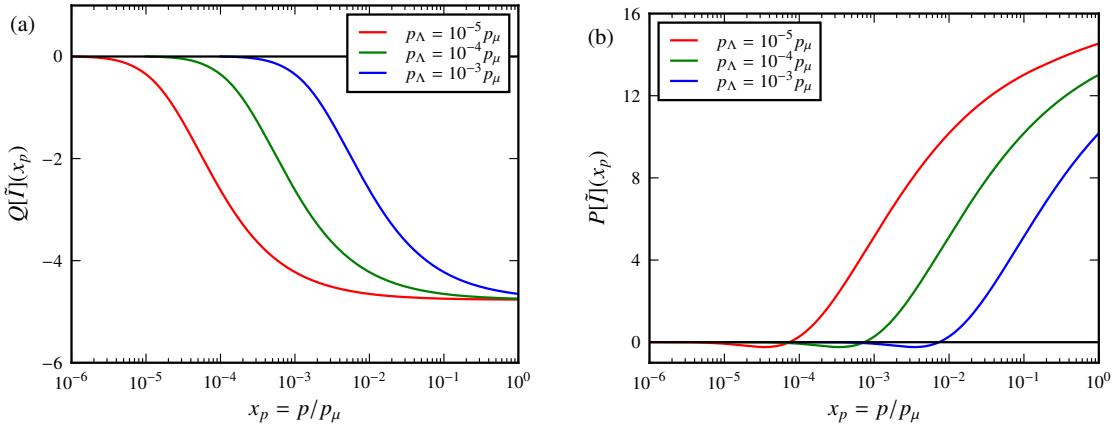

Figure 5.6: The particle flux $Q[\tilde{I}](x_p)$ and the energy flux $P[\tilde{I}](x_p)$ calculated from the rescaled scattering integral $\tilde{I}(x_p)$ are shown as functions of the rescaled momentum x_p in panel (a) and (b) respectively. The evaluation has been done at the analytically predicted scaling exponents, i.e. at $\kappa = 4/3$ for $Q[\tilde{I}](x_p)$ and $\kappa = 5/3$ for $P[\tilde{I}](x_p)$.

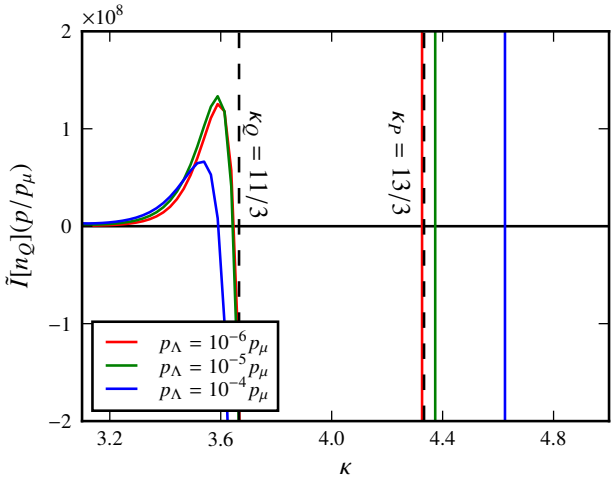

Figure 5.7: Dependence of the strong-wave-Boltzmann scattering integral $I[n](p)$ for free particles in $d = 3$ spatial dimensions, at the momentum $p = 0.001 p_\mu$, on the momentum scaling exponent κ characterizing the occupation number distribution $n(p) \sim p^{-\kappa}$. The vertical dashed lines mark, from the left, the particle-cascade exponent $\kappa_Q = 11/3$, and the energy-cascade exponent $\kappa_P = 13/3$. In the figure, the rescaled integral $\tilde{I}[n_Q](p)$ is shown, see Eq. (5.6). The different colors correspond to different values of the IR cutoff p_Λ, as indicated in the legend. As the cutoff is lowered, the zeroes approach the predicted values. The sign of the slope $\partial I[n]/\partial\kappa$ at the zeroes determines the direction of the cascade.

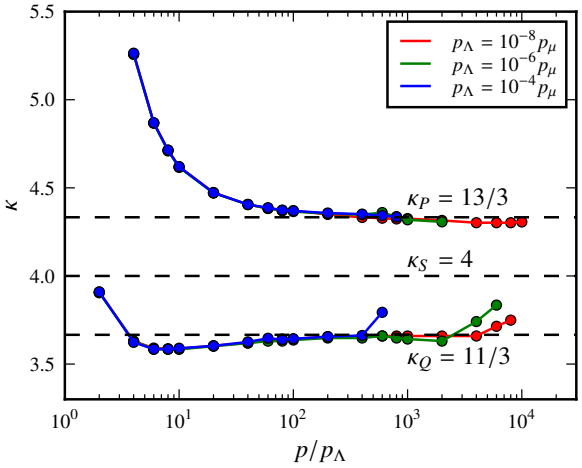

Figure 5.8: Scaling exponents κ of occupation number distribution $n(p) \sim p^{-\kappa}$ for which the wave-Boltzmann scattering integral $I[n](p)$ for free particles in $d = 3$ spatial dimensions has a zero. The figure applies to the IR region of large occupation numbers where the effective many-body coupling describing collective scattering scales with $\gamma_\kappa = 2$ and modifies the scaling properties. The colors mark different choices of the IR cutoff scale p_Λ. The upper line corresponds to an energy cascade and approaches $\kappa_P = d + 4/3$ for $p_\Lambda \to 0$, as obtained from Eq. (3.17) with $\gamma_\kappa = 2$, while the lower line approaches the particle-cascade exponent $\kappa_Q = d + 2/3$, cf. Eq. (3.16).

tions come closer to the predicted values, $\kappa_Q = 11/3$ and $\kappa_P = 13/3$, see Eq. (3.27). However, there is a limit to this where lowering the cutoff further does not bring the solutions down to the predicted values. We will come back to this issue again in the Bogoliubov calculation.

The fluxes are calculated using Eqs. (5.20) and (5.21). The results are shown in Fig. 5.9. There is no a fully developed plateau of the quasiparticle flux as in the weak-wave case. For the energy flux, we lose the numerical accuracies around $p \sim 10^3 p_\Lambda$, however, the energy exponent curve in Fig. 5.8 (the upper curve) is not yet saturated at $\kappa = 3$ at the approximately same scale so it is more likely that there is no flat plateau of the energy flux in the momentum window we calculated. If this is the case, it means there is no turbulence cascade in the nonperturbative regime where the energy spectrum is quadratic.

Bogoliubov quasiparticles

We now use the self-energy in Eq. (4.159) for the coupling g_{eff} and replace the Λ scale with Eq. (4.158). The rescaled integral $\tilde{I}[n_Q](x_p)$ as a function of κ is shown in Fig. 5.10 for $x_p = 0.001$. Two stationary solutions are presented and both of them approach the predicted values $\kappa_Q = 8/3$ and $\kappa_P = 3$ as the infrared cutoff is lowered, see Eq. (3.30). In Fig. 5.11, we see the shift of the solutions towards to the predicted values but departing again as $p_\Lambda \to 0$. Here, it is clear that the particle and the

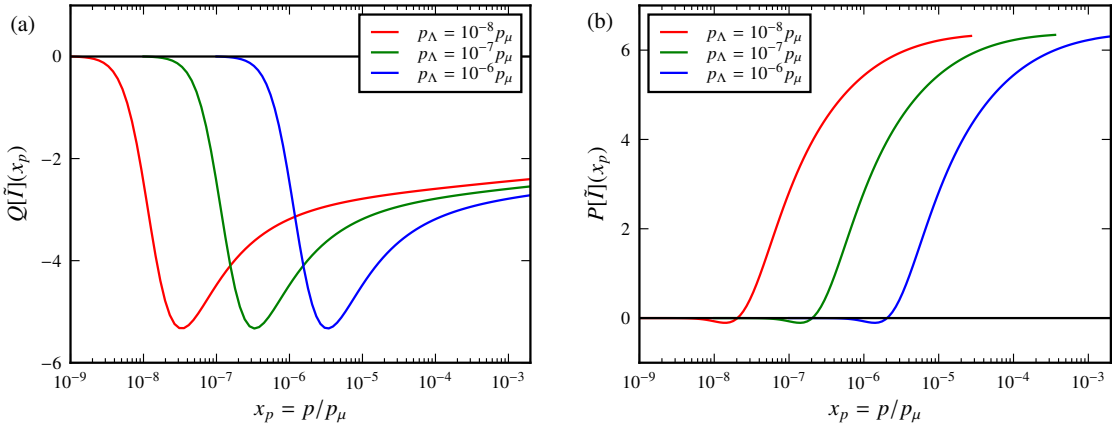

Figure 5.9: The particle flux $Q[\tilde{I}](x_p)$ and the energy flux $P[\tilde{I}](x_p)$ calculated from the rescaled scattering integral $\tilde{I}(x_p)$ are shown as functions of rescaled momentum x_p in panel (a) and (b) respectively. The evaluation has been done at the analytically predicted scaling exponents, i.e. at $\kappa = 11/3$ for $Q[\tilde{I}](x_p)$ and $\kappa = 13/3$ for $P[\tilde{I}](x_p)$.

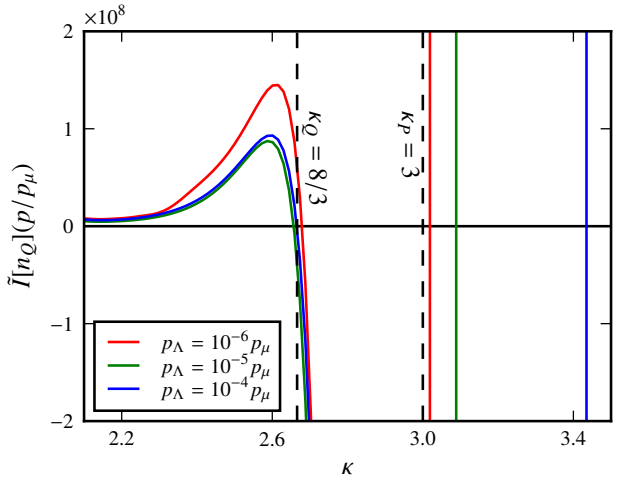

Figure 5.10: Dependence of the strong-wave-Boltzmann scattering integral $I[n_Q](p)$ for Bogoliubov sound in $d = 3$ spatial dimensions, at the momentum $p = 0.001\, p_\mu$, on the momentum scaling exponent κ characterizing the occupation number distribution $n_Q(p) \sim p^{-\kappa}$. The vertical dashed lines mark, from the left, the quasiparticle-cascade exponent $\kappa_Q = 8/3$, and the energy-cascade exponent $\kappa_P = 3$. In the figure, the resscaled integral $\tilde{I}[n_Q](p)$ is shown, see Eq. (5.19). The different colors correspond to different values of the IR cutoff p_Λ, as indicated in the legend. As the cutoff is lowered, the zeroes approach the predicted values. The sign of the slope $\partial \tilde{I}[n_Q]/\partial\kappa$ at the zeroes determines the direction of the cascade.

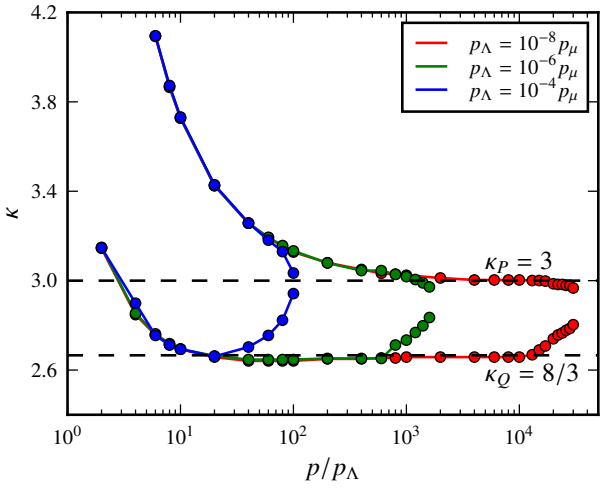

Figure 5.11: Scaling exponents κ of the quasiparticle distribution $n_Q(p) \sim p^{-\kappa}$ for which the wave-Boltzmann scattering integral $I[n_Q](p)$ in the IR collective scattering region, in $d = 3$ has a zero, for different momenta p in units of the IR cutoff scale p_Λ, for three different p_Λ. As in Fig. 5.5, the lower data marks the quasiparticle cascade, with the zeroes approaching $\kappa_Q = 8/3$, while the upper data marks the energy cascade, approaching $\kappa_P = 3$.

energy solutions merge at some scale and leave the further momentum regime without a stationary solution. We do not have a concrete description why the solutions disappear at a particular momentum scale but we do know that it is bound to happen.

The stationary solutions predicted by Eq. (3.30) (or Eq. (3.27) in the free particle case) only exist within the momentum window where g_{eff} grows as p^2. This means we should see the predicted solutions only in a certain window. From Figs. 4.3, 4.4, 4.5 and 4.6, we can estimate such a window to be bounded by p_Λ and p_μ. However, the integral has been done on the 2-dimensional plane so determining the actual window is more complicated.

Inside the area bounded by the curves of the stationary solutions, the integral is negative. This means the time evolution with a decreasing in the number distribution must take place within this area. This includes the self-similar evolution where the number of quasiparticles within the scaling regime needs to decrease to fulfil the global conservation laws. Thus, the self-similar solution κ_S must stay between κ_Q and κ_P. Only the nonperturbative free particle calculation fulfils this condition, see Fig. 5.8.

We calculate the fluxes with Eqs. (5.20) and (5.22). The results are shown in Fig. 5.12. We again lose the numerical accuracies before we can make a concrete statement. However, the quasiparticle flux shows an overlap of curves calculated from two different infrared cutoffs which gives a promising trend of a flat plateau. The energy flux also shows a similar behaviour but not as good as appearing in the particle flux.

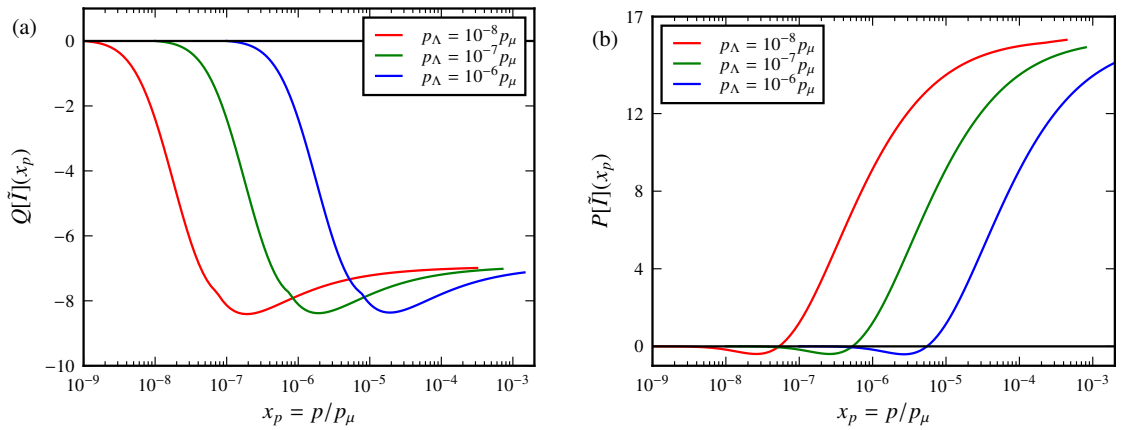

Figure 5.12: The particle flux $Q[\tilde{I}](x_p)$ and the energy flux $P[\tilde{I}](x_p)$ calculated from the rescaled scattering integral $\tilde{I}(x_p)$ are shown as functions of the rescaled momentum x_p in panel (a) and (b) respectively. The evaluation has been done at the analytically predicted scaling exponents, i.e. at $\kappa = 8/3$ for $Q[\tilde{I}](x_p)$ and $\kappa = 3$ for $P[\tilde{I}](x_p)$.

5.2.3 Self-similar solutions

The self-similar exponents can be verified through the momentum scaling of the scattering integral. We only discuss the self-similar solutions in the nonperturbative regime because the particle cascade is expected to manifest in the perturbative regime due to the well developed particle fluxes presented in Figs. 5.3 and 5.6.

Free particles

Eqs. (3.32) and (3.61) give $\kappa_S = 4$ for the free particle case and we evaluated the rescaled integral $\tilde{I}[n_Q](x_p)$ at this exponent with varying x_p for several values of the infrared cutoff. Fig. 5.13 shows an absolute value of the rescaled integral $p'^4 \tilde{I}_S[n_Q](p')$ as a function of the another rescaled momentum $p' = p/p_\Lambda$ on a double-logarithmic scale. The first bump shows a regime where the integral is positive, before it turns inegative and the plateau in the negative domain exhibits the power-law fall-off $I[n_Q](p) \sim p^{-4}$. Not only $\kappa_S = 4$ fulfils the requirements of a self-similar exponent, it also results where the scattering integral is negative which ensures the decreasing of the local occupation number and conserves the global conservation laws, see Fig. 2.1.

Bogoliubov quasiparticle

In the linear dispersion regime, $\kappa_S = 5/2$, cf. Eqs. (3.32) and (3.61). The rescaled integral $\tilde{I}(x_p)$ is evaluated with $n_Q(p) \sim p^{-5/2}$. Fig. 5.14 presents the rescaled integral $p'^{5/2} \tilde{I}_S[n_Q](p')$ as a function of $p' = p/p_\Lambda$ on a double-logarithmic scale. The integral is all positive including where the plateau shows up. Therefore, the occupation number is increasing self-similarly in time instead of decreasing. Since the time-evolution violates the global conservation laws, we conclude that this situation is

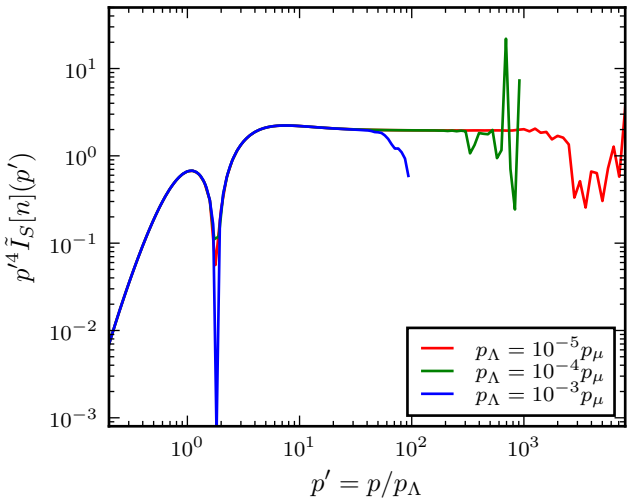

Figure 5.13: Momentum dependence of the scattering integral (3.4) multiplied by $p'^4 = (p/p_\Lambda)^4$, for free particles ($z = 2$, $n = n_Q$) in $d = 3$ dimensions. The integral is evaluated in the collective-scattering regime, with effective many-body T-matrix, Eqs. (3.25), (4.129), (4.142), for different values of the IR cutoff scale p_Λ (colors), and the results are scaled on top of each other by showing $p'^4 \tilde{I}_S[n_Q](p') = x_{p_\Lambda}^4 \tilde{I}[n_Q](x_p)$, see details in Sect. 5.3. The horizontal plateau demonstrates the power-law dependence $I[n_Q](p) \sim p^{-4}$ predicted by $\kappa_S = 4$, cf. Eq. (3.32).

unlikely to occur although the $\kappa_S = 5/2$ satisfies the requirement of a self-similar exponent.

5.3 Dynamical exponents

So far, the numerical integration of scattering integrals recovered all exponents that are determined by the momentum scaling alone. Although we can infer the dynamics with the analysis from global conservation laws, the calculations are, in general, time-independent. The only temporal scaling exponent that is accessible by means of our numerical integration is the exponent μ from Eq. (3.42) but this is only the case if there is only one time-dependent scale, p_Λ. We have no p_λ in our calculation and Λ can be related to p_Λ using Eqs. (4.141) and (4.158) for the free particles and the Bogoliubov quasiparticles respectively. This also means μ we evaluated here is subject to the condition that there is no time evolution in the noncondensed quasiparticle numbers, $\rho_{\rm nc} = \text{const.}$.

We again restrict our calculation in the nonperturbative regime. In this case,

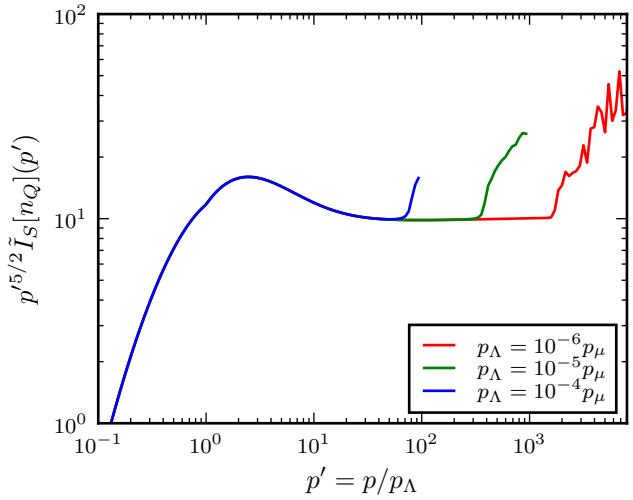

Figure 5.14: Momentum dependence of the scattering integral (3.4) multiplied by $p'^{5/2} = (p/p_\Lambda)^{5/2}$, for Bogoliubov quasiparticles ($z = 1$) in $d = 3$ dimensions. The integral is evaluated in the collective-scattering regime, with the effective many-body T-matrix, Eqs. (3.25), (4.129), (4.159), for different values of the IR cutoff scale p_Λ (colors), and the results are scaled on top of each other by showing $p'^{5/2}\,\tilde{I}_S[n_Q](p') = x_{p_\Lambda}^{2.5}\tilde{I}[n_Q](x_p)$, see more details in Sect. 5.3. The horizontal plateau demonstrates the power-law dependence $I[n_Q](p) \sim p^{-5/2}$ predicted by $\kappa_S = 5/2$, cf. Eq. (3.32).

Eqs. (3.44), (3.60) and (3.64) give

$$\begin{aligned}\mu &= 2d + 2\Big(2(z-1) - \eta/2\Big) - z - 3\alpha/\beta \\ &= -d + 2 + 3(d + z - 2 - \alpha/\beta) - \eta \\ &= -d + 2 - \eta\,, \end{aligned} \tag{5.23}$$

where we have used the constraint, $\alpha/\beta = d+z-2$, which is obtained from Eq. (3.64) in the case $\delta = 0$. In our calculation where $d = 3$ (and $\eta = 0$ due to the choices of spectral functions), the exponent μ takes a universal value, $\mu = -1$, in both the free particle and the Bogoliubov quasiparticle cases.

Under the assumption that only p_Λ scale is time-dependent, we need to include only a prefactor $x_\Lambda^\kappa = (\Lambda/p_\mu)^\kappa$ into the rescaled integral $\tilde{I}[n_Q](x_p)$. The idea is to generate a time-independent self-similar function $\tilde{I}_S[n_Q](p/p_\Lambda)$ from the rescaled integral,

$$I_S[n_Q]\Big(\frac{p}{p_\Lambda}\Big) = x_{p_\Lambda}^{-\mu}\Big[x_\Lambda^{3\kappa}\tilde{I}[n_Q](x_p)\Big]\,. \tag{5.24}$$

Eq. (5.24) can be viewed as a rescaled version of Eq. (3.42). To proceed, we numerically evaluate the $\tilde{I}[n_Q](x_p)$ as a function of x_p for several values of p_Λ keeping the κ exponent fixed. Then, we create plots of $\tilde{I}[n_Q](x_p)$ versus p/p_Λ by simply rescaling x_p with x_{p_Λ}. Last, the factor $x_{p_\Lambda}^{-\mu}x_\Lambda^{3\kappa}$ is multiplied to $\tilde{I}[n_Q](x_p)$ with a specific

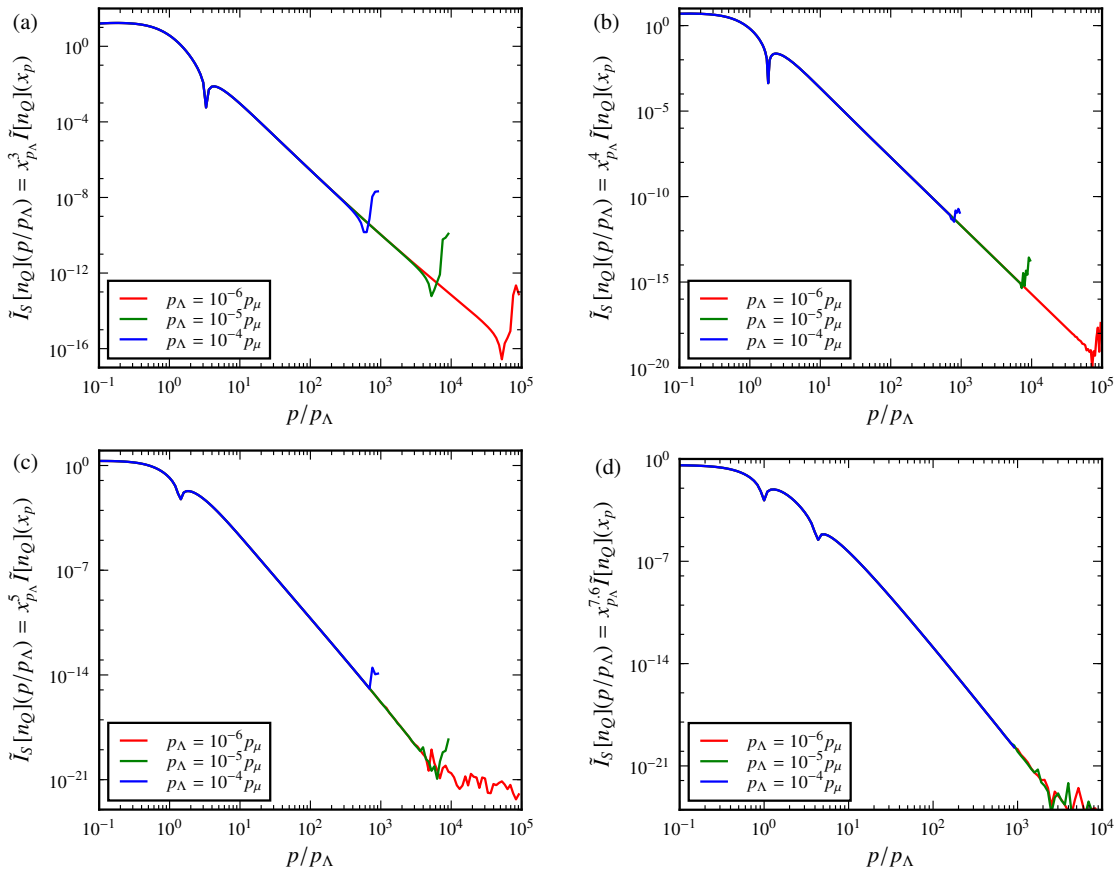

Figure 5.15: The figure shows the time-independent function $I_S[n_Q](p/p_\Lambda)$ as a function of p/p_Λ for the free particle case. The κ exponents are $11/3, 4, 13/3$ and 5.2 presented in subfigures (a), (b), (c) and (d) respectively. Eq. (4.141) gives the conversion $x_\Lambda^\kappa \sim x_{p_\Lambda}^{\kappa-3}$, thus, the multiplication factor making all curves lie on top of each other becomes $x_{p_\Lambda}^{3(\kappa-3)-\mu}$. All subfigures give the universal value $\mu = -1$.

value of μ that makes curves corresponding to different p_Λ lie on top of each other, hence, creating a cutoff independent function $I_S[n_Q](p/p_\Lambda)$ which is equivalent to a time-independent function in our context.

Figs. 5.15 and 5.16 show the time-independent function $I_S[n_Q](p/p_\Lambda)$ as a function of p/p_Λ for the free particle and the Bogoliubov quasiparticle case respectively. Each panel represents different values of κ exponents with the different infrared cutoffs labelled by different colours. All panels are obtained with an exponent $\mu = -1$. We emphasize further that this is the case for all other exponents κ that are not presented here. Thus, the numerical results confirm that $\mu = -1$, independent of the values of κ exponents. We can see that curves lie on top of each other even outside the power law regime.

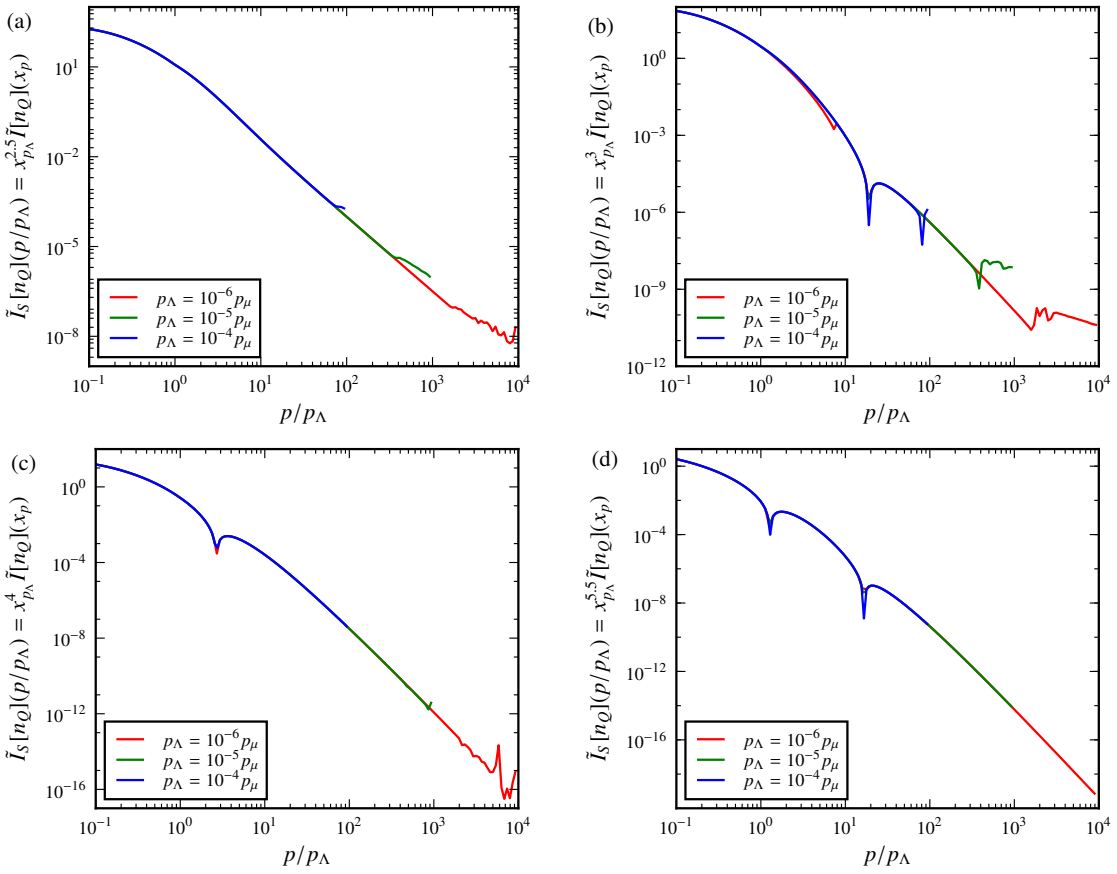

Figure 5.16: The figure shows the time-independent function $I_S[n_Q](p/p_\Lambda)$ as a function of p/p_Λ for the Bogoliubov quasiparticle case. The κ exponents are $2.5, 8/3, 3$ and 3.5 presented in subfigures (a), (b), (c) and (d) respectively. Eq. (4.158) gives the conversion $x_\Lambda^\kappa \sim x_{p_\Lambda}^{\kappa-2}$, thus, the multiplication factor making all curves lie on top of each other becomes $x_{p_\Lambda}^{3(\kappa-2)-\mu}$. All subfigures give the universal value $\mu = -1$.

5.4 Time evolution of Bose gas in the kinetic regime

So far, we concentrated on recovering the momentum scaling exponents and there are three of them in general: an inverse particle cascade exponent κ_Q, a direct energy cascade exponent κ_P and a self-similar exponent κ_S. We have also two momentum scales that separate the momentum window into two regimes. The inverse healing length scale, p_ξ, separate the quadratic (free particle) from the sound wave (Bogoliubov quasiparticle) regimes, while, the scale p_μ, the inverse healing length defined with only noncondensed particles, separates the perturbative (weak-wave) from the nonperturbative (strong-wave) regime. In this section, we would like to discuss which types of time evolution should occur in each momentum regime assuming that the kinetic description can be applied.

In the perturbative regime i.e. for $p \gg p_\mu$ whether it is quadratic or sound wave, the particle cascade is expected to occur. This comes from the fact that all exponents in the perturbative regime lie in the window of the particle cascade, see Eqs. (3.20), (3.23) and (2.25). Moreover, we have seen a well established quasiparticle flux in Figs. 5.3 and 5.6. This observation agrees with previous studies [15–17], an inverse particle cascade takes place in the perturbative regime.

In the nonperturbative regime, there is a difference between the free particle and the Bogoliubov quasiparticle cases. In the free particle case, all scaling solutions are in the self-similar windows, $3 < \kappa < 5$, suggesting that particle number and energy are dominantly in the infrared and the ultraviolet ends respectively. If the global conservation laws are taken into account, the only possibility to fulfil the particle and the energy conservation is to evolve self-similarly in time. This agrees with Fig. 5.13 where we have seen that the self-similar exponent $\kappa_S = 4$ manifests in the regime where the scattering integral is negative, implying a decrease of the number occupation as time progresses. In te Bogoliubov quasiparticle case, the scaling solutions lie in the particle cascade window, $\kappa < 3$, except the energy cascade solution $\kappa_P = 3$ that stays right at the border which implies a logarithmic divergence in both the infrared and the ultraviolet ends. We have ruled out the possibility of self-similar evolution in this case. Therefore, we conclude that an inverse particle cascade takes place in the nonperturbative sound wave regime.

In the window of nonperturbative quadratic regime, $p_\xi \ll p \ll p_\mu$, we expect the scaling evolution to be self-similar type with a critically slowing down wave front towards the infrared. Further down in the infrared, $p \ll p_\xi$, where the dispersion becomes that of sound waves, an inverse particle cascade takes place instead. However, the nonperturbative sound wave regime is very close to the coherent regime where structural defects like vortices are likely to be formed. It might not be possible to observe it at all unless the vortices have gone. The subdominance of the scaling exponents in the kinetic theory is emphasized in Fig. 5.17. The occupation number presented in Fig. 5.17 is taken from the classical statistical calculation at very late times where the last vortex ring has disappeared. The incompressible part (blue dots) exhibits the power law, $n(p) \sim p^{-\zeta}$, where $\zeta = 3.6$. This exponent seems to coincide with our inverse particle cascade solutions, $\kappa_Q = 11/3$ in the quadratic and

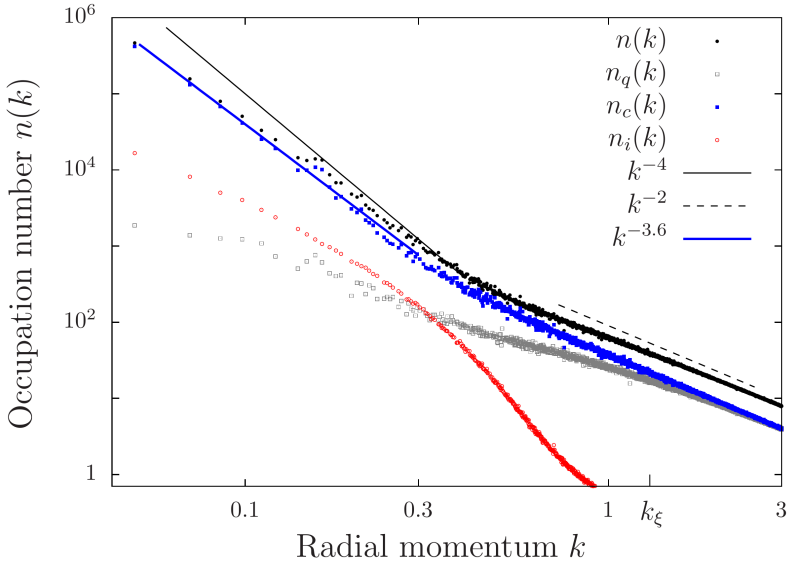

Figure 5.17: The figure shows the occupation number spectra of the late-stage evolution of a closed system after an initial quench, briefly after the last vortex ring has disappeared, cf. Fig. 15 of Ref. [28]. The compressible component (blue dots), cf. Ref. [28], is starting to be a dominant component of the total occupation number (black dots) in an absence of vortices. The blue solid line represents $n(p) \sim p^{-3.6}$. The figure is taken from Ref. [51].

$\kappa_Q = 8/3$ in the sound wave cases, see Eq. (2.22). However, we rather conclude that this exponent, if it is applied in the kinetic regime, is an inverse particle cascade as a result of sound wave turbulence due to the previous discussion that the self-similar evolution takes place in the quadratic regime. The same exponent $\zeta = 3.6$ has been obtained with functional renormalization group methods in Ref. [51].

5.5 Summary

We have numerically evaluated the Boltzmann integral in the kinetic equation derived in Ch. 4 and recovered the Kolmogorov-Zakharov exponents predicted in Ch. 3 by means of scaling arguments. Apart from the value of exponents, the direction of transport can be read off from the plots of the scattering integral versus κ as it has been analysed in Ref. [10]. The fluxes of transport are calculated at these exponents to cross check whether they are indeed momentum independent. The results show that the particle flux is well established in the perturbative regime and the nonperturbative sound wave regime, see Figs. 5.3, 5.6 and 5.12.

Apart from the Kolmogorov-Zakharov exponents, we determine the self-similar exponents from the scaling behaviour of the scattering integral. We infer from Eq. (3.46) that an exponent will be a self-similar exponent if it makes the Boltzmann integral scaling in the same way as the occupation number. Apparently, it works in

Table 5.1: Scaling exponents. The table summarizes the scaling exponents for universal scaling evolutions following a cooling quench, for the case of free particles ($z = 2$) and sound quasiparticles ($z = 1$). Only transport to lower momenta is relevant for such a quench. The self-similar and cascade evolutions in the collective scattering regime ($p \ll p_\mu$) have a positive β and slow down algebraically at large times due to their proximity to a non-thermal fixed point (NTFP). In contrast, $\beta < 0$ for the build-up of a weak-wave-turbulence (WWT) inverse (quasi)particle cascade in the wave-Boltzmann two-body scattering regime ($p \gg p_\mu$), implying a critically accelerated wave-front evolution. The NTFP self-similar solution is valid only for z within the interval $z_- \leq z \leq z_+$ where $z_\pm = 4(2 \pm 1)/3$. In the either regimes we have set $\eta = 0$. The rightmost column derives from $\zeta = \kappa + 2 - z$, cf. Eq. (2.22).

	α/β	β	α'/β'	β'/β	$\kappa - d$	$\zeta - d$
free particles ($z = 2$)						
NTFP $p \ll p_\mu$	d	$\frac{1}{z}$	$d + z$	-1	$\frac{3z-4}{2}$	$\frac{z}{2}$
WWT cascade $p \gg p_\mu$	κ	$\frac{1}{z - 8/3}$	0	0	$z - \frac{8}{3}$	$-\frac{2}{3}$
sound waves ($z = 1$)						
NTFP (cascade) $p \ll p_\mu \ll p_\xi$	κ	$\frac{1}{z}$	0	0	$z - \frac{8}{6}$	$\frac{4}{6}$
WWT cascade $p_\mu \ll p \ll p_\xi$	κ	$\frac{1}{z - 8/3}$	0	0	$z - \frac{8}{3}$	$-\frac{2}{3}$

our case as the self-similar exponent predicted in Ch. 3 satisfies such behaviour. We argue that the self-similar evolution needs the particles and energy in the infrared and ultraviolet ends respectively, therefore, the occupation number has to go down as depicted in Fig. 2.1 if p_Λ and p_λ move to the infrared and the ultraviolet direction respectively. Thus, only the free particle case in the nonperturbative regime is expected to show the self-similar scaling.

We then turn our interest to the temporal scaling μ. In the numerical approach, we are able to evaluate μ in the case of $\rho_{\mathrm{nc}} = $ const. and the result is universal, $\mu = -1$ in $d = 3$ dimensions.

Last, we have discuss the universal dynamics of Bose gas based on our results in the kinetic regime in Sect. 5.4 and summarized the scaling exponents according to the dynamics taking place in each regime after scaling exponents before according to Table 5.1.

Chapter 6

Conclusion

The universal dynamics of a dilute Bose gas in the kinetic regime has three possible scenarios: an inverse particle transport, a direct energy transport or a self-similar evolution. In each case, the global conservation laws and the kinetic equation constrain the scaling exponents in both momentum and time. These exponents are apparently universal in the sense that they do not strongly depend on the underlying microscopic theory but only few parameters such as the dimension, the dispersion relation and the scaling of T-matrix, and the global conservation laws.

We approached the problem by means of nonequilbrium quantum field theory and nonperturbatively derived the kinetic equation which is not subject to the weak-wave approximations. The structure of the kinetic equation is the same as the kinetic equation derived from weak-wave approximations but with a momentum dependent effective coupling. We evaluated the effective coupling analytically from the ansatz of the free particle and the Bogoliubov quasiparticle in the linear regime with an infrared regularization. The mommentum scalings of the effective coupling are universal, see Eqs. (4.148) and (4.166), and notably different from the ones obtained from dimensional counting where the divergences and the regularization scales are neglected. Using the momentum scaling of the effective coupling, we evaluated an effective T-matrix and determined the momentum scaling exponents: the Kolmogorov-Zakharov exponents for turbulence cascades and the self-similar scaling exponents. The results are given in the first column of Tables 3.1 and 3.2 for the perturbative and the nonperturbative regimes respectively and they are confirmed by our numerical integration presented in Sect. 5.2. Because the momentum exponents strongly depend on the scaling behaviour of the effective coupling, then, having a correct momentum scaling of the effective coupling is crucial.

We studied the time evolution, mainly, the scaling exponents β and β' of the regularization scales $p_\Lambda(t) \sim t^{-\beta}$ and $p_\lambda(t) \sim t^{-\beta'}$ respectively. We have shown that the other exponents related to time evolution can be expressed in the terms of β and β', see Table 2.1. To determine the values of β and β', we need both the global conservation laws and the kinetic equation. We found that there are some inconsistencies, especially in the self-similar time evolution depicted in Fig. 2.1, if the quasiparticle does not coincide with a particle, or equivalently, any cases where $z \neq 2$. The quasiparticle conservation violates the particle conservation for the cases with $z \neq 2$, therefore, some other momentum scales, such as p_μ, are now time-dependent.

This makes a difference between the momentum scaling and the time scaling of the effective T-matrix that are used to constrain and evaluate the exponents β and β' respectively. We have shown that the inconsistencies disappear under the condition that there is no other time-dependent scales except p_Λ, p_λ and Λ. The arguments apply in both the perturbative and the nonperturbative regimes. It should be noted that the momentum scales p_Λ, p_λ and Λ are the only time-dependent momentum scales appearing in the analysis concerning the global conservation laws. Nevertheless, if we neglect the inconsistencies and follow the general procedure by keeping the quasiparticle and the energy conservation at the infrared and the ultraviolet ends respectively, we find the universal scaling $\beta = (z - \eta)^{-1}$ in the nonperturbative regime regardless of whether the type of dynamics represents an inverse cascade or a self-similar shift in time. This may predict a nonthermal fixed point in the nonperturbative regime.

We ended with the description of dynamics of a dilute Bose gas in the kinetic regime based on our results. In the perturbative regime, we expect the turbulence transport with an accelerating wave front and such a scenario has been observed numerically in earlier works. In the nonperturbative within the momentum window $p_\xi \ll p \ll p_\mu$, we predicted the self-similar evolution with the momentum exponent $\kappa_S = 4$ and a critically slowed down wave front $p_\Lambda(t) \sim t^{-1/2}$. Further in the infrared where $p \ll p_\xi$, the inverse cascade of sound-wave turbulence is expected to occur with the momentum exponent $\kappa_Q = 8/3$ and the critically slow down wave front $p_\Lambda(t) \sim t^{-1}$. Beyond this window, we believe the dynamics is governed by superfluid turbulence which is not captured by the kinetic equation.

As a side result we find that the momentum scaling exponent $\kappa = 3.5$ observed in the recent experiment [41] for a direct wave-turbulent energy cascade, can be interpreted to deviate from the predicted value $\kappa_P = 3$ due to finite-size effects in the trap.

Appendix A

Convention and useful symmetries

The Fourier transform in $d+1$-dimensional space-time reads

$$\mathcal{F}[f(p)](x) = f(x) = \int_{-\infty}^{\infty} \frac{\mathrm{d}^{d+1}p}{(2\pi)^{d+1}} \exp\{-ipx\} f(p)\,, \tag{A.1}$$

$$\mathcal{F}[f(x)](p) = f(p) = \int_{-\infty}^{\infty} \mathrm{d}^{d+1}x \exp\{ipx\} f(x)\,, \tag{A.2}$$

where the term px is an inner product in $d+1$ dimensions with the Minkowski metric $(+---)$,

$$px = p_0 x_0 - \boldsymbol{p}\cdot\boldsymbol{x}\,. \tag{A.3}$$

Therefore, the Fourier transform of the Dirac delta distribution becomes

$$\delta^{d+1}(x-y) = \int_{-\infty}^{\infty} \frac{\mathrm{d}^{d+1}p}{(2\pi)^{d+1}} \exp\{-i(x-y)p\}\,. \tag{A.4}$$

In Ch. 4, we study the field theory of a complex scalar Bose field which, in general, is not different from the real-field representation presented in [45–47]. However, the symmetries do not always coincide. First, $F(x,y)$ and $\rho(x,y)$ defined in Eqs. (4.26) and (4.27) are no more symmetric and anti-symmetric functions respectively. Instead, their symmetry properties are

$$F_{ab}(x,y) = F^*_{ba}(y,x) \tag{A.5}$$

$$\rho_{ab}(x,y) = -\rho^*_{ba}(y,x). \tag{A.6}$$

These relations can be verified directly from Eqs. (4.26) and (4.27), for example, Eq. (4.26) gives

$$\begin{aligned} F_{ab}(y,x) &= \frac{1}{2}\langle\{\Phi_a(y),\Phi_b^\dagger(x)\} = \frac{1}{2}\langle\Phi_a(y)\Phi_b^\dagger(x) + \Phi_b^\dagger(x)\Phi_a(y)\rangle\rangle \\ &= \frac{1}{2}\langle\Phi_b(x)\Phi_a^\dagger(y) + \Phi_a^\dagger(y)\Phi_b(y)\rangle^* \\ &= \frac{1}{2}\langle\{\Phi_b(x),\Phi_a^\dagger(y)\}\rangle^* = F^*_{ba}(x,y). \end{aligned} \tag{A.7}$$

The procedure is similar for $\rho(x,y)$. In the homogeneous case, two-point functions depend solely on the difference $x-y$ which means there is a translational invariance.

Choosing $y = 0$, the Fourier transform of $F_{ab}(x, y) = F_{ab}(x - y)$ becomes

$$\begin{aligned} F_{ab}(x,0) &= \frac{1}{2}\langle\{\Phi_a(x), \Phi_b^\dagger(0)\}\rangle \\ &= \frac{1}{2}\langle\{\int \frac{\mathrm{d}^{d+1}p}{(2\pi)^{d+1}}\Phi_a(p)e^{-ipx}, \Phi_b^\dagger(0)\}\rangle \\ &= \int \frac{\mathrm{d}^{d+1}p}{(2\pi)^{d+1}}e^{-ipx}\frac{1}{2}\langle\{\Phi_a(p), \Phi_b^\dagger(0)\}\rangle = \int \frac{\mathrm{d}^{d+1}p}{(2\pi)^{d+1}}e^{-ipx}F_{ab}(p)\,, \end{aligned} \tag{A.8}$$

where $\mathcal{F}[F_{ab}(x)](p) = \langle\{\Phi_a(p), \Phi_b^\dagger(0)\}\rangle/2$. Similarly, we also have

$$\begin{aligned} F_{ba}(0,x) &= \frac{1}{2}\langle\{\Phi_b(0), \Phi_a^\dagger(x)\}\rangle \\ &= \frac{1}{2}\langle\{\Phi_b(0), \int \frac{\mathrm{d}^{d+1}p}{(2\pi)^{d+1}}\Phi_a^\dagger(p)e^{ipx}\}\rangle \\ &= \int \frac{\mathrm{d}^{d+1}p}{(2\pi)^{d+1}}\frac{1}{2}\langle\{\Phi_b(0), \Phi_a^\dagger(-p)\}\rangle = \int \frac{\mathrm{d}^{d+1}p}{(2\pi)^{d+1}}e^{-ipx}F_{ba}(-p)\,. \end{aligned} \tag{A.9}$$

The same calculation applies for the Fourier transform of $\rho(x)$ and $\rho(-x)$. Then, the symmetries of $F(p)$ and $\rho(p)$ can be read off directly,

$$F_{ab}(p) = F_{ba}^*(p) \quad , F_{ab}(-p) = F_{ba}^*(-p) \tag{A.10}$$

$$\rho_{ab}(p) = -\rho_{ba}^*(p) \quad , \rho_{ab}(-p) = -\rho_{ba}^*(-p)\,. \tag{A.11}$$

Notice that in momentum space, $F(p)$ and $\rho(p)$ are completely separated from $F(-p)$ and $\rho(-p)$. Although the symmetries of F and ρ are different from the ones obtained in the real-field representation, the symmetries of traced objects are identical, for example,

$$(F \cdot F)(x) = F_{ab}(-x)F_{ba}(x) = (F \cdot F)(-x)\,, \tag{A.12}$$

$$(\rho \cdot \rho)(x) = \rho_{ab}(-x)\rho_{ba}(x) = (\rho \cdot \rho)(-x)\,, \tag{A.13}$$

$$\begin{aligned} (\rho \cdot F - F \cdot \rho)(x) &= (\rho_{ab}(x)F_{ba}(-x) - F_{ab}(x)\rho_{ab}(-x)) \\ &= -(\rho \cdot F - F \cdot \rho)(-x)\,. \end{aligned} \tag{A.14}$$

The Fourier transform of traced objects can be obtained directly,

$$\begin{aligned} F_{ab}(x)F_{ba}(-x) &= \Big(\int \frac{\mathrm{d}^{d+1}p}{(2\pi)^{d+1}}e^{-ipx}F_{ab}(p)\Big)\Big(\int \frac{\mathrm{d}^{d+1}q}{(2\pi)^{d+1}}e^{-iqx}F_{ba}(-q)\Big) \\ &= \int \frac{\mathrm{d}^{d+1}p}{(2\pi)^{d+1}}\int \frac{\mathrm{d}^{d+1}q}{(2\pi)^{d+1}}e^{-i(p+q)x}F_{ab}(p)F_{ba}(-q) \\ &= \int \frac{\mathrm{d}^{d+1}p}{(2\pi)^{d+1}}e^{-ipx}\int \frac{\mathrm{d}^{d+1}q}{(2\pi)^{d+1}}F_{ab}(p-q)F_{ba}(-q) \\ &= \int \frac{\mathrm{d}^{d+1}p}{(2\pi)^{d+1}}e^{-ipx}(F_{ab} * F_{ba})(p)\,, \end{aligned} \tag{A.15}$$

where the $*$ operator defined by

$$(F_{ab} * F_{ba})(p) = \int \frac{\mathrm{d}^{d+1}q}{(2\pi)^{d+1}} F_{ab}(p-q)F_{ba}(-q). \tag{A.16}$$

Note that there is an extra factor $(2\pi)^{-(d+1)}$ from the definition in Eq. (4.74) because the convolution is done in momentum space. Thus, it can be verified that

$$[F * F](p) = 2\Pi^F(-p) = 2\Pi^F(p)\,, \tag{A.17}$$
$$[\rho * F - F * \rho](p) = 2\Pi^\rho(-p) = -2\Pi^\rho(p)\,. \tag{A.18}$$

From the symmetries of $F(p)$ and $\rho(p)$, we can prove the following relation,

$$\Pi^{\rho *}(p) = \Pi^\rho(-p) = -\Pi^\rho(p)\,, \tag{A.19}$$
$$\begin{aligned}(\theta * \Pi^\rho)(-p) &= \int dq^0 \theta(-p^0 - q^0)\Pi^\rho(-q^0, -\boldsymbol{p}) \\ &= -\int dq^0 \theta^-(p^0 - q^0)\Pi^\rho(-q^0, \boldsymbol{p}) = -(\theta^- * \Pi^\rho)(p)\,,\end{aligned} \tag{A.20}$$
$$\begin{aligned}(\theta * \Pi^\rho)^*(p) &= \int dq^0 \theta^*(p^0 - q^0)\Pi^{\rho *}(-q^0, \boldsymbol{p}) \\ &= -\int dq^0 \theta^-(p^0 - q^0)\Pi^\rho(-q^0, \boldsymbol{p}) = -(\theta^- * \Pi^\rho)(p)\,,\end{aligned} \tag{A.21}$$

where $\theta(p)$ is a Fourier transform of the Heaviside function $\theta(x)$

$$\theta(p^0) = \frac{i}{p^0 + i\epsilon}\,, \tag{A.22}$$
$$\theta(-p^0) = \theta^*(p^0) = \frac{-i}{p^0 - i\epsilon} = \theta^-(p^0)\,. \tag{A.23}$$

Note that $\theta(x)$ and its Fourier transform $\theta(p)$ depend only on the temporal component of the respective 4-vector. Thus, the operations $\cdot$ and $*$ with $\theta(x)$ or $\theta(p)$ are done only in the temporal component.

In Ch. 4, we have evaluated the effective coupling function,

$$\begin{aligned}g^2_{\text{eff}}(p) &= \frac{g^2}{|1 + g\Pi^R(p)|^2} \\ &= \frac{g^2}{[1 + g\Pi^R(p)][1 + g\Pi^{R*}(p)]}\end{aligned} \tag{A.24}$$

where $\Pi^R(p) = -(\theta * \Pi^\rho)(p)$. It is straightforward to see that $g^2_{\text{eff}}(p) = g^2_{\text{eff}}(-p)$. From there, we can evaluate more symmetries of $I^F(p)$ and $I^\rho(p)$, see Eqs. (4.84)

and (4.85),

$$I^F(p) = \hbar(\Pi^F \cdot g_{\text{eff}}^2)(p) = I^F(-p)\,, \tag{A.25}$$
$$I^\rho(p) = \hbar(\Pi^\rho \cdot g_{\text{eff}}^2)(p) = -I^\rho(-p)\,, \tag{A.26}$$
$$I^{F*}(p) = I^F(p)\,, \tag{A.27}$$
$$I^{\rho*}(p) = -I^\rho(p)\,, \tag{A.28}$$
$$(I^F * F_{ba})(p) = (I^F * F_{ab})^*(p)\,, \tag{A.29}$$
$$(I^\rho * F_{ba})(p) = -(I^\rho * F_{ab})^*(p)\,, \tag{A.30}$$
$$(I^F * \rho_{ba})(p) = -(I^F * \rho_{ab})^*(p)\,. \tag{A.31}$$

These symmetries imply, see Eqs. (4.93) and (4.94),

$$\Sigma^F_{ab}(p) = \Sigma^{F*}_{ba}(p) \tag{A.32}$$
$$\Sigma^\rho_{ab}(p) = -\Sigma^{\rho*}_{ba}(p)\,. \tag{A.33}$$

We can use the symmetries in the momentum space to identify the symmetries in the configuration space,

$$I^F(-x) = I^{F*}(x) = I^F(x)\,, \tag{A.34}$$
$$I^\rho(-x) = -I^{\rho*}(x) = -I^\rho(x)\,, \tag{A.35}$$
$$\Sigma^F_{ab}(-x) = \Sigma^{F*}_{ba}(x)\,, \tag{A.36}$$
$$\Sigma^\rho_{ab}(-x) = -\Sigma^{\rho*}_{ba}(x)\,. \tag{A.37}$$

Note that self-energy functions, $\Sigma^F(x)$ and $\Sigma^\rho(x)$ share the same symmetries with $F_{ab}(x)$ and $\rho_{ab}(x)$ respectively.

Appendix B

Nonequilibrium quantum field theory

B.1 Closed-time-path integral

The Closed-time-path (CTP) formalism (also known as the Schwinger-Keldysh formalism) is an essential tool for studying nonequilibrium dynamics due to its property of preserving causality.

B.1.1 Single-time-contour formalism

In equilibrium, a conventional single time path can substitute the closed time path without costs. To see why this is the case, we recall the vacuum-to-vacuum transition amplitude from quantum field theory,[1]

$$Z[J] = \langle \Omega | \Omega \rangle_J \tag{B.1}$$

where the state $|\Omega\rangle$ is a vacuum state of an interacting theory at a particular time t_0. The subscript J is used to remind that the quantities are evaluated with an external source-dependent Hamiltonian

$$H_J(t_0) = H(t_0) + \int d^d x \Phi_S(\boldsymbol{x}) J(t_0, \boldsymbol{x}) \,, \tag{B.2}$$

where $\Phi_S(\boldsymbol{x})$ is a field in the Schrödinger picture and it coincides with the Heisenberg field $\Phi(x)$ at time t_0. Note that if $J = 0$, $Z[0]$ has to be normalized, i.e. $Z[0] = 1$. The Heisenberg field at time t reads

$$\Phi(x) = U_J^\dagger(t, t_0) \Phi_s(\boldsymbol{x}) U_J(t, t_0) \,, \tag{B.3}$$

where

$$U_J(t, t') = T\Big\{ \exp[-\frac{i}{\hbar} \int_{t'}^{t} dt_1 H_J(t_1)] \Big\} \,. \tag{B.4}$$

The operator T is the time-ordering operator which makes operators evaluated at time $t > t'$ to stand to the left of operator evaluated at time t'. In the following

[1] We used $Z[J]$ in the discussion because the observables that we are interested in are n-point functions which are generated from $Z[J]$. Otherwise, one can inspect an expectation value of any time-dependent observables to reach the same conclusion.

discussion, we will treat the source-dependent term as an interaction part of the Hamiltonian in the interaction picture, therefore the interaction picture representation of the field operator is defined by

$$\Phi_I(x) = U^\dagger(t,t_0)\Phi_s(\boldsymbol{x})U(t,t_0) \tag{B.5}$$

where

$$U(t,t') = T\Big\{\exp[-\frac{i}{\hbar}\int_{t'}^{t} dt_1 H(t_1)]\Big\}\,. \tag{B.6}$$

Supposing a Fock basis at time t_0 is labelled by $|\alpha\rangle$, the interaction picture representation of the state vector at time t reads[2]

$$|\alpha(t)\rangle_I = U^\dagger(t,t_0)|\alpha(t)\rangle_S = U^\dagger(t,t_0)U_J(t,t_0)|\alpha\rangle = S_J(t,t_0)|\alpha\rangle\,. \tag{B.7}$$

It is straightforward to verify that

$$S_J(t,t') = T\Big\{\exp[-\frac{i}{\hbar}\int_{t'}^{t} dt_1 \Phi_I(t_1,\boldsymbol{x})J(t_1,\boldsymbol{x})]\Big\}\,. \tag{B.8}$$

We remark that setting $J = 0$ gives $S_{J=0}(t,t') = 1$ implying that the interaction picture coincides with the Heisenberg picture.[3] The vacuum state $|\Omega\rangle$ can now be expressed in the terms of the free vacuum in the infinite past and future using Gell-Mann-Low formulas [107, 108],

$$|\Omega\rangle_J = S_J(t_0,-\infty)|0(-\infty)\rangle\,, \tag{B.9}$$

$$\langle\Omega|_J = \langle 0(+\infty)|S_J(+\infty,t_0)\,. \tag{B.10}$$

Using these relations requires several assumptions. First, states $|0(\pm\infty)\rangle$ will represent the vacuum of the free theory only if the source J vanishes at $t \to \pm\infty$. Second, these relations will be valid only in an adiabatic process, otherwise, there may not be an overlap between $|\Omega\rangle_J$ and $|0(\pm\infty)\rangle$. This explains why the "bra" is connected to $\langle 0(+\infty)|$ instead of $\langle 0(-\infty)|$, the vacuum evolves uniquely to be the vacuum at a different time. These requirements are fulfilled in equilibrium or near-equilibrium processes but fail in nonequilibrium where the dynamics is more violent to be considered adiabatic. Now we are able to rewrite Eq. (B.1) explicitly in terms of the source J,

$$\begin{aligned} Z[J] &= \frac{1}{Z_0}\langle 0(+\infty)|S_J(\infty,-\infty)|0(-\infty)\rangle \\ &= \frac{1}{Z_0}\langle 0(+\infty)|T\Big\{\exp[-\frac{i}{\hbar}\int_{-\infty}^{\infty} dt_1 \Phi_I(t_1,\boldsymbol{x})J(t_1,\boldsymbol{x})]\Big\}|0(-\infty)\rangle\,, \end{aligned} \tag{B.11}$$

[2]Since $S(t,t_0) = S(t,t')S(t',t_0)$, the state at the time t is linked to state at time t' by $|\alpha(t)\rangle_I = S_J(t,t')|\alpha(t')\rangle_I$.

[3]Because of this, one can say that the time-independent Heisenberg state ($J = 0$) becomes a time-dependent state under the influence of an external source J [44].

where $Z_0 = \langle 0(+\infty)|0(-\infty)\rangle$. Here, we interpret $|0(\pm\infty)\rangle$ as a Heisenberg vacuum state at time $t \to \pm\infty$ and $|0(\infty)\rangle \neq |0(-\infty)\rangle$ in general because the vacuum state at time $t \to -\infty$ is defined to be a state that is annihilated by the operator $a(t)$ at time $t \to -\infty$,

$$a(-\infty)|0(-\infty)\rangle = 0\,. \tag{B.12}$$

Since the operator $a(\infty) = U^\dagger(\infty,-\infty)a(-\infty)U(\infty,-\infty)$, it is not necessary that $|0(-\infty)\rangle$ will also be annihilated by $a(\infty)$. Therefore, Z_0 is not normalized in general and the factor $1/Z_0$ is needed in the Eq. (B.11) to keep $Z[J=0]$ normalized.

The n-point functions encoded in $Z[J]$ are defined as a time-order products of the Heisenberg fields

$$G^{(n)}(x_1, x_2, \cdots x_n) = \langle\Omega|T\Big(\Phi(x_1)\Phi(x_2)\cdots\Phi(x_n)\Big)|\Omega\rangle\,. \tag{B.13}$$

Here, the expectation value was made with respect to the vacuum at time t_0. Nevertheless, we can use the form that was introduced by turning the Heisenberg fields into interaction fields, $\Phi(x_i) = S^\dagger(t,t_0)\Phi_I(x_i)S(t,t_0)$,

$$\begin{aligned} G^{(n)}(x_1, x_2, \cdots x_n) = \frac{1}{Z_0}\langle 0(+\infty)|S(+\infty,t_1)\Phi_I(x_1)S(t_1,t_2)\Phi_I(x_2)\cdots \\ \times\,\Phi_I(x_n)S(t_n,-\infty)|0(-\infty)\rangle\,, \end{aligned} \tag{B.14}$$

where we assumed $t_1 > t_2 > \cdots > t_n$ and added the normalization factor $1/Z_0$. Eq. (B.14) is the usual form in S-matrix theory and can be understood that the n-point function is a collective evolution from $t \to -\infty$ to t_n to t_{n-1} and so on until it reaches $t \to +\infty$. The evolution from $t \to -\infty$ to $t \to +\infty$ motivates the name a " single time contour". This approach makes the task of calculating dynamical in-out matrix elements a boundary value problem since the n-point functions here are bounded by two different states: $|0(-\infty)\rangle$ and $|0(+\infty)\rangle$. This is another crucial point because nonequilibrium processes in closed systems are determined by the initial state only. The presence of $|0(+\infty)\rangle$ also demands that the n-point function contains $S(+\infty,t_1)$ which means the contributions at $t' > t_1$ are needed to evaluate n-point functions even though the latest time is t_1.

B.1.2 Closed-time-path formalism

The problems that were mentioned can be fixed by using the state $|\Omega\rangle$ in all expectation values. To do this, we employ the Schwinger-Keldysh formalism by redefinition of the generating function,

$$Z[J_1, J_2] = \langle\Omega|S_{J_2}(t_0,t^*)S_{J_1}(t^*,t_0)|\Omega\rangle\,, \tag{B.15}$$

where

$$\begin{aligned} S_{J_1}(t^*,t_0) &= T\Big\{\exp[-\frac{i}{\hbar}\int_{t_0}^{t^*} dt_1\Phi_I^1(t_1,\boldsymbol{x})J_1(t_1,\boldsymbol{x})]\Big\}\,, \\ S_{J_2}(t_0,t^*) &= \tilde{T}\Big\{\exp[-\frac{i}{\hbar}\int_{t^*}^{t_0} dt_1\Phi_I^2(t_1,\boldsymbol{x})J_2(t_1,\boldsymbol{x})]\Big\}\,. \end{aligned} \tag{B.16}$$

Here, $\tilde{T}$ is an anti-time-ordering operator and it is needed to indicate that $S_{J_2}(t_0, t^*)$ is a backward time-evolution. The first different from Eq. (B.11) is that there is no need of a normalizing factor here because $Z[J, J] = 1$ automatically. Next, there are two sources (J_1 and J_2) and two fields (Φ_I^1 and Φ_I^2) instead of J and Φ_I. This is needed to distinguish the "forward time path" ($t_0 \to t^*$) from the "backward time path" ($t^* \to t_0$). Combining the paths sequentially gives the "closed time path" (CTP). The generating function in Eq. (B.15) is defined within the time window $t_0 < t < t^*$ where t^* serves as an arbitrary time but should be larger than the time scale of any observable of interest. This point will become clear when we write down n-point functions. In fact, n-point functions on the CTP are not so straightforward because the fields Φ_I can live on either the forward or the backward time path and the time ordering must respect the closed time contour. For example, if $t_1 > t_2$, $\Phi_I(x_1)$ will stay on the left side of $\Phi_I(x_2)$ in the case that both of them live on the forward time branch but $\Phi_I(x_1)$ will be on the right side of $\Phi_I(x_2)$ if both of them live on backward time branch. If they live on different time branches, fields on the forward time branch will always be on the right side of fields on the backward path. Because of this, the number of n-point functions are duplicated on the CTP, i.e. there are two 1-point functions,

$$G_1^{(1)}(x) = \phi_1(x) = \langle\Omega|S_{J_2}(t_0, t^*)S_{J_1}(t^*, t)\Phi_I^1(x)S_{J_1}(t, t_0)|\Omega\rangle\,, \tag{B.17}$$

$$G_2^{(1)}(x) = \phi_2(x) = \langle\Omega|S_{J_2}(t_0, t)\Phi_I^2(x)S_{J_2}(t, t^*)S_{J_1}(t^*, t_0)|\Omega\rangle\,, \tag{B.18}$$

however, they collapse to the same function if we choose $J_1 = J_2 = J$,[4]

$$\phi(x) = \langle\Omega|S_J(t_0, t)\Phi_I(x)S_J(t, t_0)|\Omega\rangle\,. \tag{B.19}$$

Notice that there is no evolution beyond t involving the calculation of a local observable at time $t' > t$. As for 2-point functions, there are four possibilities,

$$G_{11}^{(2)}(x_1, x_2) = \langle\Omega|T[\Phi^1(x_1)\Phi^1(x_2)]|\Omega\rangle\,, \tag{B.20}$$

$$G_{12}^{(2)}(x_1, x_2) = \langle\Omega|\Phi^2(x_2)\Phi^1(x_1)|\Omega\rangle\,, \tag{B.21}$$

$$G_{21}^{(2)}(x_1, x_2) = \langle\Omega|\Phi^2(x_1)\Phi^1(x_2)|\Omega\rangle\,, \tag{B.22}$$

$$G_{22}^{(2)}(x_1, x_2) = \langle\Omega|\tilde{T}[\Phi^2(x_1)\Phi^2(x_2)]|\Omega\rangle\,, \tag{B.23}$$

where $\Phi(x)$ is a Heisenberg field. Setting $J_1 = J_2 = J$, we obtain similar expressions as in Eq. (B.19),

$$G_{21}^{(2)}(x_1, x_2) = \langle\Omega|S_J(t_0, t_1)\Phi_I(x_1)S_J(t_1, t_2)\Phi_I(x_2)S_J(t_2, t_0)|\Omega\rangle\,, \tag{B.24}$$

$$G_{12}^{(2)}(x_1, x_2) = \langle\Omega|S_J(t_0, t_2)\Phi_I(x_2)S_J(t_2, t_1)\Phi_I(x_1)S_J(t_1, t_0)|\Omega\rangle\,, \tag{B.25}$$

$$G_{11}^{(2)}(x_1, x_2) = G_{21}^{(2)}(x_1, x_2)\Theta(t_1 - t_2) + G_{12}^{(2)}(x_1, x_2)\rangle\Theta(t_2 - t_1)\,, \tag{B.26}$$

$$G_{22}^{(2)}(x_1, x_2) = G_{12}^{(2)}(x_1, x_2)\Theta(t_1 - t_2) + G_{21}^{(2)}(x_1, x_2)\rangle\Theta(t_2 - t_1)\,. \tag{B.27}$$

[4]The short cut to Eq. (B.19) is to realize that the Heisenberg field is linked to the interaction field by $\Phi(x) = S_J^\dagger(t, t_0)\Phi_I(x)S_J(t, t_0)$. Therefore, $\langle\Omega|\Phi(x)|\Omega\rangle = \langle\Omega|S_J^\dagger(t, t_0)\Phi_I(x)S_J(t, t_0)|\Omega\rangle$ automatically. This shows that the closed time path is an appropriate contour for evaluating the expectation value of the operators.

Again, no evolution beyond t_1 is needed. Note that not all 2-point functions are independent, only two out of four are needed. Moreover, all observables together now form a "true" expectation value with respect to the same initial state $|\Omega\rangle$ [97], therefore for all Hermitian operators, the observables will be real. Hence in the CTP formalism, observables are real and respect causality. We remark that causality is obeyed because the Hamiltonian on the forward and backward time paths are assumed to be identical. Otherwise, $\Phi_I^1(x)$ would be different from $\Phi_I^2(x)$ due to the different Hamiltonians and S_{J_1} can not be combined with S_{J_2} even if the sources J_1 and J_2 are set to be the same.

B.1.3 Path integral representation of CTP formalism and its effective action

We would like to recover the path-integral representation on the CTP as we did in the single-time formalism. Since the structure is the same all properties of path-integrals also apply in the CTP formalism. One can argue that the closed-time contour is, more or less, similar to two single-time contours. Therefore, if t^* is sent to ∞ and t_0 is pushed to $-\infty$, a closed-time contour now consists of two single-time contours, the first one runs from $t_0 \to -\infty$ to $t^* \to \infty$ and the second one from $t^* \to \infty$ to $t_0 \to -\infty$. The difference compared to the single-time formalism is that these two time contours are not fully independent. There is a constraint condition at $t^* \to \infty$. For example, $J_1 = J_2$ and $\Phi^1 = \Phi^2$ to ensure that these two single-time contours form one closed-time contour. Moreover, at $t^* \to \infty$, the path integral is not only considered with $|0(\infty)\rangle$ but with a complete set of some eigenstates,

$$Z[J_1, J_2] = \sum_\alpha \langle \Omega, -\infty | \alpha, +\infty \rangle_{J_2} \langle \alpha, +\infty | \Omega, -\infty \rangle_{J_1} , \tag{B.28}$$

where $|\Omega, -\infty\rangle$ is the very same state $|\Omega\rangle$ but we deliberately chose $t_0 \to -\infty$. From now on, we would like to assume that the Schrödinger field operator $\Phi_S(\boldsymbol{x})$ is a real scalar boson field operators with commutation relations

$$[\Phi_S(\boldsymbol{x}), \Pi_S(\boldsymbol{x}')] = \delta^d(\boldsymbol{x} - \boldsymbol{x}') , \tag{B.29}$$
$$[\Phi_S(\boldsymbol{x}), \Phi_S(\boldsymbol{x}')] = [\Pi_S(\boldsymbol{x}), \Pi_S(\boldsymbol{x}')] = 0 , \tag{B.30}$$

where $\Pi_S(x)$ is the conjugate momentum field operator of $\Phi_S(\boldsymbol{x})$ in the Schrödinger picture. The Heisenberg field $\Phi_H(x) = U_J^\dagger(t, t_0)\Phi_S(\boldsymbol{x})U_J(t, t_0)$ satisfies the same set of commutation relations but at equal times,

$$[\Phi_H(\boldsymbol{x}, t), \Pi_H(\boldsymbol{x}', t)] = \delta^d(\boldsymbol{x} - \boldsymbol{x}') , \tag{B.31}$$
$$[\Phi_H(\boldsymbol{x}, t), \Phi_H(\boldsymbol{x}', t)] = [\Pi_H(\boldsymbol{x}, t), \Pi_H(\boldsymbol{x}', t)] = 0 . \tag{B.32}$$

Here, we explicitly labelled the Heisenberg field with subscript H to avoid confusion. As the $\Phi_S(\boldsymbol{x})$ at different space points commute with each other, there is a complete

set of simultaneous eigenstates $|\Phi\rangle$ with eigenvalue $\Phi(\boldsymbol{x})$,

$$\Phi_S(\boldsymbol{x})|\Phi\rangle = \Phi(\boldsymbol{x})|\Phi\rangle\,, \tag{B.33}$$

$$\int[\mathrm{d}\Phi]|\Phi\rangle\langle\Phi| = \mathbb{1}\,. \tag{B.34}$$

In the Heisenberg picture, the eigenstates of $\Phi(x)$ with an eigenvalue $\Phi(\boldsymbol{x})$ are denoted by $|\Phi, t\rangle$

$$\Phi_H(x)|\Phi, t\rangle = \Phi(\boldsymbol{x})|\Phi, t\rangle\,, \tag{B.35}$$

$$\int[\mathrm{d}\Phi]|\Phi, t\rangle\langle\Phi, t| = \mathbb{1}\,. \tag{B.36}$$

where $|\Phi, t\rangle = U_J^\dagger(t, t_0)|\Phi\rangle$. It should be pointed out that $|\Phi, t\rangle$ is totally different from $|\Phi(t)\rangle = U_J(t, t_0)|\Phi\rangle$ which is a Schrödinger time-dependent state. $|\Phi, t\rangle$ is only an eigenstate of the Heisenberg field at different times with the same eigenvalue as at time t_0. The same arguments also apply to the momentum operator $\Pi(x)$, therefore, the matrix element $\langle\alpha, +\infty|\Omega, -\infty\rangle_{J_1}$ (and also $\langle\Omega, -\infty|\alpha, +\infty\rangle_{J_2}$) can be treated as in quantum mechanics [109, 110]. By slicing the matrix element with $\int[\mathrm{d}\Phi]|\Phi, t\rangle\langle\Phi, t|$ at the discrete set of times $\{t_N\}$, i.e.[5]

$$\begin{aligned}\langle\alpha, +\infty|\Omega, -\infty\rangle_{J_1} = \int &[\mathrm{d}\Phi_N][\mathrm{d}\Phi_{N-1}]\cdots[\mathrm{d}\Phi_1][\mathrm{d}\Phi_0] \\ &\times \langle\alpha, +\infty|\Phi_N, t_N\rangle\langle\Phi_N, t_N|\Phi_{N-1}, t_{N-1}\rangle\langle\Phi_{N-1}, t_{N-1}|\cdots \\ &\times \langle\Phi_1, t_1|\Phi_0, t_0\rangle\langle\Phi_0, t_0|\Omega, -\infty\rangle_{J_1}\,,\end{aligned} \tag{B.37}$$

one obtains a path-integral representation of the matrix element,

$$\langle\alpha, +\infty|\Omega, -\infty\rangle_{J_1} = \int \mathcal{D}'\Phi_1 \exp\Big[\frac{i}{\hbar}\int_{-\infty}^{\infty}\mathrm{d}t\int\mathrm{d}^dx\Big(\mathcal{L}[\Phi_1] + J_1(x)\Phi_1(x)\Big)\Big]\,, \tag{B.38}$$

$$\langle\Omega, -\infty)|\alpha, +\infty\rangle_{J_2} = \int \mathcal{D}'\Phi_2 \exp\Big[\frac{i}{\hbar}\int_{\infty}^{-\infty}\mathrm{d}t\int\mathrm{d}^dx\Big(\mathcal{L}[\Phi_2] + J_2(x)\Phi_2(x)\Big)\Big]\,, \tag{B.39}$$

where $\mathcal{L}[\Phi]$ is a Lagrangian density of the system. The prime on the integral over field configurations indicates that there are boundary conditions due to the first and last matrix elements. They are $\langle\Phi, t_0|\Omega, -\infty\rangle$ and $\langle\alpha, +\infty|\Phi, t_N\rangle$ on the forward time path and $\langle\Phi, t_N|\Omega, -\infty\rangle$ and $\langle\alpha, +\infty|\Phi, t_0\rangle$ on the backward time path.

By defining an action $S[\Phi] = \int_{-\infty}^{\infty}\mathrm{d}t\int\mathrm{d}^dx\mathcal{L}[\Phi]$, we obtain

$$\begin{aligned}Z[J_1, J_2] &= \int\mathrm{d}\Phi_\alpha\int\mathcal{D}'\Phi_1\mathcal{D}'\Phi_2\exp\Big\{\frac{i}{\hbar}\Big[(S[\Phi_1] - S[\Phi_2]) + \int_x(J_1\Phi_1 - J_2\Phi_2)\Big]\Big\} \\ &= \int^{\mathcal{C}}\mathcal{D}'\Phi\exp\Big\{\frac{i}{\hbar}\Big[S_{\mathcal{C}}[\Phi] + \int_x^{\mathcal{C}}J(x)\Phi(x)\Big]\Big\}\,,\end{aligned} \tag{B.40}$$

[5] The times t_0 and t_N are set to be $-\infty$ and $+\infty$ respectively. Also, it is convenient to choose $|\alpha, +\infty\rangle$ to be $|\Phi, +\infty\rangle$ because the only requirement of the state $|\alpha, +\infty\rangle$ is to be a complete set. A subscript i where $i \in \{0, 1, \cdots, N\}$ has been used to distinguish each completeness identity for each time slicing. In this notation we write $\Phi_H(x)|\Phi_i, t\rangle = \Phi_i(\boldsymbol{x})|\Phi_i, t\rangle$. The time-dependent field $\Phi(\boldsymbol{x}, t)$ is a result of the interpolation $\Phi_i(\boldsymbol{x})$ between the discrete times t_N [109].

where $\int_x$ stands for $\int_{-\infty}^{\infty} \mathrm{d}t \int \mathrm{d}^d x$ and $S_{\mathcal{C}}[\Phi]$ is defined by $S[\Phi_1] - S[\Phi_2]$. The integral $\mathrm{d}\Phi_\alpha$ is a sum over all possible configurations at $t \to \infty$ and we drop it by introducing the notation $\mathcal{C}$ to indicate that the integral over time is performed on the closed time contour so sum over all possible configurations of the fields at any time along the closed time contour. Also, the prime over the integration is a reminder that there is an initial condition at t_0.

It is helpful to see that $Z[J_1, J_2]$ is a generating functional in the CTP formalism. Starting with 1-point functions, both of them can be obtained through the functional derivative of $Z[J_1, J_2]$,

$$\begin{aligned} \frac{\hbar}{i}\frac{\delta Z[J_1,J_2]}{\delta J_1(x)} &= \sum_\alpha \langle \Omega, -\infty|\alpha, +\infty\rangle_{J_2}\langle \alpha, +\infty|\Phi_H^1(x)|\Omega, -\infty\rangle_{J_1} \\ &= \langle \Omega, -\infty|\Phi_H(x)|\Omega, -\infty\rangle_J = \phi(x) \qquad ; J_1 = J_2 = J\,, \end{aligned} \tag{B.41}$$

$$\begin{aligned} -\frac{\hbar}{i}\frac{\delta Z[J_1,J_2]}{\delta J_2(x)} &= \sum_\alpha \langle \Omega, -\infty|\Phi_H^2(x)|\alpha, +\infty\rangle_{J_2}\langle \alpha, +\infty|\Omega, -\infty\rangle_{J_1} \\ &= \langle \Omega, -\infty|\Phi_H(x)|\Omega, -\infty\rangle_J = \phi(x) \qquad ; J_1 = J_2 = J\,. \end{aligned} \tag{B.42}$$

The same applies to 2-point functions,

$$\begin{aligned} \left(\frac{\hbar}{i}\right)^2 \frac{\delta^2 Z[J_1,J_2]}{\delta J_1(x)\delta J_1(y)} &= \sum_\alpha \langle \Omega, -\infty|\alpha, +\infty\rangle_{J_2}\langle \alpha, +\infty|T[\Phi_H^1(x)\Phi_H^1(y)]|\Omega, -\infty\rangle_{J_1} \\ &= \langle \Omega, -\infty|T[\Phi_H(x)\Phi_H(y)]|\Omega, -\infty\rangle_J = G_{11}^{(2)}(x,y)\,, \end{aligned} \tag{B.43}$$

$$-\left(\frac{\hbar}{i}\right)^2 \frac{\delta^2 Z[J_1,J_2]}{\delta J_1(x)\delta J_2(y)} = \langle \Omega, -\infty|\Phi_H(y)\Phi_H(x)|\Omega, -\infty\rangle_J = G_{12}^{(2)}(x,y)\,, \tag{B.44}$$

$$-\left(\frac{\hbar}{i}\right)^2 \frac{\delta^2 Z[J_1,J_2]}{\delta J_2(x)\delta J_1(y)} = \langle \Omega, -\infty|\Phi_H(x)\Phi_H(y)|\Omega, -\infty\rangle_J = G_{21}^{(2)}(x,y)\,, \tag{B.45}$$

$$\left(-\frac{\hbar}{i}\right)^2 \frac{\delta^2 Z[J_1,J_2]}{\delta J_2(x)\delta J_2(y)} = \langle \Omega, -\infty|\tilde{T}[\Phi_H(x)\Phi_H(y)]|\Omega, -\infty\rangle_J = G_{22}^{(2)}(x,y)\,, \tag{B.46}$$

and higher-order of n-point functions. As in the single-time formalism, these n-point functions consist of both connected and disconnected contributions. The sources in both time branches must be set to be equal, $J_1 = J_2 = J$, before we can claim they are n-point functions in the canonical formalism [111, 112].

The generating function $W[J_1, J_2]$ that generates only connected diagrams is defined in a similar way as in the single-time formalism,

$$W[J_1, J_2] = -i\hbar \ln Z[J_1, J_2]\,, \tag{B.47}$$

and the effective action is a Legendre transform of $W[J_1, J_2]$

$$\Gamma[\phi_1, \phi_2] = W[J_1, J_2] - \int_x \Big[\phi_1(x)J_1(x) - \phi_2(x)J_2(x)\Big]\,, \tag{B.48}$$

where $\phi_a(x) = (-1)^{a-1}\delta W[J_1, J_2]/\delta J_a(x); a = 1, 2$ which are 1-point functions. It is straightforward to show that

$$\frac{\delta\Gamma[\phi_1, \phi_2]}{\delta\phi_1(x)} = -J_1(x)\,, \tag{B.49}$$

$$\frac{\delta\Gamma[\phi_1, \phi_2]}{\delta\phi_2(x)} = J_2(x)\,. \tag{B.50}$$

Once the sources J_1 and J_2 are set to zero, we obtain dynamic equations of ϕ_1 and ϕ_2 respectively. Even though there are two field variables and two dynamical equations on each time branch, $\delta\Gamma/\delta\phi_{1,2} = 0$, these equations are supposed to coincide in the limit $J_1 = J_2$. This can be seen from the vanishing of the effective action in that limit

$$\Gamma[\phi, \phi] = -i\hbar \ln Z[J, J] - \int_x (J\phi - J\phi) = 0\,, \tag{B.51}$$

where we used $Z[J, J] = 1$. We then introduce the new field variables

$$\phi_+ = \frac{1}{2}(\phi_1 + \phi_2)\,, \tag{B.52}$$

$$\phi_- = \phi_1 - \phi_2\,, \tag{B.53}$$

and expand the effective action in these new variables

$$\begin{aligned}\Gamma[\phi_+, \phi_-] \;=\; & \phi_-(x)N_1(x) + \phi_+(x)M_1(x) + \frac{1}{2}\phi_-(x)N_2(x, x')\phi_-(x') \\ & + \frac{1}{2}\phi_+(x)M_2(x, x')\phi_+(x') + \frac{1}{2}\phi_+(x)D_2(x, x')\phi_-(x') + \dots\,.\end{aligned} \tag{B.54}$$

Since Γ has to vanish when $J_1 = J_2$, all terms that contain only ϕ_+ and no ϕ_- are zero. This condition enforces all M functions to be zero. Then, the dynamics of ϕ_+ obtained from $\delta\Gamma/\delta\phi_+ = 0$ is trivial in the limit $\phi_1 = \phi_2$, and only non-trivial dynamics lies in the ϕ_- [113].

So far, we assumed pure states in the sense that the observables are expectation values with respect to a single state, a vacuum state. In the case that mixed states are involved, we need to incorporate the density operator into the generating functional. We use the observation that in the operator language, the expectation value of an observable reads

$$\langle\mathcal{O}\rangle = \mathrm{Tr}\left[\mathcal{O}\rho_0\right]\,, \tag{B.55}$$

where ρ_0 is a density operator, presumingly is defined at initial time. The generating functional then shall be redefined by

$$Z[J_1, J_2; \rho_0] = \mathrm{Tr}\{S_{J_2}(t_0, t^*)S_{J_1}(t^*, t_0)\rho_0\}\,. \tag{B.56}$$

As a result, n-point functions can be evaluated by tracing with the density operator, for example,

$$\phi(x) = \mathrm{Tr}\{\Phi_H(x)\rho_0\}\,, \tag{B.57}$$

$$G^{(2)}_{11}(x, y) = \mathrm{Tr}\{T[\Phi_H(x)\Phi_H(y)\rho_0]\}\,, \tag{B.58}$$

where we have set $J_1 = J_2 = J$. To recover the path-integral representation, we perform the very same time slicing as we did before, however, the generating functional in Eq. (B.56) is written in S-matrix form. Hence, we use interaction-picture fields $\Phi_I(x)$ instead of Heisenberg fields $\Phi_H(x)$. Since the $\Phi_I(x)$ also commute at an equal times, there exists a complete set of simultaneously eigenstates $|\Phi, t\rangle_I$ of $\Phi_I(x)$ with eigenvalues $\Phi(\boldsymbol{x})$,

$$\Phi_I(x)|\Phi, t\rangle_I = \Phi(\boldsymbol{x})|\Phi, t\rangle_I \,, \tag{B.59}$$

$$\int [\mathrm{d}\Phi]|\Phi, t\rangle_I\langle\Phi, t|_I = \mathbb{1} \,, \tag{B.60}$$

where $|\Phi, t\rangle_I = U^\dagger(t, t_0)|\Phi\rangle$. Again, the state $|\Phi, t\rangle_I$ has nothing to do with a time-dependent state in the interaction picture $|\Phi(t)\rangle_I = S_J(t, t_0)|\Phi\rangle$. The path integral representation can be formed using these eigenstates,

$$Z[J_1, J_2; \rho_0] = \int [\mathrm{d}\Phi^-] \int [\mathrm{d}\Phi^+]\langle\Phi^+|\rho_0|\Phi^-\rangle\langle\Phi^-|S_{J_2}(t_0, t^*)S_{J_1}(t^*, t_0)|\Phi^+\rangle \,, \tag{B.61}$$

where $|\Phi^\pm\rangle = |\Phi^\pm, t_0\rangle_I$. The first factor in the integrand in Eq. (B.61) is a matrix element at time t_0, therefore this term is interpreted as the initial condition. The second factor is a path integral over a closed-time path and dynamics is encoded here. Time slicing by the completeness identity will be done in this second factor,

$$\begin{aligned}
&\langle\Phi^-|S_{J_2}(t_0, t^*)S_{J_1}(t^*, t_0)|\Phi^+\rangle \\
&\quad = \int [\mathrm{d}\Phi_N][\mathrm{d}\Phi_{N-1}]\cdots[\mathrm{d}\Phi_1][\mathrm{d}\Phi_0]\langle\Phi^-|S_{J_2}(t_0, t_N)|\Phi_N, t_N\rangle_I \\
&\qquad \times \langle\Phi_N, t_N|_I S_{J_2}(t_N, t_{N-1})|\Phi_{N-1}, t_{N-1}\rangle_I\langle\Phi_{N-1}, t_{N-1}|_I \cdots \\
&\qquad \times \langle\Phi_1, t_1|_I S_{J_1}(t_1, t_0)|\Phi, t_0\rangle_I\langle\Phi, t_0|_I\Phi^+\rangle \,.
\end{aligned} \tag{B.62}$$

Note that S_J which occurs in each factor can be rewritten in terms of $\langle\Phi_f|U_J(t_f, t_i)|\Phi_i\rangle$,

$$\begin{aligned}
\langle\Phi_f, t_f|_I S_J(t_f, t_i)|\Phi_i, t_i\rangle_I &= \langle\Phi_f|U(t_f, t_0)S_J(t_f, t_0)S_J(t_0, t_i)U^\dagger(t_i, t_0)|\Phi_i\rangle \\
&= \langle\Phi_f|U(t_f, t_0)\Big(U^\dagger(t_f, t_0)U_J(t_f, t_0)\Big) \\
&\qquad \times \Big(U^\dagger(t_i, t_0)U_J(t_i, t_0)\Big)^\dagger U^\dagger(t_i, t_0)|\Phi_i\rangle \\
&= \langle\Phi_f|U_J(t_f, t_0)U_J^\dagger(t_i, t_0)|\Phi_i\rangle \\
&= \langle\Phi_f|U_J(t_f, t_i)|\Phi_i\rangle \,.
\end{aligned} \tag{B.63}$$

Therefore the path integral takes the same form as in Eq. (B.40) and thus, Eq. (B.61) becomes

$$Z[J_1, J_2; \rho_0] = \int [\mathrm{d}\Phi^-][\mathrm{d}\Phi^+]\langle\Phi^+|\rho_0|\Phi^-\rangle \int_{\Phi^+}^{\mathcal{C}\,\Phi^-} \mathcal{D}'\Phi \exp\Big\{\frac{i}{\hbar}\Big[S_{\mathcal{C}}[\Phi] + \int_x^{\mathcal{C}} J(x)\Phi(x)\Big]\Big\} \,, \tag{B.64}$$

again, we use $\mathcal{C}$ to remind that the time integration is done over the closed-time contour and the refer to $\Phi^\pm$ at the integral limits the constraints at the beginning and the end of the path. We end this section by recalling that all formulations are assumed to be for a real scalar field. The extension to more than one component or the complex scalar field is straightforward.

B.2 2-particle irreducible effective action

We have seen that the dynamic equations for mean fields $\phi(x)$ can be obtained through the relation $\delta\Gamma[\phi]/\delta\phi(x) = 0$. This relation is a direct consequence of having the local external source $J(x)$ in the generating functional $Z[J]$. In this section, we are going to show that the presence of nonlocal external sources gives the dynamic equations for higher n-point functions. However, we will mainly focus on the 2PI formalism and dynamic equations for 1- and 2-point functions.

B.2.1 The generating of n-particle irreducible (nPI) formalism

The nPI generating functional takes the form

$$Z[J_a, K_{ab}, ..] = \int^{\mathcal{C}} \mathcal{D}\Phi\mathcal{D}\Phi^* \exp\Big[\frac{i}{\hbar}\Big\{S_{\mathcal{C}}[\Phi,\Phi^*] + \int_x^{\mathcal{C}} J_a(x)\Phi_a(x) \tag{B.65}$$

$$+ \frac{1}{2}\int_{xy}^{\mathcal{C}} K_{ab}(x,y)\Phi_a(x)\Phi_b^*(y) + \frac{1}{6}\int_{xyz}^{\mathcal{C}} K_{abc}(x,y,z)\Phi_a(x)\Phi_b^*(y)\Phi_c(z) + \dots\Big\}\Big], \tag{B.66}$$

where all K terms represent nonlocal sources in the sense that they are the functions of more than one space-time point. The indices $a = 1, 2$ label the field and its complex conjugate i.e. $\Phi_1(x) = \Phi(x)$ and $\Phi_2(x) = \Phi^*(x)$. In this convention, $\Phi_1(x)$ and $\Phi_2(x)$ are related by the transformation $\Phi_a^*(x) = \sigma^1_{ab}\Phi_b(x)$ where σ^1 is the first Pauli metrix. Also the label $\mathcal{C}$ is used to remind that the integration, whether in space-time or field variables, is to be understood within the CTP formalism. There are some useful symmetries of the kernels K that will be needed later on. We start with $K_{ab}(x,y)$, observing that

$$\int_{xy}^{\mathcal{C}} K_{ab}(x,y)\Phi_a(x)\Phi_b^*(y) = \int_{xy}^{\mathcal{C}} K_{ab}(x,y)\Phi_b^*(y)\Phi_a(x)$$

$$\int_{xy}^{\mathcal{C}} K_{ab}(x,y)\sigma^1_{aa'}\Phi_{a'}^*(x)\sigma^1_{bb'}\Phi_{b'}(y) = \int_{xy}^{\mathcal{C}} K_{ba}(y,x)\Phi_a^*(x)\Phi_b(y)\,. \tag{B.67}$$

By interchanging primed and un-primed indices on the LHS, it can be seen that

$$K_{ba}(y,x) = \sigma^1_{aa'}\sigma^1_{bb'}K_{a'b'}(x,y)\,. \tag{B.68}$$

The other K have similar properties, namely, the relation in Eq. (B.68) holds for any pairs of indices ab that are contracted with $\Phi_a\Phi_b^*$ but for a pair of indices ab contracted with $\Phi_a\Phi_b$ or $\Phi_a^*\Phi_b^*$, they are completely symmetric. For example, taking $K_{abc}(x,y,z)$, we have the following relations,

$$K_{bac}(y,x,z) = \sigma^1_{aa'}\sigma^1_{bb'}K_{a'b'c}(x,y,z)\,, \tag{B.69}$$

$$K_{acb}(x,z,y) = \sigma^1_{bb'}\sigma^1_{cc'}K_{ab'c'}(x,y,z)\,, \tag{B.70}$$

$$K_{cba}(z,y,x) = K_{abc}(x,y,z)\,. \tag{B.71}$$

The connected generating functional is defined by

$$W[J_a, K_{ab}, \ldots] \equiv -i\hbar \ln Z[J_a, K_{ab}, \ldots] \,, \tag{B.72}$$

and the effective action is a multiple Legendre transformation of $W[J_a, K_{ab}, \ldots]$

$$\begin{aligned}\Gamma[\phi_a, G_{ab}, \ldots] = W[J_a, K_{ab}, \ldots] &- \int_x^{\mathcal{C}} J_a(x)\phi_a(x) \\ &- \frac{1}{2}\int_{xy}^{\mathcal{C}} K_{ab}(x,y)\Big[\phi_a(x)\phi_b^*(y) + \hbar G_{ab}(x,y)\Big] \\ &- \frac{1}{6}\int_{xyz}^{\mathcal{C}} K_{abc}(x,y,z)\Big[\phi_a(x)\phi_b^*(y)\phi_c(z) + \hbar\phi_a(x)G_{cb}(z,y) \\ &\qquad + \hbar\sigma^1_{cc'}\phi_b^*(y)G_{ac'}(x,z) + \hbar\phi_c(z)G_{ab}(x,y) + \hbar^{3/2}G_{abc}(x,y,z)\Big] \\ &- \ldots \,,\end{aligned} \tag{B.73}$$

where the mean field $\phi_a(x)$ is defined by the functional derivative with respect to the local source $J_a(x)$.

$$\frac{\delta W}{\delta J_a(x)} = \phi_a(x) \,, \tag{B.74}$$

and the nonlocal kernels $G_{ab}(x,y), G_{abc}(x,y,z), \ldots$ are defined by

$$\frac{\delta W}{\delta K_{ab}(x,y)} = \frac{1}{2}\Big\{\phi_a(x)\phi_b^*(y) + \hbar G_{ab}(x,y)\Big\} \tag{B.75}$$

$$\begin{aligned}\frac{\delta W}{\delta K_{abc}(x,y,z)} = \frac{1}{6}\Big\{&\phi_a(x)\phi_b^*(y)\phi_c(z) + \hbar\phi_a(x)G_{cb}(z,y) \\ &+ \hbar\sigma^1_{cc'}\phi_b^*(y)G_{ac'}(x,z) + \hbar\phi_c(z)G_{ab}(x,y) \\ &+ \hbar^{3/2}G_{abc}(x,y,z)\Big\},\end{aligned} \tag{B.76}$$

and so on. It can be seen that $\delta W/\delta K_{ab} = \delta^2 Z/\delta J_b^*\delta J_a$ which is the total 2-point functions containing both connected and disconnected contributions. Therefore, by including $\phi_a(x)\phi_b^*(y)$ in Eq. (B.75) which are the disconnected contribution of the 2-point functions, G_{ab} become the connected 2-point functions once external sources on both time branches have been set to be equal i.e. $J_1 = J_2 = J$. A similar procedure is followed for the other G, for example in Eq. (B.76), $\delta W/\delta K_{abc}$ are 3-point functions so we need to explicitly add disconnected contributions to make G_{abc} being a connected 3-point function. The first term is a product of three 1-point functions which is straightforward. The tricky terms are the combinations of 1- and 2-point functions because of the rule that the index b must be a conjugate index (contraction with Φ^*). To form these terms, we pair two of three indices abc and turn the pair into G. For example, if we pair ab, we get $\phi_c G_{ab}$ which is fine because the second index of G_{ab} is a conjugate index. If we now want to pair ac, it becomes

problematic because neither a nor c are conjugate indices and it is impossible to form G_{ac}. To overcome this problem, we observe that

$$\Phi_a(x)\Phi_b^*(y)\Phi_c(z) = \sigma^1_{cc'}\Phi_a(x)\Phi_b^*(y)\Phi_{c'}^*(z)\,, \tag{B.77}$$

so instead pairing indices ac directly, we pair ac' with the cost of having $\sigma^1_{cc'}$ in the expression. As for a pair bc, one can use the same procedure

$$\Phi_a(x)\Phi_b^*(y)\Phi_c(z) = \sigma^1_{bb'}\sigma^1_{cc'}\Phi_a(x)\Phi_{b'}(y)\Phi_{c'}^*(z)\,, \tag{B.78}$$

such that one gets $\sigma^1_{bb'}\sigma^1_{cc'}G_{b'c'}(y,z)$ as a result of pairing $b'c'$ gives $G_{cb}(z,y)$ since it shares the structure of $K_{ab}(x,y)$.[6] The corresponding inverse transformations are[7]

$$\begin{aligned}\frac{\delta\Gamma}{\delta\phi_a(x)} = &-J_a(x) - \int_y^{\mathcal{C}} \phi_b^*(y)K_{ab}(x,y) \\ &- \frac{1}{2}\int_{yz}^{\mathcal{C}} K_{abc}(x,y,z)\Big[\phi_b^*(y)\phi_c(z) + \hbar G_{cb}(z,y)\Big] \\ &- \ldots,\end{aligned} \tag{B.79}$$

$$\frac{\delta\Gamma}{\delta G_{ab}(x,y)} = -\frac{\hbar}{2}K_{ab}(x,y) - \frac{\hbar}{2}\int_z^{\mathcal{C}} K_{abc}(x,y,z)\phi_c(z) - \ldots, \tag{B.80}$$

$$\frac{\delta\Gamma}{\delta G_{abc}(x,y,z)} = -\frac{\hbar^{3/2}}{6}K_{abc}(x,y,z) - \ldots, \tag{B.81}$$

and so on. Setting all the external sources to zero yields the nonperturbative dynamic equations for the connected n-point functions. The set of equation forms the BBGKY hierarchy in the sense that the equation of motion for an n-point function requires information about the dynamics of higher m-point functions, $m > n$. However, in the limit of vanishing sources, $J = 0$ and $K = 0$, the hierarchy disappears and dynamic equations for n-point functions are in closed form. Thus, one may keep only a finite number of sources or, in the other words, the generating functional is defined to have up to nth power of Φ. This n-particle-irreducible formalism (nPI) gives an nonperturbative approach to evaluate up to n-point functions.

B.2.2 2-particle-irreducible (2PI) effective action

In this study, we are mainly interested in propagators or 2-point functions and would like to have a dynamic equation for 2-point functions, therefore, we need to keep only

[6] One can easily see that the term $G_{cb}(y,z)$ comes from the pair $\Phi_c(z)\Phi_b^*(y)$ nevertheless.

[7] As we have done in the Ch. 4, the functional differentiation rules $\delta\phi_a(x)/\delta\phi_b(y) = \delta_{ab}\delta^{\mathcal{C}}(x-y)$ and $\delta\phi_a^*(x)/\delta\phi_b(y) = \delta\phi_a(x)/\delta\phi_b^*(y) = \sigma^1_{ab}\delta^{\mathcal{C}}(x-y)$ are needed as well as the relations in Eq. (B.68) for the kernels K and to show that for the 2-point function G, the differentiation is straightforward, for example, $\delta G_{ab}(x,y)/\delta G_{cd}(u,v) = \delta_{ac}\delta_{bd}\delta^{\mathcal{C}}(x-u)\delta^{\mathcal{C}}(y-v)$. This is the case because we do not include K^* or G^* directly in the generating function to avoid overcounting.

terms up to quadratic order in $\Phi_a(x)$ in the generating functional,

$$Z[J_a, K_{ab}] = \int^{\mathcal{C}} \mathcal{D}\Phi\mathcal{D}\Phi^* \exp\Big[\frac{i}{\hbar}\Big\{S_{\mathcal{C}}[\Phi,\Phi^*] + \int_x^{\mathcal{C}} J_a(x)\Phi_a(x) + \frac{1}{2}\int_{xy}^{\mathcal{C}} K_{ab}(x,y)\Phi_a(x)\Phi_b^*(y)\Big\}\Big]. \tag{B.82}$$

The corresponding effective action is

$$\Gamma[\phi_a, G_{ab}] = W[J_a, K_{ab}] - \int_x^{\mathcal{C}} J_a(x)\phi_a(x) - \frac{1}{2}\int_{xy}^{\mathcal{C}} K_{ab}(x,y)\Big[\phi_a(x)\phi_b^*(y) + \hbar G_{ab}(x,y)\Big], \tag{B.83}$$

where the 2PI connected generating functional is $W[J_a, K_{ab}] = -i\hbar \ln Z[J_a, K_{ab}]$. The dynamical equations are now in the closed form,

$$\frac{\delta\Gamma}{\delta\phi_a(x)} = -J_a(x) - \int_y^{\mathcal{C}} K_{ab}(x,y)\phi_b^*(y), \tag{B.84}$$

$$\frac{\delta\Gamma}{\delta G_{ab}(x,y)} = -\frac{\hbar}{2}K_{ab}(x,y). \tag{B.85}$$

The further step is to express the effective action $\Gamma[\phi_a, G_{ab}]$ in terms of the classical action and the quantum correction terms. To do this, we employ a background field method by stating that $\Phi(x)$, the fluctuation field in the path integral in Eq. (B.83), can be separated into a mean field $\phi(x)$ and its quantum fluctuation $\varphi(x)$,

$$\Phi_a(x) = \phi_a(x) + \varphi_a(x). \tag{B.86}$$

Taking an exponential, $\Gamma[\phi_a, G_{ab}]$ can also be written in the form of a path integral,

$$\begin{aligned}\exp\frac{i}{\hbar}\Gamma[\phi_a, G_{ab}] &= \int^{\mathcal{C}} \mathcal{D}\Phi\mathcal{D}\Phi^* \exp\frac{i}{\hbar}\Big\{S_{\mathcal{C}}[\Phi,\Phi^*] + \int_x^{\mathcal{C}} J_a(x)[\Phi_a(x) - \phi_a(x)] \\ &\quad + \frac{1}{2}\int_{xy}^{\mathcal{C}} K_{ab}(x,y)[\Phi_a(x)\Phi_b^*(y) - \phi_a(x)\phi_b^*(y) - \hbar G_{ab}(x,y)]\Big\} \\ &= \int^{\mathcal{C}} \mathcal{D}\varphi\mathcal{D}\varphi^* \exp\frac{i}{\hbar}\Big\{S_{\mathcal{C}}[\phi+\varphi,\phi^*+\varphi^*] + \int_x^{\mathcal{C}} J_a(x)\varphi_a(x) \\ &\quad + \frac{1}{2}\int_{xy}^{\mathcal{C}} K_{ab}(x,y)[\varphi_a(x)\varphi_b^*(y) + \varphi_a(x)\phi_b^*(y) \\ &\quad + \phi_a(x)\varphi_b^*(y) - \hbar G_{ab}(x,y)]\Big\},\end{aligned} \tag{B.87}$$

where we applied Eq. (B.86) and assumed that all fluctuations are encoded in φ. The expansion of the classical action around the mean field $\phi(x)$ reads[8]

$$S_{\mathcal{C}}[\phi+\varphi,\phi^*+\varphi^*] = S_{\mathcal{C}}[\phi,\phi^*] + \int_x^{\mathcal{C}} \frac{\delta S_{\mathcal{C}}}{\delta\Phi_a(x)}\Big|_{\Phi=\phi}\varphi_a(x) + \frac{1}{2}\int_{xy}^{\mathcal{C}} \frac{\delta^2 S_{\mathcal{C}}}{\delta\Phi_b^*(y)\delta\Phi_a(x)}\Big|_{\Phi=\phi}\varphi_a(x)\varphi_b^*(y) + S_Q, \tag{B.88}$$

[8]Note that , while $\delta S/\delta\Phi_a \neq \delta S/\delta\Phi_a^*$ one has $\int_x \varphi_a^*\,\delta S/\delta\Phi_a = \int_x \varphi_a^*\,\delta S/\delta\Phi_a^*$ because it is summed over field indices a. Therefore, it is possible to interchange Φ and Φ^*.

where S_Q contains the higher-order expansion in φ,

$$S_Q = \frac{1}{3!}\int_{xyz}^{\mathcal{C}} \frac{\delta^3 S_{\mathcal{C}}}{\delta\Phi_c(z)\delta\Phi_b^*(y)\delta\Phi_a(x)}\Big|_{\Phi=\phi}\varphi_a(x)\varphi_b^*(y)\varphi_c(z) + \frac{1}{4!}\int_{xyzw}^{\mathcal{C}} \frac{\delta^4 S_{\mathcal{C}}}{\delta\Phi_d^*(w)\delta\Phi_c(z)\delta\Phi_b^*(y)\delta\Phi_a(x)}\Big|_{\Phi=\phi}\varphi_a(x)\varphi_b^*(y)\varphi_c(z)\varphi_d^*(w) + \cdots . \tag{B.89}$$

Putting the expansion back into Eq. (B.87) and rearranging the terms, we obtain

$$\exp\frac{i}{\hbar}\Gamma[\phi_a, G_{ab}] = \int^{\mathcal{C}} \mathcal{D}\varphi\mathcal{D}\varphi^* \exp\frac{i}{\hbar}\Big\{ S_{\mathcal{C}}[\phi,\phi^*] + \int_x^{\mathcal{C}} \Big[\frac{\delta S_{\mathcal{C}}}{\delta\Phi_a(x)}\Big|_{\Phi=\phi} - \frac{\delta\Gamma}{\delta\phi_a(x)}\Big]\varphi_a(x) + \frac{1}{2}\int_{xy}^{\mathcal{C}} \Big[\frac{\delta^2 S_{\mathcal{C}}}{\delta\Phi_b^*(y)\delta\Phi_a(x)}\Big|_{\Phi=\phi} - \frac{2}{\hbar}\frac{\delta\Gamma}{\delta G_{ab}(x,y)}\Big]\varphi_a(x)\varphi_b^*(y) + \int_{xy}^{\mathcal{C}} \frac{\delta\Gamma}{\delta G_{ab}(x,y)} G_{ab}(x,y) + S_Q\Big\}, \tag{B.90}$$

where Eqs. (B.84) and (B.85) have been used to turn J and K into ϕ and G. The terms that have no φ can be pulled out of path integral

$$\Gamma[\phi_a, G_{ab}] = S_{\mathcal{C}}[\phi,\phi^*] + \int_{xy}^{\mathcal{C}} \frac{\delta\Gamma}{\delta G_{ab}(x,y)} G_{ab}(x,y) + \tilde{\Gamma}_2[\phi_a, G_{ab}], \tag{B.91}$$

where the rest of path integral is included in $\tilde{\Gamma}_2[\phi_a, G_{ab}]$,

$$\tilde{\Gamma}_2[\phi_a, G_{ab}] = -i\hbar \ln\Big[\int^{\mathcal{C}} \mathcal{D}\varphi\mathcal{D}\varphi^* \exp\frac{i}{\hbar}\Big\{\int_x^{\mathcal{C}} \Big[\frac{\delta S_{\mathcal{C}}}{\delta\Phi_a(x)}\Big|_{\Phi=\phi} - \frac{\delta\Gamma}{\delta\phi_a(x)}\Big]\varphi_a(x) + \frac{1}{2}\int_{xy}^{\mathcal{C}} \Big[\frac{\delta^2 S_{\mathcal{C}}}{\delta\Phi_b^*(y)\delta\Phi_a(x)}\Big|_{\Phi=\phi} - \frac{2}{\hbar}\frac{\delta\Gamma}{\delta G_{ab}(x,y)}\Big]\varphi_a(x)\varphi_b^*(y) + S_Q\Big\}\Big]. \tag{B.92}$$

Notice that $\tilde{\Gamma}_2[\phi_a, G_{ab}]$ itself takes a similar form as $\Gamma[\phi_a, G_{ab}]$ in Eq. (B.87) [112, 113]. The differences lie in the external sources which, in $\tilde{\Gamma}_2[\phi_a, G_{ab}]$, are not fully independent quantities, for example, $\tilde{J}_a(x) = \delta S_{\mathcal{C}}/\delta\Phi_a - \delta\Gamma/\delta\phi_a$ depend fully on ϕ_a (and presumably G_{ab} as well). However, one can see that there is not yet a definite classical action and this can be used for our advantage.[9] Since the quadratic terms in φ in Eq. (B.92) are the only quadratic terms in $\tilde{\Gamma}$ (S_Q starts with a cubic term), these terms must serve as the free term in the classical action and the nonlocal source $\tilde{K}_{ab}(x,y)$ in the case that we demand $\tilde{\Gamma}$ being a 2PI-effective action. We then make an ansatz

$$\frac{\delta^2 S_{\mathcal{C}}}{\delta\Phi_b^*(y)\delta\Phi_a(x)}\Big|_{\Phi=\phi} - \frac{2}{\hbar}\frac{\delta\Gamma}{\delta G_{ab}(x,y)} = iG_{ab}^{-1}(x,y) + \tilde{K}_{ab}(x,y), \tag{B.93}$$

[9] The interpretation here is analogue to the arguments for the 1PI effective action in Ref. [42].

where we deliberately choose $G^{-1}_{ab}(x,y)$ on the RHS to be an inverse of $G_{ab}(x,y)$ which are the propagators of a theory with classical action $S_{\mathcal{C}}$. Using the ansatz in Eq. (B.93), the effective action $\Gamma[\phi_a, G_{ab}]$ becomes

$$\begin{aligned}\Gamma[\phi_a, G_{ab}] &= S_{\mathcal{C}}[\phi,\phi^*] + \frac{\hbar}{2}\int_{xy}^{\mathcal{C}}\Big[\frac{\delta^2 S_{\mathcal{C}}}{\delta\Phi^*_b(y)\delta\Phi_a(x)}\Big|_{\Phi=\phi} - iG^{-1}_{ab}(x,y) - \tilde{K}_{ab}(x,y)\Big]G_{ab}(x,y) \\ &\quad + \tilde{\Gamma}_2[\phi_a, G_{ab}] \\ &= S_{\mathcal{C}}[\phi,\phi^*] + \frac{\hbar}{2}\int_{xy}^{\mathcal{C}}\Big[\frac{\delta^2 S_{\mathcal{C}}}{\delta\Phi^*_b(y)\delta\Phi_a(x)}\Big|_{\Phi=\phi} G_{ab}(x,y) - \frac{i\hbar}{2}\ln\det{}_{\mathcal{C}}G \\ &\quad + \Gamma_2[\phi_a, G_{ab}] + \text{const}\,, \end{aligned} \tag{B.94}$$

where $\Gamma_2[\phi_a, G_{ab}]$ is

$$\begin{aligned}\Gamma_2[\phi_a, G_{ab}] = -i\hbar\ln\Big[&\det{}^{-1/2}(\hbar G)\int^{\mathcal{C}}\mathcal{D}\varphi\mathcal{D}\varphi^* \\ &\times \exp\frac{i}{\hbar}\Big\{\Big(\frac{1}{2}\int_{xy}^{\mathcal{C}} iG^{-1}_{ab}(x,y)\varphi_a(x)\varphi^*_b(y) + S_Q\Big) \\ &\quad + \int_x^{\mathcal{C}}\Big[\frac{\delta S_{\mathcal{C}}}{\delta\Phi_a(x)}\Big|_{\Phi=\phi} - \frac{\delta\Gamma}{\delta\phi_a(x)}\Big]\varphi_a(x) \\ &\quad + \frac{1}{2}\int_{xy}^{\mathcal{C}}\tilde{K}_{ab}(x,y)\Big[\varphi_a(x)\varphi^*_b(y) - \hbar G_{ab}(x,y)\Big\}\Big] \end{aligned}$$

$$\begin{aligned}= -i\hbar\ln\Big[&\det{}^{-1/2}(\hbar G)\int^{\mathcal{C}}\mathcal{D}\varphi\mathcal{D}\varphi^*\exp\frac{i}{\hbar}\Big\{S^{\Gamma_2}_{\mathcal{C}}[\varphi,\varphi^*] + \int_x^{\mathcal{C}}\tilde{J}_a(x)\varphi_a(x) \\ &\quad + \frac{1}{2}\int_{xy}^{\mathcal{C}}\tilde{K}_{ab}(x,y)\Big[\varphi_a(x)\varphi^*_b(y) - \hbar G_{ab}(x,y)\Big]\Big\}\Big]\,. \end{aligned} \tag{B.95}$$

What we need to do to get Eq. (B.94) are shifting back the $\tilde{K}_{ab}G_{ab}$ term into $\tilde{\Gamma}_2$ and pulling out the 1-loop contribution, $i\hbar/2\ln\det{}_{\mathcal{C}}G$, so the $\Gamma_2[\phi_a, G_{ab}]$ contains only contributions from two- and higher-loop diagrams. The source terms can be expressed in terms of $\Gamma_2[\phi_a, G_{ab}]$ by replacing $\Gamma[\phi_a, G_{ab}]$ with Eq. (B.94),

$$\tilde{J}_a(x) = -\Big(\frac{\hbar}{2}\int_{yz}^{\mathcal{C}}\frac{\delta^3 S_{\mathcal{C}}[\phi,\phi^*]}{\delta\phi_a(x)\delta\phi^*_c(z)\delta\phi_b(y)}G_{bc}(y,z) + \frac{\delta\Gamma_2}{\delta\phi_a(x)}\Big)\,, \tag{B.96}$$

$$\tilde{K}_{ab}(x,y) = -\frac{2}{\hbar}\frac{\delta\Gamma_2}{\delta G_{ab}(x,y)}\,. \tag{B.97}$$

The classical action in $\Gamma_2[\phi_a, G_{ab}]$ now reads

$$S^{\Gamma_2}_{\mathcal{C}}[\varphi,\varphi^*] = \frac{1}{2}\int_{xy}^{\mathcal{C}} iG^{-1}_{ab}(x,y)\varphi_a(x)\varphi^*_b(y) + S_Q\,. \tag{B.98}$$

This action is different from $S_{\mathcal{C}}[\phi,\phi^*]$. It explicitly contains the free-kinetic part $\int_{xy}^{\mathcal{C}} iG^{-1}_{ab}(x,y)\varphi_a(x)\varphi^*_b(y)$ where the free propagators are $G_{ab}(x,y)$ and the interaction

is now determined by S_Q. Then, the lines in the Feynman diagrams generated by Γ_2 are full propagators $G_{ab}(x,y)$ instead of free propagators and the vertices are governed by the interaction S_Q. The unique structure of Γ_2 can be seen by performing the functional derivative of Γ in Eq. (B.94) with respect to $G_{ab}(x,y)$,

$$iG^{-1}_{ab}(x,y) = \frac{\delta^2 S_{\mathcal{C}}}{\delta\Phi^*_b(y)\delta\Phi_a(x)}\bigg|_{\Phi=\phi} + K_{ab}(x,y) + \frac{2}{\hbar}\frac{\delta\Gamma_2}{\delta G_{ab}(x,y)}\,. \tag{B.99}$$

Setting $K_{ab}(x,y) = 0$, we see that the inverse propagator $iG^{-1}_{ab}(x,y)$ is the sum of the free propagator and $2/\hbar\delta\Gamma/\delta G_{ab}$ so we can conclude that the term $2/\hbar\delta\Gamma/\delta G_{ab}$ is the self-energy. Since the self-energy has to be a sum of 1PI diagrams, Γ_2 itself must be a sum of 2PI diagrams. We can conclude this because lines in Γ_2 represent full propagators G, such that $\delta\Gamma/\delta G_{ab}$ can be interpreted as cutting a line in the diagrams. To be a 1PI diagram after one line has been cut, the diagram has to stay connected even after cutting two lines. Hence, Γ_2 consists of 2-particle-irreducible diagrams only. So in practice, we will not use Eq. (B.95) to evaluate Γ_2 but calculate it from a sum of 2PI vacuum diagrams instead. In general, it is not possible to sum all 2PI diagrams for a given interaction, such that truncations are in order. Once Γ_2 is known, $\phi_a(x)$ and $G_{ab}(x,y)$ can be evaluated directly from Eqs. (B.84) and (B.85),

$$\frac{\delta\Gamma}{\delta\phi_a(x)} = 0\,, \tag{B.100}$$

$$\frac{\delta\Gamma}{\delta G_{ab}(x,y)} = 0\,, \tag{B.101}$$

where the sources $J_a(x)$ and $K_{ab}(x,y)$ are set to zero. We end this section by mentioning that Eq. (B.94) can also be written as

$$\begin{aligned}\Gamma[\phi_a, G_{ab}] = S_{\mathcal{C}}[\phi,\phi^*] + \frac{\hbar}{2}\int_{xy}^{\mathcal{C}}\bigg[\frac{\delta^2 S_{\mathcal{C}}}{\delta\Phi_b(y)\delta\Phi^*_a(x)}\bigg|_{\Phi=\phi} G_{ba}(y,x) - \frac{i\hbar}{2}\ln\det{}_{\mathcal{C}} G \\ + \Gamma_2[\phi_a, G_{ab}] + \text{const}\,,\end{aligned} \tag{B.102}$$

which is completely equivalent to Eq. (B.94) but it is derived with a different convention for the functional derivative. As $\delta\Gamma/\delta\phi^*_a$ leads to the conjugate equation of ϕ_a, inserting the effective action in Eq. (B.102) into $\delta\Gamma/\delta G_{ba}$ yields the conjugate equation of G_{ab}.

B.3 Nonequilibrium Quantum Field Theory

There are few things that are needed for a nonequilibrium description of quantum field theory. The first is an initial state at an initial time t_0, encoded in density operator ρ_0 whether in a mixed or pure state. The second is time-evolution equations of the relevant observables. In the closed system, the time evolution must be fully determined by the Hamitonian or the action in the case of the path integral

formulation. We have discussed that the CTP formalism is a necessary tool to form a meaningful initial value problem, and therefore, the CTP is required in the nonequilibrium description. However, this solves only the first half of the problem as we have seen that the CTP within the IPI formalism yields only the dynamic equation for mean field $\phi(x)$ or 1-point function. In realistic situations, higher-order n-point functions can and normally will build up during the time evolution. This is where that nPI formalism comes into play. It gives access to dynamic equations of n-point function in a nonperturbative way. As in our study we focus on 2-point functions, the 2PI approach is sufficient.

In Sect. B.2, we have introduced the 2PI formalism in the context of pure states but it can be used equally well with mixed initial states, see Sect. B.1.3. Therefore, the results resembles Eq. (B.64) in the sense that the path integral consists of two parts: an initial part and a dynamics part. We emphasize that in the case that the initial condition has Gaussian form, the initial part can be absorbed into the dynamics part as source terms [48].

Appendix C

Spectral function of free and Bogoliubov particles

In this appendix, we present the means to obtain the spectral functions for both free nonrelativistic and Bogoliubov quasiparticle fields. The field is a complex scalar Bose field Φ, therefore it satisfies the equal-time commutation relation,

$$[\Phi(t,\boldsymbol{x}),\Phi^\dagger(t,\boldsymbol{y})]=\delta^d(\boldsymbol{x}-\boldsymbol{y})\,,\qquad [\Phi(t,\boldsymbol{x}),\Phi(t,\boldsymbol{y})]=[\Phi^\dagger(t,\boldsymbol{x}),\Phi^\dagger(t,\boldsymbol{y})]=0\,. \tag{C.1}$$

The Hamiltonian of free nonrelativistic field reads

$$H=-\int \mathrm{d}^d x\Phi^\dagger(t,\boldsymbol{x})\frac{\nabla^2_{\boldsymbol{x}}}{2m}\Phi(t,\boldsymbol{x})\,, \tag{C.2}$$

where m is a particle mass. The field $\Phi(t,\boldsymbol{x})$ need to satisfy the free Schrödinger's equation which, in turn, yields a free dispersion relation $\varepsilon_{\boldsymbol{p}}=p^2/2m$. Therefore, the Fourier transforms of $\Phi(t,\boldsymbol{x})$ and $\Phi^\dagger(t,\boldsymbol{x})$ become

$$\begin{aligned}\Phi(t,x)&=\int \mathrm{d}^d p e^{i\boldsymbol{p}\cdot\boldsymbol{x}}e^{-i\varepsilon_{\boldsymbol{p}}t}\Phi(\boldsymbol{p})\\&=\int_p e^{-ipx}\,(2\pi)\delta(p_0-\varepsilon_{\boldsymbol{p}})\Phi(\boldsymbol{p})\,, \qquad \text{(C.3)}\\ \Phi^\dagger(t,x)&=\int_p e^{-ipx}\,(2\pi)\delta(p_0+\varepsilon_{\boldsymbol{p}})\Phi^\dagger(-\boldsymbol{p})\,. \qquad \text{(C.4)}\end{aligned}$$

The delta distribution, $\delta(p_0+\varepsilon_{\boldsymbol{p}})$, indicates a constraint from the free Schrödinger equation. It is now straightforward to calculate equal-time commutators in momentum space,

$$[\Phi(\boldsymbol{p}),\Phi^\dagger(\boldsymbol{q})]=(2\pi)^d\delta^d(\boldsymbol{p}-\boldsymbol{q})\,,\qquad [\Phi(\boldsymbol{p}),\Phi(\boldsymbol{q})]=[\Phi^\dagger(\boldsymbol{p}),\Phi^\dagger(\boldsymbol{q})]=0\,. \tag{C.5}$$

Thus, the Hamiltonian in momentum space becomes

$$H=\int\frac{\mathrm{d}^d p}{(2\pi)^d}\,\varepsilon_{\boldsymbol{p}}\Phi^\dagger(\boldsymbol{p})\Phi(\boldsymbol{p})\,. \tag{C.6}$$

This form of the Hamiltonian indicates that the field Φ is a free field. Recalling that $\rho_{ab}(x,y)=i\langle[\Phi_a(x),\Phi_b^\dagger(y)]\rangle$ where $\Phi_1(t,\boldsymbol{x})=\Phi(t,\boldsymbol{x})$ and $\Phi_2(t,\boldsymbol{x})=\Phi^\dagger(t,\boldsymbol{x})$, we can

evaluate the Fourier transform for each element of $\rho_{ab}(x,y)$,

$$\begin{aligned}\rho_{11}(x,y) &= i\langle[\Phi(x),\Phi^\dagger(y)]\rangle \\ &= i\int_{pq}(2\pi)^2\delta(p_0-\varepsilon_{\boldsymbol{p}})\delta(q_0-\varepsilon_{\boldsymbol{q}})e^{-ipx+iqy}\langle[\Phi(\boldsymbol{p}),\Phi^\dagger(\boldsymbol{q})]\rangle \\ &= i\int_{pq}(2\pi)^2\delta(p_0-\varepsilon_{\boldsymbol{p}})\delta(q_0-\varepsilon_{\boldsymbol{q}})e^{-ipx+iqy}(2\pi)^d\delta^d(\boldsymbol{p}-\boldsymbol{q}) \\ &= \int_p e^{-i(x-y)p}(2\pi i)\delta(p_0-\varepsilon_{\boldsymbol{p}})\,, \qquad \text{(C.7)}\\ \rho_{22}(x,y) &= i\langle[\Phi^\dagger(x),\Phi(y)]\rangle \\ &= i\int_{pq}(2\pi)^2\delta(p_0-\varepsilon_{\boldsymbol{p}})\delta(q_0-\varepsilon_{\boldsymbol{q}})e^{ipx-iqy}\langle[\Phi^\dagger(\boldsymbol{p}),\Phi(\boldsymbol{q})]\rangle \\ &= \int_p e^{-i(x-y)p}(-2\pi i)\delta(p_0+\varepsilon_{\boldsymbol{p}})\,, \qquad \text{(C.8)}\end{aligned}$$

where $\rho_{12}(x,y)=\rho_{21}(x,y)=0$ due to the commutation relation (C.5) and thus, give the vanishing Fourier transforms. The elements of $\rho_{ab}(p)$ can be read off from the Fourier transforms of $\rho_{ab}(x,y)$,

$$\rho_{11}(p) = 2\pi i\delta(p_0-\varepsilon_{\boldsymbol{p}}) = \rho_{22}^*(-p) = -\rho_{22}(-p)\,, \qquad \text{(C.9)}$$
$$\rho_{12}(p) = \rho_{21}(p) = 0\,. \qquad \text{(C.10)}$$

We turn to the interacting case, recalling the Hamiltonian in Eq. (2.1),

$$H = \int \mathrm{d}^d x\,\left[-\Phi^\dagger(x)\frac{\nabla^2}{2m}\Phi(x) + \frac{g}{2}\,\Phi^\dagger(x)\Phi^\dagger(x)\Phi(x)\Phi(x)\right]. \qquad \text{(C.11)}$$

The Hamiltonian can be transformed into momentum space[1],

$$\begin{aligned}H = \int \frac{\mathrm{d}^d p}{(2\pi)^d}\Big[&\varepsilon_{\boldsymbol{p}}\Phi^\dagger(\boldsymbol{p},t)\Phi(\boldsymbol{p},t) \\ &+ \frac{g}{2}\int\frac{\mathrm{d}^d k}{(2\pi)^d}\frac{\mathrm{d}^d q}{(2\pi)^d}\Phi^\dagger(\boldsymbol{k}+\boldsymbol{q},t)\Phi^\dagger(\boldsymbol{p}-\boldsymbol{q},t)\Phi(\boldsymbol{k},t)\Phi(\boldsymbol{p},t)\Big]\,, \qquad \text{(C.12)}\end{aligned}$$

which Bogoliubov mean-field theory can now be applied to. In the condensate phase where there are sufficiently large numbers of particles in the zero-mode, the zero-mode operator $\Phi(\boldsymbol{p}=0,t)$ can be replaced by a complex-valued number ϕ_0 where the condensate density $\rho_0\sim\phi_0^2$ is of the same order as the total density ρ_{tot}. The large occupation of the zero mode can be used to approximate the Hamiltonian such that there are only quadratic terms in the Hamiltonian [68],

$$\begin{aligned}H =& \frac{g\rho_{\mathrm{tot}}^2}{2} + \int_{\boldsymbol{p}\neq 0}\frac{\mathrm{d}^d p}{(2\pi)^d}\Big[\big(\varepsilon_{\boldsymbol{p}}+g\rho_0\big)\Phi^\dagger(\boldsymbol{p},t)\Phi(\boldsymbol{p},t) \\ &+ \frac{g\rho_0}{2}\big(\Phi^\dagger(-\boldsymbol{p},t)\Phi^\dagger(\boldsymbol{p},t)+\Phi(-\boldsymbol{p},t)\Phi(\boldsymbol{p},t)\big)\Big]\,. \qquad \text{(C.13)}\end{aligned}$$

[1] Notice that the integral in Eq. (2.1) sums over the spatial variable $\boldsymbol{x}$, and thus, in Eq. (C.12) only the spatial dependence is Fourier transformed, leaving $x_0=t$ in the momentum dependent field operator $\Phi(\boldsymbol{p},t)$.

The Hamiltonian in Eq. (C.13) can be diagonalized by the Bogoliubov canonical transformation to another set of bosonic operators $\Phi_Q(\boldsymbol{p},t)$. The transformation reads

$$\Phi(\boldsymbol{p},t) = u_{\boldsymbol{p}}\Phi_Q(\boldsymbol{p},t) + v_{\boldsymbol{p}}\Phi_Q^\dagger(-\boldsymbol{p},t)\,, \tag{C.14}$$

with a constraint $u_{\boldsymbol{p}}^2 - v_{\boldsymbol{p}}^2 = 1$ to preserve the canonical equal-time commutation relations,

$$[\Phi_Q(\boldsymbol{p},t), \Phi_Q^\dagger(\boldsymbol{q},t)] = (2\pi)^d\,\delta^d(\boldsymbol{p}-\boldsymbol{q})\,, \tag{C.15}$$

$$[\Phi_Q(\boldsymbol{p},t), \Phi_Q(\boldsymbol{q},t)] = [\Phi_Q^\dagger(\boldsymbol{p},t), \Phi_Q^\dagger(\boldsymbol{q},t)] = 0\,. \tag{C.16}$$

The commutation relation is necessary for reordering the fields such that the $\Phi_Q^\dagger(\boldsymbol{p},t)$ stays on the left of $\Phi(\boldsymbol{p},t)$, for example[2]

$$\Phi_Q(\boldsymbol{p},t)\Phi_Q^\dagger(\boldsymbol{q},t) = \Phi_Q^\dagger(\boldsymbol{q},t)\Phi_Q(\boldsymbol{p},t) + (2\pi)^d\,\delta^d(\boldsymbol{p}-\boldsymbol{q})\,. \tag{C.17}$$

The Hamiltonian can be diagonalized in terms of the quasiparticle operators $\Phi_Q(\boldsymbol{p},t)$ and $\Phi_Q^\dagger(\boldsymbol{p},t)$ [68]

$$H = C_0 + \int_{\boldsymbol{p}} \frac{\mathrm{d}^d p}{(2\pi)^d}\,\omega_{\boldsymbol{p}}\Big[\Phi_Q^\dagger(\boldsymbol{p},t)\Phi_Q(\boldsymbol{p},t) + \frac{1}{2}\Big]\,, \tag{C.18}$$

where C_0 is a constant, depending on the total density. The Hamiltonian (C.18) can be interpreted as the Hamiltonian of free quasiparticles associated with Φ_Q and $\Phi_Q^\dagger$ operators whose energy spectrum is given by the Bogoliubov dispersion $\omega(\boldsymbol{p})$,

$$\omega_{\boldsymbol{p}} = \Big[\varepsilon_{\boldsymbol{p}}\Big(\varepsilon_{\boldsymbol{p}} + 2g\rho_0\Big)\Big]^{1/2}\,. \tag{C.19}$$

The diagonalization requires a specific form of Bogoliubov mode functions $u_{\boldsymbol{p}}$ and $v_{\boldsymbol{p}}$,

$$u_{\boldsymbol{p}} = \left(\frac{\varepsilon_{\boldsymbol{p}} + g\rho_0 + \omega_{\boldsymbol{p}}}{2\omega_{\boldsymbol{p}}}\right)^{1/2}\,, \qquad v_{\boldsymbol{p}} = \left(\frac{\varepsilon_{\boldsymbol{p}} + g\rho_0 - \omega_{\boldsymbol{p}}}{2\omega_{\boldsymbol{p}}}\right)^{1/2}\,. \tag{C.20}$$

The Bogoliubov transformation allows us to write down the Fourier transforms of $\Phi(x)$ in terms of Φ_Q and $\Phi_Q^\dagger$, instead of $\Phi(\boldsymbol{p})$,

$$\begin{aligned}\Phi(t,\boldsymbol{x}) &= \int \frac{\mathrm{d}^d p}{(2\pi)^d} e^{i\boldsymbol{p}\cdot\boldsymbol{x}}\Big[u_{\boldsymbol{p}}e^{-i\omega_{\boldsymbol{p}}t}\Phi_Q(\boldsymbol{p}) + v_{\boldsymbol{p}}e^{i\omega_{\boldsymbol{p}}t}\Phi_Q^\dagger(-\boldsymbol{p})\Big] \\ &= \int_p e^{-ipx}(2\pi)\Big[\delta(p_0-\omega_{\boldsymbol{p}})u_{\boldsymbol{p}}\Phi_Q(\boldsymbol{p}) + \delta(p_0+\omega_{\boldsymbol{p}})v_{\boldsymbol{p}}\Phi_Q^\dagger(-\boldsymbol{p})\Big]\,, \qquad \text{(C.21)}\\ \Phi^\dagger(t,\boldsymbol{x}) &= \int_p e^{-ipx}(2\pi)\Big[\delta(p_0+\omega_{\boldsymbol{p}})u_{\boldsymbol{p}}\Phi_Q^\dagger(-\boldsymbol{p}) + \delta(p_0-\omega_{\boldsymbol{p}})v_{\boldsymbol{p}}\Phi_Q(\boldsymbol{p})\Big]\,, \qquad \text{(C.22)}\end{aligned}$$

[2] In the case that $\boldsymbol{p} = \boldsymbol{q}$, the relation (C.17) might not seem well-defined because of $\delta^d(0)$. However, we can argue from the Fourier transform of $\delta^d(\boldsymbol{p})$ that $\delta^d(0)$ is actually the momentum-space volume, thus, by rescaling Eq. (C.17) with the momentum-space volume, we obtain $\Phi_Q(\boldsymbol{p},t)\Phi_Q^\dagger(\boldsymbol{q},t) = \Phi_Q^\dagger(\boldsymbol{q},t)\Phi_Q(\boldsymbol{p},t) + 1$ where the field operators are now a rescaled version of the original ones.

where we have used $u(-\boldsymbol{p}) = u(\boldsymbol{p})$, $u^*(\boldsymbol{p}) = u(\boldsymbol{p})$ and similarly for $v(\boldsymbol{p})$. The matrix elements of $\rho_{ab}(x,y)$ for the Hamiltonian (C.11), in the Bogoliubov mean-field approximation, are evaluated from the commutators of $\Phi(t,\boldsymbol{x})$ and $\Phi^\dagger(t,\boldsymbol{x})$, for example the element $\rho_{11}(x,y)$,

$$\begin{aligned}
\rho_{11}(x,y) &= i\langle[\Phi(x),\Phi^\dagger(y)]\rangle \\
&= i\int_{pq} e^{-i(px-qy)}(2\pi)^2\Big\langle\Big[\delta(p_0-\omega_{\boldsymbol{p}})u_{\boldsymbol{p}}\Phi_Q(\boldsymbol{p})+\delta(p_0+\omega_{\boldsymbol{p}})v_{\boldsymbol{p}}\Phi_Q^\dagger(-\boldsymbol{p}) \\
&\qquad\qquad , \delta(q_0-\omega_{\boldsymbol{q}})v_{\boldsymbol{q}}\Phi_Q(\boldsymbol{p})+\delta(q_0+\omega_{\boldsymbol{q}})u_{\boldsymbol{q}}\Phi_Q^\dagger(-\boldsymbol{p})\Big]\Big\rangle \\
&= i\int_{pq} e^{-i(px-qy)}(2\pi)^2\Big\{\delta(p_0-\omega_{\boldsymbol{p}})\delta(q_0+\omega_{\boldsymbol{q}})u_{\boldsymbol{p}}u_{\boldsymbol{q}}(2\pi)^d\delta^d(\boldsymbol{p}+\boldsymbol{q}) \\
&\qquad\qquad -\delta(p_0+\omega_{\boldsymbol{p}})\delta(q_0-\omega_{\boldsymbol{q}})v_{\boldsymbol{p}}v_{\boldsymbol{q}}(2\pi)^d\delta^d(-\boldsymbol{p}-\boldsymbol{q})\Big\} \\
&= \int_p e^{-i(x-y)p}(2\pi i)\Big[\delta(p_0-\omega_{\boldsymbol{p}})u_{\boldsymbol{p}}^2-\delta(p_0+\omega_{\boldsymbol{p}})v_{\boldsymbol{p}}^2\Big]\,. \qquad \text{(C.23)}
\end{aligned}$$

The other elements can be found in the similar ways,

$$\begin{aligned}
\rho_{12}(x,y) &= i\langle[\Phi(x),\Phi(y)]\rangle \\
&= \int_p e^{-i(x-y)p}(2\pi i)u_{\boldsymbol{p}}v_{\boldsymbol{p}}\Big[\delta(p_0-\omega_{\boldsymbol{p}})-\delta(p_0+\omega_{\boldsymbol{p}})\Big]\,, \qquad \text{(C.24)} \\
\rho_{21}(x,y) &= i\langle[\Phi^\dagger(x),\Phi^\dagger(y)]\rangle \\
&= \int_p e^{-i(x-y)p}(2\pi i)u_{\boldsymbol{p}}v_{\boldsymbol{p}}\Big[\delta(p_0-\omega_{\boldsymbol{p}})-\delta(p_0+\omega_{\boldsymbol{p}})\Big]\,, \qquad \text{(C.25)} \\
\rho_{22}(x,y) &= i\langle[\Phi^\dagger(x),\Phi(y)]\rangle \\
&= \int_p e^{-i(x-y)p}(2\pi i)\Big[\delta(p_0-\omega_{\boldsymbol{p}})v_{\boldsymbol{p}}^2-\delta(p_0+\omega_{\boldsymbol{p}})u_{\boldsymbol{p}}^2\Big]\,. \qquad \text{(C.26)}
\end{aligned}$$

We read off the Fourier transforms of each element to determine the elements of $\rho_{ab}(p)$,

$$\begin{aligned}
\rho_{11}(p) &= (2\pi i)\Big[\delta(p_0-\varepsilon_{\boldsymbol{p}})u_{\boldsymbol{p}}^2-\delta(p_0+\varepsilon_{\boldsymbol{p}})v_{\boldsymbol{p}}^2\Big] \\
&= -\rho_{22}(-p) = \rho_{22}^*(-p)\,, \qquad \text{(C.27)} \\
\rho_{12}(p) &= (2\pi i)u_{\boldsymbol{p}}v_{\boldsymbol{p}}\Big[\delta(p_0-\varepsilon_{\boldsymbol{p}})-\delta(p_0+\varepsilon_{\boldsymbol{p}})\Big] \\
&= -\rho_{21}(-p) = \rho_{21}^*(-p) = \rho_{21}(p)\,. \qquad \text{(C.28)}
\end{aligned}$$

Appendix D

Evaluation of integrals

This appendix is going to evaluate the integrals that are needed in Ch. 4 and Ch. 5.

D.1 Integrals involving the many-body coupling

The first integral is in Eq. (4.143). The integral variable y can be rescaled such that the branch points are at ± 1. For a positive x, the integral becomes

$$\tilde{\pi}_\kappa(x) = \frac{2}{\sqrt{\pi}} \frac{\Gamma(\frac{\kappa}{2})}{\Gamma(\frac{\kappa-3}{2})} \Big[x^2 \int_0^\infty \mathrm{d}z \frac{z}{(1+z^2\,x^2)^{\kappa/2}} \ln\Big(\frac{1+z+i\epsilon}{1-z+i\epsilon}\Big)\Big], \tag{D.1}$$

where $z = y/x$. In the case of negative x, it becomes

$$\tilde{\pi}_\kappa(x) = \frac{2}{\sqrt{\pi}} \frac{\Gamma(\frac{\kappa}{2})}{\Gamma(\frac{\kappa-3}{2})} \Big[-|x|^2 \int_0^\infty \mathrm{d}z \frac{z}{(1+z^2\,x^2)^{\kappa/2}} \ln\Big(\frac{1+z-i\epsilon}{1-z-i\epsilon}\Big)\Big], \tag{D.2}$$

where $z = y/|x|$. Apart from the minus sign of the small imaginary part and prefactor, both integrals are the same. If $\kappa > 2$, it is possible to perform the integration by parts and thus, get rid of logarithms in the integrand,

$$\begin{aligned}
&\int_0^\infty \mathrm{d}z \frac{z\,x^2}{(1+z^2\,x^2)^{\kappa/2}} \Big(\ln(1+z\pm i\epsilon) - \ln(1-z\pm i\epsilon)\Big) \\
&\quad = \mathrm{d}\Big(\frac{(1+z^2\,x^2)^{1-\kappa/2}}{2-\kappa} \ln(1+z\pm i\epsilon)\Big)\Big|_0^\infty - \mathrm{d}\Big(\frac{(1+z^2\,x^2)^{(1-\kappa/2)}}{2-\kappa} \ln(1-z\pm i\epsilon)\Big)\Big|_0^\infty \\
&\qquad - \int_0^\infty \mathrm{d}z \frac{(1+z^2\,x^2)^{1-\kappa/2}}{2-\kappa} \frac{1}{1+z\pm i\epsilon} - \int_0^\infty \mathrm{d}z \frac{(1+z^2\,x^2)^{1-\kappa/2}}{2-\kappa} \frac{1}{1-z\pm i\epsilon} \\
&\quad = \int_0^\infty \mathrm{d}z \frac{(1+z^2\,x^2)^{1-\kappa/2}}{\kappa-2} \Big(\frac{2(1\pm i\epsilon)}{(1\pm i\epsilon)^2 - z^2}\Big) \\
&\quad = \int_0^\infty \mathrm{d}z^2 \frac{z^{-1}}{\kappa-2} (1+z^2\,x^2)^{1-\kappa/2} \Big(1 - \frac{z^2}{(1\pm i\epsilon)^2}\Big)^{-1} \\
&\quad = \int_0^\infty \mathrm{d}y \frac{y^{-1/2}}{(\kappa-2)|x|} (1+y)^{1-\kappa/2} \Big(1 - \frac{y}{(1\pm i\epsilon)^2\,x^2}\Big)^{-1} \\
&\quad = \frac{1}{|x|} \frac{\Gamma(\frac{1}{2})\Gamma(\frac{\kappa-1}{2})}{(\kappa-2)\Gamma(\frac{\kappa}{2})} {}_2F_1\Big(1, \frac{1}{2}; \frac{\kappa}{2}; 1 + [(1\pm i\epsilon)x]^{-2}\Big),
\end{aligned} \tag{D.3}$$

where we have used

$$\frac{\Gamma(c-b)\Gamma(b)}{\Gamma(c)}{}_2F_1(a,b;c;1-z)=\int_0^\infty \mathrm{d}s s^{b-1}(1+s)^{a-c}(1+sz)^{-a}, \tag{D.4}$$

with the conditions $\mathrm{Re}(c)>\mathrm{Re}(b)>0$ and $|\arg(z)|<\pi$ [114]. The aboved result in (D.3) is valid only for $\kappa>2$ when the boundary terms vanish. Substituting Eq. (D.3) into Eq. (D.1) (or Eq. (D.2)), we obtain

$$\tilde{\pi}_\kappa(x)=\frac{1}{x}\frac{\kappa-3}{\kappa-2}{}_2F_1\Big(1,\frac{1}{2};\frac{\kappa}{2};1+[(1\pm i\epsilon)x]^{-2}\Big), \tag{D.5}$$

as it has been presented in Eq. (4.143). The sign of the imaginary part is needed to distinguish the results of positive and negative x.

Another integral is in Eq. (4.157), for the Bogoliubov quasiparticle case. The strategy is similar to what we have done in the free particle case. Rescaling the integration variable such that the branch points are at ±1, for positive values of the external variable x, one gets

$$\widetilde{\Pi}'_f(x)=\left(\frac{\Lambda}{p_\Lambda}\right)^\kappa\left[x\int_0^\infty \mathrm{d}z\,(1+z\,x)^{-\kappa}\,\ln\left(\frac{1+z+i\epsilon}{1-z+i\epsilon}\right)\right], \tag{D.6}$$

where $z=y/x$ and for negative values of x

$$\widetilde{\Pi}'_f(x)=\left(\frac{\Lambda}{p_\Lambda}\right)^\kappa\left[-|x|\int_0^\infty \mathrm{d}z\,(1+z\,|x|)^{-\kappa}\,\ln\left(\frac{1-z-i\epsilon}{1+z-i\epsilon}\right)\right], \tag{D.7}$$

where $z=y/|x|$. To do the integration by parts to get rid of logarithms, we now need $\kappa>1$

$$\begin{aligned}
&\int_0^\infty \mathrm{d}z\,|x|\,(1+z\,|x|)^{-\kappa}\Big((\ln(1+z\pm i\epsilon)-\ln(1-z\pm i\epsilon)\Big)\\
&\quad=\mathrm{d}\Big(\frac{(1+z\,|x|)^{1-\kappa}}{(1-\kappa)}\ln(1+z\pm i\epsilon)\Big)\Big|_0^\infty-\mathrm{d}\Big(\frac{(1+z\,|x|)^{1-\kappa}}{(1-\kappa)}\ln(1-z\pm i\epsilon)\Big)\Big|_0^\infty\\
&\qquad-\int_0^\infty \mathrm{d}z\frac{(1+z\,|x|)^{1-\kappa}}{(1-\kappa)}(1+z\pm i\epsilon)^{-1}-\int_0^\infty \mathrm{d}z\frac{(1+z\,|x|)^{1-\kappa}}{(1-\kappa)}(1-z\pm i\epsilon)^{-1}\\
&\quad=\frac{1}{(\kappa-1)|x|}\Big[\int_0^\infty dy(1+y)^{1-\kappa}\Big(1+\frac{y}{(1\pm i\epsilon)|x|}\Big)^{-1}\\
&\qquad\qquad+\int_0^\infty \mathrm{d}y(1+y)^{1-\kappa}\Big(1-\frac{y}{(1\pm i\epsilon)|x|}\Big)^{-1}\Big]\\
&\quad=\frac{1}{|x|}\frac{\Gamma(1)\Gamma(\kappa-1)}{(\kappa-1)\Gamma(\kappa)}\Big({}_2F_1\Big(1,1;\kappa;1-[(1\pm i\epsilon)|x|]^{-1}\Big)\\
&\qquad\qquad+{}_2F_1\Big(1,1;\kappa;1+[(1\pm i\epsilon)|x|]^{-1}\Big)\Big),
\end{aligned} \tag{D.8}$$

where Eq. (D.4) has been used to turn the integral into a Guassian hypergeometric function. Note that the result in Eq. (D.8) is only valid for $\kappa>1$. Inserting

Eq. (D.8) back into Eq. (D.6) (or Eq. (D.7)), we obtain the results that we presented in Eq. (4.157):

$$\widetilde{\Pi}'_f(x) = \left(\frac{\Lambda}{p_\Lambda}\right)^\kappa \frac{1}{(\kappa-1)^2 x}\Big({}_2F_1\Big(1,1;\kappa;1-[(1\pm i\epsilon)x]^{-1}\Big) + {}_2F_1\Big(1,1;\kappa;1+[(1\pm i\epsilon)x]^{-1}\Big)\Big)\,. \tag{D.9}$$

Again the results for positive and negative x are distinguished by the sign of the small imaginary part.

D.2 Evaluation of the scattering integral

In this section, we will evaluate explicitly six different integrals which contribute to the scattering integrals. Two integrals I_1^{free} and I_2^{free} belong to the scattering integral of free particles and four integrals $I_1^{\text{bog}}, I_2^{\text{bog}}, I_3^{\text{bog}}$ and I_4^{bog} contribute to the scattering integral of Bogoliubov quasiparticles.

D.2.1 Evaluation of I_1^{free} and I_2^{free}

Due to the structure of the delta function $\delta(p^2+k^2-q^2-|\boldsymbol{p}-\boldsymbol{r}'|^2)$ that appears in both integrals, it is more convenient to introduce new variables u and v,

$$u = \frac{1}{\sqrt{2}}(k^2+q^2)\,, \qquad\qquad v = \frac{1}{\sqrt{2}}(k^2-q^2)\,, \tag{D.10}$$

such that the delta function depends on a single variable i.e. v. The integral I_1^{free} in (u,v) variables becomes

$$I_1^{\text{free}}(\boldsymbol{p},\boldsymbol{r}') = \frac{1}{4}\int_{-\infty}^{\infty}\mathrm{d}v\int_{u(v)}^{\infty}\mathrm{d}u\,\delta(p^2-|\boldsymbol{p}-\boldsymbol{r}'|^2+\sqrt{2}v) \times\left(\frac{2^{\kappa/2}}{(\sqrt{2}(u-v)+2p_\Lambda^2)^{\kappa/2}}-\frac{2^{\kappa/2}}{(\sqrt{2}(u+v)+2p_\Lambda^2)^{\kappa/2}}\right), \tag{D.11}$$

where $u(v)=\frac{2v^2+r'^4}{2\sqrt{2}r'^2}$. We intentionally perform the integration over u first because the delta function is in v. The integration domain is now bound by a parabola in these (u,v) variables. For an upper bound, $q=k+r'$ yeilds

$$\begin{aligned} q^2 &= k^2+r'^2+2kr' \\ \Rightarrow q^2-k^2 &= r'^2+2r'k \\ \Rightarrow -\sqrt{2}v &= r'^2+2r'\sqrt{\frac{u+v}{\sqrt{2}}} \\ \Rightarrow (-\sqrt{2}v-r'^2)^2 &= (\sqrt{2}v+r'^2)^2 = 4r'^2\frac{u+v}{\sqrt{2}}\,, \end{aligned} \tag{D.12}$$

and for a lower bound, $q = |k - r']$ gives

$$\begin{aligned} q^2 &= k^2 + r'^2 - 2kr \\ \Rightarrow (\sqrt{2}v - r'^2)^2 &= 4r'^2 \frac{u+v}{\sqrt{2}}\,, \end{aligned} \tag{D.13}$$

which is exactly the same parabola as we obtained from the upper limit. By expanding and rearranging the terms, we have a parabola $u(v)$ that will be used for the lower limit of the u-integration. The integration over u is now straightforward,

$$\begin{aligned} I_1^{\text{free}}(\boldsymbol{p}, \boldsymbol{r}') &= \frac{2^{\kappa/2-1}}{4} \int_{-\infty}^{\infty} \mathrm{d}(\sqrt{2}v)\, \delta(p^2 - |\boldsymbol{p} - \boldsymbol{r}'|^2 + \sqrt{2}v) \\ &\quad \times \frac{1}{1-\kappa/2} \Big[\Big(\sqrt{2}(u(v) + v) + 2p_\Lambda^2 \Big)^{1-\kappa/2} - \Big(\sqrt{2}(u(v) - v) + 2p_\Lambda^2 \Big)^{1-\kappa/2} \Big] \\ &= \frac{2^{\kappa/2}}{4(\kappa-2)} \int_{-\infty}^{\infty} \mathrm{d}(\sqrt{2}v)\, \delta(p^2 - |\boldsymbol{p} - \boldsymbol{r}'|^2 + \sqrt{2}v) \\ &\quad \times \Big[\Big(\frac{(\sqrt{2}v - r'^2)^2}{2r'^2} + 2p_\Lambda^2 \Big)^{1-\kappa/2} - \Big(\frac{(\sqrt{2}v + r'^2)^2}{2r'^2} + 2p_\Lambda^2 \Big)^{1-\kappa/2} \Big] \\ &= \frac{2^{\kappa/2}}{4(\kappa-2)} \Big[\Big(\frac{(p^2 - |\boldsymbol{p} - \boldsymbol{r}'|^2 + r'^2)^2}{2r'^2} + 2p_\Lambda^2 \Big)^{1-\kappa/2} \\ &\qquad - \Big(\frac{(p^2 - |\boldsymbol{p} - \boldsymbol{r}'|^2 - r'^2)^2}{2r'^2} + 2p_\Lambda^2 \Big)^{1-\kappa/2} \Big]\,, \end{aligned} \tag{D.14}$$

$$\begin{aligned} I_1^{\text{free}}(\boldsymbol{p}, \boldsymbol{p} - \boldsymbol{r}) &= \frac{2^{\kappa/2}}{4(\kappa-2)} \Big[\Big(\frac{(p^2 - r^2 + |\boldsymbol{p} - \boldsymbol{r}|^2)^2}{2|\boldsymbol{p} - \boldsymbol{r}|^2} + 2p_\Lambda^2 \Big)^{1-\kappa/2} \\ &\qquad - \Big(\frac{(p^2 - r^2 - |\boldsymbol{p} - \boldsymbol{r}|^2)^2}{2|\boldsymbol{p} - \boldsymbol{r}|^2} + 2p_\Lambda^2 \Big)^{1-\kappa/2} \Big]\,, \end{aligned} \tag{D.15}$$

where we replaced $\boldsymbol{r}'$ by $|\boldsymbol{p} - \boldsymbol{r}|$. The same variable transformation is also needed for I_2^{free}. The integral I_2^{free} in (u, v) variables becomes

$$\begin{aligned} I_2^{\text{free}}(\boldsymbol{p}, \boldsymbol{r}') &= \frac{1}{4} \int_{-\infty}^{\infty} \mathrm{d}v \int_{u(v)}^{\infty} \mathrm{d}u\, \delta(p^2 - |\boldsymbol{p} - \boldsymbol{r}'|^2 + \sqrt{2}v) \\ &\qquad \times \Big[\Big(\frac{u - v}{\sqrt{2}} + p_\Lambda^2 \Big) \Big(\frac{u + v}{\sqrt{2}} + p_\Lambda^2 \Big) \Big]^{-\kappa/2} \\ &= \frac{2^{\kappa-1}}{4} \int_{-\infty}^{\infty} \mathrm{d}(\sqrt{2}v)\, \delta(p^2 - |\boldsymbol{p} - \boldsymbol{r}'|^2 + \sqrt{2}v) \\ &\qquad \times \int_{\sqrt{2}u(v)}^{\infty} \mathrm{d}(\sqrt{2}u) \Big[(\sqrt{2}u + 2p_\Lambda^2)^2 - 2v^2 \Big]^{-\kappa/2} \\ &= \frac{2^{\kappa-1}}{4} \int_{-\infty}^{\infty} \mathrm{d}(\sqrt{2}v)\, \delta(p^2 - |\boldsymbol{p} - \boldsymbol{r}'|^2 + \sqrt{2}v) \\ &\qquad \times \frac{(u(v) + 2p_\Lambda^2)^{1-\kappa}}{\kappa - 1} {}_2F_1\Big(\frac{\kappa}{2}, \frac{\kappa-1}{2}; \frac{\kappa+1}{2}; \Big(\frac{\sqrt{2}v}{u(v) + 2p_\Lambda^2} \Big)^2 \Big)\,. \end{aligned} \tag{D.16}$$

The last equality needs to evaluate the following integral,

$$\int_A^\infty \mathrm{d}x(x^2-y^2)^{-\alpha} \tag{D.17}$$

where A is positive which is the case here since $A=\sqrt{2}u(v)+2p_\Lambda^2$. This integral can be written in terms of a hypergeometric function,

$$\begin{aligned}
\int_A^\infty \mathrm{d}x(x^2-y^2)^{-\alpha} &= A^{1-2\alpha}\int_1^\infty \mathrm{d}x'(x'^2-\frac{y^2}{A^2})^{-\alpha} && ;x'=\frac{x}{A}\\
&= A^{1-2\alpha}\int_1^\infty \mathrm{d}x'^2\frac{1}{2x'}(x'^2-\frac{y^2}{A^2})^{-\alpha}\\
&= \frac{A^{1-2\alpha}}{2}\int_1^\infty \mathrm{d}x''x''^{-1/2}(x''-\frac{y^2}{A^2})^{-\alpha} && ;x''=x'^2\\
&= \frac{A^{1-2\alpha}}{2\alpha-1}{}_2F_1(\alpha,\alpha-\frac{1}{2};\alpha+\frac{1}{2};\frac{y^2}{A^2})\,,
\end{aligned} \tag{D.18}$$

where we used the following integral representations of the hypergeometric function [115],

$${}_2F_1(a,b;c;z^{-1}) = \frac{\Gamma(c)}{\Gamma(b)\Gamma(c-b)}\int_1^\infty \mathrm{d}s(s-1)^{c-b-1}s^{a-c}(s-z^{-1})^{-a}\,. \tag{D.19}$$

Integrating the v variable, I_2^{free} becomes

$$\begin{aligned}
I_2^{\mathrm{free}}(\boldsymbol{p},\boldsymbol{p}-\boldsymbol{r}) = \frac{2^{\kappa-1}}{4(\kappa-1)}&\Big(\frac{(p^2-r^2)^2+|\boldsymbol{p}-\boldsymbol{r}|^4}{2|\boldsymbol{p}-\boldsymbol{r}|^2}+2p_\Lambda^2\Big)^{1-\kappa}\\
&\times {}_2F_1\Big(\frac{\kappa}{2},\frac{\kappa-1}{2};\frac{\kappa+1}{2};\Big(\frac{p^2-r^2}{\frac{(p^2-r^2)^2+|\boldsymbol{p}-\boldsymbol{r}|^4}{2|\boldsymbol{p}-\boldsymbol{r}|^2}+2p_\Lambda^2}\Big)^2\Big)\,.
\end{aligned} \tag{D.20}$$

D.2.2 Evaluation of I_1^{bog}, I_2^{bog}, I_3^{bog} and I_4^{bog}

The procedure is similar to the evaluation in the free particle case. A set of variables is needed such that the integration over the delta function can be done last. Due to the different structure of delta functions that appear in I_1^{bog}, I_2^{bog} and I_3^{bog}, I_4^{bog}, the details are slightly different.

Evaluation I_1^{bog} and I_2^{bog}

The integration variables (u,v) are defined by

$$u=\frac{1}{\sqrt{2}}(k+q)\,, \qquad v=\frac{1}{\sqrt{2}}(k-q)\,, \tag{D.21}$$

and the delta function again depends on only v with a similar structure as compared to the free particle case. In this set of variables, it is equivalent to rotate the axes

of (k, q) clockwise by $\pi/4$. Therefore, the integration domain is unchanged. The integral I_1^{bog} becomes

$$\begin{aligned} I_1^{\mathrm{bog}}(\boldsymbol{p}, \boldsymbol{r}') &= \int_{-r'/\sqrt{2}}^{r'/\sqrt{2}} \mathrm{d}v \int_{r'/\sqrt{2}}^{\infty} \mathrm{d}u\, \delta(p - |\boldsymbol{p} - \boldsymbol{r}'| + \sqrt{2}v) \\ &\qquad \times \left[\left(\frac{u - v}{\sqrt{2}} + p_\Lambda \right)^{-\kappa} - \left(\frac{u + v}{\sqrt{2}} + p_\Lambda \right)^{-\kappa} \right] \\ &= \frac{2^{\kappa-1}}{1 - \kappa} \int_{-r'}^{r'} \mathrm{d}(\sqrt{2}v)\, \delta(p - |\boldsymbol{p} - \boldsymbol{r}'| + \sqrt{2}v) \\ &\qquad \times \left[\left(r' + \sqrt{2}v + 2p_\Lambda \right)^{1-\kappa} - \left(r' - \sqrt{2}v + 2p_\Lambda \right)^{1-\kappa} \right] \\ &= \frac{2^{\kappa-1}}{\kappa - 1} \left[\left(r' + p - |\boldsymbol{p} - \boldsymbol{r}'| + 2p_\Lambda \right)^{1-\kappa} - \left(r' - p + |\boldsymbol{p} - \boldsymbol{r}'| + 2p_\Lambda \right)^{1-\kappa} \right] \\ &\qquad \times \Theta(r' - \left| p - |\boldsymbol{p} - \boldsymbol{r}'| \right|), \end{aligned} \tag{D.22}$$

$$I_1^{\mathrm{bog}}(\boldsymbol{p}, \boldsymbol{p} - \boldsymbol{r}) = \frac{2^{\kappa-1}}{\kappa - 1} \left[\left(|\boldsymbol{p} - \boldsymbol{r}| + p - r + 2p_\Lambda \right)^{1-\kappa} - \left(|\boldsymbol{p} - \boldsymbol{r}| - p + r + 2p_\Lambda \right)^{1-\kappa} \right]. \tag{D.23}$$

The Heaviside function appears because the integration over $\mathrm{d}v$ is not done on the entire real axis, and the integral is nonzero only if $-r' < p - |\boldsymbol{p} - \boldsymbol{r}'| < r'$. However, this constraint is always fulfilled as can be seen by substituting $\boldsymbol{r}' = \boldsymbol{p} - \boldsymbol{r}$ which gives $|\boldsymbol{p} - \boldsymbol{r}| - |p - r| \geq 0$. The integral I_2^{bog} can also be done by changing the variables to (u, v),

$$\begin{aligned} I_2^{\mathrm{bog}}(\boldsymbol{p}, \boldsymbol{r}') &= \int_{-r'/\sqrt{2}}^{r'/\sqrt{2}} \mathrm{d}v \int_{r'/\sqrt{2}}^{\infty} \mathrm{d}u\, \delta(p - |\boldsymbol{p} - \boldsymbol{r}'| + \sqrt{2}v) \\ &\qquad \times \left[\left(\frac{u - v}{\sqrt{2}} + p_\Lambda \right) \left(\frac{u + v}{\sqrt{2}} + p_\Lambda \right) \right]^{-\kappa} \\ &= 2^{2\kappa-1} \int_{-r'}^{r'} \mathrm{d}(\sqrt{2}v)\, \delta(p - |\boldsymbol{p} - \boldsymbol{r}'| + \sqrt{2}v) \\ &\qquad \times \int_{r'}^{\infty} \mathrm{d}(\sqrt{2}u) \left[(\sqrt{2}u + 2p_\Lambda)^2 - 2v^2 \right]^{-\kappa} \\ &= 2^{2\kappa-1} \int_{-r'}^{r'} \mathrm{d}(\sqrt{2}v)\, \delta(p - |\boldsymbol{p} - \boldsymbol{r}'| + \sqrt{2}v) \\ &\qquad \times \frac{(r' + 2p_\Lambda)^{2\kappa-1}}{2\kappa - 1} {}_2F_1\left(\kappa, \kappa - \frac{1}{2}, \kappa + \frac{1}{2}; \left(\frac{\sqrt{2}v}{r' + 2p_\Lambda} \right)^2 \right) \\ &= \frac{2^{2\kappa-1}}{2\kappa - 1} (r' + 2p_\Lambda)^{2\kappa-1} {}_2F_1\left(\kappa, \kappa - \frac{1}{2}, \kappa + \frac{1}{2}; \left(\frac{p - |\boldsymbol{p} - \boldsymbol{r}'|}{r' + 2p_\Lambda} \right)^2 \right) \\ &\qquad \times \Theta(r' - \left| p - |\boldsymbol{p} - \boldsymbol{r}'| \right|), \end{aligned} \tag{D.24}$$

$$I_2^{\mathrm{bog}}(\boldsymbol{p}, \boldsymbol{p} - \boldsymbol{r}) = \frac{2^{2\kappa-1}}{2\kappa - 1} (|\boldsymbol{p} - \boldsymbol{r}| + 2p_\Lambda)^{2\kappa-1} {}_2F_1\left(\kappa, \kappa - \frac{1}{2}, \kappa + \frac{1}{2}; \left(\frac{p - r}{|\boldsymbol{p} - \boldsymbol{r}| + 2p_\Lambda} \right)^2 \right), \tag{D.25}$$

where we use the result in Eq. (D.18) to integrate over du and the Heaviside function is treated the same way we did for $I_1^{\rm bog}$. The results for $I_1^{\rm bog}$ and $I_2^{\rm bog}$ are similar to $I_1^{\rm free}$ and $I_2^{\rm free}$ because of the similar energy conservation (delta function) and the similar structures of the many-body couplings (arguments in the many-body coupling function).

Evaluation $I_3^{\rm bog}$ and $I_4^{\rm bog}$

The strategy is still the same, we change the integration variables to (u, v) defined by,

$$u = \frac{1}{2}(r+q)\,, \qquad\qquad v = \frac{1}{2}(r-q)\,. \tag{D.26}$$

The integral $I_3^{\rm bog}$ can be evaluated in (u, v) variables,

$$\begin{aligned}
I_3^{\rm bog}(\boldsymbol{p}, \boldsymbol{k}') &= \int_{k'/\sqrt{2}}^{\infty} \mathrm{d}u \int_{-k'/\sqrt{2}}^{k'/\sqrt{2}} \mathrm{d}v\, \delta(p + |\boldsymbol{k}' + \boldsymbol{p}| - \sqrt{2}u) \\
&\qquad \times \left[\Big(\frac{u-v}{\sqrt{2}} + p_\Lambda \Big)^{-\kappa} + \Big(\frac{u+v}{\sqrt{2}} + p_\Lambda \Big)^{-\kappa} \right] \\
&= \frac{2^{\kappa-1}}{1-\kappa} \int_{k'}^{\infty} \mathrm{d}(\sqrt{2}u)\, \delta(p + |\boldsymbol{k}' + \boldsymbol{p}| - \sqrt{2}u) \\
&\qquad \times \Big\{ - [(\sqrt{2}u - k' + 2p_\Lambda)^{1-\kappa} - (\sqrt{2}u + k' + 2p_\Lambda)^{1-\kappa}] \\
&\qquad\qquad + [(\sqrt{2}u + k' + 2p_\Lambda)^{1-\kappa} - (\sqrt{2}u - k' + 2p_\Lambda)^{1-\kappa}] \Big\} \\
&= 2\,\frac{2^{\kappa-1}}{\kappa-1} \Big[(p + |\boldsymbol{k}' - \boldsymbol{p}| - k' + 2p_\Lambda)^{1-\kappa} - (p + |\boldsymbol{k}' - \boldsymbol{p}| + k' + 2p_\Lambda)^{1-\kappa} \Big] \\
&\qquad \times \Theta(p + |\boldsymbol{k}' - \boldsymbol{p}| - k')\,,
\end{aligned} \tag{D.27}$$

$$I_3^{\rm bog}(\boldsymbol{p}, \boldsymbol{k}+\boldsymbol{p}) = 2\,\frac{2^{\kappa-1}}{\kappa-1} \Big[(p + k - |\boldsymbol{k} + \boldsymbol{p}| + 2p_\Lambda)^{1-\kappa} - (p + k + |\boldsymbol{k} + \boldsymbol{p}| + 2p_\Lambda)^{1-\kappa} \Big]\,, \tag{D.28}$$

and similarly for the integral $I_4^{\rm bog}$,

$$\begin{aligned}
I_4^{\rm bog}(\boldsymbol{p}, \boldsymbol{k}') &= \int_{k'/\sqrt{2}}^{\infty} \mathrm{d}u \int_{-k'/\sqrt{2}}^{k'/\sqrt{2}} \mathrm{d}v\, \delta(p + |\boldsymbol{k}' + \boldsymbol{p}| - \sqrt{2}u) \\
&\qquad \times \left[\Big(\frac{u-v}{\sqrt{2}} + p_\Lambda \Big) \Big(\frac{u+v}{\sqrt{2}} + p_\Lambda \Big) \right]^{-\kappa} \\
&= 2^{2\kappa-1} \int_{k'}^{\infty} \mathrm{d}(\sqrt{2}u)\, \delta(p + |\boldsymbol{k}' + \boldsymbol{p}| - \sqrt{2}u) \\
&\qquad \times \int_{-k'}^{k'} \mathrm{d}(\sqrt{2}v) \left[(\sqrt{2}u + 2p_\Lambda)^2 - 2v^2 \right]^{-\kappa}
\end{aligned}$$

$$= 2^{2\kappa-1}\int_{k'}^{\infty} \mathrm{d}(\sqrt{2}u)\,\delta(p+|\boldsymbol{k}'+\boldsymbol{p}|-\sqrt{2}u) \\ \times\Big(\frac{2k'}{(\sqrt{2}u+2p_\Lambda)^{2\kappa}}\Big){}_2F_1\Big(\kappa,\frac{1}{2};\frac{3}{2};\Big(\frac{k'}{\sqrt{2}u+2p_\Lambda}\Big)^2\Big)\,, \tag{D.29}$$

$$I_4^{\mathrm{bog}}(\boldsymbol{p},\boldsymbol{k}+\boldsymbol{p}) = 2\,\frac{2^{2\kappa-1}|\boldsymbol{k}+\boldsymbol{p}|}{(p+k+2p_\Lambda)^{2\kappa}}\,{}_2F_1\Big(\kappa,\frac{1}{2};\frac{3}{2};\Big(\frac{|\boldsymbol{k}+\boldsymbol{p}|}{p+k+2p_\Lambda}\Big)^2\Big)\,. \tag{D.30}$$

The following integral is needed,

$$\begin{aligned}\int_{-A}^{A}\mathrm{d}x(y^2-x^2)^{-\alpha} &= \frac{2}{y^{2\alpha-1}}\int_0^{A/y}\mathrm{d}x'(1-x'^2)^{-\alpha} \qquad ; x'=x/y \\ &= \frac{2A}{y^{2\alpha}}\int_0^{\pi/2}\mathrm{d}t\frac{\cos(t)}{(1-\frac{A^2}{y^2}\sin^2(t))^{\alpha}} \qquad ; x'=\frac{A}{y}\sin(t) \\ &= \frac{2A}{y^{2\alpha}}{}_2F_1(\alpha,\frac{1}{2};\frac{3}{2};\frac{A^2}{y^2}).\end{aligned} \tag{D.31}$$

The last line can be obtained by the following integral representation of the hypergeometric function [115],

$${}_2F_1(a,b;c;z) = \frac{2\Gamma(c)}{\Gamma(b)\Gamma(c-b)}\int_0^{\pi/2} dt\frac{(\sin(t))^{2b-1}(\cos(t))^{2c-2b-1}}{(1-z\sin^2(t))^a}\,, \tag{D.32}$$

and the identity ${}_2F_1(a,b;c;z) = {}_2F_1(b,a;c;z)$.

Appendix E

Expansion of the hypergeometric functions

The hypergeometric function has the following series expansion [114],

$$ {}_2F_1(a,b;c;z) = \sum_{n=0}^{\infty} \frac{(a)_n (b)_n}{(c)_n} \frac{z^n}{n!}\,, \tag{E.1} $$

where $(a)_n$ is a Pochhammer symbol defined by $(a)_n = \Gamma(a+n)/\Gamma(a)$ and $c \neq 0, -1, -2, \cdots$. In the case $\mathrm{Re}(c-a-b) > 0$, the series is absolute convergent within the radius $|z| < 1$. The logarithmic branch-cuts extend from the branch-points $z = \pm 1$, and thus, analytic continuation is needed to evaluate the series for $z \geq 1$. Here, we are interested in the leading-oder expansion of the hypergeometric function that takes the form, ${}_2F_1(a,b;c;1+z)$, which appears in Eqs. (4.143) and (4.160). We start by observing one of the relations between Kummer's 24 solutions [115],

$$ \begin{aligned} {}_2F_1(a,b;c;z) = {} & A_1\, {}_2F_1(a,b;-c'+1;1-z) \\ & + A_2\,(1-z)^{c'}\, {}_2F_1(c-a,c-b;c'+1;1-z)\,, \end{aligned} \tag{E.2} $$

where $A_1 = \frac{\Gamma(c)\Gamma(c')}{\Gamma(c-a)\Gamma(c-b)}$ and $A_2 = \frac{\Gamma(c)\Gamma(-c')}{\Gamma(a)\Gamma(b)}$ with $c' = c-a-b$. The $\Gamma(c')$ and $\Gamma(-c')$ in the numerators require noninteger c'.

The hypergeometric function ${}_2F_1\big(1, \frac{1}{2}; \frac{\kappa}{2}; 1 + [(1 \pm i\epsilon)x]^{-2}\big)$ can be transformed using Eq. (E.2) such that we can express them by means of hypergeometric functions the arguments z of which stay within the radius of convergence, $|z| < 1$,

$$ \begin{aligned} & {}_2F_1\Big(1, \frac{1}{2}; \frac{\kappa}{2}; 1 + [(1 \pm i\epsilon)x]^{-2}\Big) \\ & \quad = \frac{\Gamma(\frac{\kappa}{2})\Gamma(\frac{\kappa-3}{2})}{\Gamma(\frac{\kappa-2}{2})\Gamma(\frac{\kappa-1}{2})}\, {}_2F_1\Big(1, \frac{1}{2}; \frac{5-\kappa}{2}; -[(1 \pm i\epsilon)x]^{-2}\Big) \\ & \qquad + \frac{\Gamma(\frac{\kappa}{2})\Gamma(\frac{3-\kappa}{2})}{\Gamma(1)\Gamma(\frac{1}{2})} \Big(-[(1 \pm i\epsilon)x]^2\Big)^{\frac{\kappa-3}{2}}\, {}_2F_1\Big(\frac{\kappa-2}{2}, \frac{\kappa-1}{2}; \frac{\kappa-1}{2}; -[(1 \pm i\epsilon)x]^{-2}\Big)\,. \end{aligned} \tag{E.3} $$

In the limit $x \gg 1$, the hypergeometric functions on the RHS of Eq. (E.3) take the form ${}_2F_1(a,b;c;-1/x^2)$ and thus, the leading-order term is approximated by the first

term ($n = 0$) in the series (E.1) which is 1. Note that we can set $\epsilon \to 0$ inside the hypergeometric function on the RHS of Eq. (E.3) because the arguments are within the radius of convergence, which has no branch cut. We then inspect the factor $\{-[(1 \pm i\epsilon)x]^2\}^{(\kappa-3)/2}$ and separate its real and imaginary parts,

$$\begin{aligned}
\Big(-[(1\pm i\epsilon)x]^{-2}\Big)^{\frac{\kappa-3}{2}} &= |x|^{3-\kappa}\Big[-\Big(\frac{1\mp\epsilon}{1-\epsilon^2}\Big)^2\Big]^{\frac{\kappa-3}{2}} \\
&= |x|^{3-\kappa}[(1\mp\epsilon)(-1\pm\epsilon)]^{\frac{\kappa-3}{2}} \\
&= -|x|^{3-\kappa}\exp\Big(\pm i\frac{\pi(\kappa-1)}{2}\Big) \\
&= -|x|^{3-\kappa}[\cos\Big(\frac{\pi}{2}(\kappa-1)\Big)\pm i\sin\Big(\frac{\pi}{2}(\kappa-1)\Big)] \\
&= -|x|^{3-\kappa}\Big[\cos\Big(\frac{\pi}{2}(\kappa-1)\Big)\pm i\frac{\pi}{\Gamma(\frac{\kappa-1}{2})\Gamma(\frac{3-\kappa}{2})}\Big]\,, \qquad \text{(E.4)}
\end{aligned}$$

where we use Euler's reflection formula,

$$\Gamma(z)\Gamma(1-z) = \frac{\pi}{\sin(\pi z)}\,. \qquad \text{(E.5)}$$

For $\kappa > 3$, the cosine term in Eq. (E.4) can be dropped because of $x \gg 1$. Assuming that this is the case, ${}_2F_1\Big(1, \frac{1}{2}; \frac{\kappa}{2}; 1+[(1\pm i\epsilon)x]^{-2}\Big)$ can be approximated by the leading-order terms of its real and imaginary parts,

$${}_2F_1\Big(1, \frac{1}{2}; \frac{\kappa}{2}; 1+[(1\pm i\epsilon)x]^{-2}\Big) \simeq \frac{\kappa-2}{\kappa-3} \mp i\sqrt{\pi}|x|^{3-\kappa}\frac{\Gamma(\frac{\kappa}{2})}{\Gamma(\frac{\kappa-1}{2})}\,, \qquad \text{(E.6)}$$

where we substitute $\Gamma(1/2) = \sqrt{\pi}$ and use the identity $\Gamma(z) = (z-1)\Gamma(z-1)$.

For $x \ll 1$, we can approximate, $1 + [(1 \pm i\epsilon)x]^{-2} \simeq [(1 \pm i\epsilon)x]^{-2}$, and then use the relation [115],

$$\begin{aligned}
{}_2F_1(a,b;c;z) = B_1\,(-z)^{-a}{}_2F_1(a, 1-c+a; 1-b+a; z^{-1}) \\
+ B_2\,(-z)^{-b}{}_2F_1(b, 1-c+b; 1-a+b; z^{-1})\,, \qquad \text{(E.7)}
\end{aligned}$$

where $B_1 = \frac{\Gamma(b-a)\Gamma(c)}{\Gamma(b)\Gamma(c-a)}$ and $B_2 = \frac{\Gamma(a-b)\Gamma(c)}{\Gamma(a)\Gamma(c-b)}$. Thus,

$$\begin{aligned}
&{}_2F_1\Big(1, \frac{1}{2}; \frac{\kappa}{2}; 1+[(1\pm i\epsilon)x]^{-2}\Big) \\
&\simeq \frac{\Gamma(-\frac{1}{2})\Gamma(\frac{\kappa}{2})}{\Gamma(\frac{1}{2})\Gamma(\frac{\kappa-2}{2})}\Big(-[(1\pm i\epsilon)x]^{-2}\Big)^{-1}{}_2F_1\Big(1, \frac{4-\kappa}{2}; \frac{3}{2}; [(1\pm i\epsilon)x]^2\Big) \\
&\quad + \frac{\Gamma(\frac{1}{2})\Gamma(\frac{\kappa}{2})}{\Gamma(1)\Gamma(\frac{\kappa-1}{2})}\Big(-[(1\pm i\epsilon)x]^{-2}\Big)^{-1/2}{}_2F_1\Big(\frac{1}{2}, \frac{3-\kappa}{2}; \frac{1}{2}; [(1\pm i\epsilon)x]^2\Big)\,. \qquad \text{(E.8)}
\end{aligned}$$

The two hypergeometric functions on the RHS of Eq. (E.8) can be approximated by 1 since we are in the small-x regime. Therefore we only need to evaluate the phase

factor of $\{-[(1 \pm i\epsilon)]^{-2}\}$,

$$\Big(- [(1 \pm i\epsilon)x]^{-2}\Big)^{-1} = [-(1 \pm i\epsilon)^{-2}]^{-1}\, x^2 = \Big(e^{\pm i\pi}\Big)^{-1} x^2 = -x^2\,, \tag{E.9}$$

$$\Big(- [(1 \pm i\epsilon)x]^{-2}\Big)^{-1/2} = [-(1 \pm i\epsilon)^{-2}]^{-1/2}\, |x| = \Big(e^{\pm i\pi}\Big)^{-1/2} |x| = \mp i\, |x|\,. \tag{E.10}$$

Inserting the results into Eq. (E.8) gives

$${}_2F_1\Big(1, \frac{1}{2}; \frac{\kappa}{2}; 1 + [(1 \pm i\epsilon)x]^{-2}\Big) \simeq (\kappa - 2)\, |x| \Big[|x| \mp \frac{i\sqrt{\pi}}{\kappa - 3} \frac{\Gamma(\frac{\kappa-2}{2})}{\Gamma(\frac{\kappa-3}{2})} \Big]\,, \tag{E.11}$$

where we use $\Gamma(-1/2) = -2\sqrt{\pi}$.

The hypergeometric functions ${}_2F_1\,(1, 1; \kappa; 1 \pm [(1 \pm i\varepsilon)|x|]^{-1})$ can be approximated in similar ways. In the limit $x \gg 1$, we can use Eq. (E.2) to rewrite the hypergeometric functions such that their arguments are within the radius of convergence. The results are

$${}_2F_1\Big(1, 1; \kappa; 1 + [(1 \pm i\varepsilon)|x|]^{-1}\Big) \simeq \frac{\kappa - 1}{\kappa - 2} \mp i\pi |x|^{2-\kappa} (\kappa - 1)\,, \tag{E.12}$$

$${}_2F_1\Big(1, 1; \kappa; 1 - [(1 \pm i\varepsilon)|x|]^{-1}\Big) \simeq \frac{\kappa - 1}{\kappa - 2}\,, \tag{E.13}$$

where we assume $\kappa > 2$ in this case. There is no imaginary part in Eq. (E.13) because the argument, $1 - [(1 \pm i\varepsilon)|x|]^{-1}$, is already within the radius of convergence. In the opposite limit, $x \ll 1$, relation (E.7) is unable to represent the function due to $a = b$ in this case. This means the poles in the complex plane are not simple poles but second-order poles. We only emphasize that the leading order contains similar terms as in Eq. (E.11) with an extra logarithmic term due to the second-order pole structure [115].

Appendix F

Evaluation of the scaling form of T-matrix elements

In this appendix, we are going to give the details of the evaluation that have been used in Sect. 3.3, the results presented in Eqs. (3.38), (3.39), (3.44) and (3.45).

The scaling of the T-matrix is derived from the scaling of the many-body coupling, cf. Eqs. (3.18), (3.21), (3.25) and (3.28). Recall Eq. (4.129) for the expression of the many-body coupling $g_{\text{eff}}(p)$,

$$g_{\text{eff}}^2(p) = \frac{g^2}{|1 + g\hbar\Pi^R(p)|^2} \tag{F.1}$$

where the 1-loop self-energy $\Pi^R(p_0, \boldsymbol{p})$ is defined by, cf. Eq. (4.80),

$$\begin{aligned}\Pi^R(p_0, \boldsymbol{p}) &= -\int_{-\infty}^{\infty} \frac{\mathrm{d}q_0}{2\pi} \frac{1}{q_0 + i\,\epsilon} \Pi^\rho(q_0 - p_0, -\boldsymbol{p}) \\ &= -\frac{1}{2}\int_{-\infty}^{\infty} \frac{\mathrm{d}q_0}{2\pi} \frac{1}{q_0 + i\,\epsilon} \int \frac{\mathrm{d}^d k\, \mathrm{d}k_0}{(2\pi)^{d+1}} \\ &\qquad \times \Big[\rho_{ab}(p_0 - q_0 - k_0, \boldsymbol{p} - \boldsymbol{k}) F_{ba}(-k_0, \boldsymbol{k}) \\ &\qquad\quad - F_{ab}(p_0 - q_0 - k_0, \boldsymbol{p} - \boldsymbol{k}) \rho_{ba}(-k_0, \boldsymbol{k})\Big] . \end{aligned} \tag{F.2}$$

There are two scaling limits of g_{eff}. In the regime where $|\Pi^R| \ll 1$, g_{eff} is reduced to the bare GPE coupling $g = 4\pi\, a/m$ and thus, the scaling exponents γ and γ_κ, defined by the following scaling hypotheses,

$$g_{\text{eff}}(s^z p_0, s\boldsymbol{p}; s^{-1/\beta} t) = s^\gamma g_{\text{eff}}(p_0, \boldsymbol{p}; t)\,, \tag{F.3}$$

$$g_{\text{eff}}(s^z p_0, s\boldsymbol{p}; t) = s^{\gamma_\kappa} g_{\text{eff}}(p_0, \boldsymbol{p}; t)\,, \tag{F.4}$$

become simply $\gamma = \gamma_\kappa = 0$ which we use to evaluate the scaling exponents m and m_κ in the perturbative regime, cf. Eqs. (3.19) and (3.22). For $|\Pi^R| \gg 1$, the scaling of g_{eff} is derived directly from the scaling of Π^R. We recall the scaling hypotheses of $F(p)$ and $\rho(p)$ [25, 49],

$$F_{ab}(s^z p_0, s\boldsymbol{p}) = s^{-2-\kappa} F_{ab}(p_0, \boldsymbol{p})\,, \tag{F.5}$$

$$\rho_{ab}(s^z p_0, s\boldsymbol{p}) = s^{-2+\eta} \rho_{ab}(p_0, \boldsymbol{p})\,, \tag{F.6}$$

where κ is the momentum exponent of the quasiparticle occupancy as we defined it in Eq. (2.21) and η is an anomalous dimension.

If the integral on the RHS of Eq. (F.2) converges, the momentum scaling of Π^R is determined by counting the dimension of momentum on the RHS of Eq. (F.2),

$$\Pi^R(s^z p_0, s\boldsymbol{p}) = s^{d+z-4-\kappa+\eta}\Pi^R(p_0, \boldsymbol{p}) \sim p^{d+z-4-\kappa+\eta}\,. \tag{F.7}$$

This is the case because no other momentum scale exists in the integral. However, if the integral on the RHS of Eq. (F.2) diverges such that a regularization scale is needed, the momentum scaling of Π^R can be different from the one presented in Eq. (F.7). The divergent integral can be expressed in terms of the regularization scale, for example, assuming that a function $f(p)$ is infrared-divergent, through

$$\int_{k_\Lambda}^{\infty} \mathrm{d}k\, f(k) \sim F(k_\Lambda), \tag{F.8}$$

where $\mathrm{d}F(k)/\mathrm{d}k = f(k)$. Since the dimension of momentum in both sides of Eq. (F.8) needs to be equal, the order of k_Λ in $F(k_\Lambda)$ is determined by the order of the divergence in the integral on the LHS of Eq. (F.8), i.e. if $f(k) \sim k^{-\alpha}$, $F(k_\Lambda) \sim k_\Lambda^{1-\alpha}$.

In the following, we assume that $F_{ab}(p_0, \boldsymbol{p})$ diverges as $\boldsymbol{p} \to 0$, while $\rho_{ab}(p)$ has a well defined peak and thus, is finite. Then, the divergence of the integral in Eq. (F.2) can be extracted from the behaviour of the integrand around the singularity. In the first terms on the RHS of Eq. (F.2), the singularity locates at $\boldsymbol{k} \to 0$. As long as the well defined peak of $\rho(p_0, \boldsymbol{p})$ is away from $\boldsymbol{p} \sim 0$, we can ignore $\rho(p_0, \boldsymbol{p})$ when we count the order of divergence. Similar arguments apply for the second term on the RHS of Eq. (F.2) where the singular point is now $\boldsymbol{k} \to \boldsymbol{p}$. Thus, the order of the divergence of Π^R, χ, is determined by the momentum unit on the RHS of Eq. (F.2) minus the momentum unit of ρ, i.e.,

$$\chi = d + z - 2 - \kappa\,. \tag{F.9}$$

Then, scaling form of Π^R in Eq. (F.2) becomes

$$\Pi^R(p) \sim p^{-2+\eta} p_\Lambda^{d+z-2-\kappa}\,. \tag{F.10}$$

Note that the momentum scaling in Eq. (F.10) comes from ρ where the infrared cutoff p_Λ has its power equal to the order of divergence χ. The structure in Eq. (F.10) can be verified by the leading-order terms of Eqs. (4.142) and (4.159) in the limit $\eta = 0$. We can infer the momentum scaling exponent γ_κ from $|\Pi^R|^{-1}$, cf. Eq. (F.1), and thus,

$$\gamma_\kappa = 2 - \eta\,. \tag{F.11}$$

The result is confirmed in the limit $\eta = 0$ by our explicit calculation in Ch. 4, cf. Eqs. (4.148) and (4.166). The m_κ can be obtained by comparing the momentum scaling in Eq. (3.3) with Eq. (4.116),

$$\begin{aligned} 2d - z + 2m_\kappa - 3\kappa &= 2d + 3z + 2\gamma_\kappa - 8 - 3\kappa + \eta \\ \Rightarrow m_\kappa &= 2(z-2) + \gamma_\kappa + \frac{\eta}{2}\,. \end{aligned} \tag{F.12}$$

Substituting Eq. (F.11) into Eq. (F.12) yields

$$m_\kappa = 2(z-1) - \frac{\eta}{2}\,. \tag{F.13}$$

Before we evaluate the temporal scaling exponents γ and m, it is helpful to investigate the temporal scaling of $n_Q(p,t)$ and $n(p,t)$. Recalling the scaling hypotheses, Eqs. (2.21) and (3.34),

$$n_Q(s\boldsymbol{p},t) = s^{-\kappa} n_Q(\boldsymbol{p},t)\,, \tag{F.14}$$

$$n_Q(s\boldsymbol{p},s^{1/\beta}t) = s^{-\alpha/\beta} n_Q(\boldsymbol{p},t)\,. \tag{F.15}$$

these imply a simple scaling form of n_Q,

$$n_Q(\boldsymbol{p},t) \sim p^{-\kappa} p_\Lambda^{\kappa-\alpha/\beta}(t)\,, \tag{F.16}$$

where we explicitly choose the time-dependent scale to be the infrared scale p_Λ with time evolution, $p_\Lambda(t) \sim t^{-\beta}$ because we assume the quasiparticles are concentrated in the infrared regime. For the occupation number $n(\boldsymbol{p},t)$, we recall Eq. (2.20),

$$n(\boldsymbol{p},t) = \left(\frac{|\boldsymbol{p}|}{\tilde{p}(t)}\right)^{z-2} n_Q(\boldsymbol{p},t)\,, \tag{F.17}$$

where $\tilde{p}$ is a momentum scale encoded in the Bogoliubov transformation, i.e. in the case $z=1$, $\tilde{p} \sim p_\xi$. It is straightforward to verify the following scaling hypotheses,

$$n(s\boldsymbol{p},t) = s^{-\kappa+z-2} n(\boldsymbol{p},t)\,, \tag{F.18}$$

$$n(s\boldsymbol{p},s^{1/\beta}t) = s^{-\tilde{\alpha}/\beta} n(\boldsymbol{p},t)\,. \tag{F.19}$$

If we assume that $\tilde{p}$ is time-independent, then

$$\tilde{\alpha}/\beta = \alpha/\beta - z + 2\,. \tag{F.20}$$

The result implies

$$n(\boldsymbol{p},t) \sim p^{-\kappa+z-2} {p_\Lambda}^{(\kappa-z+2)-\tilde{\alpha}/\beta}(t)\,, \tag{F.21}$$

$$\rho_{\mathrm{nc}}(t) = \int \mathrm{d}^d p\, n(\boldsymbol{p},t) \sim p_\Lambda^{d-\tilde{\alpha}/\beta}(t)\,. \tag{F.22}$$

If we assume $\rho_{\mathrm{nc}}(t) \sim t^{-2\delta} \sim p_\Lambda^{2\delta/\beta}(t)$, we obtain the relation

$$2\delta/\beta = d + z - 2 - \alpha/\beta\,. \tag{F.23}$$

To evaluate γ, we claim that the exponent κ in $F(p)$ has its origin from the quasiparticle occupation, i.e. we assume the following scaling hypotheses in F,

$$F_{ab}(s^z p_0, s\boldsymbol{p}; t) = s^{-2-\kappa} F_{ab}(p_0, \boldsymbol{p}; t)\,, \tag{F.24}$$

$$F_{ab}(s^z p_0, s\boldsymbol{p}; s^{1/\beta}t) = s^{-2-\alpha/\beta} F_{ab}(p_0, \boldsymbol{p}; t)\,. \tag{F.25}$$

We do not account for time dependence of ρ because ρ has no dynamics at the level of the kinetic equations we derived in Ch. 4. This means the momentum and temporal scalings of ρ are identical. Then, the temporal scaling of Π^R can be read off from Eq. (F.2),

$$\begin{aligned}\Pi^R(s^z p_0, s\boldsymbol{p}; s^{-1/\beta} t) &= s^{d-4+z+\eta-\alpha/\beta}\Pi^R(p_0, \boldsymbol{p}; t) \\ &= s^{-2+\eta+2\delta/\beta}\Pi^R(p_0, \boldsymbol{p}; t)\,. \end{aligned} \tag{F.26}$$

This means

$$\gamma = 2 - \eta - 2\delta/\beta\,. \tag{F.27}$$

The result is confirmed by our calculation in Ch. 4, cf. Eqs. (4.148) and (4.166). For the temporal scaling of the T-matrix, m, we determine by comparing the temporal scaling of Eqs. (3.3) with (4.116),

$$\begin{aligned} 2d - z + 2m - 3\alpha/\beta &= 2d + 3z + 2\gamma - 8 - 3\alpha/\beta + \eta \\ \Rightarrow m &= 2(z-2) + \gamma + \frac{\eta}{2}\,. \end{aligned} \tag{F.28}$$

Inserting Eq. (F.27) into Eq. (F.28) yields

$$m = 2(z-1) - \frac{\eta}{2} - \frac{2\delta}{\beta}\,. \tag{F.29}$$

Bibliography

[1] S. N. Bose, Plancks Gesetz und Lichtquantenhypothese, [Am. J. Phys. **44**, 1056 (1976)] Z. Phys. **26**(3), 178 (1924).

[2] A. Einstein, Quantentheorie des einatomigen idealen Gases, Sitzungsber. Kgl. Preuss. Akad. Wiss., Phys. Math. Kl. **1924**, 261 (1924).

[3] A. Einstein, Quantentheorie des einatomigen idealen Gases. Zweite Abhandlung, Sitzungsber. Kgl. Preuss. Akad. Wiss., Phys. Math. Kl. **1925**, 3 (1925).

[4] M. H. Anderson, J. R. Ensher, M. R. Matthews, C. E. Wieman, and E. A. Cornell, Observation of Bose-Einstein Condensation in a Dilute Atomic Vapor, Science **269**, 198 (1995).

[5] C. C. Bradley, C. A. Sackett, J. J. Tollett, and R. G. Hulet, Evidence of Bose-Einstein Condensation in an Atomic Gas with Attractive Interactions, Phys. Rev. Lett. **75**, 1687 (1995).

[6] K. B. Davis, M.-O. Mewes, M. R. Andrews, N. J. van Druten, D. S. Durfee, D. M. Kurn, and W. Ketterle, Bose-Einstein Condensation in a Gas of Sodium Atoms, Phys. Rev. Lett. **75**, 3969 (1995).

[7] Y. Kagan and B. V. Svistunov, Kinetics of the onset of long-range order during Bose condensation in an interacting gas, [Zh. Eksp. Teor. Fiz. 105, 353 (1994)] Sov. Phys. JETP **78**(2), 187 (1994).

[8] C. Townsend, W. Ketterle, and S. Stringari, Bose-Einstein condensation, Physics World **10**(3), 29 (1997).

[9] W. Ketterle, Nobel lecture: When atoms behave as waves: Bose-Einstein condensation and the atom laser, Rev. Mod. Phys. **74**, 1131–1151 (2002).

[10] V. E. Zakharov, V. S. L'vov, and G. Falkovich, *Kolmogorov Spectra of Turbulence I: Wave Turbulence*, Springer, Berlin, 1992.

[11] S. Nazarenko, *Wave turbulence*, Number 825 in Lecture Notes in Physics, Springer, Heidelberg, 2011.

[12] A. Newell, Wave Turbulence, Ann. Rev. Fluid Mech. **43**(1) (2011).

[13] E. Levich and V. Yakhot, Time evolution of a Bose system passing through the critical point, Phys. Rev. B **15**(1), 243 (1977).

[14] E. Levich and V. Yakhot, Time development of coherent and superfluid properties in the course of a λ-transition, J. Phys. A: Math. Gen. **11**(11), 2237 (1978).

[15] B. Svistunov, Highly nonequilibrium Bose condensation in a weakly interacting gas, J. Mosc. Phys. Soc. **1**, 373 (1991).

[16] D. V. Semikoz and I. I. Tkachev, Kinetics of Bose Condensation, Phys. Rev. Lett. **74**, 3093–3097 (1995).

[17] D. Semikoz and I. Tkachev, Condensation of Bosons in the kinetic regime, Phys. Rev. D **55**(2), 489 (1997).

[18] H. T. C. Stoof, Formation of the condensate in a dilute Bose gas, Phys. Rev. Lett. **66**, 3148 (1991).

[19] H. T. C. Stoof, Nucleation of Bose-Einstein condensation , Phys. Rev. A **45**(12), 8398 (1992).

[20] H. T. C. Stoof, Initial Stages of Bose-Einstein Condensation, Phys. Rev. Lett. **78**(5), 768 (1997).

[21] H. T. C. Stoof, Coherent Versus Incoherent Dynamics During Bose-Einstein Condensation in Atomic Gases, J. Low Temp. Phys. **114**(1/2), 11 (1999).

[22] Y. Kagan, B. V. Svistunov, and G. V. Shlyapnikov, Kinetics of Bose condensation in an interacting Bose gas, [Zh. Eksp. Teor. Fiz. 101, 528 (1992)] Sov. Phys. JETP **74**, 279 (1992).

[23] Y. Kagan and B. V. Svistunov, Evolution of Correlation Properties and Appearance of Broken Symmetry in the Process of Bose-Einstein Condensation, Phys. Rev. Lett. **79**(18), 3331 (1997).

[24] N. G. Berloff and B. V. Svistunov, Scenario of strongly nonequilibrated Bose-Einstein condensation, Phys. Rev. A **66**(1), 013603 (2002).

[25] J. Berges, A. Rothkopf, and J. Schmidt, Non-thermal fixed points: Effective weak-coupling for strongly correlated systems far from equilibrium, Phys. Rev. Lett. **101**, 041603 (2008).

[26] J. Berges and G. Hoffmeister, Nonthermal fixed points and the functional renormalization group, Nucl. Phys. **B813**, 383 (2009).

[27] B. Nowak, D. Sexty, and T. Gasenzer, Superfluid Turbulence: Nonthermal Fixed Point in an Ultracold Bose Gas, Phys. Rev. B **84**, 020506(R) (2011).

[28] B. Nowak, J. Schole, D. Sexty, and T. Gasenzer, Nonthermal fixed points, vortex statistics, and superfluid turbulence in an ultracold Bose gas, Phys. Rev. A **85**, 043627 (2012).

[29] B. Nowak, J. Schole, and T. Gasenzer, Universal dynamics on the way to thermalisation, New J. Phys. **16**, 093052 (2014).

[30] M. J. Davis, T. M. Wright, T. Gasenzer, S. A. Gardiner, and N. P. Proukakis, Formation of Bose-Einstein condensates, (2016).

[31] M. Imamovic-Tomasovic and A. Griffin, Quasiparticle Kinetic Equation in a Trapped Bose Gas at Low Temperatures, Journal of Low Temperature Physics **122**(5), 617–655 (2001).

[32] R. Walser, J. Williams, J. Cooper, and M. Holland, Quantum kinetic theory for a condensed bosonic gas, Phys. Rev. A **59**(5), 3878 (1999).

[33] R. Walser, J. Cooper, and M. Holland, Reversible and irreversible evolution of a condensed bosonic gas, Phys. Rev. A **63**, 013607 (2000).

[34] J. Wachter, R. Walser, J. Cooper, and M. Holland, Equivalence of kinetic theories of Bose-Einstein condensation, Phys. Rev. A **64**, 053612 (2001).

[35] N. P. Proukakis, Self-consistent quantum kinetics of condensate and non-condensate via a coupled equation of motion formalism, Journal of Physics B: Atomic, Molecular and Optical Physics **34**(23), 4737 (2001).

[36] N. P. Proukakis, K. Burnett, and H. T. C. Stoof, Microscopic treatment of binary interactions in the nonequilibrium dynamics of partially Bose-condensed trapped gases, Phys. Rev. A **57**, 1230 (1998).

[37] S. Dyachenko, A. C. Newell, A. Pushkarev, and V. E. Zakharov, Optical turbulence: weak turbulence, condensates and collapsing filaments in the nonlinear Schrödinger equation, Phys. D: Nonlin. Phen. **57**(1-2), 96 (1992).

[38] Y. Lvov, S. Nazarenko, and R. West, Wave turbulence in Bose–Einstein condensates, Physica D: Nonlinear Phenomena **184**(1), 333–351 (2003), Complexity and Nonlinearity in Physical Systems – A Special Issue to Honor Alan Newell.

[39] U. Frisch, *Turbulence: The Legacy of A. N. Kolmogorov*, Cambridge University Press, 2004.

[40] A. N. Kolmogorov, The local structure of turbulence in incompressible viscous fluid for very large Reynolds numbers, Proc. USSR Acad. Sci. **30**, 299 (1941), [Proc. R. Soc. Lond. A 434, 9 (1991)].

[41] N. Navon, A. L. Gaunt, R. P. Smith, and Z. Hadzibabic, Emergence of a turbulent cascade in a quantum gas, Nature **539**(7627), 72–75 (2016).

[42] R. Jackiw, Functional evaluation of the effective potential, Phys. Rev. D **9**, 1686–1701 (1974).

[43] J. M. Cornwall, R. Jackiw, and E. Tomboulis, Effective action for composite operators, Phys. Rev. D **10**, 2428 (1974).

[44] E. A. Calzetta and B. L. Hu, Nonequilibrium Quantum Fields: Closed Time Path Effective Action, Wigner Function And Boltzmann Equation, Phys. Rev. D **37**, 2878 (1988).

[45] J. Berges, Controlled nonperturbative dynamics of quantum fields out of equilibrium, Nucl. Phys. **A699**, 847 (2002).

[46] G. Aarts and J. Berges, Classical Aspects of Quantum Fields Far from Equilibrium, Phys. Rev. Lett. **88**, 041603 (2002).

[47] G. Aarts, D. Ahrensmeier, R. Baier, J. Berges, and J. Serreau, Far-from-equilibrium dynamics with broken symmetries from the $1/N$ expansion of the 2PI effective action, Phys. Rev. D **66**, 045008 (2002).

[48] J. Berges, Nonequilibrium Quantum Fields: From Cold Atoms to Cosmology, in *Proc. Int. School on Strongly Interacting Quantum Systems Out of Equilibrium, Les Houches*, edited by T. Giamarchi et al., OUP, Oxford, 2016.

[49] C. Scheppach, J. Berges, and T. Gasenzer, Matter-wave turbulence: Beyond kinetic scaling, Phys. Rev. A **81**(3), 033611 (2010).

[50] A. Piñeiro-Orioli, K. Boguslavski, and J. Berges, Universal self-similar dynamics of relativistic and nonrelativistic field theories near nonthermal fixed points, Phys. Rev. D **92**(2), 025041 (2015).

[51] S. Mathey, T. Gasenzer, and J. M. Pawlowski, Anomalous scaling at nonthermal fixed points of Burgers' and Gross-Pitaevskii turbulence, Phys. Rev. A **92**, 023635 (2015).

[52] R. Walz, K. Boguslavski, and J. Berges, Large-N kinetic theory for highly occupied systems, ArXiv e-prints:1710.11146 (2017).

[53] J. Cardy, *Scaling and Renormalization in Statistical Physics*, Cambridge Lecture Notes in Physics, CUP, Cambridge, UK, 1996.

[54] A. Polkovnikov, K. Sengupta, A. Silva, and M. Vengalattore, Colloquium: Nonequilibrium dynamics of closed interacting quantum systems, Rev. Mod. Phys. **83**(3), 863 (2011).

[55] P. C. Hohenberg and B. I. Halperin, Theory of Dynamic Critical Phenomena, Rev. Mod. Phys. **49**, 435–479 (1977).

[56] H. Janssen, Field-theoretic methods applied to critical dynamics, in *Dynamical critical phenomena and related topics, Lecture Notes in Physics, vol. 104*, page 26, Springer, Heidelberg 1979, 1979.

[57] H. K. Janssen, B. Schaub, and B. Schmittmann, New universal short-time scaling behaviour of critical relaxation processes, Z. Phys. B Cond. Mat. **73**(4), 539–549 (1989).

[58] H. Janssen, On the renormalized field theory of nonlinear critical relaxation, in *From phase transitions to chaos*, page 68, World Scientific, Singapore 1992, 1992.

[59] P. Calabrese and A. Gambassi, Aging in ferromagnetic systems at criticality near four dimensions, Phys. Rev. E **65**, 066120 (2002).

[60] P. Calabrese and A. Gambassi, Ageing properties of critical systems, J. Phys. A: Math. Gen. **38**(18), R133 (2005).

[61] A. Gambassi, Slow dynamics at critical points: the field-theoretical perspective, J. Phys. Conf. Ser. **40**(1), 13 (2006).

[62] C. Godrèche and J. M. Luck, Response of non-equilibrium systems at criticality: ferromagnetic models in dimension two and above, Journal of Physics A: Mathematical and General **33**(50), 9141 (2000).

[63] C. Godrèche and J. M. Luck, Nonequilibrium critical dynamics of ferromagnetic spin systems, Journal of Physics: Condensed Matter **14**(7), 1589 (2002).

[64] M. Tsubota, Quantum Turbulence, J. Phys. Soc. Jpn. **77**, 111006 (2008).

[65] W. Vinen, An Introduction to Quantum Turbulence, J. Low Temp. Phys. **145**, 7 (2006).

[66] M. Karl, B. Nowak, and T. Gasenzer, Tuning universality far from equilibrium, Scientific Reports **3** (2013).

[67] M. Karl, B. Nowak, and T. Gasenzer, Universal scaling at non-thermal fixed points of a two-component Bose gas, Phys. Rev. A **88**, 063615 (2013).

[68] C. Pethick and H. Smith, *Bose-Einstein condensation in dilute gases*, CUP, Cambridge, UK, 2006.

[69] J. Berges and D. Sexty, Bose condensation far from equilibrium, Phys. Rev. Lett. **108**, 161601 (2012).

[70] J. Schole, B. Nowak, and T. Gasenzer, Critical Dynamics of a Two-dimensional Superfluid near a Non-Thermal Fixed Point, Phys. Rev. A **86**, 013624 (2012).

[71] M. Karl and T. Gasenzer, Strongly anomalous non-thermal fixed point in a quenched two-dimensional Bose gas, New Journal of Physics **19**(9), 093014 (2017).

[72] J. Berges and D. Sexty, Strong versus weak wave-turbulence in relativistic field theory, Phys. Rev. D **83**, 085004 (2011).

[73] K. Huang, *Statistical Mechanics*, Wiley, New York, 1987.

[74] R. Kraichnan, Inertial Ranges in Two-Dimensional Turbulence, Phys. Fl. **10**(7), 1417 (1967).

[75] J. Jiménez, The Contributions of A. N. Kolmogorov to the theory of turbulence, Arbor **178**(704), 589–606 (2004).

[76] S. Orszag, *Lectures on the Statistical Theory of Turbulence*, Flow research report, MIT, 1974.

[77] G. Falkovich and K. R. Sreenivasan, Lessons from hydrodynamics turbulence, Phys. Today **39**(7), 43 (2006).

[78] J. Cardy, G. Falkovich, K. Gawędzki, S. Nazarenko, and O. Zaboronski, *Non-equilibrium Statistical Mechanics and Turbulence*, London Mathematical Society Le, Cambridge University Press, 2008.

[79] H. L. Grant, R. W. Stewart, and A. Moilliet, Turbulence spectra from a tidal channel, Journal of Fluid Mechanics **12**(2), 241–268 (1962).

[80] F. H. Champagne, The fine-scale structure of the turbulent velocity field, Journal of Fluid Mechanics **86**(1), 67–108 (1978).

[81] J. Maurer, P. Tabeling, and G. Zocchi, Statistics of Turbulence between Two Counterrotating Disks in Low-Temperature Helium Gas, EPL (Europhysics Letters) **26**(1), 31 (1994).

[82] D. J. Benney and P. G. Saffman, Nonlinear Interactions of Random Waves in a Dispersive Medium, Proceedings of the Royal Society of London. Series A, Mathematical and Physical Sciences **289**(1418), 301–320 (1966).

[83] M. M. Farazmand, N. K.-R. Kevlahan, and B. Protas, Controlling the dual cascade of two-dimensional turbulence, Journal of Fluid Mechanics **668**, 202–222 (2011).

[84] L. Biven, S. Nazarenko, and A. Newell, Breakdown of wave turbulence and the onset of intermittency, Physics Letters A **280**(1), 28–32 (2001).

[85] V. E. Zakharov and N. N. Filonenko, Weak turbulence of capillary waves, Journal of Applied Mechanics and Technical Physics **8**(5), 37–40 (1967).

[86] A. Pushkarev and V. Zakharov, Turbulence of capillary waves - theory and numerical simulation, Physica D: Nonlinear Phenomena **135**(1), 98–116 (2000).

[87] E. Falcon, C. Laroche, and S. Fauve, Observation of gravity-capillary wave turbulence, Phys. Rev. Lett. **98**(9), 94503 (2007).

[88] C. Falcón, E. Falcon, U. Bortolozzo, and S. Fauve, Capillary wave turbulence on a spherical fluid surface in low gravity, EPL (Europhysics Letters) **86**(1), 14002 (2009).

[89] G. V. Kolmakov, A. A. Levchenko, M. Y. Brazhnikov, L. P. Mezhov-Deglin, A. N. Silchenko, and P. V. E. McClintock, Quasiadiabatic Decay of Capillary Turbulence on the Charged Surface of Liquid Hydrogen, Phys. Rev. Lett. **93**, 074501 (2004).

[90] G. V. Kolmakov, M. Y. Brazhnikov, A. A. Levchenko, A. N. Silchenko, P. V. E. McClintock, and L. P. Mezhov-Deglin, Nonstationary Nonlinear Phenomena on the Charged Surface of Liquid Hydrogen, Journal of Low Temperature Physics **145**(1), 311–335 (2006).

[91] P. A. Hwang, D. W. Wang, E. J. Walsh, W. B. Krabill, and R. N. Swift, Airborne Measurements of the Wavenumber Spectra of Ocean Surface Waves. Part I: Spectral Slope and Dimensionless Spectral Coefficient, Journal of Physical Oceanography **30**(11), 2753–2767 (2000).

[92] P. A. Hwang and D. W. Wang, Field Measurements of Duration-Limited Growth of Wind-Generated Ocean Surface Waves at Young Stage of Development, Journal of Physical Oceanography **34**(10), 2316–2326 (2004).

[93] V. E. Zakharov, Theoretical interpretation of fetch limited wind-drivensea observations, Nonlinear Processes in Geophysics **12**(6), 1011–1020 (2005).

[94] C. Connaughton, C. Josserand, A. Picozzi, Y. Pomeau, and S. Rica, Condensation of classical nonlinear waves, Phys. Rev. Lett. **95**(26), 263901 (2005).

[95] S. Nazarenko and M. Onorato, Wave turbulence and vortices in Bose-Einstein condensation, Phys. D: Nonlin. Phen. **219**(1), 1 (2006).

[96] M. Schiffer, Generalized Boltzmann equation for quasi-condensates in 1D, Bachelor thesis (unpublished), Universität Heidelberg, 2016.

[97] R. D. Jordan, Effective field equations for expectation values, Phys. Rev. D **33**, 444–454 (1986).

[98] J. Schwinger, Brownian Motion of a Quantum Oscillator, J. Math. Phys. **2**, 407 (1961).

[99] L. V. Keldysh, Diagram Technique For Nonequilibrium Processes, [Sov. Phys. JETP **20**, 1018 (1965)] Zh. Eksp. Teor. Fiz. **47**, 1515 (1964).

[100] P. Dirac, *Lectures on Quantum Mechanics*, Belfer Graduate School of Science, monograph series, Dover Publications, 2001.

[101] R. Jackiw, (Constrained) quantization without tears, in *2nd Workshop on Constraint Theory and Quantization Methods Montepulciano, Italy, June 28-July 1, 1993*, pages 163–175, 1993.

[102] J. Berges and J. Serreau, Parametric Resonance in Quantum Field Theory, Phys. Rev. Lett. **91**, 111601 (2003).

[103] J. Berges and T. Gasenzer, Quantum versus classical statistical dynamics of an ultracold Bose gas, Phys. Rev. **A76**, 033604 (2007).

[104] G. Aarts and J. Berges, Nonequilibrium time evolution of the spectral function in quantum field theory, Phys. Rev. **D64**, 105010 (2001).

[105] S. Juchem, W. Cassing, and C. Greiner, Quantum dynamics and thermalization for out-of-equilibrium ϕ^4-theory, Phys. Rev. D **69**, 025006 (2004).

[106] A. Branschädel and T. Gasenzer, 2PI nonequilibrium versus transport equations for an ultracold Bose gas, J. Phys. B **41**, 135302 (2008).

[107] M. Peskin and D. Schroeder, *An Introduction to Quantum Field Theory*, Advanced book classics, Addison-Wesley Publishing Company, 1995.

[108] K. Hagen and S. Verena, *Critical Properties Of Phi4- Theories*, World Scientific Publishing Company, 2001.

[109] S. Weinberg, *The Quantum Theory of Fields: Foundations*, Number v. 1 in The Quantum Theory of Fields 3 Volume Hardback Set, Cambridge University Press, 1995.

[110] H. Kleinert, *Path Integrals in Quantum Mechanics, Statistics, Polymer Physics, and Financial Markets*, EBL-Schweitzer, World Scientific, 2009.

[111] C. Itzykson and J. Zuber, *Quantum Field Theory*, Dover Books on Physics, Dover Publications, 2012.

[112] V. Nair, *Quantum Field Theory: A Modern Perspective*, Graduate Texts in Contemporary Physics, Springer New York, 2006.

[113] E. Calzetta and B. Hu, *Nonequilibrium Quantum Field Theory*, Cambridge Monographs on Mathem, Cambridge University Press, 2008.

[114] M. Abramowitz and I. Stegun, *Handbook of Mathematical Functions: With Formulas, Graphs, and Mathematical Tables*, Applied mathematics series, Dover Publications, 1964.

[115] H. Bateman and B. M. Project, *Higher Transcendental Functions*, Number v. 1 in Bateman Manuscript Project California Institute of Technology, McGraw-Hill, 1955.